INVESTIGATING THE DIVERSE ROLE OF METALS

IN PROTEIN STRUCTURE AND FUNCTION

by

Katherine M. F. Paulsen

A dissertation in partial fulfillment of
the requirements for the degree of

Doctor of Philosophy

(Chemistry)

at the

UNIVERSITY OF WISCONSIN—MADISON

2013

Date of Final Oral Examination: April 18th, 2013

The dissertation is approved by the following members of the Final Oral Committee:
Judith N. Burstyn, Professor, Department of Chemistry
Silvia Cavagnero, Professor, Department of Chemistry
Joshua C. Coon, Professor, Department of Chemistry
Thomas C. Brunold, Professor, Department of Chemistry
Edward G. Ruby, Professor, Department of Medical Microbiology & Immunology

INVESTIGATING THE DIVERSE ROLE OF METALS IN PROTEIN STRUCTURE AND FUNCTION

by

Katherine M. F. Paulsen

Under the supervision of Professor Judith N. Burstyn

At the University of Wisconsin—Madison

Metal ions are essential to life where they play a critical role in over a third of all proteins. The ability of metals to gain and lose electrons enables a variety of functions ranging from electron transport and reaction catalysis to structural stabilization. This thesis explores how exogenous and native metal ions interact with proteins to disrupt structure or to provide structural stability. This work examines: 1) how a synthetic copper protease disrupts protein structure during cleavage; 2) how two heme-containing proteins are regulated allosterically; 3) the identity of the Fe(III) cysteine(thiolate) ligand in the regulator of CO metabolism (RcoM) from *Burkholderia xenovorans*; and 4) the insertion of CoPPIX into human cystathionine β-synthase (hCBS).

Utilization of a variety of spectroscopic techniques revealed that incubating bovine serum albumin (BSA), aldolase and glyceraldehyde-3-phopshate dehydrogenase (GAPDH) with [Cu(1,4,7-triazocyclononane)]Cl_2 results in cleavage and protein aggregation via disruption of tertiary structures, but does not induce fibril formation. In-gel trypsin digestion coupled with MALDI-MS was used to identify the sites of aldolase cleavage. The copper complex accessed buried residues during cleavage.

Mass spectrometry enabled studies on two allosterically regulated proteins, the CO-sensing carbon monoxide oxidation activator (CooA) protein from *Rhodospirillum rubrum* and CBS from *Drosophila melanogaster* (*Dm*CBS). Initial hydrogen/deuterium exchange MS experiments with CooA confirmed that the DNA-binding and the heme-binding domains are independently folded. Mass spectrometry revealed that *Dm*CBS does not bind the allosteric regulator AdoMet, even under saturating conditions, unlike AdoMet-regulated hCBS.

The *Bx*RcoM protein is a CO-responsive transcription factor that binds heme with an Fe(III) Cys/His ligation motif. Expression and purification of variants at all three cysteines in *Bx*RcoM, C94S, C127S and C130S, allowed spectroscopic identification of Cys^{94} is as the native cysteine(thiolate) ligand to the Fe(III) heme in *Bx*RcoM.

CBS is a PLP-dependent enzyme bearing a heme cofactor believed to be involved in structural stabilization. Metal analysis and spectroscopic characterization of CoPPIX-substituted human CBS (CoCBS) revealed that CoCBS contained 92% CoPPIX and retained the native His/Cys metal coordination. CoCBS was fully active. Together these results support a structural role for heme in hCBS.

Approved: _____ Date: _____

Judith N. Burstyn

Professor of Chemistry

Acknowledgements

First and foremost I would like to thank my wonderful advisor, Professor Judith Burstyn, or as I like to call her, Fearless Leader. I am grateful Judith took a risk accepting a student from the analytical division who admittedly knew minimal inorganic chemistry into her research group. I have learned a tremendous amount of inorganic chemistry, molecular biology, spectroscopy, protein chemistry and a lot about myself during my time in Judith's group. I am truly appreciative of the open relationship I have shared with Judith; I am glad she did not try to force me to be someone I am not; rather, she showed me great compassion. Judith, I can say without a doubt, I would choose you as my advisor time and time again – thank you. Wherever my future endeavors take me I hope I can emulate the passion and joy I have seen in Judith for her research.

To the Burstyn research group, both past and present, thank you for the wonderful work environment, it was a pleasure to come to work each day. I am particularly grateful to have met one of my best friends, the crazy smart and caring, Dr. Aaron Smith, in the Burstyn group. A shoutout to my wonderful undergraduate students, past and present, Wenlu Gu and Debra Statz, for keeping work lighthearted and fun while helping me become a better teacher and scientist. A special thanks, to my favorite Burstyn-group-post-doc, Dr. Dan Stevens for always helping me in the lab and guiding me intellectually. I would be remiss if I did not acknowledge, an extension of the Burstyn group family, Dr. Bob Kerby, my favorite *E. coli* whisper who taught me everything I know about protein expression and purification.

My deepest gratitude goes to my family and my friends, particularly my parents. I will be forever indebted to my parents for their constant love and support. I am truly blessed my parents financed my many, many, many years education and encouraged to me set my goals

high. I am sure I will never fully know the sacrifices my parents made enabling me to be where I am today. I hope one day I can provide financially and intellectually for my children in the same manner my parents have provided for me. Mary and Rob Freeman, mom and dad, thank you. Much thanks to my number one fan, my grandfather, Thomas Reagan, for keeping me grounded reminding me that it is the people in our lives that make life. Papa, your carefree, silly nature always lightened the mood and kept a smile on my face, thank you. Thank you to my best friend, Laura Fuhrman. She has been my go-to-girl for many years. Even though Laura claims chemistry is foreign to her, she has always been there to listen through the good times and the bad times. Laura, thank you for your constant support and friendship, keeping me grounded.

Last but not least, thank you to my amazing husband, Eirik Paulsen, for graciously sharing me with graduate school these past few years. He has been a constant source of support, understanding and help. Eirik has brought me much joy and laughter through these daunting past few years of graduate school. Without his love and support… Thank you, Eirik, I love you.

Table of Contents

List of Tables

Chapter 2

Chapter 4

Chapter 5

List of Figures

Chapter 1

Chapter 2

List of Abbreviations

A

αS, alpha-synuclein, major constituent of Lewy bodies in Parkinson's dieseas

Aβ, amyloid beta peptide, the main component of deposits in brains of Alzheimer's patients

ABCB6, ATP-binding cassette protein family responsible for heme intermediate transport across mitochondrial outer membrane prior to iron insertion

AD, Alzheimer's disease

AdoMet, *S*-adenosyl-L-methionine

ALA, 5-amino-levulinic acid or δ-amino-levulinic acid

ALAS, amino-levulinic acid synthase

ALS, amyotrophic lateral sclerosis

APP, amyloid precursor protein, proteolysis generates Aβ

ATP7A, ATPase Cu^{+} transporting alpha protein, associated with Menkes disease

ATP7B, ATPase Cu^{+} transporting beta protein, associated with Wilson's disease

Atox1, antioxidant protein 1 copper chaperone for ATPases in secretory pathway

*Ax*PDEA1, *Acetobacter xylinum* phosphodiesterase A1, a heme-containing oxygen sensor

B

BCA, bicinchoninic acid

BMAL1, brain and muscle Arnt-like protein-1, a transcription factor

BSA, bovine serum albumin

*Bx*RcoM-1, a CO-sensing heme-containing transcription factor protein homolog from *Burkholderia xenovorans*

*Bx*RcoM-2, a CO-sensing heme-containing transcription factor protein homolog from *Burkholderia xenovorans*

C

cAMP, cyclic adenosine monophosphate

CBS, cystathionine β-synthase

CCO, cytochrome *c* oxidase

CCS, copper chaperone for superoxide dismutase

CD, circular dichroism spectroscopy

*Ch*CooA, a CooA homologue from the thermophilic bacterium *Carboxydothermus hydrogenoformans*

Ch LL-CooA, a CooA homologue from the thermophilic bacterium *Carboxydothermus hydrogenoformans* locked "on" due to Asn127L and Ser128L mutations

CHES, 2-(*N*-cyclohexylamino)ethanesulfonic acid

CJD, Creutzfeld-Jakob disease, a prion disease

CNS, central nervous system

CO, carbon monoxide

CoCBS, cobalt-substituted human CBS

CooA, a CO-sensing transcription regulator heme protein in *Rhodospirillum rubrum*

CoPPIX, cobalt PPIX

Cox17, cytochrome *c* oxidase copper chaperon

CR, Congo Red dye

CRP, cAMP receptor protein

Ctr1, high-affinity copper uptake protein 1 responsible for absorption of copper

$Cu([9]aneN_3)Cl_2$, 1,4,7-triazocyclononane copper(II) dichloride

D

DCT1, divalent cation transporter, another name for DMT1, Fe^{2+} transporter into intestine

DCYTB, duodenal cytochrome b, a ferrireductases responsible for reduction of iron (Fe^{3+} to Fe^{2+}) present in food before Fe^{2+} is absorbed into the intestine

DEAE, diethylaminoethanol

DHBA, dihydroxybenzoic acid

DHR51, *Drosophila melanogaster* hormone receptor 51

*Dm*CBS, *Drosophila melanogaster* CBS

DMT1, divalent metal transporter 1, transports Fe^{2+} into the intestine

DNR, *Pseudomonas aeruginosa* dissimilative nitrate respiration regulator

DOS, a heme-binding PAS protein, a direct oxygen sensor

DTT, dithiothreitol

E

E75, a heme-containing protein from *Drosophila melanogaster*

EA, electronic absorption

*Ec*Dos, heme-containing direct oxygen sensor in *Escherichia coli*

EDTA, ethylenediaminetetraacetic acid

eIF2α, heme-regulated eukaryotic initiation factor 2α kinase

EM, electron microscopy

EPPS, 3-[4-(2-hydroxyethyl)-1-piperazinyl]propanesulfonic acid

EPR, electronic paramagnetic resonance

F

FBXL5, F-box and leucine-rich repeat protein 5

FECH, ferrochelatase, mitochondrial enzyme responsible for iron insertion into PPIX

FePPIX, iron PPIX (heme)

FixL, an O_2-sensing heme protein that regulates gene expression associated with N_2 fixation

FLAG, polypeptide protein tag of sequence DYKDDDDK

FPN1, ferroportin, cellular iron exporter

Fre, metalloreducatse

FT, Fourier transform

Ftmt, mitoferritin, mitochondrial-specific iron storage protein

G

GAPDH, glyceraldehyde-3-phosphate dehydrogenase

GdnHCl, guanidine hydrochloride

GLRX5, glutaredoxin 5 protein associated with anemia

GST, glutathione S-transferase

H

HBD, heme-binding domain

hCBS, human cystathionine β-synthase

H/D, hydrogen/deuterium

HemAT, heme-based aerotactic transducer (oxygen sensor) from *Bacillus subtilis*

HEPES, 4-(2-hydroxylethyl)-1-piperazineethanesulfonic acid

HFE, hemochromatosis protein functions to regulate iron absorption

HH, hemochromatosis an iron-overload disease

HIF, hypoxia-inducible factor

HO, heme oxygenase responsible catabolism of heme and release of iron

HRI, heme-regulated eukaryotic initiation factor 2α kinase

I

ICP-OES, inductively-coupled plasma optical-emission spectroscopy

IPTG, isopropyl β-D-1-thiogalactopyranoside

IRE, iron-response element

IRP, iron-regulatory protein

ISC, iron-sulfur cluster

IscU, iron-sulfur cluster assembly protein U

IT, ion trap

J

JAK, Janus kinase, tyrosine kinase transfers phosphate group from ATP to protein during phosphorylation

K

L

Lcn2, lipocalin 2, siderophore-like iron scavenger and/or carrier

LMCT, ligand-to-metal-charge-transfer transition

LytTR, a DNA-binding domain, potential winged helix-turn-helix domain of ~100 amino acids present in bacterial transcriptional regulators of the algR/argA/lytR family

M

MALDI, matrix-assisted laser desorption/ionization

MAO, monoamine oxidase

Mb, myoglobin

MCD, magnetic circular dichroism

MES, 2-(*N*-morpholino)ethanesulfonic acid

MnPPIX, manganese PPIX

MOPS, 3-(*N*-morpholino)propanesulfonic acid

MS, mass spectrometry

N

NH_4HCO_3, ammonium bicarbonate

Ni-NTA, nickel nitrilotriacetic acid

NO, nitric oxide

NPAS2, neuronal PAS domain protein 2, a heme CO-sensor eukaryotic transcriptional regulator

NRAMP2, natural resistance-associated macrophage protein 2, another name for DMT1, transporter of Fe^{2+} into intestine

NTBI, non-transferrin-bound iron, 'free' iron associated with reactive oxygen species formation via Fenton chemistry

O

P

PAS, a domain structure named for the proteins in which the motif was first identified: Period, aryl hydrocarbon receptor nuclear translocator (ARNT), Simple-minded proteins

PD, Parkinson's disease

PDB, protein databank, repository for 3-D structures of large biomolecules

PLP, pyridoxal-5'-phosphate

PPIX, protoporphyrin IX

PrP, prion protein

PrP^{Sc}, disease-causing scrapie isoform of prion protein, protease resistant

Q

R

ROS, reactive oxygen species

rR, resonance Raman

*Rr*CooA, a CO-sensing transcription factor in *Rhodospirillum rubrum*

S

sGC, soluble guanylyl cyclase, an NO-sensing heme protein that catalyzes the conversion of GTP to cGMP

SDS-PAGE, sodium dodecyl sulfate polyacrylamide gel electrophoresis

SOD, superoxide dismutase, provides protection against oxidative stress

SPROX, stability of proteins from rates of oxidation

STEAP3, six-transmembrane epithelial antigen of prostate-3, an endosomal iron reductase

SUPREX, stability of unpurified proteins from rates of H/D exchange

T

TACN, 1,4,7-triazocyclononane

TCA, tricholoracetic acid

TCEP, tris(2-carboxyethyl)phosphine

TEM, transmission electron microscopy

Tf, transferrin, transporter of Fe^{3+} to either the liver or bone marrow

TFA, trifluoroacetic acid

TfR, transferrin receptor

ThT, thioflavin T, a fluorescent dye sensitive to fibrils

TMAO, trimethylamine-N-oxide

Tris, tris(hydroxymethyl)aminomethane

U

UTR, untranslated regions

V

VHL, von Hippel-Lindau factor, ubiquitin ligase responsible for degradation of hypoxia-inducible transcription factors that control hepcidin expression

W

WT, wild-type

X

Y

yCBS, yeast cystathionine β-synthase

Z

Dedicated to my wonderfully supportive family and friends. Words cannot describe how much your love and support has meant these past few years, especially when times were tough or when I was feeling tired, you kept me going and grounded to what really matters in life – the people in our lives.

Chapter One

More Questions Than Answers: How Mammalian Cells Regulate the Redox Active Transition Metals Iron and Copper

Introduction

Metal ions have unique chemical properties that allow them to play diverse roles in the chemistry of life. Consequently, they are essential components of over one third of all proteins (*1*). Metal ions are essential for electron transport, enzymatic reactions, structural stability and are used as therapeutic agents. Two particularly intriguing and diverse metal ions in the chemistry of life are iron and copper. Both iron and copper are essential for eukaryotes, but they can also be toxic. The ease by which iron and copper can gain or lose electrons can result in the exchange of electrons with oxygen, resulting in the generation of superoxide anions and the hydroxyl radical through Fenton-like chemistry (see Scheme 1.1). These oxygen metabolites in turn readily attack and damage cellular macromolecules such as proteins, DNA and RNA. Thus, the acquisition, transport and storage of iron and copper poses challenges. Therefore, the regulation of accumulation and turnover of these metal ions is extremely important.

Importance of Iron in Physiology

Iron is a transition metal that lies in the *d*-block of the periodic table. Iron has the ability to cycle between multiple oxidation states with the most common species being oxidized Fe^{3+} and reduced Fe^{2+}. The redox potential of iron is greatly affected by the nature of attached ligands; depending on the ligand environment, iron's redox potential may span from +1000 to -550 mV (*2*). The broad redox range of iron is essential to mammalian metabolism, where iron serves as a cofactor for hemoproteins and non-heme iron-containing proteins, including many enzymes. Hemoproteins are involved in numerous biological functions such as oxygen binding and transport (hemoglobins), oxygen metabolism (catalases and peroxidases), and cellular

respiration and electron transport (cytochromes). Proteins containing non-heme iron are important for fundamental cellular processes such as DNA synthesis, cell proliferation and differentiation (ribonucleotide reductase), gene regulation, drug metabolism, and steroid synthesis (ferredoxin-1 transfers electrons from NADPH to P450) (*3*).

The multitude of functionalities for iron-containing proteins is due to the ease by which iron can gain or lose electrons. The oxidation state of iron is not only important for biological function but also dramatically affects the solubility of iron in water. In the earliest days of life on earth, there was little or no oxygen and, as a result, iron was most often found in the Fe^{2+} state. In the Fe^{2+} state iron is very soluble in water; thus in the early days of life on earth, iron was readily available. As life evolved, the levels of atmospheric oxygen increased resulting in iron preferring the Fe^{3+} state, which is very insoluble in water. As iron predominately existed in the Fe^{3+} state, acquiring iron became more difficult necessitating the need for specialized iron-acquisition machinery (*4*). Thus, the acquisition and transport of iron poses challenges and mammalian cells tightly regulate the cytosolic concentration of iron.

Intestinal Absorption of Iron

The absorption of dietary iron is highly regulated and involves transport across the apical membrane of absorptive intestinal cells where iron is bound by ferritin before export through ferroportin into the blood plasma (Figure 1.1). This transport requires enzymes that switch the oxidation state of iron. Iron present in food, particularly red meat, legumes and dairy products, primarily occurs as Fe^{3+} or heme. The absorption of iron involves reduction of Fe^{3+} to Fe^{2+} by ascorbate and/or ferrireductases, such as duodenal cytochrome *b* (DCYTB), coupled to transport of Fe^{2+} across the apical membrane by divalent metal transporter 1 (DMT1) (*5*), also

known as natural resistance-associated macrophage protein 2 (NRAMP2) or divalent cation transporter (DCT1) (*6-8*). The mechanism of heme absorption remains poorly understood and may involve either direct transport of heme or receptor-mediated endocytosis (*9*). Once heme is absorbed, heme oxygenase-1 and -2 (HO-1 and HO-2, respectively) catabolize heme in macrophages and enterocytes, which yields bioavailable iron (*10*).

Iron absorbed by DMT1 enters the cytosol of the absorptive intestinal cell where iron can be either stored in the cytosolic iron-storage molecule ferritin or exported into plasma by the iron exporter ferroportin. Ferroportin, the only known cellular iron exporter, is found embedded in the cell envelope of all cell types involved in iron export, including duodenal mucosa, macrophages and cells of the placenta (*11-13*). The export of iron by ferroportin is coupled to the reoxidation of Fe^{2+} to Fe^{3+}. This process is mediated by the circulating ferroxidase hephaestin, or its homologue ceruloplasmin, both of which are copper-containing enzymes (*14, 15*). In an antagonistic manner, copper deficiency limits the incorporation of copper into ceruloplasmin, therefore rendering ceruloplasmin unable to convert Fe^{2+} to Fe^{3+}. Humans with mutations in ceruloplasmin exhibit iron overload; the most striking phenotype is seen in the brain where iron overload leads to progressive neurological failings (*16*). In the absence of a functional ferroxidase, Fe^{2+} cannot be exported through ferroportin and accumulates in the cytosolic iron-storage molecule ferritin, resulting in iron overload. In cases of iron overload, the serum ferritin level is extremely high at ~1000 ng/mL; the normal range for males is 12 – 300 ng/mL and for women is 12 – 150 ng/mL (*17*).

Delivery of Iron to Tissues

Transferrin.

Iron that is exported from cells into the plasma by ferroportin is bound to transferrin, an 80 kDa glycoprotein with homologous N-terminal and C-terminal iron-binding domains. Transferrin is widely distributed and is synthesized in the liver, retina, testis and brain. Transferrin can bind two atoms of Fe^{3+} with a dissociation constant (K_d) of 10^{-23} M at neutral pH. An anion, usually carbonate, is required to complete the coordination sphere of iron and stabilize Fe^{3+} binding to transferrin (*18*).

Under normal physiological conditions, only ~20-30% of circulating transferrin contains iron. The high iron-binding affinity of transferrin and the presence of a high concentration of apotransferrin (iron-free transferrin) allows an efficient buffering of increased plasma free-iron levels, preventing the buildup of non-transferrin-bound iron (NTBI). In iron overload states, transferrin gradually becomes fully saturated with iron and loses buffering capacity. When transferrin's buffering capacity is compromised NTBI can promote oxidative damage when taken up by tissue parenchymal cells (i.e., heart, liver, brain cells) (*19*).

The transferrin-Fe^{3+} complex in the plasma is transported into cells via one of two cell-surface transferrin receptors, TfR1 or TfR2. TfR1 is expressed on all dividing cells and is particularly enriched on precursors of red blood cells because these cells have the highest demand for iron. Erythrocytes in all species are terminally differentiated cells with a finite lifespan (~120 days for humans). At the end of their lifespan erythrocytes are ingested by macrophages and degraded in lysosomes where HO catabolizes heme, thereby releasing iron into the macrophage cytosol, where the released iron can be stored in ferritin or exported by ferroportin (*20*).

The role of transferrin receptor-1 (TfR1).

TfR1 is a homodimer of two identical transmembrane subunits linked by disulfide bonds (*20*). Each subunit consists of a large extracellular C-terminal domain, a hydrophobic membrane-spanning domain and a small cytoplasmic N-terminal domain. The extracellular domain binds one molecule of transferrin per subunit, forming the multimeric transferrin-TfR1 complex depicted in Figure 1.2 (*21*).

The transferrin-TfR1 complex is the main vehicle by which the transfer of transferrin-bound iron from plasma to cells of peripheral tissues is mediated. After binding the cell surface receptor, the complex of Fe^{3+}-transferrin-TfR1 is rapidly internalized by receptor-mediated endocytosis through clathrin protein-coated pits. Inside the cells, the internalized complex localizes to an endosome that is acidified by an ATP-dependent proton pump lowering the pH to ~5.5. Acidification produces a conformational change in both transferrin-Fe^{3+} and TfR1 with the concomitant release of iron (*22, 23*). At acidic pH, apotransferrin remains bound to TfR1 and the complex is recycled to the cell surface. At the more neutral plasma pH, apotransferrin dissociates from TfR1 and is free to bind iron and initiate additional rounds of receptor-mediated endocytosis (*24, 25*). The released Fe^{3+} is reduced to Fe^{2+} by six-transmembrane epithelial antigen of prostate-3 (STEAP3) (*26*). Fe^{2+} is transported across the endosomal membrane into the cytosol by DMT1 in most cells, or by its homologue NRAMP1 in macrophages (*8, 27, 28*). Newly assimilated cytosolic iron is transported to intracellular sites for either local use or for storage in ferritin (see Figure 1.2 for schematic representation).

Iron storage.

Cellular iron in excess of metabolic needs is stored in ferritin as iron oxide. Ferritin is a multimer of 24 subunits comprised of H (for heavy or heart) and L (for light or liver) protein subunits (*29*). In humans, the H subunit is 21 kDa and the L subunit is 19 kDa. Ferritin is an evolutionarily conserved, ubiquitous protein that can accommodate up to 4500 iron atoms within its inner shell (*30*).

Channels within the ferritin shell may facilitate the entry and exit of iron. The ferroxidase activity of H-ferritin converts Fe^{2+} to Fe^{3+}, which is necessary for the deposition of iron into the nanocage. L-ferritin induces iron nucleation and increases the rate of turnover of the ferroxidase activity. The mechanism by which iron is delivered to ferritin remains elusive. The levels of serum ferritin increase in response to the body's iron load or infection (*31*). Ferritin secretion may provide a mechanism for limiting iron storage after a shift from high to low iron concentrations (*32*).

Mitochondrial Handling of Iron

Mitochondria are the cell's powerhouse, and iron influences many aspects of mitochondrial metabolism. Imported iron is utilized for the biosynthesis of heme and iron-sulfur clusters (ISCs), and excess iron is stored in the mitochondria-specific storage protein mitoferritin (Ftmt).

Heme Synthesis.

Heme synthesis begins and ends in mitochondria, but intermediate steps occur in the cytoplasm (*33*). The first step is the condensation of succinyl coenzyme A and glycine in the

mitochondrial matrix to form 5-amino-levulinic acid (ALA), which is catalyzed by erythroid-specific ALA synthase 2 (ALAS2) or housekeeping ALAS1 in nonerythroid cells (*34*). ALA is then exported across mitochondrial membranes into the cytosol. The transporters or receptors that mediate ALA mitochondrial transit are not known. Subsequently, in a series of reactions in the cytosol, ALA is converted to coproporphyrinogen. ABCB6, a member of the ATP-binding cassette (ABC) family, transports coproporphyrinogen, a heme precursor, across the mitochondrial outer membrane for iron insertion (*35*). The final step in a series of reactions carried out in the mitochondria is insertion of iron into protoporphyrin, catalyzed by mitochondrial ferrochelatase (Fech) (*33*) (see Figure 1.3).

Heme biosynthesis has been extensively studied, but the process by which heme is shuttled across mitochondrial membranes into the cytosol for association with globins and apo-cytochromes remains unknown. No specific transporters or receptors that facilitate mitochondrial export of heme have been described.

Biogenesis of iron-sulfur clusters (ISCs).

Mitochondrial iron is also utilized for the synthesis of iron-sulfur clusters (ISCs). These cofactors consist of iron cations, sulfide anions and thiolates of cysteine residues. In mammals, ISC assembly protein U (IscU) assembles the ISCs. Loading of iron onto IscU is likely mediated by mitochondrial frataxin (*36*). Although the majority of ISC biogenesis takes place inside mitochondria, ISCs may also be synthesized in the cytoplasm (*37*). While mediators of cytosolic ISC biogenesis are not well understood, the mitochondrial inner membrane protein, ABCB7, is important for the maturation of cytosolic ISCs (*38*). ABCB7 may traffic ISCs or ISC precursors across mitochondrial membranes to the cytoplasm (*39*).

Biological iron chelator lipocalin 24p3.

Mitochondria are central for the regulation of cellular iron metabolism, and the majority of iron imported into the cell is utilized within this organelle for the synthesis of heme and ISCs. As described above, very little is known about intracellular iron transport pathways that facilitate mitochondrial iron import. However, studies to identify the nature of molecules that chaperone iron and facilitate iron intracellular trafficking are underway. Initial studies indicate the existence of low-molecular weight iron-binding compounds or siderophore-like (from Greek, meaning "iron carriers") molecules capable of binding iron in mammalian cells (*40, 41*). Microorganisms use siderophores for scavenging and delivering iron.

Lipocalin 24p3, also known as lipocalin 2 (Lcn2) or siderocalin, is a member of the lipocalin family of proteins. This family includes more than 20 small, secreted proteins that transport and deliver small hydrophobic molecules such as lipids and steroids. The lipocalin family of proteins influence many cellular responses because they deliver their cargo to cell surface receptors (*42, 43*). Iron binding in lipocalin 24p3 is mediated by a cofactor, presumably 2,5-dihydroxybenzoic acid (DHBA) (*44*), similar to *E. coli* enterobactin siderophore that consists of three 2,3-DHBA and three serine molecules used for iron scavenging (*45*). Considering that mitochondria are evolutionary relics of aerobic bacteria, the presence of a phylogenetically conserved siderophore-like molecule whose structure and biogenesis are evolutionarily linked to archaea siderophores is unsurprising.

Regulation of Cellular Iron Homeostasis

Transcriptional and post-transcriptional mechanisms regulate iron acquisition and storage. The mechanism of post-transcriptional control of ferritin and TfR1 involves iron-

regulatory proteins (IRPs) (*46, 47*). When iron is limiting, IRPs bind iron-regulatory elements (IREs), which are evolutionarily conserved stem-loop structures of 25-30 nucleotides that are found in non-coding regions of mRNAs that encode proteins involved in iron metabolism. The binding of IRPs to IREs in the 5'-untranslated regions (UTRs) of mRNA blocks translation. Conversely, binding at the 3'-untranslated region stabilizes the mRNA and prevents degradation. TfR1 mRNA contains multiple IREs within their long 3' UTR, while the mRNAs encoding H- and L-ferritin contain a single IRE in their 5' UTRs (*48*).

In iron deficiency, IRPs bind with high affinity ($K_d \approx 10^{-12}$ M) to target IREs. Binding to the 3' UTR results in stabilization of TfR1 mRNA and binding to the 5' UTR causes steric inhibition of ferritin mRNA translation. Under these conditions, accumulation of TfR1 promotes the uptake of cellular iron from plasma Tf, while inhibition of ferritin biosynthesis prevents storage of iron, allowing metabolic utilization of iron. Conversely, in response to excess cellular iron, IRPs are inactivated, which leads to TfR1 mRNA degradation and ferritin mRNA translation. This process minimizes further internalization of iron via TfR1, and promotes the storage of excessive intracellular iron in ferritin (*49*) (see Figure 1.4).

Iron Response Proteins (IRPs).

Two IRP molecules, IRP1 and IRP2, have been identified. IRP1 and IRP2 are homologous to mitochondrial aconitase, which catalyzes the isomerization of citrate to isocitrate and uses an iron-sulfur cluster (ISC) in the active site of mitochondrial aconitase. Under increased iron levels, IRP1 assembles an ISC and functions as cytosolic aconitase. The ISC keeps IRP1 in a closed conformation, which prevents access of IREs. Iron deficiency

promotes loss of the ISC and a conformational change enabling IRE binding activity. Thus, IRP1 is regulated by an ISC switch (*31, 50*).

Regardless of IRP2's extensive homology with IRP1, IRP2 does not assemble an ISC and is regulated by a distinct mechanism. IRP2 remains stable in iron-starved or hypoxic cells and undergoes ubiquitination and proteasomal degradation in response to iron and oxygen. This mechanism involves FBXL5 (F-box and leucine-rich repeat protein 5), an E3 ubiquitin ligase that contains an N-terminal hemerythrin-like domain (*51, 52*). Iron deficiency and/or hypoxia leads to disassembly of the diiron unit in the hemerythrin-like domain, which destabilizes FBXL5 and allows proteasome-mediated degradation of FBXL5, inversely promoting accumulation of IRP2. The IRE-IRP system is a highly integrated system used by mammals to maintain iron homeostasis.

Hormonal Regulation of Bioavailable Iron by Hepcidin

Iron entry into plasma either from intestinal absorption or from macrophage iron recycling is regulated in response to various physiological inputs. For example, in the gut, iron absorption is tuned based on iron need and availability, and is increased in response to ineffective erythropoiesis or hypoxia (*53*). In response to inflammation, iron export to plasma is decreased. The trafficking of iron into plasma is largely controlled by the iron-regulatory hormone hepcidin. This liver-derived peptide binds to ferroportin on the plasma membrane of enterocytes, macrophages, hepatocytes, and other cells, promoting its JAK-dependent phosphorylation and internalization that leads to lysosomal degradation of ferroportin (*54*). Ferroportin is the only known exporter of iron in mammalian cells. Consequently, inactivation of ferroportin causes intracellular iron retention (*55, 56*). Hepcidin has also been shown to

promote proteasomal degradation of DMT1 (responsible for iron uptake/absorption) (*55*) (see Figure 1.5).

Hepcidin is generated in hepatocytes and other cell types, as a precursor propeptide of 84 amino acids (*57, 58*). Hepcidin negatively regulates iron transport into plasma by binding to ferroportin, causing ferroportin to be phosphorylated, internalized, ubiquitinylated, and degraded in lysosomes (*54, 59*). Removal of ferroportin from the cell surface prevents iron export, leading to increased levels of cytosolic iron, which is stored in ferritin. Iron export is reduced by the removal of cell-surface ferroportin, not the inhibition of iron-transport activity (*60*).

Hepcidin levels can also be negatively regulated. Hypoxic conditions decrease hepcidin expression, resulting in increased iron export into the plasma (*61*). Hypoxia is primarily sensed in vertebrates by the hypoxia-inducible factor (HIF) family of transcription factors. In the absence of oxygen or iron, HIF proteins are stabilized and are capable of regulating transcription. Under normal conditions, hydroxylation of HIF by an iron-containing prolyl hydroxylase results in HIF recognition by an ubiquitin ligase, von Hippel-Lindau (VHL) factor, which targets HIF for degradation. (*62*). The dominant factor that negatively regulates mammalian hepcidin expression is erythropoiesis. Defective erythropoiesis results in increased iron export from enterocytes regardless of the status of liver iron stores (*63*).

Disorders of Iron Metabolism: Overload and Deficiency

Iron-overload disorders.

Iron-overload results when the amount of absorbed plasma iron exceeds the binding capacity of transferrin (*64, 65*), and arises from the inability to down-regulate iron absorption

appropriately in response to increased iron stores. Hereditary hemochromatosis (HH) is a term describing iron-overload disease that occurs as a result of genetic dysregulation of iron acquisition. Presently, HH has been associated with defects in four genes; three are recessively inherited disorders and a fourth shows dominant inheritance. All three recessive disorders result from inadequate hepcidin production relative to body iron stores (*57*). Based on current understanding, the molecular pathogensis of hemochromatosis can be divided into three classes. First, mutations in the hepcidin gene itself cause hemochromatosis by preventing the production of functional hepcidin protein (*66*). Second, mutations in the genes encoding human hemochromatosis protein (HFE), TfR2, and hemojuvelin inactivate signaling pathways that normally up-regulate hepcidin expression. Finally, mutations in the gene encoding ferroportin can cause hemochromatosis by rendering the transporter unresponsive to hepcidin regulation (*60, 67*).

Iron-deficiency disorders.

Iron deficiency anemia continues to be a major public health problem worldwide, with an estimated 2 billion people (30% of the world's population) affected. The vast majority of cases of iron deficiency are acquired, resulting from blood loss (e.g., from intestinal parasitosis), from insufficient dietary iron intake, or both (*68*). In addition, rare genetic defects can also cause iron deficiency anemia. Mutations in the genes encoding DMT1 (SLC11A2) and glutaredoxin 5 (GLRX5) are associated with autosomal recessive anemia (*69, 70*). Another anemia, hypotransferrinemia is deficiency of serum transferrin, due to mutations in the TF gene (*71*) which interrupt iron delivery to erythroid precursors, triggering a massive but futile increase in intestinal iron absorption and consequent tissue iron deposition. Deficiency of

another major plasma protein, ceruloplasmin, also causes mild iron deficiency anemia resulting in iron accumulation in the liver and brain (*72*); in this case, iron deficiency stems from a lack of ferroxidase activity needed to mobilize iron from storage. A final type of anemia, termed "anemia of chronic disease," is an acquired disorder of iron homeostasis. A common explanation for this type of anemia in chronically ill patients is associated with proinflammatory cytokines (*73*). Hepcidin secretion is increased in response to inflammatory cytokines, inducing internalization of ferroportin and preventing the export of iron from cellular iron stores, and thereby lowering the amount of bioavailable iron.

Iron Regulation Conclusions

Mammalian cells have evolved sophisticated mechanisms for coping with the challenges of iron acquisition and handling, and remarkable progress has been made in understanding the biochemical processes that regulate mammalian iron metabolism. Mammals primarily control dietary iron absorption and bioavailable iron trafficking via hepcidin, a hormonal peptide that responds to physiological stimuli. Cellular iron uptake, storage, and utilization are regulated by the IRE-IRP system, and fine-tuning is achieved by further regulatory pathways, which operate at the systemic and cellular levels. Yet, while the basic mechanisms for mammalian iron homeostasis are fairly well understood, several key issues remain unanswered: 1) How is iron sensed by hepcidin and the IRE-IRP pathways? 2) What is the iron trafficking network inside cells? and 3) What is the significance of the mammalian siderophore 24p3? Future studies on mammalian iron homeostasis will undoubtedly focus on at least these areas.

Physiological Importance of Copper

Copper, another transition metal that lies in the *d*-block of the periodic table, is a micronutrient that plays essential roles in human physiology due to copper's redox-active properties. The physiologically relevant oxidation states of copper are the oxidized Cu^{2+} state and the reduced Cu^{+} state. The coordination chemistry of copper is dependent upon oxidation state, with Cu^{2+} preferring nitrogen donors such as histidine or oxygen donors such as glutamate or aspartate, whereas Cu^{+} prefers sulfur donor ligands, such as cysteine or methionine (*74, 75*). The variability of oxidation states and ligand environments allows copper to serve as a catalytic and structural cofactor for enzymes that function in a variety of processes such as energy generation, iron acquisition, oxygen transport, cellular metabolism, peptide hormone maturation, blood clotting, and even signal transduction. However, similar to iron, the process of shuttling between the Cu^{2+} and Cu^{+} oxidation states may generate hydroxyl radicals through adventitious Fenton-like chemistry (Scheme 1.1). Hydroxyl radicals can damage proteins, nucleic acids, and lipids (*76*). Therefore, elaborate mechanisms are used to tightly regulate acquisition and distribution of copper, providing cells protection against copper toxicity.

Copper Entry into Cells

Absorption of copper.

Dietary copper is acquired via the small intestine through a process that is not fully understood. One mode for specific copper import into eukaryotic cells is through the high-affinity copper uptake protein 1 (Ctr1), an integral membrane protein that is structurally and functionally conserved from yeast to humans (*77-79*). A single Ctr1 polypeptide harbors three

transmembrane domains, a methionine-rich N terminus, a cysteine-histidine cluster in the C terminus, and a MX_3M motif in the second transmembrane domain. This MX_3M motif is essential for copper uptake (*80*) (Figure 1.6). There is substantial evidence that Ctr1 is highly specific for Cu^+ based on studies of yeast Ctr1 that have shown a requirement of a cell surface Cu^{2+}/Fe^{3+} metalloreductase, Fre1 and Fre2, for maximal activity (*81*). The Fre1 and Fre2 proteins are analogous to mammalian STEAP proteins. STEAP proteins are localized to both the plasma membrane and intracellular membranes suggesting the possibility that human Ctr1 might function in concert with a metalloreductase for Cu^+ movement across membranes (*26*). How Cu^+ is maintained in its reduced state in the presence of oxygen before uptake by Ctr1 is not currently understood.

Perhaps Ctr1 might function in Cu^+ transport both at the plasma membrane and on intracellular vesicles, considering that Ctr1 is found predominantly on the plasma membrane or intracellular vesicles in different cells and tissues (*82, 83*). A similar mode of action has been proposed for the Fe^{2+}-transporting DMT1 protein (*84*). Ctr1 may both deliver Cu^+ across the plasma membrane and mobilize Cu^+ out of the endosomal compartments into the cytosol, where Cu^+ may be made available to cytosolic copper transporters.

Copper Chaperones

Relatively little is known about how eukaryotic cells store and mobilize copper. The current model for copper homeostasis suggests that upon entry into the cell through Ctr1, copper binds to one of three specialized cytosolic copper chaperones: CCS (copper chaperone for superoxide dismutase), Atox1 (antioxidant protein 1) or Cox17 (cytochrome *c* oxidase copper chaperone); these chaperones then transfer copper to the specific cellular destinations.

CCS activates cytosolic Cu/Zn-dependent superoxide dismutase (SOD1) by direct insertion of the copper cofactor. Atox1 transfers copper to the copper-transporting ATPases in the secretory pathway. And Cox17 initiates a series of transfer reactions that result in copper delivery to cytochrome *c* oxidase (CCO) in the mitochondria (*85*) (see Figure 1.7).

Controlling cytosolic copper.

When Cu/Zn superoxide dismutase (Cu/Zn SOD1) is lacking copper the enzyme is catalytically inactive for superoxide disproportionation, and thus organisms lacking either Ctr1 or SOD1 lack protection from oxidative stress (*86, 87*). Copper delivery to Cu/Zn SOD1 requires CCS docking with either the apo or zinc-loaded monomer of SOD. In an oxygen-dependent mechanism accompanied by Cu/Zn SOD intramolecular disulfide bond formation, and a series of ligand exchange reactions between CCS and Cu/Zn SOD, copper is transferred from CCS to four histidine ligands of Cu/Zn SOD, with water as the fifth ligand bound to Cu^{2+} in square pyramidal coordination geometry (*88, 89*) (see Figure 1.8). Both CCS and Cu/Zn SOD are localized in the mitochondrial intermembrane space as well as in the cytoplasm, where active Cu/Zn SOD protects cells from the significant quantities of superoxide given off from the incomplete reduction of oxygen during mitochondrial electron transport (*90-92*).

Copper delivery to secretory compartments.

The Atox1 copper chaperone binds a relatively solvent-exposed Cu^{+} atom for delivery to the secretory compartment (*93, 94*). The Cu^{+} ion is transferred from the surface of Atox1 to a metal binding domain in the N-termini of the Cu^{+}-transporting ATPases of ATP7A and ATP7B; these domains contain repeat the consensus sequence of GMTCXXC, and the copper

ion is bound via the electron-rich cysteine ligands (*95, 96*). Transfer of copper to the ATPase occurs via a series of interprotein ligand-exchange reactions. ATP hydrolysis couples the movement of Cu^+ across the transmembrane helices in both ATP7A and ATP7B, ultimately leading to efflux across the basolateral membrane of intestinal epithelial cells for bile excretion (ATP7A) or out of hepatocytes (ATP7B) (*97*). Currently unknown are the mechanisms by which Cu^+ is transferred from the N-terminal Cu^+-binding domain of the ATPases to the transmembrane domain for transfer across the membrane. However, the current consensus in the field is that the N-termini simply "sense" the presence of Cu^+ but that these copper atoms are not actually the ones pumped across the membrane. According to this theory, Atox1 then brings more Cu^+ to the enzyme that is now "primed" for pumping copper across the membrane.

Copper delivery to mitochondria.

Mitochondria may serve as organelles of copper storage. Recently, the steady state copper levels in the mitochondrial matrix were found to be nearly an order of magnitude above that predicted to be required for the activation of the abundant mitochondrial Cu-dependent enzyme cytochrome *c* oxidase (CCO) (*98*). The Cu^+ chaperone, Cox17, originally identified in yeast as required for cytochrome oxidase assembly (*99*), is a small cysteine-rich protein that has been reported to coordinate between one and four Cu^+ atoms (*100, 101*). The proposed mechanism of copper delivery to CCO requires the Cu_B site of the Cox1 subunit to be inserted by the sequential transfer of copper from Cox17 to the integral membrane protein Cox11 that facilitates copper insertion into Cox1. The Cu_A site on the Cox2 subunit is filled via a Cox17 transfer to Sco1 (*102*) (see Figure 1.8 and Figure 1.9). Exactly how copper is moved from the site of transport via Ctr1 to the mitochondrial intermembrane space is not well understood.

Regulation of Copper Transport

Human copper transporters change their cellular location in response to various stimuli (*103-105*). The trafficking to/from specific compartments represents an important mechanism through which mammalian cells allocate copper and modulate intracellular copper levels. When copper levels are diminished, Cu-specific ATPases are found in the Golgi network (protein packaging machinery). Increased copper levels allow Cu-specific ATPases to relocate to endosomes (*105*) where they are thought to sequester copper in the vesicles. These vesicles then fuse with the plasma membrane and copper is released to the extracellular medium. Interestingly, copper, unlike iron, can be eliminated in bile. Only a small fraction of the total Cu-specific ATPases are found at the plasma membrane (*106*), likely due to rapid endocytosis (*107*). Recycling of these Cu-specific ATPases may provide a mechanism for acute regulatory response to changes in copper levels.

Disorders of Copper Homeostasis

Defects in copper homeostasis are directly responsible for human diseases and are implicated in additional pathophysiologies. For example, mutations in *ATP7A* or *ATP7B* genes, encoding Cu^{+}-transporting ATPase pumps, cause Menkes and Wilson's diseases, respectively. Menkes disease (ATP7A) is an X-linked lethal disorder. The clinical hallmarks of the disease are intestinal copper hyperaccumulation causing severe copper deficiency in peripheral tissues with subsequent deficits in Cu-dependent enzymes (*108*). Mutations in ATP7B leads to Wilson's disease, an autosomal recessive disease characterized by hepatic and neuronal copper overload, hepatotoxicity, neuropsychological and other defects. Wilson's disease can be managed with therapies to enhance copper excretion or reduce copper absorption (*108*).

Dysregulation of copper is also responsible for a familial form of amyotrophic lateral sclerosis (ALS) characterized by metal-free mutant forms of Cu/Zn SOD prone to unfolding and aggregation. The aggregation of the SOD protein is not believed to be toxic in ALS cases; rather, the lack of superoxide scavenging activity is believed to exert toxicity leading to motor neuron death. (*109*).

In addition to these genetically determined diseases of copper dysregulation, alterations in copper homeostasis have been linked to changes in senile plaque deposition in Alzheimer's disease (*110, 111*). Copper binding to α-synuclein has also been linked to the aggregation of this protein, which is strongly correlated with instances of Parkinson's disease (*112, 113*). Furthermore, N-terminal octapeptide repeats in the prion protein (PrP) have been demonstrated to serve as high-affinity Cu^{2+} binding sites that inhibit conversion to fibrils associated with prion disease (*114-117*). There is considerable investigation into whether transition-metal dysregulation is a cause or a consequence of these neurodegenerative diseases.

Copper Regulation Conclusions

The fundamental components that mediate copper acquisition and distribution have been recently identified. However, many questions remain to be answered with respect to mammalian copper homeostasis; specifically: 1) How do copper chaperones bind Cu^{+}, and is this process prioritized depending on the needs of cells? 2) How is the import of copper tuned with subsequent mobilization from intracellular stores? 3) What is the chemical nature of copper ligands that shuttle copper around cells and throughout the bloodstream or across the blood brain barrier? There are more questions than answers with respect to copper homeostasis.

Further investigation of the fundamental biochemistry, genetics, cell biology, physiology and chemistry of copper will be critical to answering these and other questions that will emerge.

Iron and Copper in Neurodegenerative Diseases

Introduction.

The brain is the command center for cognitive and motor function; therefore, it may not be surprising that the brain demands the highest concentrations of metal ions in the body (*118, 119*) and has the highest consumption of oxygen in the body on a per-weight basis (*120*). For example, in humans, the brain constitutes only 2% of total body mass but consumes 20% of the oxygen that is taken in through respiration (*120*). Due to the high oxygen demand and cellular complexity, relatively high metal levels pervade all regions of the brain and central nervous system. The *d*-block metals are significant components in both neurophysiology and neuropathology, particularly with respect to aging and neurodegenerative diseases. Abnormal accumulations of metals such as iron, copper and zinc have been reported in neurological pathologies, most notably, Alzheimer's (AD), Parkinson's (PD) and prion diseases. These metal ions play very important roles in neurodegeneration and have an impact on both protein structure (folding/misfolding) and oxidative stress (generation of reactive oxygen species (ROS) by iron and copper). Yet, metal ions are required to sustain a large number of cellular functions, including neuronal processes. For example, in the central nervous system iron, copper and zinc are required for many enzymatic activities, mitochondrial function, neurotransmission, in addition to learning and memory (*121*). In order to maintain metal ion homeostasis, cells employ sophisticated machinery whose failure might lead to disease states including neurodegenerative disorders. Metal binding affects the aggregation process of

amyloid β (Aβ) and α-synuclein (αS) in AD and PD, respectively. In both AD and PD, copper and iron are associated with ROS generation via Fenton-like reactions that form the highly reactive hydroxyl radical (*122-126*) (refer to Scheme 1.1).

Iron.

Iron is essential for normal neurological function due to the role of iron both in oxidative metabolism and as a cofactor in the synthesis of neurotransmitters and myelin. The high requirement for iron in the brain is consistent with the massive energy needs of the brain; there is a considerable demand for ATP to maintain membrane ionic gradients, synaptic transmission and axon transport (*127*). Iron is an essential component of cytochromes, cytochrome oxidase and iron-sulfur clusters in the oxidative metabolism pathway producing ATP. The synthesis of neurotransmitters requires enzymes where iron is a cofactor, specifically, tyrosine hydroxylase (conversion of Tyr to L-DOPA) and tryptophan hydroxylase (involved in synthesis of serotonin) (*127*). In addition, iron-dependent enzymes include ribonucleoside reductase, the rate-limiting enzyme of DNA synthesis, and succinate dehydrogenase and aconitase of the Krebs cycle. Finally, iron is essential for the biosynthesis of lipids and cholesterol, important substrates in the synthesis of myelin, essential to propagating impulses in the nervous system (*128*).

How the brain regulates fluxes and storage of iron in neurons, astrocytes and glial cells is still unclear (*129*). Generally, the brain regions responsible for motor functions have more iron than non-motor related regions; unsurprisingly, movement disorders are often associated with iron loading. Interestingly, as an individual ages, iron concentration in the brain is observed to increase (*130*). Transferrin receptors seem to control iron uptake in the gray matter,

whereas, ferritin receptors seem to control iron uptake in the white matter. In AD and PD, iron levels are higher than expected due to normal aging, but the mechanisms associated with such accumulation are still elusive (*131*). In addition, altered metal transport in the brain has been proposed to result in unutilized iron in the intracellular space where the metal exists as a labile iron pool (LIP) of Fe^{2+} and Fe^{3+}. Because iron is a redox active metal and may participate in Fenton-like chemistry, iron may adventitiously react with hydrogen peroxide, generated for instance by monoamine oxidase (MAO) during dopamine metabolism, initiating hydroxyl radical generation. These hydroxyl radicals may initiate a cascade of deleterious reactions leading to neurological oxidative stress and tissue degradation (*132*).

Oxidative stress is associated with the progression of PD, a severe, progressive motor disorder caused by changes in the CNS that are associated with degeneration of dopaminergic neurons. Inherited forms of PD are linked to mutations in genes encoding α-synuclein, the key Parkinson's disease protein. The hallmark of this disease is the presence of the Lewy bodies that house fibrous α-synuclein deposits (*133*). No consensus has been reached for the role of α-synuclein, and the mechanism initiating conversion of α-synuclein to species tending to aggregate remains a puzzle. The most likely factors involved in aggregation are interactions with transition metal ions (*134*). Altered metal homeostasis has been reported in patients afflicted with PD, as are reduced expression levels of ferritin. In theory, the reduced expression of ferritin compromises the ability of neurons to sequester iron and results in elevated levels of labile, redox active iron (*135*). Elevated iron levels may contribute to oxidative stress and deposition of intracellular inclusion bodies, facilitating the progression of PD pathology.

Copper.

Copper is required for cellular respiration, peptide amidation, neurotransmitter biosynthesis, pigment formation and connective tissue strength. The central nervous system is dependent on copper as a cofactor for numerous enzymes (*108*). Again, owing to the oxidative metabolism and large oxygen capacity of brain tissues, neurons and glia alike require copper for the basic respiratory and antioxidant enzymes cytochrome *c* oxidase and Cu/Zn superoxide dismutase, respectively (*136*). In addition, copper is a necessary cofactor for many brain-specific enzymes that control homeostasis of neurotransmitters and neuropeptides. Included are dopamine-β-hydroxylase (converts dopamine to norepinephrine), peptidylglycine α-amidating mono-oxygenase and tyrosinase (rate limiting for controlling production of melanin). There are other enzymes dependent on copper in the brain including, the ferroxidases ceruloplasmin and hephaestin responsible for the oxidation of Fe^{2+} to Fe^{3+} (*137*).

Understanding of copper transport within the CNS is incomplete, although the proteins involved in copper homeostasis in peripheral tissues have been shown to be present in the brain (*138, 139*). The distribution of copper within the CNS varies according to species. In humans, the highest copper concentration is in the hippocampus (*140*), an organ responsible for long- and short-term memory. As with iron, copper concentration increases with aging. Copper is also a redox-active metal that may participate in Fenton-like chemistry. In Alzheimer's-like dementia, copper content in the CNS is 2-fold higher than in age-matched controls (*141, 142*). The harmful side reactions that occur due to copper's redox activity, coupled with higher accumulations of copper in the CNS during aging, may contribute to neurodegenerative diseases.

Alzheimer's disease, the most common form of dementia, is characterized by the extracellular deposition of amyloid plaques and tau tangles. Amyloid plaques are formed by aggregated amyloid β peptide, which is generated upon cleavage from its parent integral membrane precursor protein (APP). Tau tangles are formed by hyperphosphorylation of tau proteins (*143*). Although the function of APP is unknown, there is recent evidence APP may play a role in maintaining copper homeostasis, possibly by employing its ferroxidase-like activity (*144-146*). The synapses of the hippocampus are the chief point of amyloid deposition (*147, 148*). Copper and iron are found at amyloid plaques in relatively high concentrations of 400 μM and 1 mM, respectively (*149*). The interplay of copper is not limited only to Aβ but extends through all the key Alzheimer's disease proteins. Initially, Cu^{+} binds the N-terminal extracellular domain of APP promoting its export out of neurons. The C-terminal domain of β-secretase, involved in APP processing, binds Cu^{+}, thereby allowing β-secretase to interact with the Cu chaperone, CCS1, which delivers Cu^{+} to Cu/Zn-SOD (*150*). The physiological implications of these metal–protein interactions remain unclear.

The implications of metal-protein interactions are also unclear in human prion diseases, a group of fatal neurodegenerative disorders that share a common pathogenic agent, the protease-resistant prion protein (PrP^{Sc}) (*151*). There are five known human prion diseases: Creutzfeld-Jakob disease (CJD), Gerstmann Straussler Scheinker disease, kuru, new variant CJD and fatal familial insomnia. Prion diseases are unusual because they can be transferred both between individuals and between species. These diseases are characterized by neural spongiosis and a deposition of amyloid-like plaques (*152*). It has been proposed that prions are self-propagating and replicate by fiber fragmentation that act as templates for monomer recruitment, thus generating (and propagating) amyloid-like plaques (*153*). Although the exact

mechanism by which the prion protein (PrP) causes neurodegeneration and cell death is unknown, the soluble form of the PrP is a known copper-binding protein (*115, 117*). The present understanding of prion diseases is that Cu^{2+} binding to PrP protects against aggregation. The Cu^{2+} ion is believed to interact with the disease-causing isoform of the prion protein (PrP^{Sc}). Not much is understood about the role of Cu^{2+} interacting with PrP^{Sc}, but ions of Cu^{2+} have been implicated in conversion of PrP to the protease-resistant species PrP^{Sc} (*154*).

Conclusions

The *d*-block metals, iron and copper, are major contributors to the complex chemistry and biology of the brain. Owing to the unique physiology, specialization, and complexity of brain tissues, iron and copper are required at unusually high levels compared with the rest of the body. The redox active capabilities of iron and copper are particularly important due to the tremendous oxygen consumption and oxidative capacity of the brain cell neurons and glia. Tightly bound forms of these metals are found as cofactors in essential metalloenzymes throughout the brain and central nervous system, and labile metal ion pools are present in all brain cells. Metals accumulate in the brain as a function of aging, and misregulation of brain metal-ion pools is linked with several neurodegenerative conditions, including Parkinson's and Alzheimer's diseases, where oxidative stress, protein misfolding and aggregation are hallmarks of their pathology. The understanding of the role of metal ions in the brain, including the mechanisms by which metal ions are tightly regulated, is an expanding area of research and, presently, there are more questions than answers.

References

1. Bertini, I., Gray, H. B., Lippard, S. J., and Valentine, J. S. (1994) *Bioinorganic Chemsitry*, University Science Books, Mill Valley, CA.
2. Nielands, J. B. (1995) Siderophores: structure and functions of microbial iron transport compounds. , *J. Biol. Chem. 27*, 26723-26726.
3. May, P. M., and Williams, D. R. (1980) *Iron in Biochemistry and Medicine*, Academic Press, New York
4. Verkhovtseva, Y. V., Filina, Y. Y., and Pukhov, D. W. (2001) Evolutionary Role of Iron in Metabolism of Prokaryotes and in Biogeochemical Processes, *J. Evol. Biochem. Phys+. 37*, 444-450.
5. McKie, A. T. (2008) The role of DcytB in ron metabolism: an update, *Biochem. Soc. Trans. 36*, 1239-1241.
6. Gunshin, H. (1997) Cloning and characterization of a mammalian proton-coupled metal-ion transporter, *Nature 388*, 482-488.
7. Fleming, M. D. (1997) Microcytic anaemia mice have a mutation in Nramp2, a candidate iron transporter gene, *Nature Genet. 16*, 383-386.
8. Fleming, M. D. (1998) Nramp2 is mutated in the anemic Belgrade (b) rat: evidence of a role for Nramp2 in endosomal iron transport, *Proc. Natl Acad. Sci. USA 95*, 1148-1153.
9. West, A. R., and Oates, P. S. (2008) Mechanisms of heme iron absorption: current questions and controversies, *World J. Gastroenterol. 14*, 4101-4110.
10. Ryter, S. W., Alam, J., and Choi, A. M. (2006) Heme oygenases-1/carbon monoxide: From basic science to therapeutic applications, *Physiol. Rev. 86*, 583-650.

11. Abboud, S., and Haile, D. J. (2000) A novel mammalian iron-regulated protein involved in intracellular iron metabolism, *J. Biol. Chem. 275*, 19906-19912.

12. Donovan, A. (2000) Positional cloning of zebrafish ferroportin1 identifies a conserved vertebrate iron exporter, *Nature 403*, 776-781.

13. McKie, A. T. (2000) A novel duodenal iron-regulated transporter, IREG1, implicated in the basolateral transfer of iron to the circulation, *Mol. Cell 5*, 299-309.

14. Osaki, S., Johnson, D. A., and Frieden, E. (1966) The possible significance of the ferrous oxidase activity of ceruloplasmin in normal human serum, *J. Biol. Chem. 241*, 2746-2751.

15. Roeser, H. P., Lee, G. R., Nacht, S., and Cartwright, G. E. (1970) The role of ceruloplasmin in iron metabolism, *J. Clin. Invest. 49*, 2408-2417.

16. Harris, Z. L., Klomp, L. W., and Gitlin, J. D. (1998) Aceruloplasminemia: an inherited neurodegenerative disease with impairment of iron homeostasis, *Am. J. Clin. Nutr. 67*, 972S-977S.

17. Hoffman, R., Benz Jr., R. J., and Shattil, S. J. (2005) *Hematology: Basic Principles and Practice*, 4th ed., Churchill Livingston, Philadelphia, PA.

18. Gkouvatsos, K., Papanikolaou, G., and Pantopoulos, K. (2012) Regulation of iron transport and the role of transferrin, *Biochim. Biophys. Acta 1820*, 188-202.

19. Brissot, P., Ropert, M., Le Lan, C., and Loreal, O. (2012) Non-transferrin bound iron: a key role in iron overload and iron toxicity, *Biochim. Biophys. Acta 1820*, 403-410.

20. Aisen, P. (2004) Transferrin receptor 1, *Int. J. Biochem. Cell Biol. 36*, 2137-2143.

21. Cheng, Y., Zak, O., Aisen, P., Harrison, S. C., and Walz, T. (2004) Structure of the human transferrin receptor-transferrin complex, *Cell 116*, 565-576.

22. Sipe, D. M., and Murphy, R. F. (1991) Binding to cellular receptors results in increased iron release from transferrin at mildly acidic pH, *J. Biol. Chem. 266*, 8002-8007.

23. Bali, P. K., Zak, O., and Aisen, P. (1991) A new role for the transferrin receptor in the release of iron from transferrin, *Biochemistry 30*, 324-328.

24. van Renswoude, J., Bridges, K. R., Harford, J. B., and Klausner, R. D. (1982) Receptor-mediated endocytosis of transferrin and the uptake of Fe in K562 cells: identification of a nonlysosomal acidic compartment, *Proc. Natl Acad. Sci. USA 79*, 6186-6190.

25. Dautry-Varsat, A., Ciechanover, A., and Lodish, H. F. (1983) pH and the recycling of transferrin during receptor-mediated endocytosis, *Proc. Natl Acad. Sci. USA 80*, 2258-2262.

26. Ohgami, R. S., Campagna, D. R., McDonald, A., and Fleming, M. D. (2006) The Steap proteins are metalloreductases, *Blood 108*, 1388-1394.

27. Fleming, M. D., Tremor, C. C., Su, M. A., Foernzler, D., Beier, D. R., Dietrich, W. F., and Andrews, N. C. (1997) Microcytic anaemia mice have a mutation in Nramp2, a candidate iron transporter gene, *Nat. Genet. 16*, 383-386.

28. Gunshin, H., Mackenzie, B., Berger, U. V., Gunshin, Y., Romero, M. F., Boron, W. F., Nussberger, S., Gollan, J. L., and Hediger, M. A. (1997) Cloning and characterization of mammalian proton-coupled metal-ion transporter, *Nature 388*, 482-488.

29. Theil, E. C. (2004) Iron, ferritin, and nutrition, *Annu. Rev. Nutr. 24*, 327-343.

30. De Domenico, I. (2006) Ferroportin-mediated mobilization of ferritin iron precedes ferritin degradation by the proteasome, *EMBO J. 25*, 5396-5404.

31. Wang, J., and Pantopoulos, K. (2011) Regulation of cellular iron metabolism *Biochem. J 434*, 365-381.

32. Arosio, P., Ingrassia, R., and Cavadini, P. (2006) Ferritins: A family of molecules for iron storage, antioxidation and more, *Biochim. Biophys. Acta 1790*, 589-599.

33. Ajioka, R. S., Phillips, J. D., and Kushner, J. P. (2006) *Biochim. Biophys. Acta 1763*, 723.

34. Sheftel, A. D., Richardson, D. R., Prchal, J., and Ponka, P. (2009) Mitochondrial iron metabolism and sideroblastic anemia, *Acta Hematol. 122*, 120-133.

35. Krishnamurthy, P. C., Du, G., Fukuda, Y., Sun, D., Sampath, J., Mercer, K. E., Wang, J., Sosa-Pineda, B., Murti, K. G., and Schuetz, J. D. (2006) Identification of a mammalian mitochondrial porphyrin transporter, *Nature 443*, 586-589.

36. Stemmler, T. L., Lesuisse, E., Pain, D., and Dancis, A. (2010) Frataxin and mitochondiral FeS cluster biogenesis, *J. Biol. Chem. 285*, 26737-26743.

37. Lill, R., and Muhlenhoff, U. (2008) Maturation of iron-sulfur proteins in eukaryotes: Mechanisms, connected process, and dieseases, *Annu. Rev. Biochem 77*, 669-700.

38. Pondarre, C., Antiochos, B. B., Campagna, D. R., Clarke, S. L., Greer, E. L., Deck, K. M., McDonald, A., Han, A. P., Medlock, A., Kutok, J. L., Anderson, S. M., Eisenstein, R. S., and Fleming, M. D. (2006) A mitochondrial ATP-binding cassette transporter Abcb7 is essential in mice and participates in cytosolic iron-sulfer cluster biogenesis, *Hum. Mol. Genet. 15*, 953-964.

39. Kispal, G., Csere, P., Prohl, C., and Lill, R. (1999) The mitochondrial proteins Atm1p and Nfs1p are essential for biogenesis of cytosolic Fe/S proteins, *EMBO J. 18*, 3981-3989.

40. Fernandez-Pol, J. A. (1977) Isolaiton and characterization of a siderophore-like growth factor from mutants of SV40-transformed cells adapted to picolinic acid, *Cell 14*, 489-499.

41. Jones, R., Peterson, C., Grady, R., and Cerami, A. (1980) Low molecular weight iron-binding factor from mammalian tissue that potentiates bacterial growth, *J. Exp. Med. 151*, 418-428.

42. Yang, J., Mori, K., Li, J. Y., and Barasch, J. (2003) Iron, lipocalin, and kidney epithelia, *Am. J. Physiol. 285*, F9-F18.

43. Richardson, D. R. (2005) 24p3 and its receptor: Dawn of a new iron age?, *Cell 123*, 1175-1177.

44. Devireddy, L. R., Hart, D. O., Goetz, D. H., and Green, M. R. (2010) A mammalian siderophore synthesized by an enzyme with a bacterial homolog involved in enterobactin production, *Cell 141*, 1006-1017.

45. Raymond, K. N., Dertz, E. A., and Kim, S. S. (2003) Enterobactin: An archetype for microbial iron transport, *Proc. Natl. Acad. Sci. U.S.A. 100*, 3584-3588.

46. Rouault, T. A. (2006) The role of iron regulatory proteins in mammalian iron homeostasis and disease, *Nature Chem. Biol. 2*, 406-414.

47. Galy, B., Ferring, D., Benesova, M., Benes, V., and Hentze, M. W. (2004) Targeted mutagenesis of the murine IRP1 and IRP2 genes reveals context-dependent RNA processing differences in vivo, *RNA 10*, 1019-1025.

48. Piccinelli, P., and Samuelsson, T. (2007) Evolution of the iron-responsive element, *RNA 13*, 952-966.

49. Arosio, P., and Levi, S. (2010) Cytosolic and mitochondrial ferritins in the regulation of cellular iron homeostasis and oxidative damage, *Biochim. Biophys. Acta 1800*, 783-792.

50. Hentze, M. W., Muckenthaler, M. U., Galy, B., and Camaschella, C. (2010) Two to tango: Regulation of mammalian iron metabolism, *Cell 142*, 24-38.

51. Vashisht, A. A., Zumbrennen, K. B., Huang, X., Powers, D. N., Durazo, A., Sun, D., Bhaskaran, N., Persson, A., Uhlen, M., Sangfelt, O., Spruck, C., Leibold, E. A., and Wohlschlegel, J. A. (2009) Control of iron homeostasis by an iron-regulated ubiquitin ligase, *Science 326*, 718-721.

52. Salahudeen, A. A., Thompson, J. W., Ruiz, J. C., Ma, H. W., Kinch, L. N., Li, Q., Grishin, N. V., and Bruick, R. K. (2009) An E3 ligase possesing an iron-responsive hemerythrin domain is a regulator of iron homeostasis, *Science 326*, 722-726.

53. Pak, M., Lopez, M. A., Gabayan, V., Ganz, T., and Rivera, S. (2006) Suppression of hepcidin during anemia requires erythropoietic activity, *Blood 108*, 3730-3735.

54. Nemeth, E. (2004) Hepcidin regulates cellular iron efflux by binding to ferroportin and inducing its internalization, *Science 306*, 2090-2093.

55. Brasse-Lagnel, C., Karim, Z., Letteron, P., Bekri, S., Bado, A., and Beaumont, C. (2011) Intestinal DMT1 cotransporter is down-regulated by hepcidin via proteasome internalization and degradation, *Gastroenterology 140*, 1261-1271 e1261.

56. Weiss, G. (2009) Iron metabolism in the anemia of chromic disease, *Biochim. Biophys. Acta 1790*, 682-693.

57. Ganz, T. (2011) Hepcidin and iron regulation, 10 years later, *Blood 117*, 4425-4433.

58. Peslova, G., Petrak, J., Kuzelova, K., Hrdy, I., Halada, P., Kuchel, P. W., Soe-Lin, S., Ponka, P., Sutak, R., Becker, E., Huang, M. L., Suryo Rahmanto, Y., Richardson, D. R.,

and Vyoral, D. (2009) Hepcidin, the hormone of iron metabolism, is bound specifically to alpha-2-macroglobulin in blood, *Blood 113*, 6225-6236.

59. De Domenico, I., Ward, D. M., Langelier, C., Vaughn, M. B., Nemeth, E., Sundquist, W. I., Ganz, T., Musci, G., and Kaplan, J. (2007) The molecular mechanism of hepcidin-mediated ferroportin down-regulation, *Mol. Biol. Cell 18*, 2569-2578.

60. De Domenico, I., Ward, D. M., Nemeth, E., Vaughn, M. B., Musci, G., Ganz, T., and Kaplan, J. (2005) The molecular basis of ferroportin-linked hemochromatosis, *Proc. Natl. Acad. Sci. U.S.A. 102*, 8955-8960.

61. Nicolas, G., Bennoun, M., Porteu, A., Mativet, S., Beaumont, C., Grandchamp, B., Sirito, M., Sawadogo, M., Kahn, A., and Vaulont, S. (2002) Severe iron deficiency anemia in transgenic mice expressing liver hepcidin, *Proc. Natl Acad. Sci. USA 99*, 4596-4601.

62. Kaelin, W. G. (2005) The von Hippel-Lindau protein, HIF hydroxylation, and oxygen sensing, *Biochem. Biophys. Res. Commun. 338*, 627-638.

63. Tanno, T., Bhanu, N. V., Oneal, P. A., Goh, S. H., Staker, P., Lee, Y. T., Moroney, J. W., Reed, C. H., Luban, N. L., Wang, R. H., Eling, T. E., Childs, R., Ganz, T., Leitman, S. F., Fucharoen, S., and Miller, J. L. (2007) High levels of GDF15 in thalassemia suppress expression of the iron regulatory protein hepcidin, *Nat. Med. 13*, 1096-1101.

64. Crosby, W. H. (1977) Hemochromatosis: the unsolved problems, *Semin. Hematol. 14*, 135-143.

65. Craven, C. M., Alexander, J., Eldridge, M., Kushner, J. P., Bernstein, S. E., and Kaplan, J. (1987) Tissue distribution and clearance kinetics of non-transferrin-bound iron in the

hypotransferrinemic mouse: a rodent model for hemochromatosis, *Proc. Natl Acad. Sci. USA 84*, 3457-3461.

66. Roetto, A., Papanikolaou, G., Politou, M., Alberti, F., Girelli, D., Christakis, J., Loukopoulos, D., and Camaschella, C. (2003) Mutant antimicrobial peptide hepcidin is associated with severe juvenile hemochromatosis, *Nature Genet. 33*, 21-22.

67. Schimanski, L. M., Drakesmith, H., Merryweather-Clarke, A. T., Edwards, J. P., Sweetland, E., Bastin, J. M., Cowley, D., Chinthammir, Y., Robson, K. J., and Townsend, A. R. (2005) In vitro functional analysis of human ferroportin (FPN) and hemochromatosis-associated FPN mutations, *Blood 105*, 4096-4102.

68. Carnicer, J., Badia, R., and Argemi, J. (1998) Helicobacter pylori gastritis and sideropenic refractory anemia, *J. Pediatr. Gastroenterol. Nutr. 25*, 441.

69. Mims, M. P., Guan, Y., Pospisilova, D., Priwitzerova, M., Indra, K., Ponka, P., Divoky, Y., and Prchal, J. T. (2005) Identification of human mutation of DMT1 in patient with microcytic anemia and iron overload, *Blood 105*, 1337-1342.

70. Priwitzerova, M., Nie, G., Sheftel, A. D., Pospisilova, D., Divoky, Y., and Ponka, P. (2005) Functional consequences of the human DMT1 (SLC11A2) mutation on protein expression and iron uptake, *Blood 106*, 3985-3987.

71. Trenor, C. C., Campagna, D. R., Sellers, V. M., Andrews, N. C., and Fleming, M. D. (2000) The molecular defect in hypotransferrinemic mice, *Blood 96*, 1113-1118.

72. Harris, Z. L., Durley, A. P., Man, T. K., and Gitlin, J. D. (1999) Targeted gene disruption reveals an essential role for ceruloplasmin in cellular iron efflux, *Proc. Natl Acad. Sci. USA 96*, 10812-10817.

73. Means, R. T. (1995) Pathogenesis of chronic disease: a cytokine-mediated anemia, *Stem Cells 13*, 32-37.

74. Linder, M. C., and Goode, C. A. (1991) *Biochemistry of Copper*, Springer-Verlag, New York, New York, USA.

75. Lippard, S. J., and Berg, J. M. (1994) *Principles of Bioinorganic Chemistry*, University Science Books, Mill Valley, California, USA.

76. Bertini, I., Gray, H. B., Stiefel, E., and Valentine, J. S. (2007) *Biological Inorganic Chemistry*, University Science Books, Sausalito, California, USA.

77. Nose, Y., Rees, E. M., and Thiele, D. J. (2006) Structure of the Ctr1 copper trans'PORE'ter reveals novel architecture, *Trends Biochem. Sci 31*, 604-607.

78. Puig, S., and Thiele, D. J. (2002) Molecular mechanisms of copper uptake and distribution, *Curr. Opin. Chem. Biol. 6*, 171-180.

79. Maryon, E., Molloy, S., Zimnicka, A., and Kaplan, J. (2007) Copper entry into human cells: progress and unanswered questions, *BioMetals 20*, 355-364.

80. Puig, S., Lee, J., Lau, M., and Thiele, D. J. (2002) Biochemical and genetic analyses of yeast and human high affinity copper transporters suggest a conserved mechanism for copper uptake, *J. Biol. Chem. 277*, 26021-26030.

81. Rees, E. M., and Thiele, D. J. (2007) Identification of a vacuole-associated metalloreductase and its role in Ctr2-mediated intracellular copper mobilization, *J. Biol. Chem. 282*, 21629-21638.

82. Lee, J., Petris, M. J., and Thiele, D. J. (2002) Characterization of mouse embryonic cells deficient in the ctr1 high affinity copper transporter. Identification of a Ctr1-independent copper transport system, *J. Biol. Chem. 277*, 40253-40259.

83. Klomp, A. E., Tops, B. B., Van Denberg, I. E., Berger, R., and Klomp, L. W. (2002) Biochemical characterization and subcellular localization of human copper transporter 1 (hCTR1), *Biochem. J. 364*, 497-505.

84. Fleming, M. D. (1998) Nramp2 is mutated in the anemic Belgrade (b) rat: evidence of a role for Nramp2 in endosomal iron transport, *Proc. Natl. Acad. Sci. USA 95*, 1148-1153.

85. Leary, S. C., Winge, D. R., and Cobine, P. A. (2009) Pulling the plug on cellular copper: the role of mitochondria in copper export, *Biochim. Biophys. Acta 1793*, 146-153.

86. Knight, S. A., Labbe, S., Kwon, L. F., Kosman, D. J., and Thiele, D. J. (1996) A widespread transposable element masks expression of a yeast copper transport gene, *Genes Dev. 10*, 1917-1929.

87. De Freitas, J. M., Liba, A., Meneghini, R., Valentine, J. S., and Gralla, E. B. (2000) Yeast lacking Cu-Zn superoxide dismutase show altered iron homeostasis. Role of oxidative stress in iron metabolism, *J. Biol. Chem. 275*, 11645-11649.

88. Lamb, A. L., Torres, A. S., O'Halloran, T. V., and Rosenzweig, A. C. (2001) Heterodimeric structure of superoxide dismutase in complex with its metallochaperone, *Nat. Struct. Biol. 8*, 751-755.

89. Furukawa, Y., Torres, A. S., and O'Halloran, T. V. (2004) Oxygen-induced maturation of SOD1: a key role for disulfide formation by the copper chaperone CCS, *EMBO J. 23*, 2872-2881.

90. Sturtz, L. A., Diekert, K., Jensen, L. T., Lill, R., and Culotta, V. C. (2001) A fraction of yeast Cu,Zn-superoxide dismutase and its metallochaperone, CCS, localize to the

intermembrane space of mitochondria. A physiological role for SOD1 in guarding against mitochondrial oxidative damage, *J. Biol. Chem. 276*, 38084-38089.

91. Okado-Matsumoto, A., and Fridovich, I. (2001) Subcellular distribution of superoxide dismutases (SOD) in rat liver: Cu,Zn-SOD in mitochondria, *J. Biol. Chem. 276*, 38388-38393.

92. Field, L. S., Furukawa, Y., O'Halloran, T. V., and Culotta, V. C. (2003) Factors controlling the uptake of yeast copper/zinc superoxide dismutase into mitochondria, *J. Biol. Chem. 278*, 28052-28059.

93. Wernimont, A. K., Huffman, D. L., Lamb, A. L., O'Halloran, T. V., and Rosenzweig, A. C. (2000) Structural basis for copper transfer by the metallochaperone for the Menkes/Wilson disease proteins, *Nat. Struct. Biol. 7*, 766-771.

94. Anastassopoulou, I., Banci, L., Bertini, I., Cantini, F., Katsari, E., and Rosato, A. (2004) Solution structure of the apo and copper(I)-loaded human metallochaperone HAH1, *Biochemistry 43*, 13046-13053.

95. Pufahl, R. A., Singer, C. P., Peariso, K. L., Lin, S. J., Schmidt, P. J., Fahrni, C. J., Culotta, V. C., Penner-Hahn, J., and O'Halloran, T. V. (1997) Metal ion chaperone function of the soluble Cu(I) receptor Atx1, *Science 278*, 853-856.

96. Banci, L., Bertini, I., Chasapis, C. T., Rosato, A., and Tenori, L. (2007) Interaction of the two soluble metal-binding domains of yeast Ccc2 with copper(I)-Atx1, *Biochem. Biophys. Res. Commun. 364*, 645-649.

97. Lutsenko, S., LeShane, E. S., and Shinde, U. (2007) Biochemical basis of regulation of human copper-transporting ATPases, *Arch. Biochem. Biophys. 463*, 134-148.

98. Cobine, P. A., Ojeda, L. D., Rigby, K. M., and Winge, D. R. (2004) Yeast contain a non-proteinaceous pool of copper in the mitochondrial matrix, *J. Biol. Chem. 279*, 14447-14455.

99. Glerum, D. M., Shtanko, A., and Tzagoloff, A. (1996) Characterization of COX17, a yeast gene involved in copper metabolism and assembly of cytochrome oxidase, *J. Biol. Chem. 271*, 14504-14509.

100. Abajian, C., Yatsunyk, L. A., Ramirez, B. E., and Rosenzweig, A. C. (2004) Yeast cox17 solution structure and copper(I) binding, *J. Biol. Chem. 279*, 53584-53592.

101. Arnesano, F., Balatri, E., Banci, L., Bertini, I., and Winge, D. R. (2005) Folding studies of Cox17 reveal an important interplay of cysteine oxidation and copper binding, *Structure 13*, 713-722.

102. Horng, Y. C., Cobine, P. A., Maxfield, A. B., Carr, H. S., and Winge, D. R. (2004) Specific copper transfer from the Cox17 metallochaperone to both Sco1 and Cox11 in the assembly of yeast cytochrome C oxidase, *J. Biol. Chem. 279*, 35334-35340.

103. Michalczyk, A., Bastow, E., Greenough, M., Camakaris, J., Freestone, D., Taylor, P., Linder, M., Mercer, J., and Ackland, M. L. (2008) ATP7B Expression in Human Breast Epithelial Cells Is Mediated by Lactational Hormones, *J. Histochem. Cytochem. 56*, 389-399.

104. Hardman, B., Michalczyk, A., Greenough, M., Camakaris, J., Mercer, J., and Ackland, L. (2007) Distinct Functional Roles for the Menkes and Wilson Copper Translocating P-type ATPases in Human Placental Cells, *Cell. Physiol. Biochem. 20*, 1073-1084.

105. Mercer, J. B., Barnes, N., Stevenson, J., Strausak, D., and Llanos, R. (2003) Copper-induced trafficking of the Cu-ATPases: A key mechanism for copper homeostasis, *BioMetals 16*, 175-184.

106. Nyasae, L., Bustos, R., Braiterman, L., Eipper, B., and Hubbard, A. (2007) Dynamics of endogenous ATP7A (Menkes protein) in intestinal epithelial cells: copper-dependent redistribution between two intracellular sites, *American Journal of Physiology - Gastrointestinal and Liver Physiology 292*, G1181-G1194.

107. Pase, L., Voskoboinik, I., Greenough, M., and Camakaris, J. (2004) Copper stimulates trafficking of a distinct pool of the Menkes copper ATPase (ATP7A) to the plasma membrane and diverts it into a rapid recycling pool, *Biochem. J 378*, 1031-1037.

108. Madsen, E., and Gitlin, J. D. (2007) Copper and iron disorders of the brain, *Annu. Rev. Neurosci. 30*, 317-337.

109. Meynard, D., Kautz, L., Darnaud, V., Canonne-Hergaux, F., Coppin, H., and Roth, M. P. (2009) *Nat. Genet. 41*, 478.

110. Adlard, P. A., and Bush, A. I. (2006) Metals and Alzheimer's disease, *J. Alzheimers Dis. 10*, 145-163.

111. Strozyk, D., Launer, L. J., Adlard, P. A., Cherney, R. A., Tsatsanis, A., Volitakis, I., Blennow, K., Petrovitch, H., White, L. R., and Bush, A. I. (2007) Zinc and copper modulate Alzheimer's Aβ levels in human cerebrospinal fluid, *Neurobiol. Aging 30*, 1069-1077.

112. Bharathi, I. S. S., and Rao, K. S. (2007) Copper- and iron-induced differential fibril formation in alpha-synuclein: TEM study, *Neurosci. Lett. 424*, 78-82.

113. Dudzik, C. G., Walter, E. D., and Millhauser, G. L. (2011) Coordination Features and Affinity of the Cu2+ Site in the α-Synuclein Protein of Parkinson's Disease, *Biochemistry 50*, 1771-1777.

114. Millhauser, G. L. (2004) Copper Binding in the Prion Protein, *Acc. Chem. Res. 37*, 79-85.

115. Bocharova, O. V., Breydo, L., Salnikov, V. V., and Baskakov, I. V. (2005) Copper(II) Inhibits in Vitro Conversion of Prion Protein into Amyloid Fibrils, *Biochemistry 44*, 6776-6787.

116. Orem, N. R., Geoghegan, J. C., Deleault, N. R., Kascsak, R., and Supattapone, S. (2006) Copper (II) ions potently inhibit purified PrPres amplification, *J. Neurochem. 96*, 1409-1415.

117. Stevens, D. J., Walter, E. D., Rodríguez, A., Draper, D., Davies, P., Brown, D. R., and Millhauser, G. L. (2009) Early Onset Prion Disease from Octarepeat Expansion Correlates with Copper Binding Properties, *PLoS Pathog 5*, e1000390.

118. Kandel, E. R., Schwartz, J. H., and Jessell, T. J. (2000) *Principles of Neural Science*, 4th ed., McGraw-Hill, New York.

119. Bush, A. I. (2000) Metals and neuroscience, *Curr. Opin. Chem. Biol. 4*, 184-191.

120. Götz, M. E., Künig, G., Riederer, P., and Youdim, M. B. H. (1994) Oxidative stress: Free radical production in neural degeneration, *Pharmacol. Ther. 63*, 37-122.

121. Frederickson, C. J., Suh, S. W., Silva, D., Frederickson, C. J., and Thompson, R. B. (2000) Importance of Zinc in the Central Nervous System: The Zinc-Containing Neuron, *J. Nutr. 130*, 1471S-1483S.

122. Bolognin, S., Messori, L., and Zatta, P. (2009) Metal Ion Physiopathology in Neurodegenerative Disorders, *Neuromolecular Med. 11*, 223-238.

123. Crichton, R., Dexter, D., and Ward, R. (2011) Brain iron metabolism and its perturbation in neurological diseases, *J. Neural Transm. 118*, 301-314.

124. Duce, J. A., and Bush, A. I. (2010) Biological metals and Alzheimer's disease: Implications for therapeutics and diagnostics, *Prog. Neurobiol. 92*, 1-18.

125. Kenche, V. B., and Barnham, K. J. (2011) Alzheimer's disease & metals: therapeutic opportunities, *Br. J. Pharmacol. 163*, 211-219.

126. Santner, A., and Uversky, V. N. (2010) Metalloproteomics and metal toxicology of [small alpha]-synuclein, *Metallomics 2*, 378-392.

127. Glinka, Y., Gassen, M., and Youdim, M. B. H. (1997) Iron and neurotransmitter function in the brain, In *Metals and oxidative damage in neurological disorders* (Connor, J. R., Ed.), pp 1-22, Plenum, New York.

128. Piñero, D. J., and Connor, J. R. (2000) Iron in the Brain: An Important Contributor in Normal and Diseased States, *Neuroscientist 6*, 435-453.

129. Götz, M. E., Double, K. A. Y., Gerlach, M., Youdim, M. B. H., and Riederere, P. (2004) The Relevance of Iron in the Pathogenesis of Parkinson's Disease, *Ann. N.Y. Acad. Sci. 1012*, 193-208.

130. Cass, W. A., Grondin, R., Andersen, A. H., Zhang, Z., Hardy, P. A., Hussey-Andersen, L. K., Rayens, W. S., Gerhardt, G. A., and Gash, D. M. (2007) Iron accumulation in the striatum predicts aging-related decline in motor function in rhesus monkeys, *Neurobiol. Aging 28*, 258-271.

131. Berg, D., and Youdim, M. B. H. (2006) Role of Iron in Neurodegenerative Disorders, *Top. Magn. Reson. Imaging 17*, 5-17.

132. Zecca, L., Youdim, M. B. H., Riederere, P., Connor, J. R., and Crichton, R. R. (2004) Iron, brain ageing and neurodegenerative disorders, *Nat. Rev. Neurosci. 5*, 863-873.

133. Brown, D. R. (2007) Interactions between metals and α-synuclein − function or artefact?, *FEBS J. 274*, 3766-3774.

134. Burré, J., Sharma, M., Tsetsenis, T., Buchman, V., Etherton, M. R., and Südhof, T. C. (2010) α-Synuclein Promotes SNARE-Complex Assembly in Vivo and in Vitro, *Science 329*, 1663-1667.

135. Sian-Hülsmann, J., Mandel, S., Youdim, M. B. H., and Riederere, P. (2011) The relevance of iron in the pathogenesis of Parkinson's disease, *J. Neurochem. 118*, 939-957.

136. Zucconi, G. G., Cipriani, S., Scattoni, R., Balgkouranidou, I., Hawkins, D. P., and Ragnarsdottir, K. V. (2007) Copper deficiency elicits glial and neuronal response typical of neurodegenerative disorders, *Neuropathol. Appl. Neurobiol. 33*, 212-225.

137. Desai, V., and Kaler, S. G. (2008) Role of copper in human neurological disorders, *The American Journal of Clinical Nutrition 88*, 855S-858S.

138. Lutsenko, S., Bhattacharjee, A., and Hubbard, A. L. (2010) Copper handling machinery of the brain, *Metallomics 2*, 596-608.

139. Tapiero, H., Townsend, D. M., and Tew, K. D. (2003) Trace elements in human physiology and pathology. Copper, *Biomed. Pharmacother. 57*, 386-398.

140. Dobrowolska, J., Dehnhardt, M., Matusch, A., Zoriy, M., Palomero-Gallagher, N., Koscielniak, P., Zilles, K., and Becker, J. S. (2008) Quantitative imaging of zinc,

copper and lead in three distinct regions of the human brain by laser ablation inductively coupled plasma mass spectrometry, *Talanta 74*, 717-723.

141. Basun, H., Forssell, L. G., Wetterberg, L., and Winblad, B. (1991) Metals and trace elements in plasma and cerebrospinal fluid in normal ageing and Alzheimer's disease, *J. Neural. Transm. Park. Dis. Dement. Sect. 3*, 231-258.

142. Hershey, C. O., Hershey, L. A., Varnes, A., Vibhakar, S. D., Lavin, P., and Strain, W. H. (1983) Cerebrospinal fluid trace element content in dementia: Clinical, radiologic, and pathologic correlations, *Neurology 33*, 1350.

143. Mattson, M. P. (2004) Pathways towards and away from Alzheimer's disease, *Nature 430*, 631-639.

144. Adlard, P. A., and Bush, A. I. (2006) Metals and Alzheimer's diease, *J. Alzheimer's Dis. 10*, 145-163.

145. Duce, J. A., Tsatsanis, A., Cater, M. A., James, S. A., Robb, E., Wikhe, K., Leong, S. L., Perez, K., Johanssen, T., Greenough, M. A., Cho, H.-H., Galatis, D., Moir, R. D., Masters, C. L., McLean, C., Tanzi, R. E., Cappai, R., Barnham, K. J., Ciccotosto, G. D., Rogers, J. T., and Bush, A. I. (2010) Iron-Export Ferroxidase Activity of β-Amyloid Precursor Protein Is Inhibited by Zinc in Alzheimer's Disease, *Cell 142*, 857-867.

146. Kong, G. K. W., Adams, J. J., Harris, H. H., Boas, J. F., Curtain, C. C., Galatis, D., Masters, C. L., Barnham, K. J., McKinstry, W. J., Cappai, R., and Parker, M. W. (2007) Structural Studies of the Alzheimer's Amyloid Precursor Protein Copper-binding Domain Reveal How it Binds Copper Ions, *J. Mol. Biol. 367*, 148-161.

147. Danscher, G., and Stoltenberg, M. (2005) Zinc-specific autometallographic in vivo selenium methods: Tracing of zinc-enriched (ZEN) terminals, ZEN pathways, and pools of zinc ions in a multitude of other ZEN cells, *J. Histochem. Cytochem. 53*, 141-153.

148. Frederickson, C. J., Giblin Iii, L. J., Balaji, R. V., Masalha, R., Frederickson, C. J., Zeng, Y., Lopez, E. V., Koh, J.-Y., Chorin, U., Besser, L., Hershfinkel, M., Li, Y., Thompson, R. B., and Krężel, A. (2006) Synaptic release of zinc from brain slices: Factors governing release, imaging, and accurate calculation of concentration, *J. Neurosci. Methods 154*, 19-29.

149. Lovell, M. A., Robertson, J. D., Teesdale, W. J., Campbell, J. L., and Markesbery, W. R. (1998) Copper, iron and zinc in Alzheimer's disease senile plaques, *J. Neurol. Sci. 158*, 47-52.

150. Bellingham, S. A., Ciccotosto, G. D., Needham, B. E., Fodero, L. R., White, A. R., Masters, C. L., Cappai, R., and Camakaris, J. (2004) Gene knockout of amyloid precursor protein and amyloid precursor-like protein-2 increases cellular copper levels in primary mouse cortical neurons and embryonic fibroblasts, *J. Neurochem. 91*, 423-428.

151. Prusiner, S. B. (1998) Prions, *Proc. Natl. Acad. Sci. USA 95*, 13363-13383.

152. Prusiner, S. (1982) Novel proteinaceous infectious particles cause scrapie, *Science 216*, 136-144.

153. Collinge, J., and Clarke, A. R. (2007) A General Model of Prion Strains and Their Pathogenicity, *Science 318*, 930-936.

154. Hong, L., and Simon, J. D. (2011) Insights into the thermodynamics of copper association with amyloid-β, α-synuclein and prion proteins, *Metallomics 3*, 262-266.

155. Saunders. (2010) Schematic absorption of iron Elsevier Inc.

156. Qian, Z. M., Li, H., Sun, H., and Ho, K. (2002) Targeted Drug Delivery via the Transferrin Receptor-Mediated Endocytosis Pathway, *Pharmacol. Rev. 54*, 561-587.

157. Anderson, C. P., Shen, M., Eisenstein, R. S., and Leibold, E. A. (2012) Mammalian iron metabolism and its control by iron regulatory proteins, *Biochim. Biophys. Acta - Mol. Cell Res. 1823*, 1468-1483.

158. Zhang, D.-L., Hughes, R. M., Ollivierre-Wilson, H., Ghosh, M. C., and Rouault, T. A. (2009) A Ferroportin Transcript that Lacks an Iron-Responsive Element Enables Duodenal and Erythroid Precursor Cells to Evade Translational Repression, *Cell Metabolism 9*, 461-473.

159. Kim, B.-E., Nevitt, T., and Thiele, D. J. (2008) Mechanisms for copper acquisition, distribution and regulation, *Nat. Chem. Biol. 4*, 176-185.

160. Festa, R. A., and Thiele, D. J. (2011) Copper: An essential metal in biology, *Curr. Biol. 21*, R877-R883.

Figure 1.1. Intestinal absorption of iron. Iron from food is first reduced from Fe^{3+} to Fe^{2+} by a ferrireductase, duodenal cytochrome *b*, before Fe^{2+} is transported into intestinal cells by DMT1. Once iron is internalized by the enterocyte, iron is either bound by ferritin or exported to the plasma through ferroportin. Export of iron to the blood plasma requires the reoxidation of iron from Fe^{2+} to Fe^{3+} by hephaestin or its homologue ceruloplasmin. Once in the blood plasma, Fe^{3+} is bound by transferrin for transport to either the liver or bone marrow. Figure adapted from (*155*).

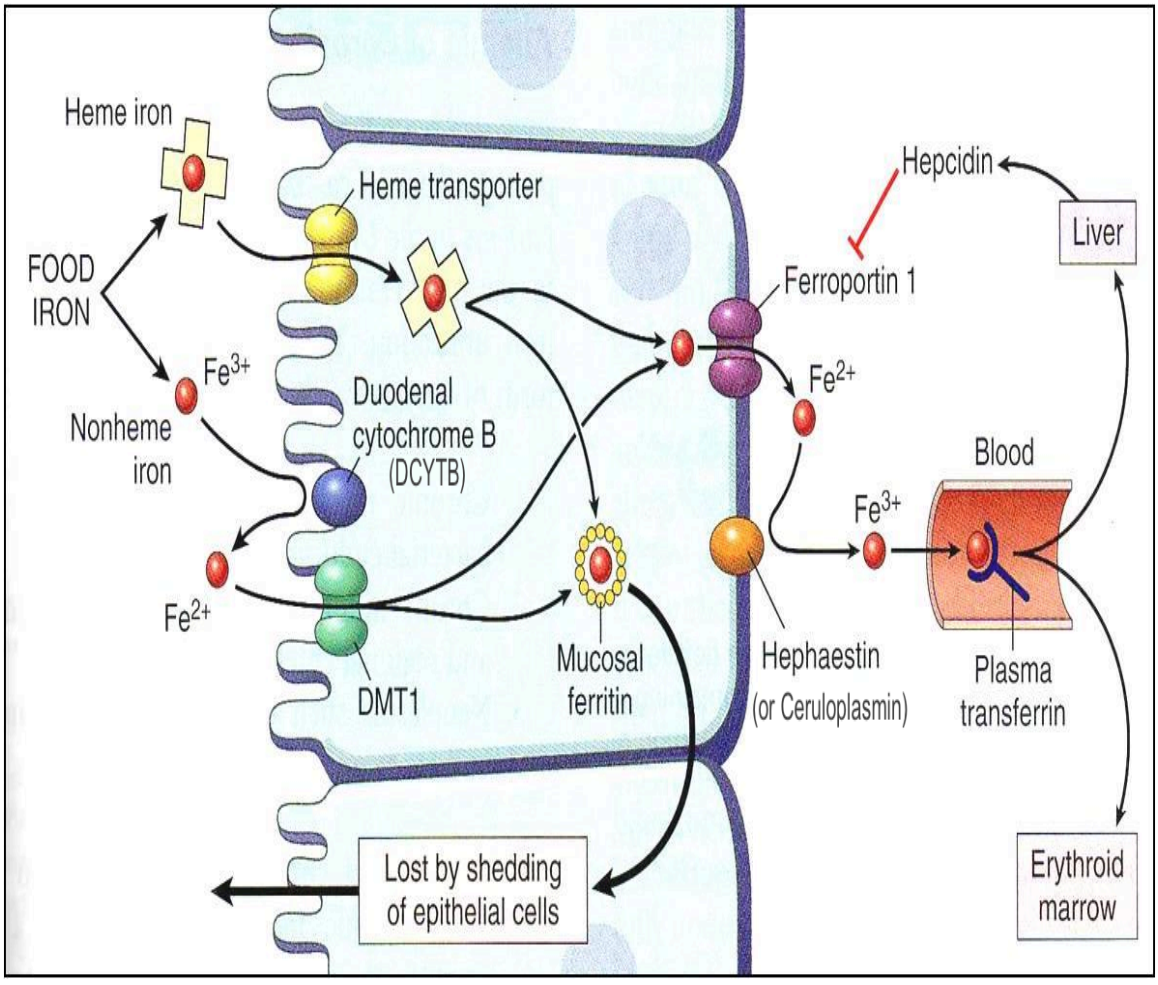

Figure 1.2. Lifecycle of transferrin. In the plasma, transferrin (Tf) binds to two atoms of Fe^{3+} (holo-Tf). Holo-Tf binds to TfR on the membrane. The Fe^{3+}-Tf-TfR complex is rapidly internalized by receptor-mediated endocytosis through clathrin-coated pits. Once inside the cell, the complex localizes to an endosome that is acidified to pH 5.5 by a proton pump. Acidification induces a conformational change resulting in release of Fe^{3+}; released Fe^{3+} is then reduced to Fe^{2+} by STEAP3. DMT1 transports Fe^{2+} across the endosomal membrane into the cytosol where iron is either stored in ferritin or utilized for heme or Fe-S cluster synthesis. Meanwhile, at acidic pH apo-Tf remains bound to TfR. The complex is recycled to the cell surface where the neutral pH results in dissociation of the apo-Tf-TfR complex and apo-Tf is free to bind Fe^{3+}, initiating additional rounds of receptor-mediated endocytosis. Figure adapted from reference (*156*).

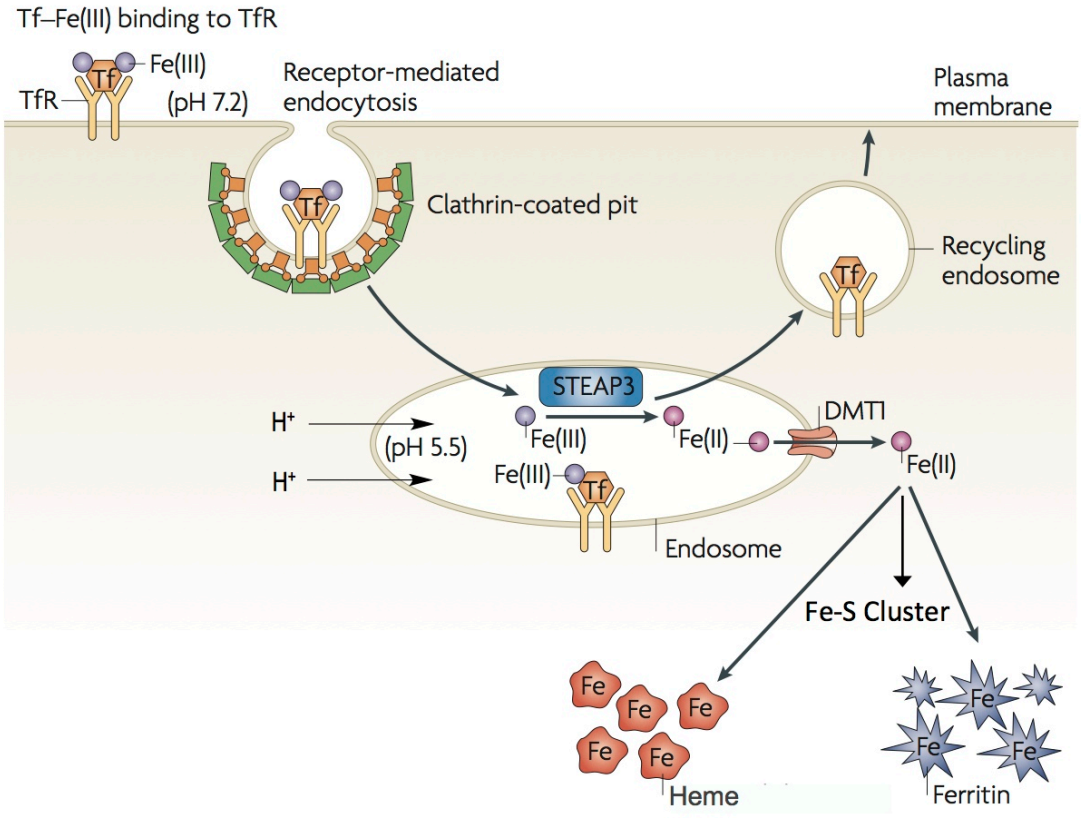

Figure 1.3. The heme biosynthetic pathway. The initial, rate-limiting step of heme synthesis is the condensation of glycine and succinyl-CoA by δ-aminolevulinic acid synthase (ALAS2) in the mitochondrion. An unknown mechanism transports δ-ALA to the cytosol for a series of reactions forming coproporphyrinogen, which is then transported back across the mitochondrial membrane by ABCB6. The final step in heme synthesis is the insertion of Fe^{2+} into protoporphyrin IX by ferrochelatase (FECH).

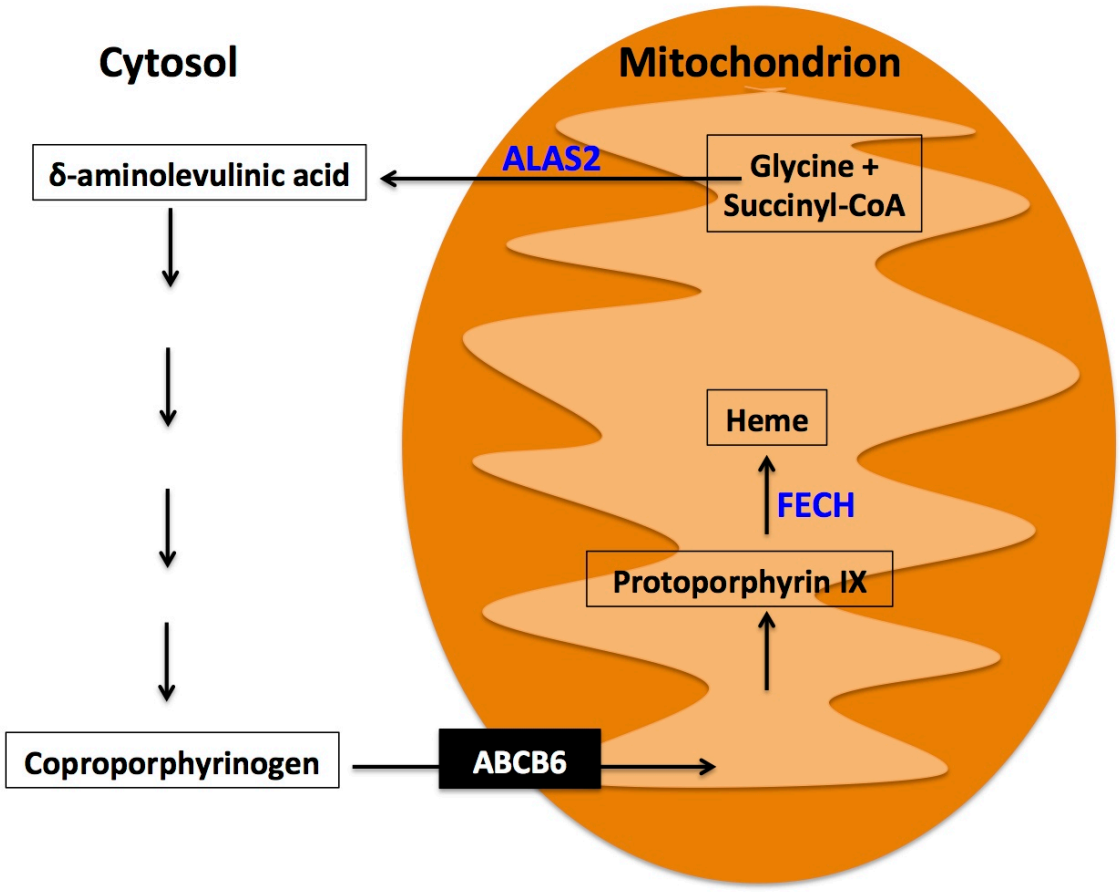

Figure 1.4. Regulation of iron response element (IRE) containing mRNAs by iron response proteins (IRPs). IRPs bind to IREs on either the 5' or 3' untranslated regions of specific mRNAs. When iron is limiting, IRPs bind with high affinity to 5' IRE mRNAs of ferritin and ferroportin repressing translation and bind to 3' IRE mRNAs of TfR1 and DMT1 stabilizing the mRNAs. When iron is abundant, IRPs do not bind IREs resulting in the translation of 5' IRE-containing mRNAs and the degradation of TfR1 and DMT1 mRNA. Abundant iron enables aconitase activity of IRP1 and promotes ubiquitin-dependent degradation of IRP2. Figure from reference (*157*).

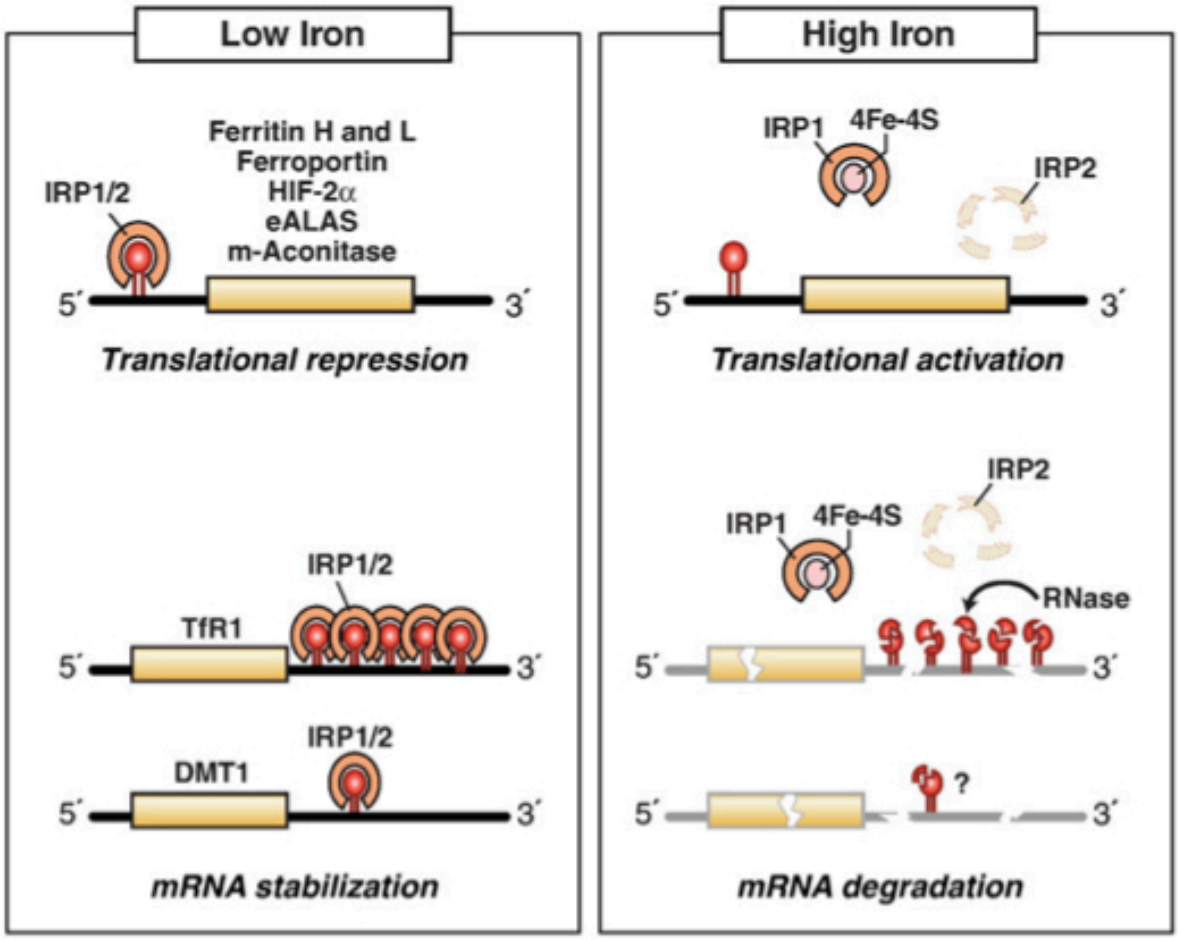

Figure 1.5. Hepcidin hormonal regulation of iron metabolism. (A) In iron-replete conditions, the liver senses Fe stores based on transferrin saturation levels and releases high levels of the iron-regulatory hormone hepcidin. Hepcidin binds to ferroportin (FPN1), an Fe exporter, resulting in FPN1 internalization and degradation. (B) In iron-deficient conditions, the liver ceases to produce hepcidin in response to the low levels of circulating Fe thus eliminating hepcidin-dependent degradation of FPN1. (C) In iron-replete conditions, the Tf/TfR1 cycle transports additional Fe into the intracellular iron pool for enhanced red cell production and heme synthesis. Increased hepcidin expression likely blocks FPN1 from exporting Fe out of cells. (D) In iron-depleted conditions, because of decreased Fe uptake from the Tf/TfR1 cycle and increased Fe export from FPN1, diminished Fe availability results in anemia characterized by decreased production of red blood cells and heme. Figure from reference (*158*).

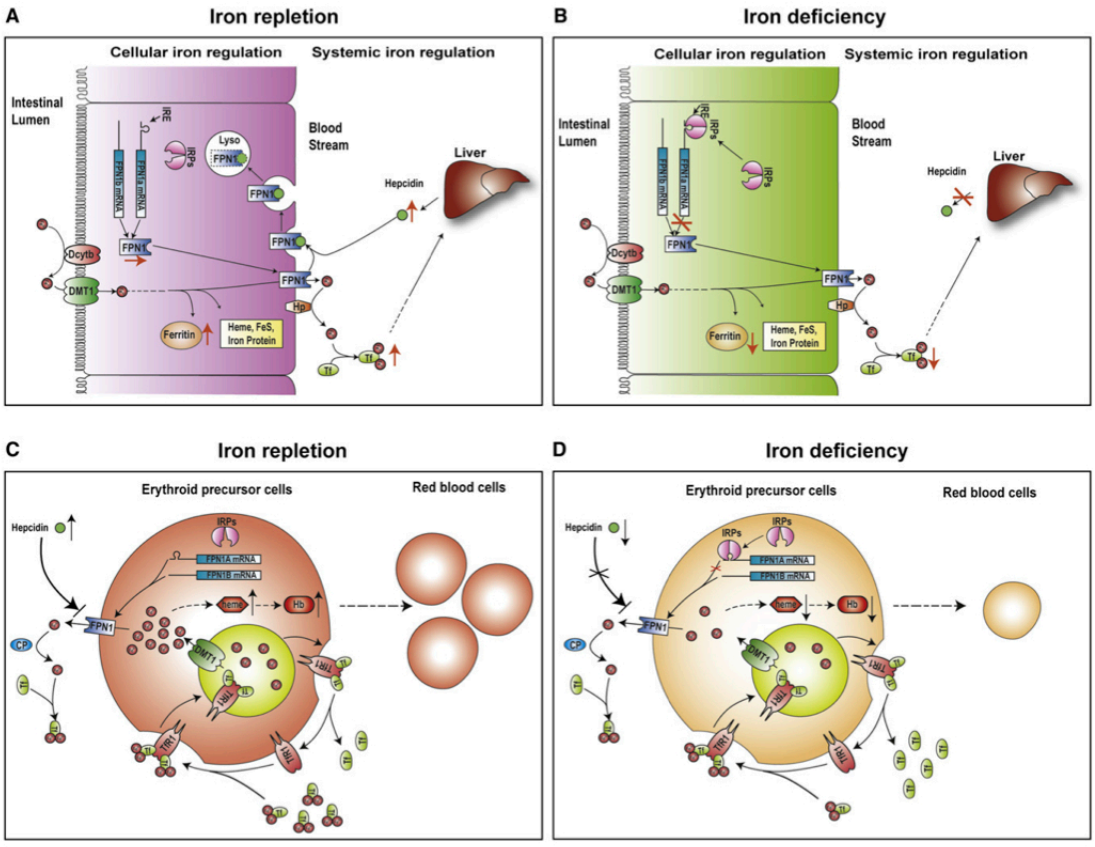

Figure 1.6. Ctr1 Cu^{+} transporter model. (A) Copper uptake protein 1 (Ctr1) has two methionine-rich (green) domains at the N-terminus that enhance Cu^{+} uptake. Three domains (orange) span the plasma membrane, and one transmembrane region has a MX_3M motif in the second domain that is essential for Cu^{+} transport. The C-terminus has a cysteine-histidine motif (purple) of unknown function. (B) Crt1 functions as a homotrimer (each monomer represented in a different color) that collectively spans the phospholipid layer of the plasma membrane in a barrel-like fashion. The arrangement of Ctr1 generates a pore for Cu^{+} (copper shown in blue) transport into cells. Image from reference (*159*).

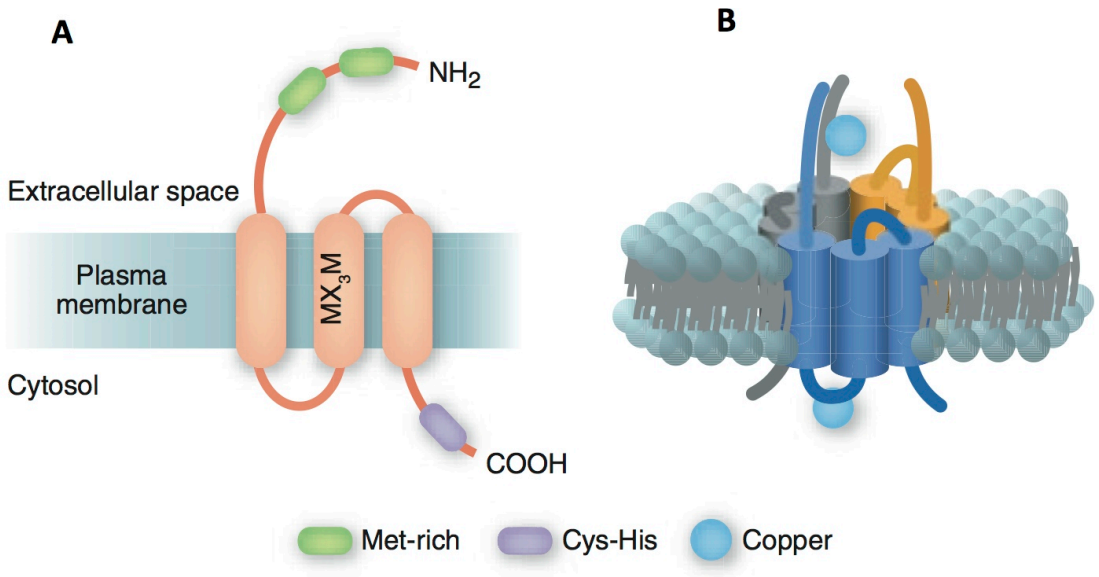

Figure 1.7. Schematic depiction of cellular copper chaperons. Ctr1 is dependent on an unidentified metalloreductase (possibly Fre1 or Fre2) for reduction of Cu^{2+} to Cu^{+} prior to import. Once inside, cellular copper is trafficked by at least three specific chaperones: CCS, Atox1 or Cox17. CCS delivers copper to Cu/Zn superoxide dismutase (SOD1). Atox1 is responsible for delivery of copper to two Cu-specific ATPases, ATP7A and ATP7B. These ATPases are necessary for delivery of copper to the Golgi for incorporation into proteins or export of copper out of the cell into the bile. Cox17 is involved in an intricate pathway resulting in delivery of copper to the mitochondria for insertion into cytochrome *c* oxidase (CCO). Image modified from reference (*160*).

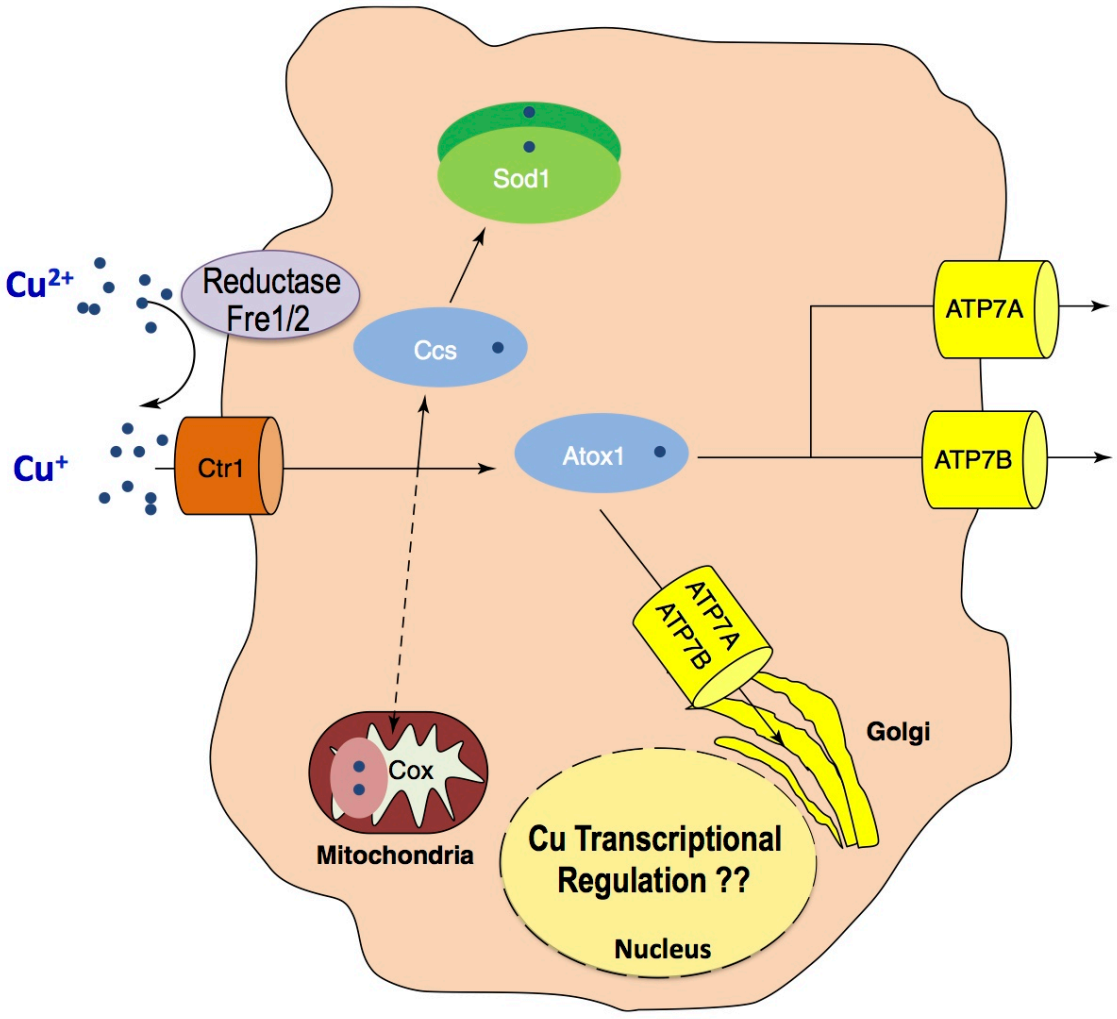

Figure 1.8. Coordination of copper ions in essential copper homeostasis enzymes. Copper is coordinated by three histidine nitrogen atoms, one histidinate nitrogen atom and one water ligand in Cu/Zn SOD. In the conserved GMTCXXC metal-binding motif of Cu-specific ATPases, the two cysteine sulfurs are responsible for binding copper. CCO has two copper centers: Cu_A in the Cox2 subunit and Cu_B in the Cox1 subunit. In the binuclear copper A center (Cu_A), the two copper atoms are coordinated by two histidines, one methionine, a protein backbone carbonyl oxygen, and two bridging cysteine residues. In the copper B center (Cu_B), the copper atom is coordinated by three histidines.

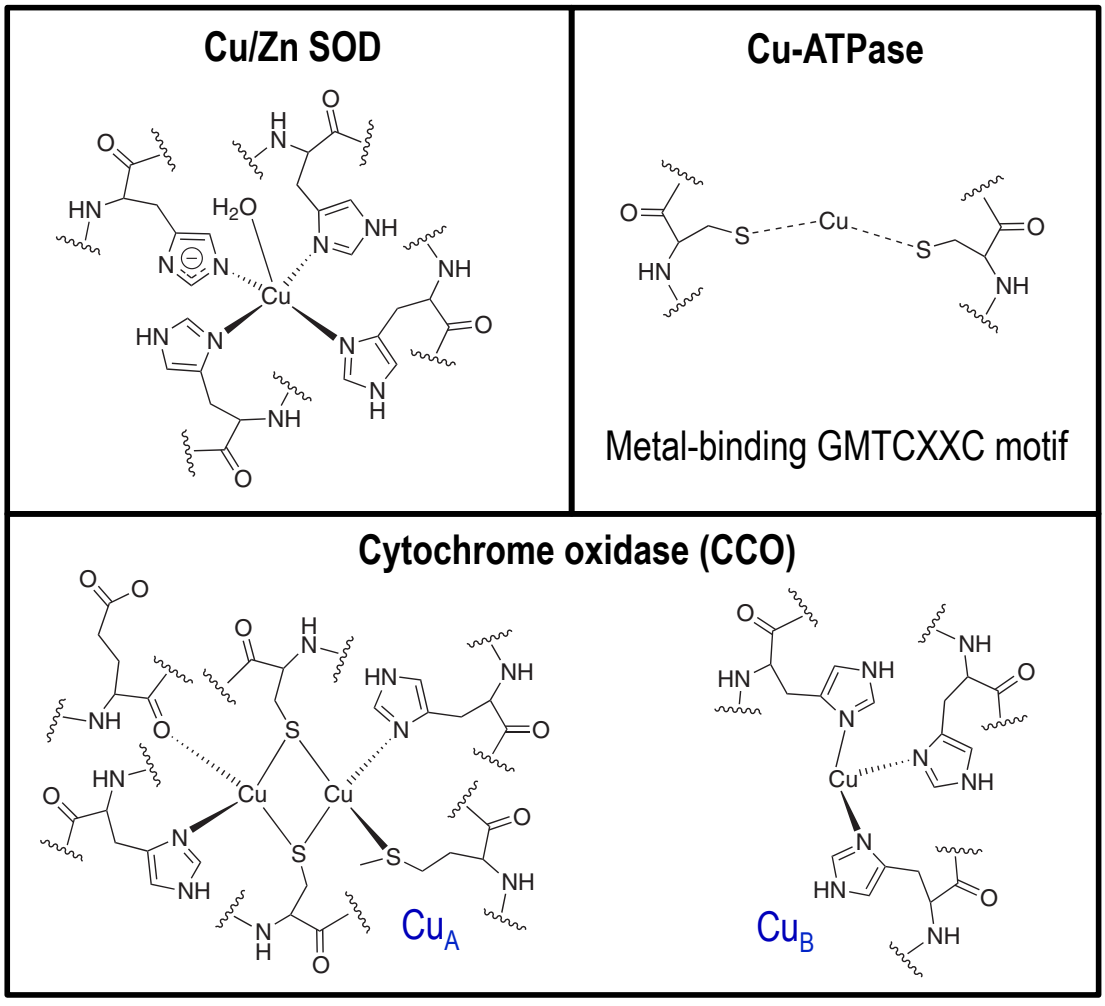

Figure 1.9. Schematic depiction of the loading of copper into mitochondrial cytochrome oxidase (CCO). How cytosolic copper imported through Ctr1 is shuttled to the mitochondria is understood. The working hypothesis is copper is delivered to Cox17 in the intermembrane space (IMS) by an unknown ligand (L). Cox17 delivers Cu^{+} to either Cox11, which delivers copper to the Cu_B site of Cox1 subunit, or Sco1, which delivers copper to the Cu_A site of Cox2 subunit of CCO. Image modified from reference (*159*).

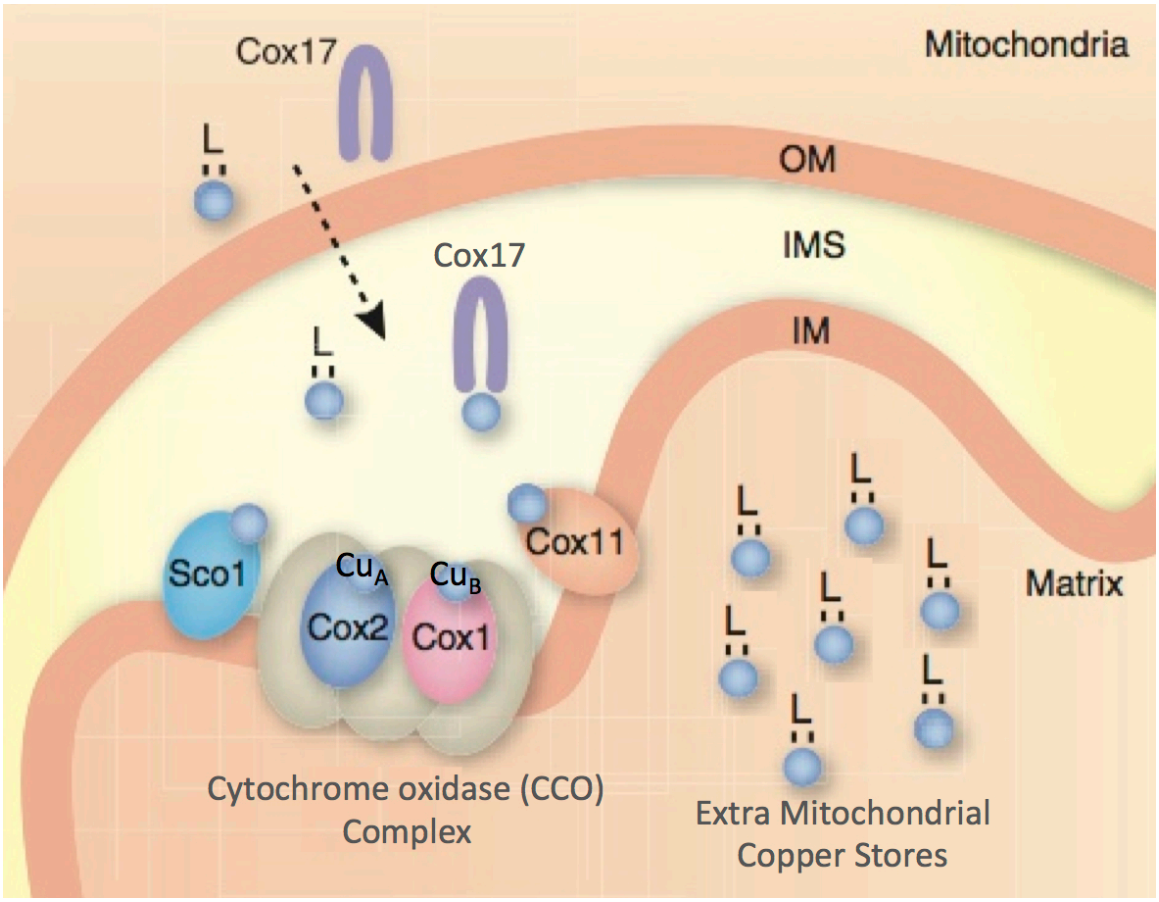

Scheme 1.1. The Fenton-like chemistry of iron and copper. Iron and copper are both redox active and are capable of generating reactive oxygen species (ROS). (A) Reduced Fe^{2+} reacts with the potent oxidant hydrogen peroxide (H_2O_2) producing hydroxide (^{-}OH), the hydroxide radical ($HO^{\bullet}$) and oxidizing iron to Fe^{3+}. Incomplete reduction of O_2 in aerobic cellular respiration is a source of superoxide ($O_2^{\bullet -}$). Subsequently $O_2^{\bullet -}$ reduces Fe^{3+} regenerating Fe^{2+} to participate in additional Fenton-like reaction cycles. (B) Reduced Cu^{+} reacts with H_2O_2 producing ^{-}OH, $HO^{\bullet}$ and oxidized Cu^{2+}. Regeneration of Cu^{+} is accomplished by reduction of Cu^{2+} by $O_2^{\bullet -}$; Cu^{+} is then available for additional Fenton-like reaction cycles. The cyclical and perpetual nature of reactive oxygen species generation is detrimental; consequently, cells have evolved extremely rigorous pathways for controlling iron and copper homeostasis.

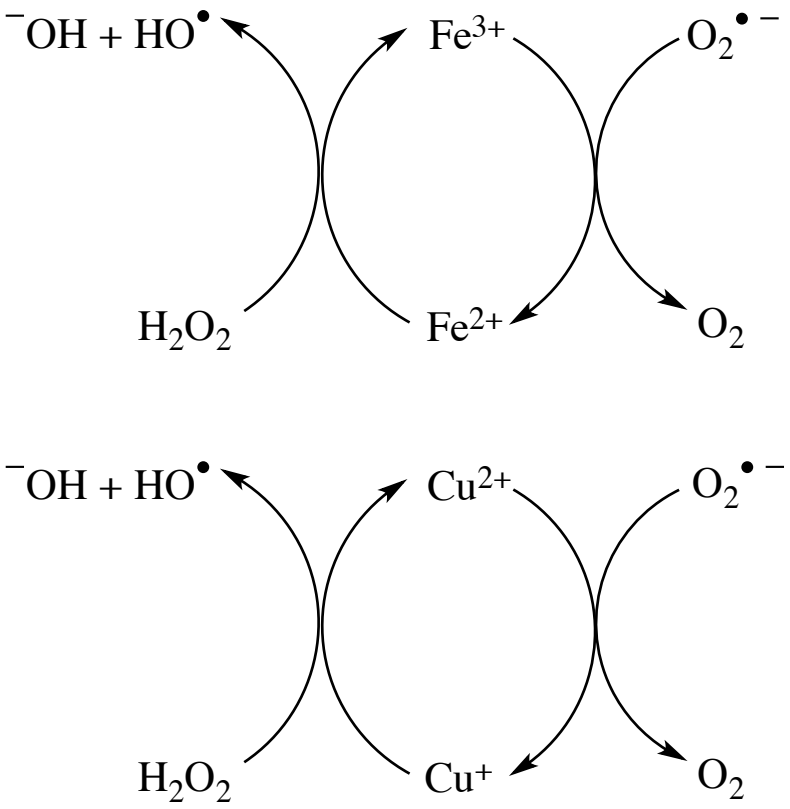

Chapter Two

Investigating the Disruption of Structure and Protein Cleavage by [Cu(1,4,7-triazocyclononane)]Cl_2 – Looking into Fibril Formation

This chapter is in preparation for submission. The authors are:

Paulsen, K. M. F.; Statz, D. A.; Polzin, G. M.; Gu, W.; Burstyn, J. N.

The in-gel trypsin digestion of aldolase fragments and identification of sites where Cu([9]aneN_3)Cl_2 cleaves aldolase were performed by Dr. Gregory Polzin in the laboratory of Professor Judith N. Burstyn at the University of Wisconsin-Madison. KMFP analyzed the Cu([9]aneN_3)Cl_2-incubated BSA, aldolase and GAPDH samples using CR EA, ThT fluorescence assay, CD spectroscopy and EM. Data interpretation and writing on this pre-manuscript were done KMFP.

Introduction

Metal ions influence the process of pathogenic aggregation of proteins in neurodegeneration. Hallmarks of certain neurodegenerative diseases are protein misfolding and conformational changes triggering the formation and deposition of toxic protein oligomers. The primary event in pathogenesis is the aggregation of the protein into cytotoxic soluble oligomers, and then into insoluble fibrils (*1*). The formation of structurally disorganized oligomers facilitates deleterious interactions of exposed amino acid side chains with cellular components. Examples of such deleterious interactions include: 1) exposure of amyloidogenic stretches with the potential to seed fibril formation; or 2) aberrant metal binding sites that can promote either peptide cross-linking or the formation of reactive oxygen species (ROS) via Fenton-like reactions involving Fe^{3+}/Fe^{2+} and/or Cu^{2+}/Cu^{+} cycling (*2, 3*). Disruption of protein secondary structure by metal ions has been implicated in both Parkinson's and Alzheimer's diseases. In Parkinson's, examination of post-mortem brain material has revealed changes in normal iron and antioxidant concentrations, and current opinion is that iron might initiate ROS-dependent oxidative stress in dopaminergic neurons (*4, 5*). The mechanism for formation of amyloid-β (Aβ) peptide aggregates, the proposed neurodegenerative agent in Alzheimer's disease, is not entirely understood, though metal ions such as Fe(III), Cu(II) and Zn(II) have been shown to facilitate Aβ aggregation (*5-7*).

Metal ions are capable of affecting oligomerization, aggregation and fibril deposition in a number of amyloidogenic proteins associated with protein misfolding (*8-11*). In addition, labile metal ions are key components in neurotransmission. These labile metal ion pools represent potential risk factors because proteins directly involved in the formation of toxic aggregates, such as the Aβ peptide, α-synuclein and the prion protein, have known metal-

binding properties. An example is copper-loaded Aβ fibrils (*5, 12, 13*). Metal ions are one of the most important factors in Aβ folding and aggregation; the binding of metal ions to Aβ induces amorphous or amyloid-type aggregation, and is dependent on metal type and stoichiometry. At physiological pH, Aβ binds up to two copper ions through N-terminal side chain residues (*14, 15*). In the presence of sub-stoichiometric Cu^{2+}, $A\beta_{1-42}$ assembles into amyloid fibrils (*16-18*); however, at higher stoichiometries, $A\beta_{1-40}$ and $A\beta_{1-42}$ form large insoluble cytotoxic amorphous aggregates (*19-22*) that are unable to seed fibril formation of $A\beta_{1-42}$ (*16*).

Not only do metal ions influence conformational changes in the proteins associated with neurodegeneration, synthetic metal-complexes provide alternatives to enzymatic proteases in cleaving proteins and peptides. Metal complexes with labile ligands may bind to the side chains of amino acid residues such as Asp, Glu, His, Lys, Trp, Cys or Met; such coordination may function as an anchor to position the metal complex for controlled hydrolysis of the protein's amide backbone (*23, 24*). In general, Pd(II) and Pt(II) coordination compounds have proven to be the most useful metal ions for cleaving peptides at defined sites. For example, various polypeptides and intact proteins are cleaved at X-Y bonds in X-Y-His and X-Y-Met sequences by Pd(II) complexes, and at Met-Z bonds by Pt(II) complexes (where X, Y and Z represent amino acid residues with non-coordinating side chains) (*25-27*). Pd(II) and Pt(II) complexes spontaneously bind to either His or Met side chains and promote nucelophilic attack of water at the aforementioned scissile peptide bonds (see Scheme 2.1). Pd(II) complexes have been used for site-specific cleavage of cytochrome *c* at the His^{18}-Thr^{19} bond (*24, 28*). Site-specific cleavage is attributed to the binding of the Pd(II) complex to His^{18} followed by hydrolysis of the adjacent amide bond. Moreover, Pd(II) complexes also have the ability to cleave proteins in

the presence of detergents, a feature useful for proteomic studies of membrane proteins where detergents are plentiful (*29*).

More abundant and less expensive transition metals have also proven to be useful metalloproteases. For example, Co(III) complexes induce selective N-terminal hydrolysis of lysozyme when the Co(III) reagent is anchored to the Trp^{108} side chain (*30*). Another alternative for sequence-specific cleavage is aqueous Ni(II). The Ni(II) ion has a strong preference for a square planar geometry and may be bound by three preceding backbone amide nitrogen atoms, while also being anchored at a His residue. The fourth anchoring backbone amide nitrogen belongs to either a Ser or Thr residue, thus allowing the hydroxyl group to act as a nucleophile toward peptide bond cleavage (*31, 32*). Recently, a Mo(VI) cluster has been shown to selectively cleave pepsin, under mild conditions without reducing agents, into three peptides with cleavage between Leu^{112}-Tyr^{113}, Leu^{166}-Leu^{167} and Leu^{178}-Asn^{179} (*33*). In contrast to the Mo(VI) cluster, polymers that contain Cu(II) complexes promote non-specific cleavage of immunoglobulins (*34, 35*). Copper ions also rapidly promote site-specific cleavage of FLAG fusion immunoglobulins (*36*). Previous work in our lab demonstrated that the metal complex, [Cu(1,4,7-triazocyclononane)]Cl_2, also known as Cu([9]aneN_3)Cl_2 (see Scheme 2.2 for structure), promotes the cleavage of bovine serum albumin (BSA) (*37*). Thus, metal complexes are capable of promoting both specific and non-specific cleavage of proteins.

Herein we report that Cu([9]aneN_3)Cl_2, **1**, rapidly cleaves, with limited specificity, three commercially available proteins, BSA, aldolase and glyceraldehyde-3-phosphate dehydrogenase (GAPDH). Previously published results demonstrated that **1** was capable of promoting hydrolysis of BSA at near neutral pH (*37*). Although the specificity was promising, the rate of hydrolysis was low, resulting in only 15% cleavage after thirteen days. In the

previous studies, BSA precipitated after only a few minutes of incubation with **1**; we speculated that the reaction conditions were inappropriate, resulting in denaturation of the protein. Upon further investigation, our hypothesis was that the observed protein aggregation was the result of an exposure of the hydrophobic protein core upon cleavage, disrupting the protein structure. Here we report in-gel trypsin digestion of Cu([9]aneN_3)Cl_2-cleaved aldolase fragments may be used to identify multiple cleavage sites. Mapping these sites onto the aldolase crystal structure revealed that the sites of Cu([9]aneN_3)Cl_2-promoted cleavage are buried, internal sites. In light of protein aggregation during the cleavage reaction with **1**, identification of internal cleavage sites, and the role of metal ions in amyloid-β fibril formation, we used a variety of spectroscopic techniques sensitive to fibril detection to investigate whether the copper complex was inducing fibril formation using. Congo Red electronic absorption, thioflavin T (ThT) fluorescence, circular dichroism (CD) spectroscopy, and electron microscopy revealed that incubating the proteins with Cu([9]aneN_3)Cl_2 results in cleavage and protein aggregation via disruption of secondary and tertiary structures, but does not induce fibril formation.

Materials and Methods

Materials. The proteins bovine serum albumin (BSA), aldolase, glyceraldehyde-3-phosphate dehydrogenase (GAPDH) and lysozyme were purchased from Sigma Aldrich in the highest purity available. Aldolase and GAPDH were purchased as isolated from rabbit muscle and sold as an essentially salt-free powder containing approximately 85% protein. Purchased BSA was isolated by cold alcohol precipitation with minimum protein content of 99% as determined by electrophoresis. Purchased lysozyme was isolated from chicken egg white containing 90% protein. All reagents used in electrophoresis were of electrophoresis grade and purchased from Sigma Aldrich. Gels were stained with PageBlue^{TM} Protein Staining Solution from Thermo Fisher. Unless otherwise stated, all other chemicals were purchased from Sigma and used as received.

Synthesis of [Cu(1,4,7-triazocyclononane)]Cl_2. The metal complex Cu([9]aneN_3)Cl_2, **1**, was prepared by the literature procedure, (*38*) with slight modification (see Scheme 2.2). $CuCl_2$•$2H_2O$ (2 mmol, 0.341 g) and triazacyclononane (TACN or [9]aneNH_3, 2 mmol, 0.477 g) were completely dissolved in 5 mL 18 MΩ H_2O. While stirring the reaction mixture was made basic by dropwise addition of 5 M NaOH to pH ~8. The reaction solution stirred for 5 minutes at room temperature before it was concentrated to half its volume. NaCl was selectively precipitated with 50:50 ethanol:water. The precipitate was removed by centrifugation then the concentration and precipitation process was repeated. The supernatant was then evaporated to dryness to yield a blue solid. The blue crystals were recrystallized from ice cold 18 MΩ H_2O. Yield of the metal complex Cu([9]aneN_3)Cl_2 was 85%.

Protein Incubation Reactions. All protein incubations were performed in sealed 1.5 mL microcentrifuge tubes at either 37 °C or 50 °C in a volume of 1 mL. For each incubation sample, 0.6 mg protein was combined with varying concentration of Cu([9]aneN$_3$)Cl$_2$ from 0.13 mM to 25.0 mM in 300 mM HEPES, pH 7. Samples were placed in an incubator at the appropriate temperature and allowed to incubate for the desired time (t = 4, 6, 12, 24 and 48 hrs). After incubation the samples were removed from the incubator and immediately stored at -20 °C until electrophoresis was performed.

The samples used for the Congo Red assay, ThT assay, CD spectroscopy and EM imaging were incubated using 0.6 mg protein with 0.625 mM Cu([9]aneN$_3$)Cl$_2$ in either 300 mM HEPES, pH 7.4 or 300 mM phosphate buffer, pH 7.4. Samples were placed in an incubator at the appropriate temperature and allowed to incubate for the desired time (t = 4, 6, 12, 24 and 48 hrs). Upon completion of incubation the samples were removed from the incubator and immediately stored at -20 °C until spectroscopic evaluation.

SDS-PAGE Electrophoresis. Separation of the protein cleavage fragments resulting from incubation with Cu([9]aneN$_3$)Cl$_2$ was performed by denaturing, sodium dodecyl sulfate polyacrylamide gel electrophoresis (SDS-PAGE) as described by Laemmli (*39*). Either 12% or 18% resolving gels overlaid with 6% stacking gels were used. All incubation samples were boiled with 20 μL 10x loading buffer for 5 minutes prior to loading into the gel. The 10x loading buffer was prepared as follows: 4.0 mL of 50% (w/v) SDS, 3.0 mL glycerol, 0.5 mL of 0.1% (w/v) bromophenol blue, 0.5 mL β-mercaptoethanol and 2.0 mL of 0.5 M Tris pH 6.8. Each gel well was loaded with 15 μL of sample to ensure an amount of cleavage product sufficient for detection by Coomasie staining. All gels were run with a molecular weight

marker lane that was loaded with ColorPlus Prestained Protein Marker, Broad Range (New England BioLabs). The gel running chamber was placed on ice while the gels ran for 60 minutes at 95 V. When electrophoresis was stopped the gels were stained according to ThermoFisher's PageBlue^{TM} protein staining protocol.

In-Gel Trypsin Digestion of Protein Fragments. In-gel digestion by trypsin was carried out according to a previously published procedure with some modification (*40*). After successful SDS-PAGE of the protein incubation sample, the gel was stained. The bands of interest were identified and excised using a sterilized scalpel. These bands were then washed twice for one hour each at 37 °C with 50 mM NH_4HCO_3:acetonitrile (1:1) to remove buffer, SDS and stain. The washings were discarded and the gel slice was dried completely in a vacuum centrifuge. The gel was rehydrated in the presence of trypsin (2 ng/mL dissolved in 50 mM NH_4HCO_3) and incubated at 37 °C for 30 minutes. After initial incubation the excess solution was removed and replaced with fresh 50 mM NH_4HCO_3 and heated at 37 °C overnight. The reaction was then stopped by the addition of trifluoroacetic acid (TFA) to a final concentration (v/v) of 1%. The supernatant was saved and the gel was washed twice with 0.1% TFA:acetonitrile (2:3) with heating to 37 °C for at least 30 minutes. The volume of the combined washings was reduced using a vacuum centrifuge for 2 hours under medium heat. The sample was then ready for MALDI-MS analysis.

MALDI-TOF Sample Preparation. Following in-gel digestion by trypsin, the supernatant was lyophilized and redissolved in acetonitrile/0.1% TFA (1:1). On the MALDI target plate, 1 μL of the sample solution was spotted and 1 μL of matrix was spotted on top of the sample. The

matrix used was a saturated solution containing α–hydroxy-4-hydroxycinnamic acid (Aldrich Chemical Co.) dissolved in methanol:H_2O (2:1). After evaporation of the volatiles, the target was ready for data acquisition.

MALDI-TOF Acquisition Conditions. MALDI-TOF was performed on a Bruker REFLEX II equipped with a 377 nm laser, a reflectron, delayed extraction and an acceleration voltage of 25 kV. Spectra were processed by the X-tof data system. Calibration was performed by the use of trypsin peaks from the autolysis of trypsin and verified by trypsin peaks located within the sample. Protein fragment identification was performed using General Protein Mass Analysis for Windows (GPMAW) version 4.02 (demo) published by Lighthouse Data © 1999. Web based search results for tryptic digestion fragments of aldolase were performed on the Peptide Mass program located on the ExPASy (Expert Protein Analysis System) proteomics server of the Swiss Institute of Bioinformatics. The sequence used in both programs was ALDOA_RABIT (UniProt accession number P00883). All modifications were considered and all mass searches were based on the monoisotopic mass.

Modeling of Cu([9]aneN$_3$)Cl$_2$ Cleavage Sites. The Cu([9]aneN$_3$)Cl$_2$ cleavage fragments identified by MALDI-MS analysis were mapped on the crystal structure of rabbit muscle aldolase chain A (PDB 1ZAH) using UCSF Chimera software (*41*).

β-Fibril Formation Control. Lysozyme was used to generate fibrils following the literature protocol (*42*). Briefly, a 1 mM lysozyme solution was prepared in 18 MΩ H_2O. To induce fibril formation, 0.5 mL of the 1 mM lysozyme stock was combined with 8.3 mL of 2 M NaCl and

7.8 mL 18 MΩ H_2O in an Erlenmyer flask and acidified to pH 2 using 1 M HCl. The solution was incubated at 37 °C with shaking at 310 rpm for 24 hours to induce fibril formation. Induced lysozyme fibrils were stored at -20 °C.

Congo Red Electronic Absorbance Assay. The Congo Red assay was adapted from the literature with slight modification (*43*). In sealed 1.5 mL microcentrifuge tubes, 1 nM Congo Red was incubated with 100 μL of Cu([9]aneN_3)Cl_2-incubated protein samples for 15 minutes at room temperature in 20 mM potassium phosphate buffered saline, pH 7.4. Electronic absorption (EA) spectra were recorded on a double-beam Varian Cary 4 Bio spectrophotometer set to a spectral bandwidth of 0.5 nm.

Thioflavin T Fluorescence Assay. Modifying the protocol published by Levine (*44*), samples were prepared in clear, disposable plastic cuvettes. The induced lysozyme fibrils were always assayed for control. Specifically, 2 μM induced lysozyme fibrils was combined with 0.1 μM Thioflavin T in 300 mM HEPES, pH 7.8. The Cu([9]aneN_3)Cl_2-incubated protein samples were assayed at 0.3 mg/mL with 0.1 μM Thioflavin T in 300 mM HEPES pH 7.8. Fluorescence measurements were taken on an ISS PC1 photon counting fluorometer (ISS Instruments, Inc., Champaign, IL) at room temperature. Emission spectra were recorded from 460 to 600 nm with an excitation wavelength of 442 nm using 1 mm slit widths for both emission and excitation monochromators.

Circular Dichroism (CD) Spectroscopy. CD experiments were performed with a MOS-450 spectropolarimeter from BioLogic (BioLogic Science Instruments, Claix, France). Lysozyme

and induced lysozyme fibrils were used as controls. CD data were collected on samples containing 0.3 mg/mL aldolase, BSA and GAPDH and 0.3 mg/mL aldolase, BSA and GAPDH incubated with 0.625 mM Cu([9]aneN_3)Cl_2 for 4 hrs in 300 mM phosphate buffer, pH 7.4. A 0.1 cm path length quartz cuvette was used (Hellma, Mlilheim, Germany). Wavelength scanning was performed in the 200-260 nm far-UV spectral region. Data were collected in 1 nm steps, with acquisition time of 20 s/nm. The instrument measures CD as ellipticity in units of millidegrees.

Transmission Electron Microscopy (TEM). The Cu([9]aneN_3)Cl_2 incubated samples of BSA, aldolase, GAPDH and the control lysozyme induced fibrils were stained with NanoW negative stain (Nanoprobes.com, Yaphank, NY), and placed on a pioloform coated grid support film (Ted Pella Inc., Redding, CA). Images were taken with a Philips CM120 transmission electron microscope (FEI Corp., Eindhoven, The Netherlands) at the UW SMPH Electron Microscope Facility.

Results

Cleavage of Bovine Serum Albumin (BSA) by Cu([9]aneN$_3$)Cl$_2$. When BSA is incubated with Cu([9]aneN$_3$)Cl$_2$, **1**, at 50 °C, cleavage is observed by SDS-PAGE. Upon mixing BSA with **1** at concentrations above 1 mM, noticeable precipitation is observed. No precipitation is observed in either the control sample without the copper complex or the reactions of BSA with lower concentrations of **1**. Cleavage of BSA by **1** is concentration dependent as seen in Figure 2.1. With an increase in concentration of **1** from 0.63 mM to 10.0 mM, the extent of cleavage proceeds to nearly 100%. Over 24 hours at 50 °C, BSA is completely cleaved in the presence of 10.0 mM **1**. The SDS-PAGE results reveal BSA cleavage product bands at 50, 46, 30 and 25 kDa, seen clearly in lanes 6 and 7 (Figure 2.1), corresponding to 5.0 and 10.0 mM **1**, respectively.

Cleavage of Aldolase by Cu([9]aneN$_3$)Cl$_2$. When aldolase is incubated with Cu([9]aneN$_3$)Cl$_2$ noticeable precipitation is observed within 90 minutes of incubation at 37 °C, independent of buffer composition or concentration of Cu([9]aneN$_3$)Cl$_2$. No precipitation is observed in the control samples of aldolase incubated in HEPES or phosphate buffer without **1**. Incubating aldolase for 24 hours with various concentrations of **1** at 37 °C results in cleavage detected by SDS-PAGE as shown in Figure 2.2. Of note is the formation of 5 distinct cleavage fragments with nominal weights of approximately 32, 25, 23, 21 and 20 kDa with 2.5 mM **1**, as observed in lane 6 of Figure 2.2. As the concentration of **1** is increased to 12.5 mM, only three bands at approximately 33, 29, and 27 kDa are observed, as shown in lane 7 of Figure 2.2. Increasing the concentration of **1** corresponds to an increase in rate and loss of specificity in protein cleavage. At a concentration of 25 mM **1**, aldolase has been completely converted to lower

molecular weight fragments; however, no specific bands are observed in lane 8 of Figure 2.2. As seen in Figure 2.3, we observe time-dependent cleavage of aldolase by Cu([9]aneN$_3$)Cl$_2$. The amounts of the three fragments observed for incubation of aldolase with 12.5 mM Cu([9]aneN$_3$)Cl$_2$ increase until 48 hours, at which time the amounts of the fragments begin to decrease until nearly all of the protein has been degraded.

Cleavage of Glyceraldehyde 3-Phosphate Dehydrogenase (GAPDH) by Cu([9]aneN$_3$)Cl$_2$. During cleavage of GAPDH by **1**, similar to the cleavage of aldolase by **1**, the protein is prone to precipitation regardless of buffer, in either HEPES or phosphate. When GAPDH is incubated for 24 hours with various concentrations of **1** at 37 °C, cleavage is observed (Figure 2.4). In addition, similar to the cleavage of aldolase by **1**, the increase in the concentration of **1** results in an increase in protein cleavage. At 25 mM **1**, the highest concentration studied (shown in lane 8 of Figure 2.4), nearly all of the protein has been converted into fragments. As with the cleavage of aldolase, five GAPDH cleavage bands are formed (see lane 7 of Figure 2.4). with approximate weights of 30, 25, 24, 23, and 21 kDa.

*Identification of Sites Where **1** Cleaves Aldolase*. Five distinct protein fragment bands are present on the SDS-PAGE gel at estimated masses of 32, 25, 23, 21 and 20 kDa when aldolase is incubated with 2.5 mM Cu([9]aneN$_3$)Cl$_2$ at 37 °C for 24 hours. Use of in-gel tryptic digestion resulted in identification of the peptides corresponding to those protein fragment bands. The resultant mass spectra were analyzed and the observable ions, both from trypsin and aldolase, were identified.

For each of the 5 aldolase protein fragments resulting from incubation with **1**, in-gel trypsin digestion was used to identify the sites of cleavage by Cu([9]aneN$_3$)Cl$_2$. In order to identify peaks corresponding to the autolysis of trypsin, a gel slice without protein was subjected to the identical tryptic digestion protocol. For ease of analysis, the peaks corresponding to the autolysis of trypsin were manually subtracted. The resultant subtraction spectrum contains only fragments that can be attributed to in-gel tryptic digestion of the aldolase protein fragment. Identification of mass peaks not corresponding to either trypsin autolysis or tryptic cleavage of aldolase, results in the location of cleavage by **1**.

Cleavage of aldolase between Gly^{75} and Val^{76} is the direct result of cleavage by **1**, generating SDS-PAGE bands observed at 32, 25 and 23 kDa. For the 32 kDa protein fragment, multiple tryptic digestion sites are identified but only a single Cu([9]aneN$_3$)Cl$_2$ cleavage site is identified (Figure 2.5). The protein fragment with the approximate mass of 25 kDa contained multiple trypsin digestion sites and two copper complex cleavage sites. In Figure 2.6, the first cleavage site by **1** is identified between Gly^{75} and Val^{76}, followed by a second cleavage site between Gln^{306} and Ala^{307}. Figure 2.7 displays the fragments of two copper cleavage sites in the aldolase protein fragment with approximate mass of 23 kDa between Gly^{75} and Val^{76} followed by cleavage between Asn^{282} and Leu^{283}. In the 21 and 20 kDa protein fragments of aldolase, only single sites corresponding to cleavage by **1** are identified among numerous tryptic digestion sites. The single **1** cleavage site in the 21 kDa protein fragment is identified between Leu^{191} and Pro^{192}, (Figure 2.8), whereas for the 20 kDa protein fragment species **1** cleaves between Ile^{185} and Val^{186}, (Figure 2.9). The limited cleavage specificity of Cu([9]aneN$_3$)Cl$_2$ on aldolase protein fragments is summarized in Table 2.1.

Modeling of Cu([9]aneN$_3$)Cl$_2$ Cleavage Sites on Aldolase. Mapping the locations of Cu([9]aneN$_3$)Cl$_2$-promoted cleavage on the crystal structure of aldolase revealed that the copper complex had access to buried protein residues during cleavage. In Figure 2.10A, the sites of **1** cleavage were mapped in red on the blue ribbon crystal structure of aldolase. The space filling structure of aldolase emphasizes the ability of Cu([9]aneN$_3$)Cl$_2$ to access sites buried in the interior of aldolase for cleavage (Figure 2.10B). Looking at the secondary structure of aldolase and considering the sites of Cu([9]aneN$_3$)Cl$_2$-promoted cleavage, the Gly^{75}-Val^{76} and the Ile^{185}-Val^{186} points of cleavage are located on beta strands, whereas the Asn^{282}-Leu^{293} and the Gln^{306}-Ala^{307} points of cleavage are located on alpha helixes, and the Leu^{191}-Pro^{192} point of cleavage is in an unstructured portion of aldolase. Therefore, it does not appear that Cu([9]aneN$_3$)Cl$_2$ has specificity for a particular secondary structural motif (i.e., α helices, β sheets or random coils).

Spectral and EM Characterization of Control Lysozyme Fibrils. Lysozyme fibrils were used as a positive control to establish protocols for detecting fibrils spectroscopically using the Congo Red electronic absorption assay, the ThT fluorescence assay, CD spectroscopy and electron microscopy. The Congo Red electronic absorbance spectrum of induced lysozyme fibrils (Figure 2.11) displays the characteristic broad, red-shifted shoulder at ~540 nm notably indicative of fibril formation (*43*). Figure 2.12 displays binding of ThT to the induced fibrils of lysozyme, resulting in enhancement of fluorescence intensity at 482 nm, as has been previously observed in amyloidogenic Aβ synthetic peptides (*44*). ThT selectively localizes to fibrils, resulting in enhancement of fluorescence. CD spectroscopy was used to probe the secondary protein structure. The crystal structure of lysozyme (PDB 1DPX) reveals the secondary

structure is 41% α-helical with 10% β-sheets and the remainder random coils. In CD spectroscopy, different structural elements give rise to characteristic CD signatures; α-helical character produces negative bands at 222 nm and 208 nm, proteins with well-defined antiparallel β-sheets have a negative band at 218 nm while disordered proteins have a negative band near 195 nm (*45*). The CD data provides a clear contrast between lysozyme before incubation and post fibril formation. The CD spectrum in Figure 2.13B (lower panel) support the predominately α-helical character of lysozyme in solution with the presence of two negative absorption bands, ~222 nm and ~208 nm. After incubation to induce fibril formation, the CD spectrum in Figure 2.13A (upper panel) reveals a single negative absorption peak at ~218 nm, indicative of the presence of fibrils. EM images of the induced lysozyme fibrils revealed short, wide fibrils that stack on one another (Figure 2.14).

*Spectral and EM Characterization of Aldolase, GAPDH and BSA Post-Incubation with **1**.* Aldolase and GAPDH revealed similar spectral characteristics indicative of protein aggregation, while spectral characterization of BSA did not reveal protein aggregation. For aldolase and GAPDH the Congo Red electronic absorbance spectra displays light scattering evidenced by high baseline absorbance in the 600-650 nm region. Detection of light scattering is an expected observation; aldolase readily aggregates when incubated with **1**, while GAPDH visibly aggregates at longer incubation times periods. Due to the light scattering in the electronic absorbance spectra of both proteins it is difficult to determine whether or not a red-shifted shoulder is forming near 540 nm; presence of a red-shifted shoulder at ~540 nm would be indicative of the formation of fibrils (*43*). To determine whether or not aldolase and GAPDH were forming fibrils during cleavage with **1** we used the ThT fluorescence assay, a more

sensitive probe of fibril formation. Combining ThT with incubated samples of aldolase and GAPDH did not result in enhancement of fluorescence, suggesting that fibrils were not present. The aggregated states of the aldolase and GAPDH samples after incubation with **1** did not permit CD characterization of the samples. We used electron microscopy to characterize the aggregated structures of aldolase and GAPDH. The EM data revealed that aldolase aggregates into big, thick protein globules, while GAPDH adopts a beads-on-a-string morphology, neither of which is similar to fibril structures (Figures 2.15 and 2.16, respectively). Taken together, these results indicate that the copper complex **1** is disrupting the protein structure, but it either 1) does not induce the formation of fibrils or, 2) induces fibril formation too transiently to be detected by conventional methods.

BSA was more tolerant of the incubation conditions with **1**, even after 48 hrs of incubation at 50 °C. The electronic absorbance Congo Red assay did not reveal light scattering in the 600-650 nm region, indicating that the BSA cleavage products remain soluble. The CR spectrum in Figure 2.17 reveals a slight red-shifted shoulder near ~540 nm indicating possible fibril formation. The red-shifted absorbance feature of BSA is not as pronounced as the spectral shift observed for the lysozyme induced fibrils (see Figure 2.11). Using the ThT fluorescence assay on **1**-incubated BSA, which is more sensitive to fibrils, did not result in enhancement of fluorescence (data not shown). CD data for BSA (Figure 2.18) supports the ThT assay data: fibrils are not formed during incubation and cleavage by **1**. A recent structure of BSA was solved and revealed nearly 74% α-helical character (PDB 3V03) (*46*). The CD spectrum of non-incubated BSA exhibits two negative absorption bands near 222 nm and 208 nm indicative of the predominantly α-helical structure of the protein. The CD spectrum of BSA incubated with **1** is identical to the CD spectrum of non-incubated BSA (Figure 2.18). Spectral

characterization of incubated BSA indicates the copper complex does not induce the formation of fibrils. The lack of fluorescence enhancement in the ThT assay, and the CD data revealing that the α-helical structure is unperturbed, suggests **1** is not inducing fibril formation upon incubation with BSA. However, EM imaging of BSA incubated with **1** reveals that $Cu([9]aneN_3)Cl_2$ does disrupt the protein structure; BSA forms snowflake-like aggregates (Figure 2.19). Both the aggregation observed in the EM images of incubated BSA and the broad absorption of Congo Red may explain the slight shoulder observed in the Congo Red electronic absorption assay (Figure 2.17) (*47*).

*Spectral and EM Characterization of Lysozyme Post-Incubation with **1**.* Lysozyme does not form fibrils during incubation with $Cu([9]aneN_3)Cl_2$. The ability of lysozyme to form amyloid fibrils under denaturing conditions at acid pH with high temperature is well-established (*42*); thus, we examined whether or not our copper complex was inducing fibril formation. The ThT fluorescence assay did not result in enhancement of fluorescence (data not shown) indicating fibrils were not present after incubating lysozyme with **1**. Lysozyme, prone to fibril formation, does not form fibrils under incubations conditions suggesting fibrils are not being formed or are formed too transiently for detection by conventional methods. These results indicate the copper complex **1** is disrupting the protein structure without inducing the formation of fibrils.

Discussion

Metal ions have a significant influence on the unfolding and/or aggregation processes of proteins associated with neurodegenerative diseases (*48-50*). In particular, divalent metals play a role in protein aggregation due to their ability to both bind proteins either in inter- or intra-molecular modes and provide electrostatic buffering capacity allowing protein residues to get close enough to interact (*51, 52*). Those factors enable proteins to assemble into aberrant states. Accumulation of peptide aggregates and neurofibrillary tangles in the brain are the key pathological markers of Alzheimer's disease (AD) (*6*). The World Health Organization estimates more than 35.6 million people worldwide have AD, and that this population is expected to double by 2030 (*53*). Elevated levels of metals such as Cu, Zn and Fe have been shown to localize with senile plaques, mainly composed of Aβ peptides (*7, 54-56*). With the understanding that metal ions can exert deleterious affects on protein conformation stability, we used a variety of spectroscopic techniques to probe the influence of $Cu([9]aneN_3)Cl_2$ on the secondary and tertiary structures of aldolase, GAPDH and BSA after incubation. Incubating these proteins with $Cu([9]aneN_3)Cl_2$ results in cleavage and disruption of the protein structure.

$Cu([9]aneN_3)Cl_2$ did not induce fibril formation; however, the copper complex does exert an adverse effect on the structures of aldolase, GAPDH and BSA during cleavage. Aldolase began to aggregate within 90 minutes of incubation with **1**, forming large protein globules (imaged by EM). Similar to aldolase, GAPDH was susceptible to protein aggregation in the presence of **1**, adopting a beads-on-a-string morphology (Figure 2.16). Spectroscopic characterization of BSA revealed that the protein secondary structure was not perturbed during incubation with $Cu([9]aneN_3)Cl_2$; significantly, the CD spectrum of **1**-incubated BSA was identical to that of native BSA. Although the secondary structure of BSA appeared unperturbed

based on spectroscopic characterization, electron microscopy revealed that the tertiary structure of BSA was disrupted. Incubation of BSA with Cu([9]aneN$_3$)Cl$_2$ induces the formation of snowflake-like aggregates.

The general understanding of metal-promoted cleavage of proteins is that metal complexes containing labile ligands may bind to the side chains of the amino acid residues Asp, Glu, His, Lys, Trp, Cys or Met. Coordinating to oxygen, nitrogen or sulfur side chains may function to anchor and position the metal for controlled hydrolysis of the protein backbone (*29-31*). Our metal complex, Cu([9]aneN$_3$)Cl$_2$, bears Cu^{2+} with two labile Cl ligands; Cu^{2+} has a preference for coordinating with oxygen and amine ligands. Considering that Cu([9]aneN$_3$)Cl$_2$-promoted aldolase cleavage products reveals Glu residues present in the cleavage fragments or nearby the sites of **1** cleavage (summarized in Table 2.1). If the copper complex anchors itself to aldolase prior to cleavage, it may do so by binding to the carboxyl of Glu residues. The presence of a Glu residue is an exception for the 25 kDa fragment resulting from cleavage between Gln^{306} and Ala^{307}; instead of a Glu residue, the fragment contains a Trp residue with a Lys near the site of cleavage. Interaction of Cu^{2+} with the positively charged side chain of Lys is unlikely due to charge repulsion, therefore, **1** may interact with the electron-rich indole of Trp to position itself for cleavage between Gln^{306} and Ala^{307}. The presence of metal-binding residues within or nearby aldolase sites of Cu([9]aneN$_3$)Cl$_2$-promoted cleavage suggests the amino acid environment may be more important in controlling cleavage rather than the identity of the individual metal complex used to promote cleavage (*57, 58*).

Lysozyme is known to form amyloid fibrils under denaturing conditions at acid pH with high temperature (*42*). The process of fibril formation and the properties of lysozyme fibrils have been studied extensively (*59, 60*). Formation of lysozyme amyloid fibrils is implicated

both in the global protein as well as in a specific protein region (*61*). Recently, a peptide located in a hydrophobic cluster, the K peptide, corresponding to residues 54-62, was identified as the core for the amyloidogenesis of lysozyme (*62*). The aromatic Trp residue at position 62 is believed to be crucial for fibrillation (*63*). Lysozyme is a well-characterized model protein for fibril formation; therefore, we probed whether or not Cu([9]aneN$_3$)Cl$_2$ induces fibril formation during incubation leading to protein cleavage. The ThT assay did not result in enhancement of fluorescence indicating fibrils were not induced by Cu([9]aneN$_3$)Cl$_2$ during incubation. (We still need to characterize the lysozyme **1**-incubated samples by CR electronic absorption, CD, EM and SDS-PAGE.) Incubating lysozyme, a fibril prone protein, with **1** does not result in fibril formation, indicating Cu([9]aneN$_3$)Cl$_2$ disrupts protein structures without inducing fibrils during protein cleavage.

Understanding how synthetic metal complexes facilitate amide cleavage has shifted efforts toward developing small molecules capable of modulating metal-induced Aβ aggregation. The strategy being employed is to design bifunctional agents that contain structural moieties for metal chelation and Aβ interaction/recognition (*55, 64*). For example, Li *et al* designed a small molecule, cyclen-curcumin, where cyclen offers metal chelation while curcumin interacts/targets Aβ peptides (see Figure 2.20). *In vitro* Aβ cleavage activity has been observed with Cu(II)-cylcen-curcumin, suggesting an additional effect in the cyclen-curcumin system (*65, 66*). The goal is to understand how metal ions associate with Aβ peptides in the brains of AD patients through the use of chemical reagents that can target metal-Aβ species, thereby elucidating the relationship between metal-Aβ-induced events and the development/pathogenesis of AD. The ability to understand how a metal complex facilitates cleavage of a peptide bond might lead to the design of metal complexes that can specifically

target Aβ fibrils, induce subsequent cleavage, and prompt eventual degradation of amyloid fibrils.

Future Directions

We have demonstrated the ability of Cu([9]aneN$_3$)Cl$_2$ to cleave bovine serum albumin (BSA), aldolase and glyceraldehyde-3-phosphate dehydrogenase (GAPDH). In-gel trypsin digestion of the aldolase cleavage fragments revealed the ability of Cu([9]aneN$_3$)Cl$_2$ to access internal, buried sites during cleavage. The process of cleavage with Cu([9]aneN$_3$)Cl$_2$ results in protein precipitation during incubation. Using Congo Red electronic absorption, Thioflavin T (ThT) fluorescence assay, circular dichroism (CD) spectroscopy and imaging with electron microscopy (EM) revealed Cu([9]aneN$_3$)Cl$_2$ disrupts the protein structures during cleavage but does not induce fibril formation. Whether or not Cu([9]aneN$_3$)Cl$_2$ cleaves with any specificity remains to be elucidated. A proteomics experiment could be utilized to establish whether or not Cu([9]aneN$_3$)Cl$_2$ cleaves with specificity by incubating cell lysate material with the copper complex followed by trypsin digestion and analysis by mass spectrometry.

References

1. Chiti, F., and Dobson, C. M. (2006) Protein Misfolding, Functional Amyloid, and Human Disease, *Annu. Rev. Biochem 75*, 333-366.
2. Powers, E. T., Morimoto, R. I., Dillin, A., Kelly, J. W., and Balch, W. E. (2009) Biological and Chemical Approaches to Diseases of Proteostasis Deficiency, *Annu. Rev. Biochem 78*, 959-991.
3. Gregersen, N., Bross, P., Vang, S., and Christensen, J. H. (2006) Protein Misfolding and Human Disease, *Annual Review of Genomics and Human Genetics 7*, 103-124.
4. Connor, J. R., Snyder, B. S., Arosio, P., Loeffler, D. A., and LeWitt, P. (1995) A Quantitative Analysis of Isoferritins in Select Regions of Aged, Parkinsonian, and Alzheimer's Diseased Brains, *J. Neurochem. 65*, 717-724.
5. Barnham, K. J., and Bush, A. I. (2008) Metals in Alzheimer's and Parkinson's Diseases, *Curr. Opin. Chem. Biol. 12*, 222-228.
6. Rauk, A. (2009) The chemistry of Alzheimer's disease, *Chem. Soc. Rev. 38*, 2698-2715.
7. Molina-Holgado, F., Hider, R., Gaeta, A., Williams, R., and Francis, P. (2007) Metals ions and neurodegeneration, *BioMetals 20*, 639-654.
8. Calabrese, M. F., Eakin, C. M., Wang, J. M., and Miranker, A. D. (2008) A regulatable switch mediates self-association in an immunoglobulin fold, *Nat. Struct. Mol. Biol. 15*, 965-971.
9. Rasia, R. M., Bertoncini, C. W., Marsh, D., Hoyer, W., Cherny, D., Zweckstetter, M., Griesinger, C., Jovin, T. M., and Fernández, C. O. (2005) Structural characterization of copper(II) binding to α-synuclein: Insights into the bioinorganic chemistry of Parkinson's disease, *Proc. Natl. Acad. Sci. USA 102*, 4294-4299.

10. Bocharova, O. V., Breydo, L., Salnikov, V. V., and Baskakov, I. V. (2005) Copper(II) Inhibits in Vitro Conversion of Prion Protein into Amyloid Fibrils†, *Biochemistry 44*, 6776-6787.

11. Brender, J. R., Hartman, K., Nanga, R. P. R., Popovych, N., de la Salud Bea, R., Vivekanandan, S., Marsh, E. N. G., and Ramamoorthy, A. (2010) Role of Zinc in Human Islet Amyloid Polypeptide Aggregation, *J. Am. Chem. Soc. 132*, 8973-8983.

12. Sarell, C. J., Wilkinson, S. R., and Viles, J. H. (2010) Substoichiometric levels of Cu2+ ions Accelerate the kinetics of fiber formation and promote cell toxicity of amyloid-β from Alzheimer disease, *The Journal of Biological Chemistry 285*, 41533-41540.

13. Millhauser, G. L. (2004) Copper Binding in the Prion Protein, *Acc. Chem. Res. 37*, 79-85.

14. Faller, P., and Hureau, C. (2009) Bioinorganic chemistry of copper and zinc ions coordinated to amyloid-[small beta] peptide, *Dalton Transactions 0*, 1080-1094.

15. Tougu, V., Tiiman, A., and Palumaa, P. (2011) Interactions of Zn(II) and Cu(II) ions with Alzheimer's amyloid-beta peptide. Metal ion binding, contribution to fibrillization and toxicity, *Metallomics 3*, 250-261.

16. Smith, D. P., Ciccotosto, G. D., Tew, D. J., Fodero-Tavoletti, M. T., Johanssen, T., Masters, C. L., Barnham, K. J., and Cappai, R. (2007) Concentration Dependent Cu2+ Induced Aggregation and Dityrosine Formation of the Alzheimer's Disease Amyloid-β Peptide, *Biochemistry 46*, 2881-2891.

17. Karr, J. W., and Szalai, V. A. (2008) Cu(II) Binding to Monomeric, Oligomeric, and Fibrillar Forms of the Alzheimer’s Disease Amyloid-β Peptide, *Biochemistry 47*, 5006-5016.

18. Sarell, C. J., Wilkinson, S. R., and Viles, J. H. (2010) Substoichiometric Levels of Cu2+ Ions Accelerate the Kinetics of Fiber Formation and Promote Cell Toxicity of Amyloid-β from Alzheimer Disease, *J. Biol. Chem. 285*, 41533-41540.

19. Yoshiike, Y., Tanemura, K., Murayama, O., Akagi, T., Murayama, M., Sato, S., Sun, X., Tanaka, N., and Takashima, A. (2001) New Insights on How Metals Disrupt Amyloid β-Aggregation and Their Effects on Amyloid-β Cytotoxicity, *J. Biol. Chem. 276*, 32293-32299.

20. Jun, S., and Saxena, S. (2007) The Aggregated State of Amyloid-β Peptide In Vitro Depends on Cu2+ Ion Concentration, *Angew. Chem. Int. Ed. 46*, 3959-3961.

21. Tõugu, V., Karafin, A., Zovo, K., Chung, R. S., Howells, C., West, A. K., and Palumaa, P. (2009) Zn(II)- and Cu(II)-induced non-fibrillar aggregates of amyloid-β (1–42) peptide are transformed to amyloid fibrils, both spontaneously and under the influence of metal chelators, *J. Neurochem. 110*, 1784-1795.

22. Jun, S., Gillespie, J. R., Shin, B.-k., and Saxena, S. (2009) The Second Cu(II)-Binding Site in a Proton-Rich Environment Interferes with the Aggregation of Amyloid-β(1−40) into Amyloid Fibrils, *Biochemistry 48*, 10724-10732.

23. Rana, T. M., and Meares, C. F. (1991) Transfer of oxygen from an artificial protease to peptide carbon during proteolysis, *Proc. Natl. Acad. Sci. USA 88*, 10578-10582.

24. Zhu, L., Qin, L., Parac, T. N., and Kostic, N. M. (1994) Site-Specific Hydrolytic Cleavage of Cytochrome c and of Its Heme Undecapeptide, Promoted by Coordination Complexes of Palladium(II), *J. Am. Chem. Soc. 116*, 5218-5224.

25. Kostic´, N. M. (1993) [24] Transition-metal complexes as spectroscopic probes for selective covalent labeling and cross-linking of proteins, In *Methods Enzymol.* (James, F. R., and Bert, L. V., Eds.), pp 565-576, Academic Press.

26. Zhu, L., and M. Kostić, N. (1994) Hydrolytic cleavage of peptides by palladium(II) complexes is enhanced as coordination of peptide nitrogen to palladium(II) is suppressed, *Inorg. Chim. Acta 217*, 21-28.

27. Korneeva, E. N., Ovchinnikov, M. V., and Kostić, N. M. (1996) Peptide hydrolysis promoted by polynuclear and organometallic complexes of palladium(II) and platinum(II), *Inorg. Chim. Acta 243*, 9-13.

28. Zhu, L., and Kostic, N. M. (1992) Toward artificial metallopeptidases: mechanisms by which platinum(II) and palladium(II) complexes promote selective, fast hydrolysis of unactivated amide bonds in peptides, *Inorg. Chem. 31*, 3994-4001.

29. Miskevich, F., Davis, A., Leeprapaiwong, P., Giganti, V., Kostić, N. M., and Angel, L. A. (2011) Metal complexes as artificial proteases in proteomics: A palladium(II) complex cleaves various proteins in solutions containing detergents, *J. Inorg. Biochem. 105*, 675-683.

30. Kumar, C. V., Buranaprapuk, A., Cho, A., and Chaudhari, A. (2000) Artificial metallopeptidases: regioselective cleavage of lysozyme, *Chem. Commun.*, 597-598.

31. Protas, A. M., Bonna, A., Kopera, E., and Bal, W. (2011) Selective peptide bond hydrolysis of cysteine peptides in the presence of Ni(II) ions, *J. Inorg. Biochem. 105*, 10-16.

32. Ariani, H. H., Polkowska-Nowakowska, A., and Bal, W. (2013) Effect of d-Amino Acid Substitutions on Ni(II)-Assisted Peptide Bond Hydrolysis, *Inorg. Chem. ASAP*.

33. Yenjai, S., Malaikaew, P., Liwporncharoenvong, T., and Buranaprapuk, A. (2012) Selective cleavage of pepsin by molybdenum metallopeptidase, *Biochem. Biophys. Res. Commun. 419*, 126-129.

34. Jang, B.-B., Lee, K.-P., Min, D.-H., and Suh, J. (1998) Immobile Artificial Metalloproteinase Containing Both Catalytic and Binding Groups, *J. Am. Chem. Soc. 120*, 12008-12016.

35. Suh, J., and Oh, S. (1996) Fast hydrolytic cleavage of proteins by coordinatively polymerized bilayer membranes, *Biorg. Med. Chem. Lett. 6*, 1067-1070.

36. Humphreys, D. P., Smith, B. J., King, L. M., West, S. M., Reeks, D. G., and Stephens, P. E. (1999) Efficient site specific removal of a C-terminal FLAG fusion from a Fab′ using copper(II) ion catalysed protein cleavage, *Protein Eng. 12*, 179-184.

37. Hegg, E. L., and Burstyn, J. N. (1995) Hydrolysis of Unactivated Peptide Bonds by a Macrocyclic Copper(II) Complex: Cu([9]aneN3)Cl2 Hydrolyzes Both Dipeptides and Proteins, *J. Am. Chem. Soc. 117*, 7015-7016.

38. Schwindinger, W. F., Fawcett, T. G., Lalancette, R. A., Potenza, J. A., and Schugar, H. J. (1980) Molecular structure of dichloro(1,4,7-triazacyclononane)copper(II), a macrocyclic triamine complex with an unusually small formation constant, *Inorg. Chem. 19*, 1379-1381.

39. Laemmli, U. K. (1970) Cleavage of structural proteins during the assembly of the head of bacteriophage T4, *Nature 227*, 680-685.

40. Hellman, U., Wernstedt, C., Gonez, J., and Heldin, C. H. (1995) Improvement of an "In-Gel" Digestion Procedure for the Micropreparation of Internal Protein Fragments for Amino Acid Sequencing, *Anal. Biochem. 224*, 451-455.

41. Pettersen, E. F., Goddard, T. D., Huang, C. C., Couch, G. S., Greenblatt, D. M., Meng, E. C., and Ferrin, T. E. (2004) UCSF Chimera—A visualization system for exploratory research and analysis, *J. Comput. Chem. 25*, 1605-1612.

42. Arnaudov, L. N., and de Vries, R. (2005) Thermally Induced Fibrillar Aggregation of Hen Egg White Lysozyme, *Biophys. J. 88*, 515-526.

43. Klunk, W. E., Jacob, R. F., and Mason, R. P. (1999) Quantifying Amyloid β-Peptide (Aβ) Aggregation Using the Congo Red-Aβ (CR–Aβ) Spectrophotometric Assay, *Anal. Biochem. 266*, 66-76.

44. LeVine III, H. (1999) [18] Quantification of β-sheet amyloid fibril structures with thioflavin T, In *Methods Enzymol.* (Ronald, W., Ed.), pp 274-284, Academic Press.

45. Kelly, S. M., and Price, N. C. (2000) The use of circular dichroism in the investigation of protein structure and function, *Curr. Protein Peptide Sci. 1*, 349-384.

46. Majorek, K. A., Porebski, P. J., Dayal, A., Zimmerman, M. D., Jablonska, K., Stewart, A. J., Chruszcz, M., and Minor, W. (2012) Structural and immunologic characterization of bovine, horse, and rabbit serum albumins, *Mol. Immunol. 52*, 174-182.

47. Eisert, R., Felau, L., and Brown, L. R. (2006) Methods for enhancing the accuracy and reproducibility of Congo red and thioflavin T assays, *Anal. Biochem. 353*, 144-146.

48. Garai, K., Sengupta, P., Sahoo, B., and Maiti, S. (2006) Selective destabilization of soluble amyloid β oligomers by divalent metal ions, *Biochem. Biophys. Res. Commun. 345*, 210-215.

49. Wang, L., and Colón, W. (2007) Effect of Zinc, Copper, and Calcium on the Structure and Stability of Serum Amyloid A, *Biochemistry 46*, 5562-5569.

50. Navarra, G., Leone, M., and Militello, V. (2007) Thermal aggregation of β-lactoglobulin in presence of metal ions, *Biophys. Chem. 131*, 52-61.

51. Remondetto, G. E., and Subirade, M. (2003) Molecular mechanisms of Fe2+ induced β-lactoglobulin cold gelation, *Biopolymers 69*, 461-469.

52. Navarra, G., Giacomazza, D., Leone, M., Librizzi, F., Militello, V., and San Biagio, P. (2009) Thermal aggregation and ion-induced cold-gelation of bovine serum albumin, *Eur. Biophys. J. 38*, 437-446.

53. (2012) Dementia: a public health priority In *Neurological Disorders*, World Health Organization.

54. Khan, A., Ashcroft, A. E., Higenell, V., Korchazhkina, O. V., and Exley, C. (2005) Metals accelerate the formation and direct the structure of amyloid fibrils of NAC, *J. Inorg. Biochem. 99*, 1920-1927.

55. Pithadia, A. S., and Lim, M. H. (2012) Metal-associated amyloid-β species in Alzheimer's disease, *Curr. Opin. Chem. Biol. 16*, 67-73.

56. Leal, S. S., Botelho, H. M., and Gomes, C. M. (2012) Metal ions as modulators of protein conformation and misfolding in neurodegeneration, *Coord. Chem. Rev. 256*, 2253-2270.

57. Krężel, A., Kopera, E., Protas, A. M., Poznański, J., Wysłouch-Cieszyńska, A., and Bal, W. (2010) Sequence-Specific Ni(II)-Dependent Peptide Bond Hydrolysis for Protein Engineering. Combinatorial Library Determination of Optimal Sequences, *J. Am. Chem. Soc. 132*, 3355-3366.

58. Kopera, E., Krężel, A., Protas, A. M., Belczyk, A., Bonna, A., Wysłouch-Cieszyńska, A., Poznański, J., and Bal, W. (2010) Sequence-Specific Ni(II)-Dependent Peptide

Bond Hydrolysis for Protein Engineering: Reaction Conditions and Molecular Mechanism, *Inorg. Chem. 49*, 6636-6645.

59. Xu, M., Shashilov, V. A., Ermolenkov, V. V., Fredriksen, L., Zagorevski, D., and Lednev, I. K. (2007) The first step of hen egg white lysozyme fibrillation, irreversible partial unfolding, is a two-state transition, *Protein Sci. 16*, 815-832.

60. Swaminathan, R., Ravi, V. K., Kumar, S., Kumar, M. V. S., and Chandra, N. (2011) Lysozyme: A model protein for amyloid research, In *Advances in Protein Chemistry and Structural Biology* (Rossen, D., Ed.), pp 63-111, Academic Press.

61. Frare, E., Polverino de Laureto, P., Zurdo, J., Dobson, C. M., and Fontana, A. (2004) A Highly Amyloidogenic Region of Hen Lysozyme, *J. Mol. Biol. 340*, 1153-1165.

62. Sugimoto, Y., Kamada, Y., Tokunaga, Y., Shinohara, H., Matsumoto, M., Kusakabe, T., Ohkuri, T., and Ueda, T. (2011) Aggregates with lysozyme and ovalbumin show features of amyloid-like fibrils, *Biochem. Cell Biol. 89*, 533-544.

63. Tokunaga, Y., Sakakibara, Y., Kamada, Y., Watanabe, K.-i., and Sugimoto, Y. (2013) Analysis of Core Region from Egg White Lysozyme Forming Amyloid Fibrils, *Int. J. Biol. Sci. 9*, 219-227.

64. Choi, J.-S., Braymer, J. J., Nanga, R. P. R., Ramamoorthy, A., and Lim, M. H. (2010) Design of small molecules that target metal-Aβ species and regulate metal-induced Aβ aggregation and neurotoxicity, *Proc. Natl. Acad. Sci. USA 107*, 21990-21995.

65. Ono, K., Hasegawa, K., Naiki, H., and Yamada, M. (2004) Curcumin has potent anti-amyloidogenic effects for Alzheimer's β-amyloid fibrils in vitro, *J. Neurosci. Res. 75*, 742-750.

66. Wu, W.-H., Lei, P., Liu, Q., Hu, J., Gunn, A. P., Chen, M.-S., Rui, Y.-F., Su, X.-Y., Xie, Z.-P., Zhao, Y.-F., Bush, A. I., and Li, Y.-M. (2008) Sequestration of Copper from β-Amyloid Promotes Selective Lysis by Cyclen-Hybrid Cleavage Agents, *J. Biol. Chem. 283*, 31657-31664.

67. Hegg, E. L., and Burstyn, J. N. (1998) Toward the development of metal-based synthetic nucleases and peptidases: a rationale and progress report in applying the principles of coordination chemistry, *Coord. Chem. Rev. 173*, 133-165.

Table 2.1. Summary of aldolase cleavage locations by Cu([9]aneN$_3$)Cl$_2$ identified using in-gel tryptic digestion and MALDI-MS. The Cu([9]aneN$_3$)Cl$_2$ cleavage fragments are shown in red with specific sites of cleavage underlined (final row of table).

Molecular Weight from SDS-PAGE	Identified Cu([9]aneN$_3$)Cl$_2$ Cleavage Location(s)	Calculated Molecular Weight (Da)	Cleavage Fragment Sequence
32 kDa	Gly^{75} and Val^{76}	31032	VILFHETLYQK
25 kDa	Gly^{75} and Val^{76} Gln^{306} and Ala^{307}	25094	VILFHETLYQK PWALTFSYGRALQ
23 kDa	Gly^{75} and Val^{76} Asn^{282} and Leu^{283}	22395	VILFHETLYQK TVPPAVTGVTFLSGGQSEEEASIN
21 kDa	Leu^{191} and Pro^{192}	20677	YASICQQNGIVPIVEPEIL
20 kDa	Ile^{185} and Val^{186}	19996	YASICQQNGIVPI

1 PHSHPALTPEQKKELSDIAHRIVAPGKGILAADESTGSIAKRLQSIGTENTEENRRFYRQ

61 LLLTADDRVNPCIGGVILFHETLYQKADDGRPFPQVIKSKGGVVGIKVDKGVVPLAGTNG

121 ETTTQGLDGLSERCAQYKKDGADFAKWRCVLKIGEHTPSALAIMENANVLARYASICQQN

181 GIVPIVEPEILPDGDHDLKRCQYVTEKVLAAVYKALSDHHIYLEGTLLKPNMVTPGHACT

241 QKYSHEEIAMATVTALRRTVPPAVTGVTFLSGGQSEEEASINLNAINKCPLLKPWALTFS

301 YGRALQASALKAWGGKKENLKAAQEEYVKRALANSLACQGKYTPSGQAGAAASESLFISN

361 HAY

Figure 2.1. Effect of varying concentrations of **1** on the cleavage of bovine serum albumin (BSA) at pH 7.8. All reactions were incubated at 50 °C for 24 hours with the following conditions: 30 mM BSA in 50 mM HEPES, pH 7.8 and various concentrations of **1**. Imaged is a 12% denaturing polyacrylamide gel (SDS-PAGE) of the appropriate incubation conditions. Lane 1: MW Ladder, lane 2: BSA control with no metal after incubating for 24 hours, lanes 3-7 show increasing concentrations of **1**: 0.63 mM, 1.25 mM, 2.5 mM, 5.0 mM, and 10.0 mM, respectively.

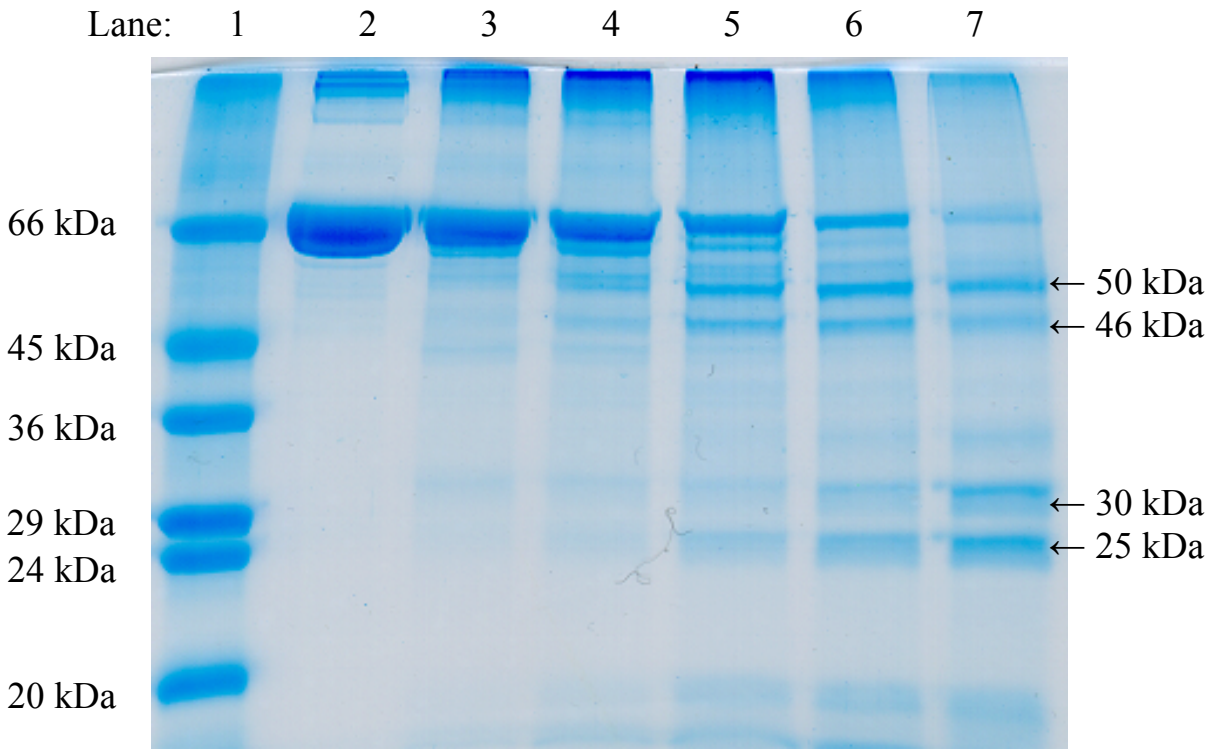

Figure 2.2. Effect of varying concentrations of **1** on the cleavage of aldolase. All incubations were performed at 37 °C for 24 hours with the following conditions: 30 mM aldolase in 50 mM HEPES, pH 7.8 and various concentrations of **1**. Imaged is an 18% denaturing polyacrylamide gel (SDS-PAGE) of the appropriate incubations. Lane 1: MW ladder, lane 2: aldolase control with no metal, lanes 3-8 show increasing concentrations of **1**: 0.13 mM, 0.25 mM, 1.25 mM, 2.5 mM, 12.5 mM, and 25.0 mM, respectively.

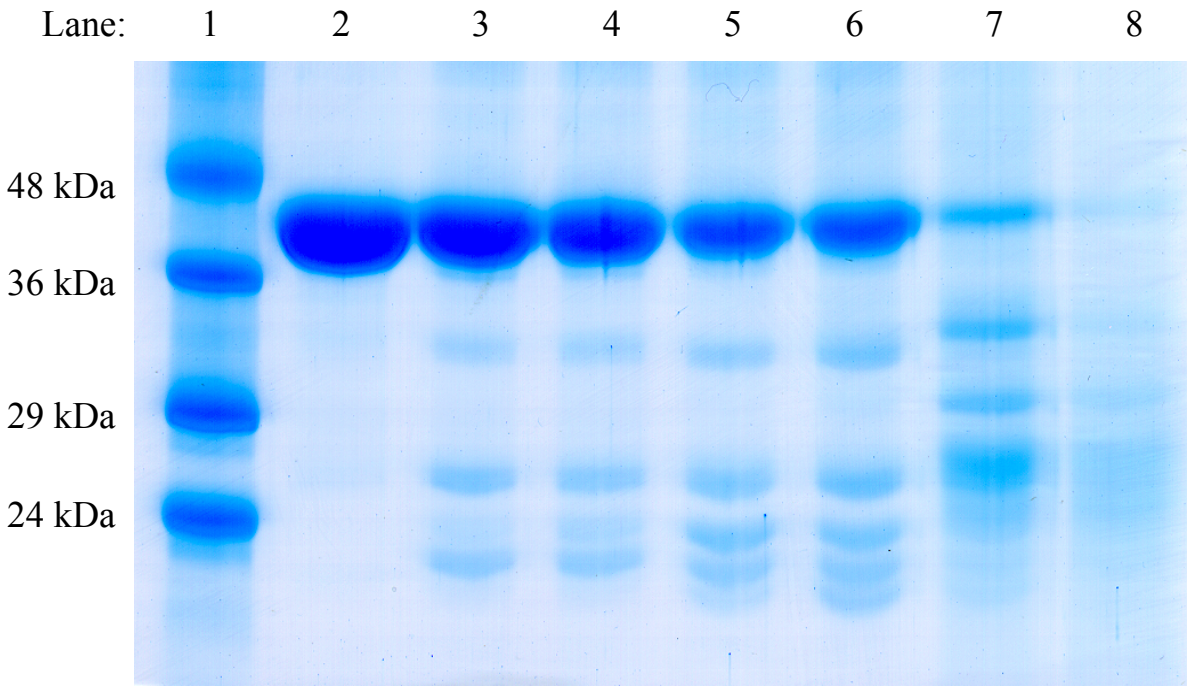

Figure 2.3. Time-dependent cleavage of aldolase by **1**. All incubations were performed at 37 °C with the following conditions: 30 mM aldolase in 50 mM HEPES, pH 7.8 with 12.5 mM Cu([9]aneN_3)Cl_2 and various durations. Imaged is an 18% denaturing polyacrylamide gel (SDS-PAGE) of the appropriate incubation. Lane 1: MW ladder, lane 2: aldolase control with no metal after 48 hours, lanes 3-7 show increasing time: 0 h, 6 h, 12 h, 24 h, and 48 h, respectively.

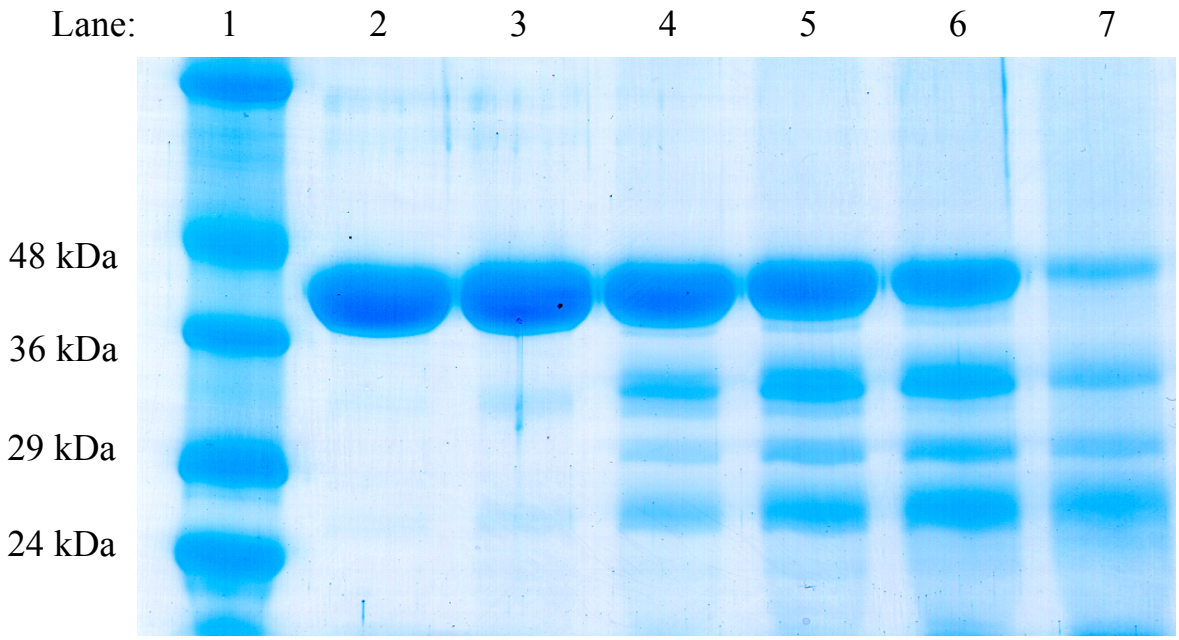

Figure 2.4. Effect of varying the concentration of **1** on the cleavage of glyceraldehyde-3-phosphate dehydrogenase (GAPDH). All incubations were performed at 37 °C for 24 hours with the following conditions: 30 mM GAPDH in 50 mM HEPES, pH 7.8 at various concentrations of **1**. Imaged is an 18% denaturing polyacrylamide gel (SDS-PAGE) of the appropriate incubations. Lane 1: MW ladder, lane 2: GAPDH control with no metal, lanes 3-8 show increasing concentrations of **1**: 0.13 mM, 0.25 mM, 1.25 mM, 2.5 mM, 12.5 mM, and 25.0 mM, respectively.

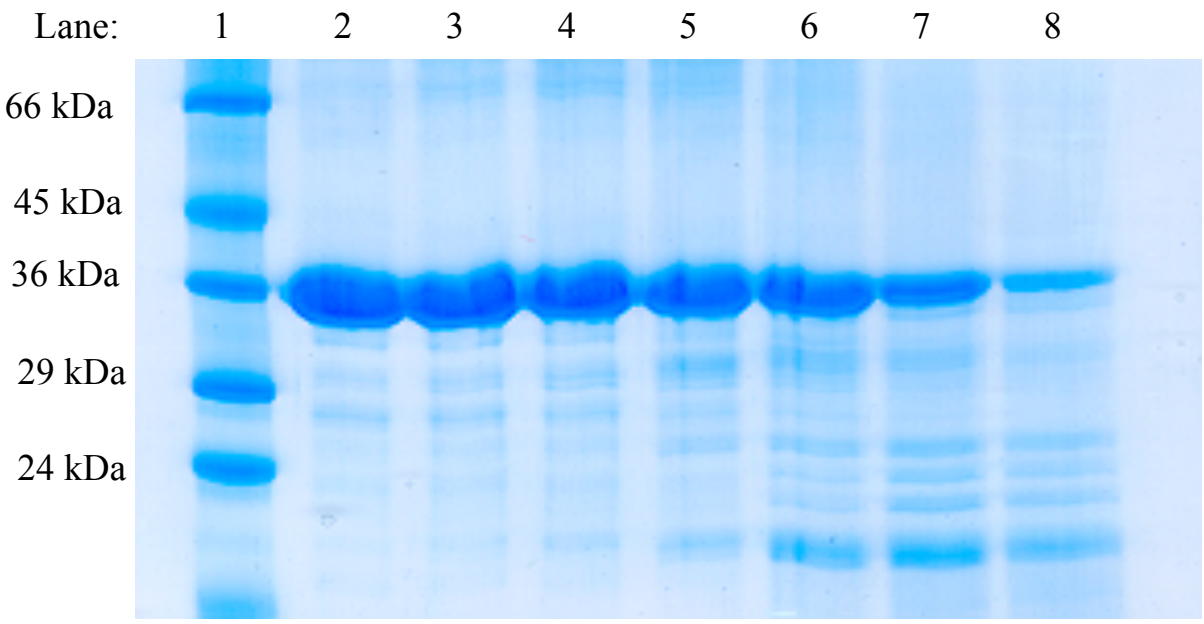

Figure 2.5. Determination of the aldolase protein fragment identity with the approximate mass of 32 kDa. Fragments identified as the result of cleavage by trypsin are listed in green and those resulting from cleavage by **1** and trypsin are shown in red. The sequence of aldolase is displayed with cleavage fragments displayed in the corresponding color. From these data the 32 kDa protein fragment is identified as the result of cleavage by **1** between amino acids Gly^{75} and Val^{76}. The resulting protein fragment has been underlined and has a predicted mass of 31032 Da.

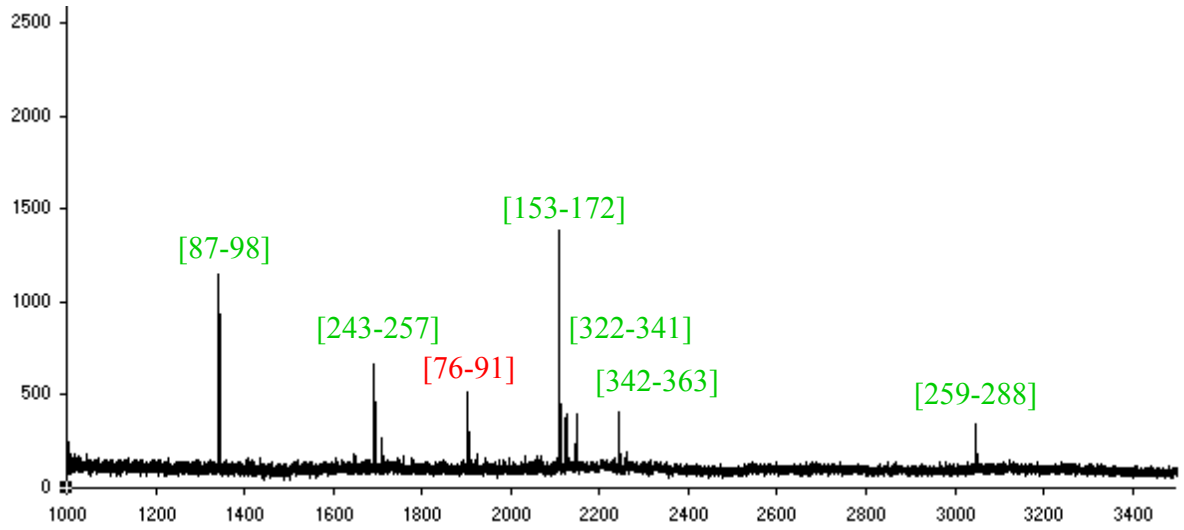

1 PHSHPALTPEQKKELSDIAHRIVAPGKGILAADESTGSIAKRLQSIGTENTEENRRFYRQ

61 LLLTADDRVNPCIGGVILFHETLYQKADDGRPFPQVIKSKGGVVGIKVDKGVVPLAGTNG

121 ETTTQGLDGLSERCAQYKKDGADFAKWRCVLKIGEHTPSALAIMENANVLARYASICQQN

181 GIVPIVEPEILPDGDHDLKRCQYVTEKVLAAVYKALSDHHIYLEGTLLKPNMVTPGHACT

241 QKYSHEEIAMATVTALRRTVPPAVTGVTFLSGGQSEEEASINLNAINKCPLLKPWALTFS

301 YGRALQASALKAWGGKKENLKAAQEEYVKRALANSLACQGKYTPSGQAGAAASESLFISN

361 HAY

Figure 2.6. Identification of the aldolase protein fragment with the approximate mass of 25 kDa. Fragments identified as the result of cleavage by trypsin are listed in green and those resulting from cleavage by **1** and trypsin are shown in red. The sequence of aldolase is displayed with cleavage fragments displayed in the corresponding color. From these data the 25 kDa protein fragment is identified as the result of cleavage by **1** between the amino acids Gly^{75} and Val^{76} followed by cleavage between amino acids Gln^{306} and Ala^{307}. The resulting protein fragment has been underlined and has a predicted mass of 25094 Da.

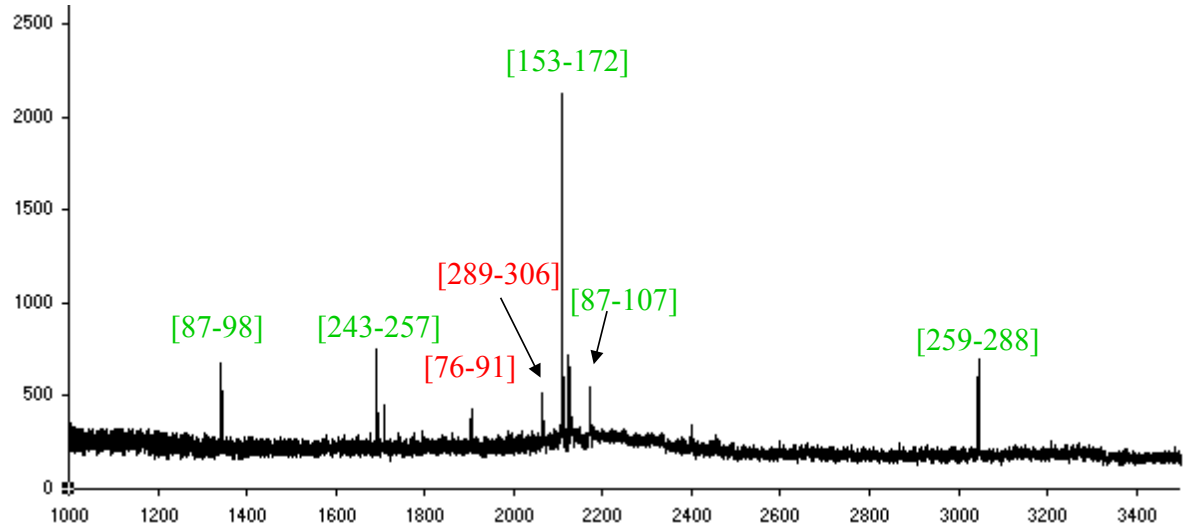

1 PHSHPALTPEQKKELSDIAHRIVAPGKGILAADESTGSIAKRLQSIGTENTEENRRFYRQ

61 LLLTADDRVNPCIGGVILFHETLYQKADDGRPFPQVIKSKGGVVGIKVDKGVVPLAGTNG

121 ETTTQGLDGLSERCAQYKKDGADFAKWRCVLKIGEHTPSALAIMENANVLARYASICQQN

181 GIVPIVEPEILPDGDHDLKRCQYVTEKVLAAVYKALSDHHIYLEGTLLKPNMVTPGHACT

241 QKYSHEEIAMATVTALRRTVPPAVTGVTFLSGGQSEEEASINLNAINKCPLLKPWALTFS

301 YGRALQASALKAWGGKKENLKAAQEEYVKRALANSLACQGKYTPSGQAGAAASESLFISN

361 HAY

Figure 2.7. Identification of the aldolase protein fragment with the approximate mass of 23 kDa. Those fragments identified as the result of cleavage by trypsin are listed in green and those resulting from cleavage by **1** and trypsin are shown in red. The sequence of aldolase is displayed with cleavage fragments displayed in the corresponding color. From these data the 23 kDa protein fragment is identified as the result of cleavage by **1** between the amino acids Gly^{75} and Val^{76} followed by cleavage between amino acids Asn^{282} and Leu^{283}. The resulting protein fragment has been underlined and has a predicted mass of 22395 Da.

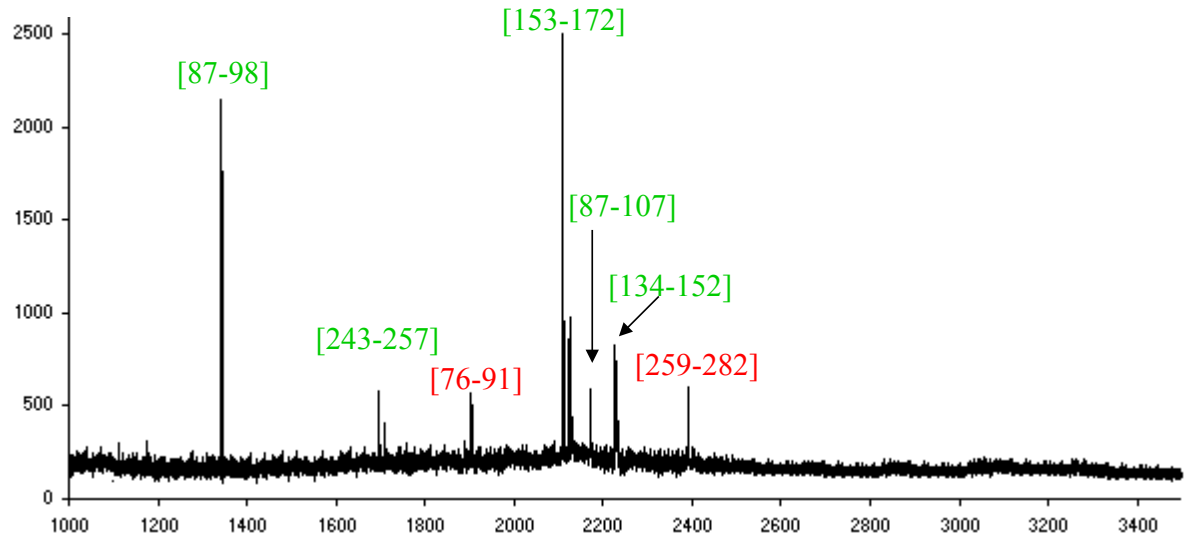

1 PHSHPALTPEQKKELSDIAHRIVAPGKGILAADESTGSIAKRLQSIGTENTEENRRFYRQ

61 LLLTADDRVNPCIGGVILFHETLYQKADDGRPFPQVIKSKGGVVGIKVDKGVVPLAGTNG

121 ETTTQGLDGLSERCAQYKKDGADFAKWRCVLKIGEHTPSALAIMENANVLARYASICQQN

181 GIVPIVEPEILPDGDHDLKRCQYVTEKVLAAVYKALSDHHIYLEGTLLKPNMVTPGHACT

241 QKYSHEEIAMATVTALRRTVPPAVTGVTFLSGGQSEEEASINLNAINKCPLLKPWALTFS

301 YGRALQASALKAWGGKKENLKAAQEEYVKRALANSLACQGKYTPSGQAGAAASESLFISN

361 HAY

Figure 2.8. Identification of the aldolase protein fragment with the approximate mass of 21 kDa. Those fragments identified as the result of cleavage by trypsin are listed in green and those resulting from cleavage by **1** and trypsin are shown in red. The sequence of aldolase is displayed with cleavage fragments displayed in the corresponding color. From these data the 21 kDa protein fragment is identified as the result of cleavage by **1** between the amino acids Leu[191] and Pro[192]. The resulting protein fragment has been underlined and has a predicted mass of 20677 Da.

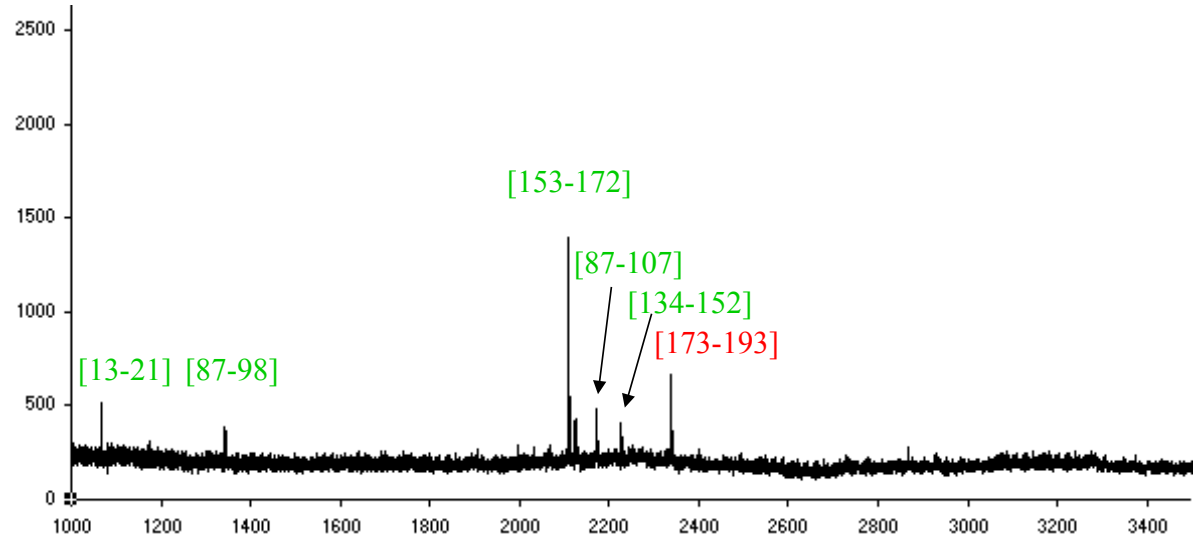

1 PHSHPALTPEQKKELSDIAHRIVAPGKGILAADESTGSIAKRLQSIGTENTEENRRFYRQ

61 LLLTADDRVNPCIGGVILFHETLYQKADDGRPFPQVIKSKGGVVGIKVDKGVVPLAGTNG

121 ETTTQGLDGLSERCAQYKKDGADFAKWRCVLKIGEHTPSALAIMENANVLARYASICQQN

181 GIVPIVEPEILPDGDHDLKRCQYVTEKVLAAVYKALSDHHIYLEGTLLKPNMVTPGHACT

241 QKYSHEEIAMATVTALRRTVPPAVTGVTFLSGGQSEEEASINLNAINKCPLLKPWALTFS

301 YGRALQASALKAWGGKKENLKAAQEEYVKRALANSLACQGKYTPSGQAGAAASESLFISN

361 HAY

Figure 2.9. Identification of the aldolase protein fragment with approximate mass of 20 kDa. Those fragments identified as the result of cleavage by trypsin are listed in green and those resulting from cleavage by **1** and trypsin are shown in red. The sequence of aldolase is displayed with cleavage fragments displayed in the corresponding color. From these data the 20 kDa protein fragment is identified as the result of cleavage by **1** between the amino acids Ile[185] and Val[186]. The resulting protein fragment has been underlined and has a predicted mass of 19996 Da.

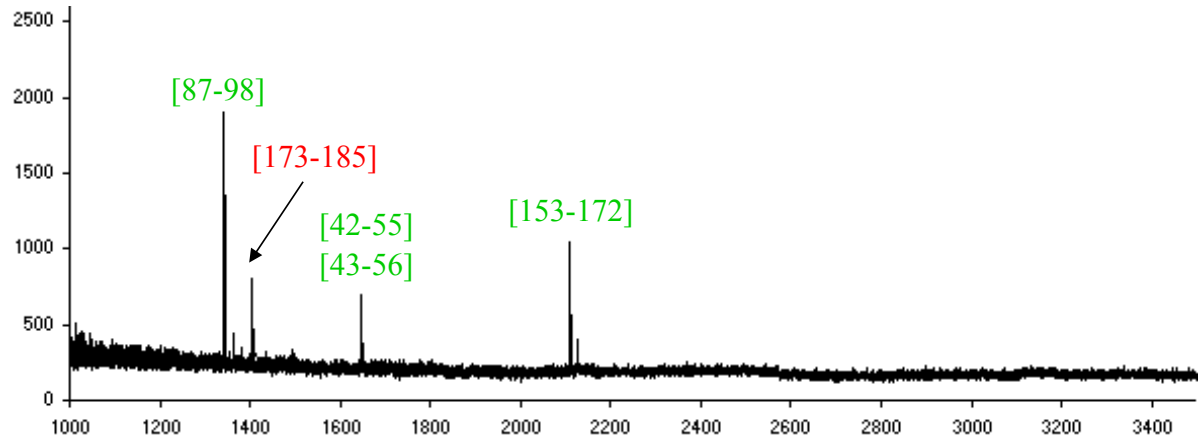

1 PHSHPALTPEQKKELSDIAHRIVAPGKGILAADESTGSIAKRLQSIGTENTEENRRFYRQ

61 LLLTADDRVNPCIGGVILFHETLYQKADDGRPFPQVIKSKGGVVGIKVDKGVVPLAGTNG

121 ETTTQGLDGLSERCAQYKKDGADFAKWRCVLKIGEHTPSALAIMENANVLARYASICQQN

181 GIVPIVEPEILPDGDHDLKRCQYVTEKVLAAVYKALSDHHIYLEGTLLKPNMVTPGHACT

241 QKYSHEEIAMATVTALRRTVPPAVTGVTFLSGGQSEEEASINLNAINKCPLLKPWALTFS

301 YGRALQASALKAWGGKKENLKAAQEEYVKRALANSLACQGKYTPSGQAGAAASESLFISN

361 HAY

Figure 2.10. A) Location of Cu([9]aneN$_3$)Cl$_2$ cleavage sites mapped on the structure of aldolase. Cleavage sites are denoted in red, remainder of the protein backbone is denoted in blue. Structure modeled from PDB file 1ZAH, chain A. B) A space-filled representation of the cleavage sites with 60% transparency is presented in B to emphasize the internal cleavage locations.

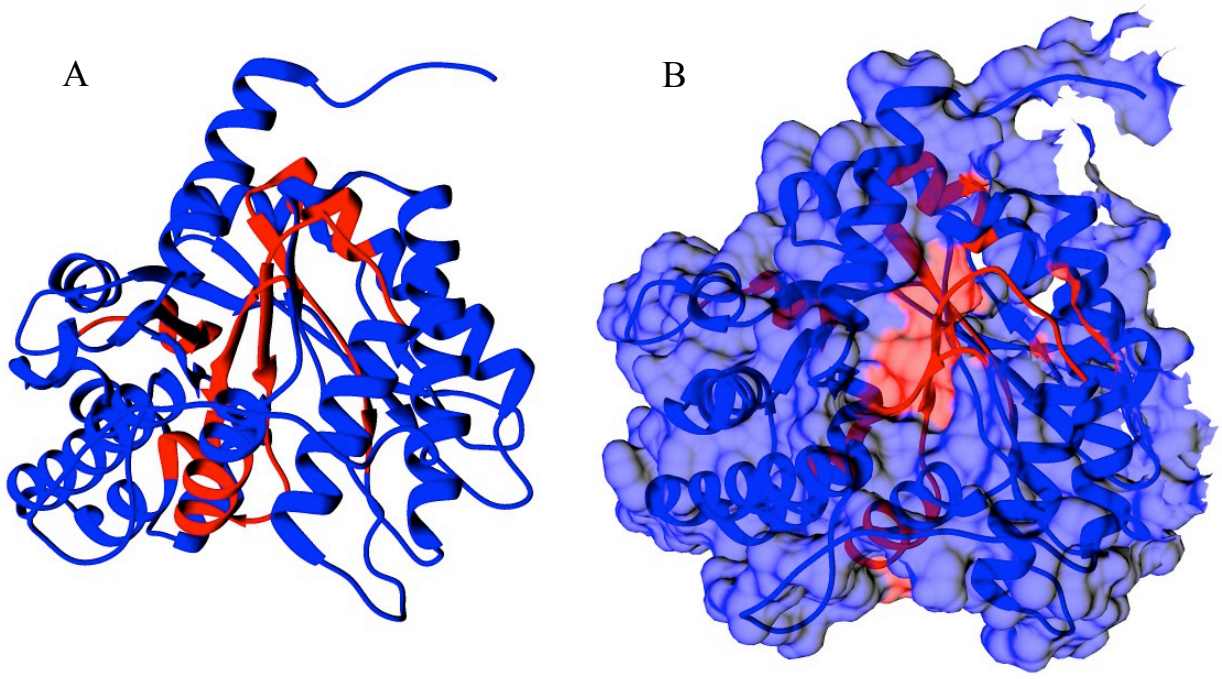

Figure 2.11. Congo Red electronic absorption spectrum of lysozyme with induced fibrils. The solid trace (—) is the absorbance of the dye. When the Congo Red dye interacts with fibrils the absorbance feature red shifts to lower energy resulting in a shoulder near 540 nm, dotted trace (…).

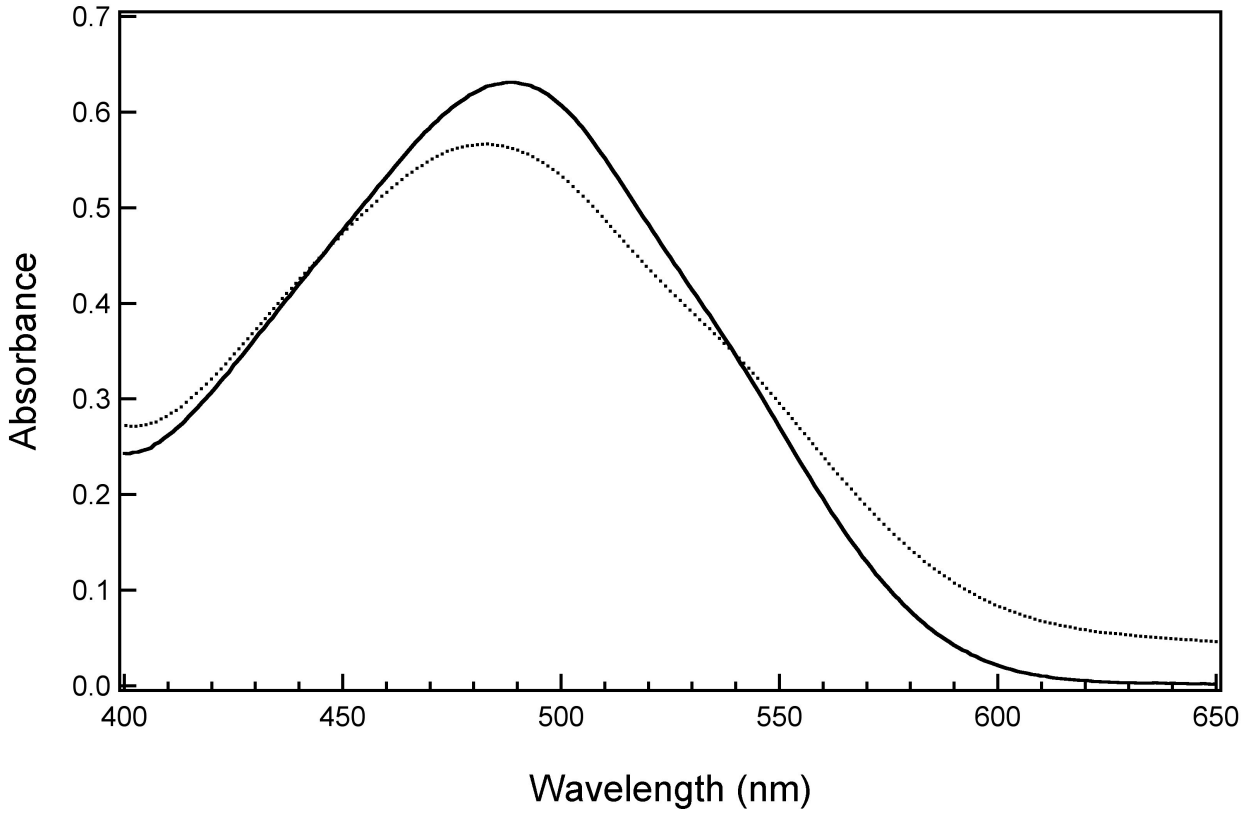

Figure 2.12. ThT fluorescence detection of lysozyme's induced fibrils. Fibrils were induced with high salt at low pH. The emission spectrum of the ThT-fibril complex (…) is significantly enhanced at 482 nm when the sample is excited at 443 nm, a hallmark of the presence of fibrils (*44*). The solid trace (—) is lysozyme fibrils without ThT.

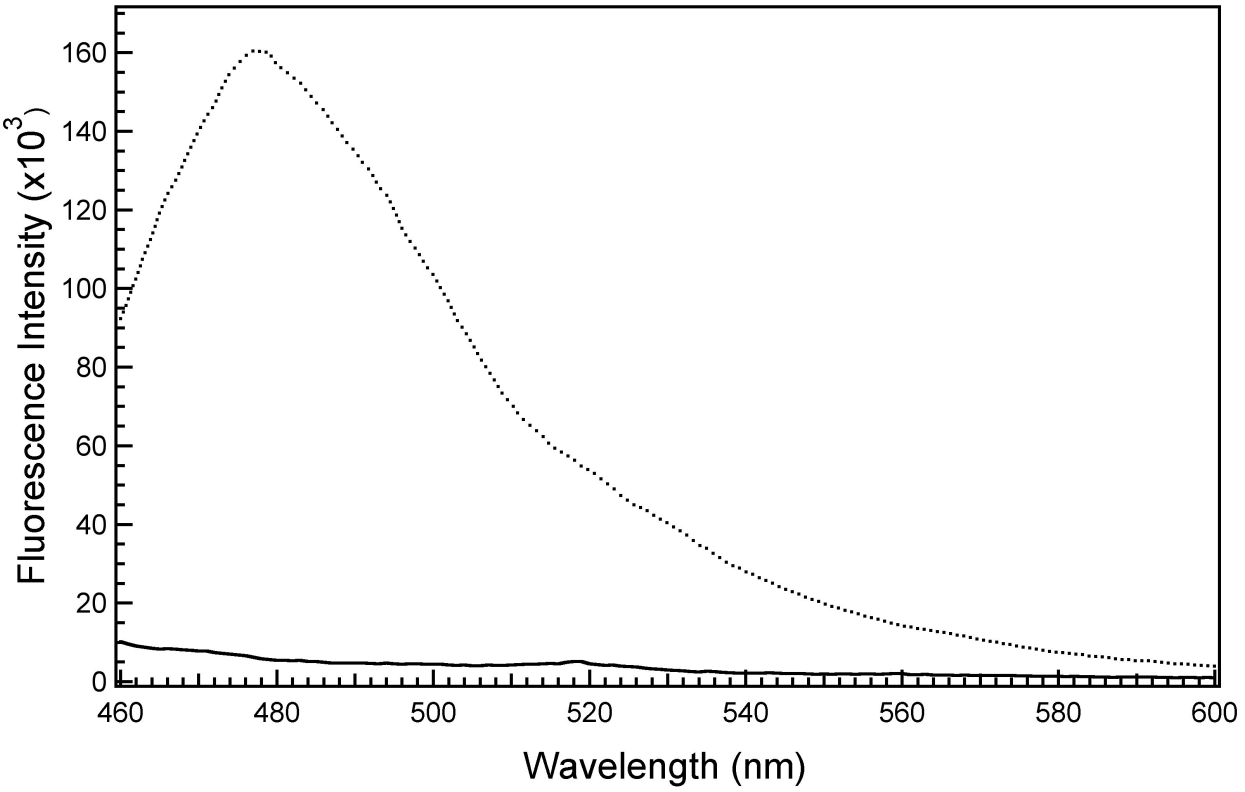

Figure 2.13. Comparison of the CD spectra of induced fibrils of lysozyme and non-treated lysozyme. The upper panel (A) is induced fibrils; the single negative absorption peak ~220 nm is evidence of the formation of β-fibrils (*45*). The lower panel (B) is non-treated hen egg white lysozyme in phosphate buffer.

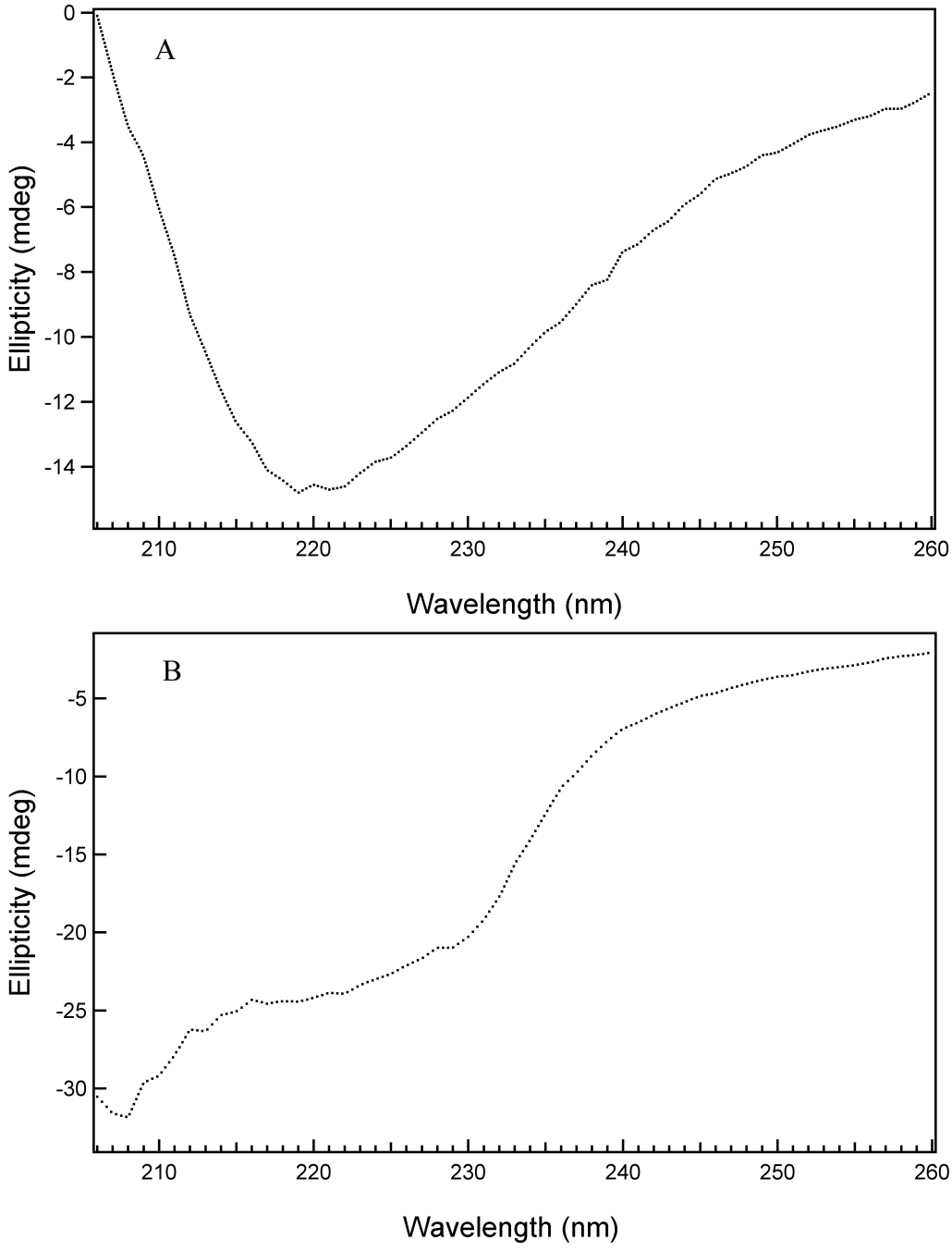

Figure 2.14. Transmission electron microscopy image of lysozyme induced fibrils. Imaged are short, wide fibrils stacking on one another.

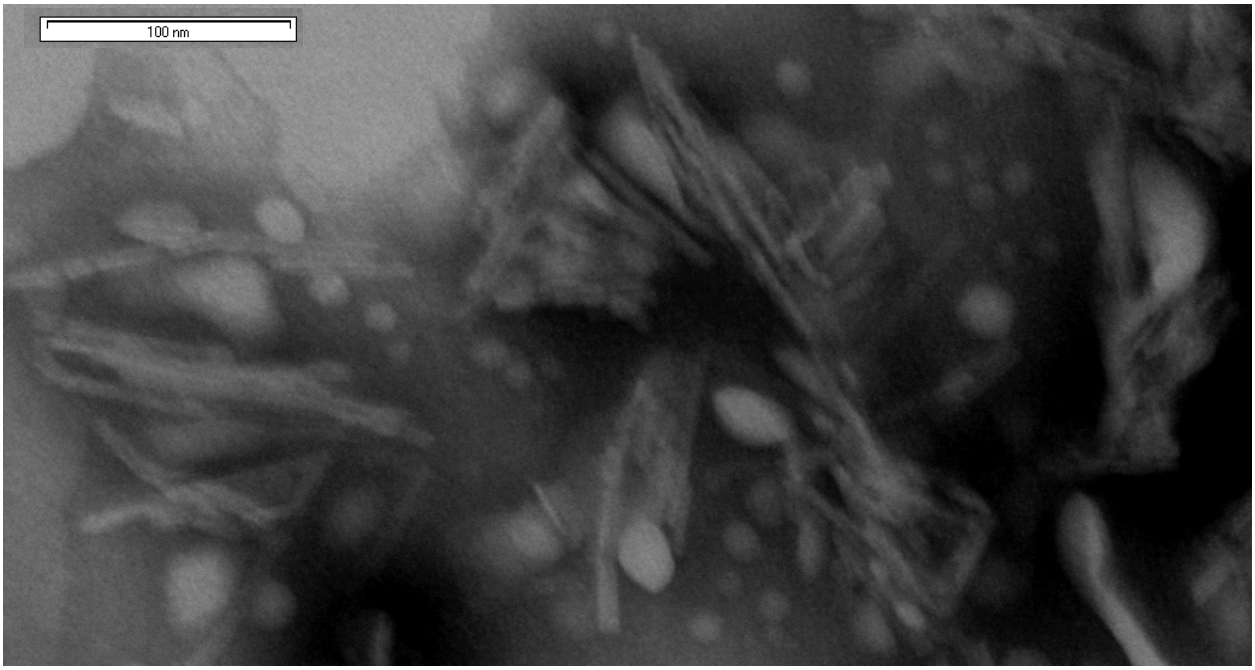

Figure 2.15. Transmission electron microscopy image of aldolase incubated with $Cu([9]aneN_3)Cl_2$. Aldolase is forming thick globules of protein upon incubation with **1**. The black area is protein with the background in gray.

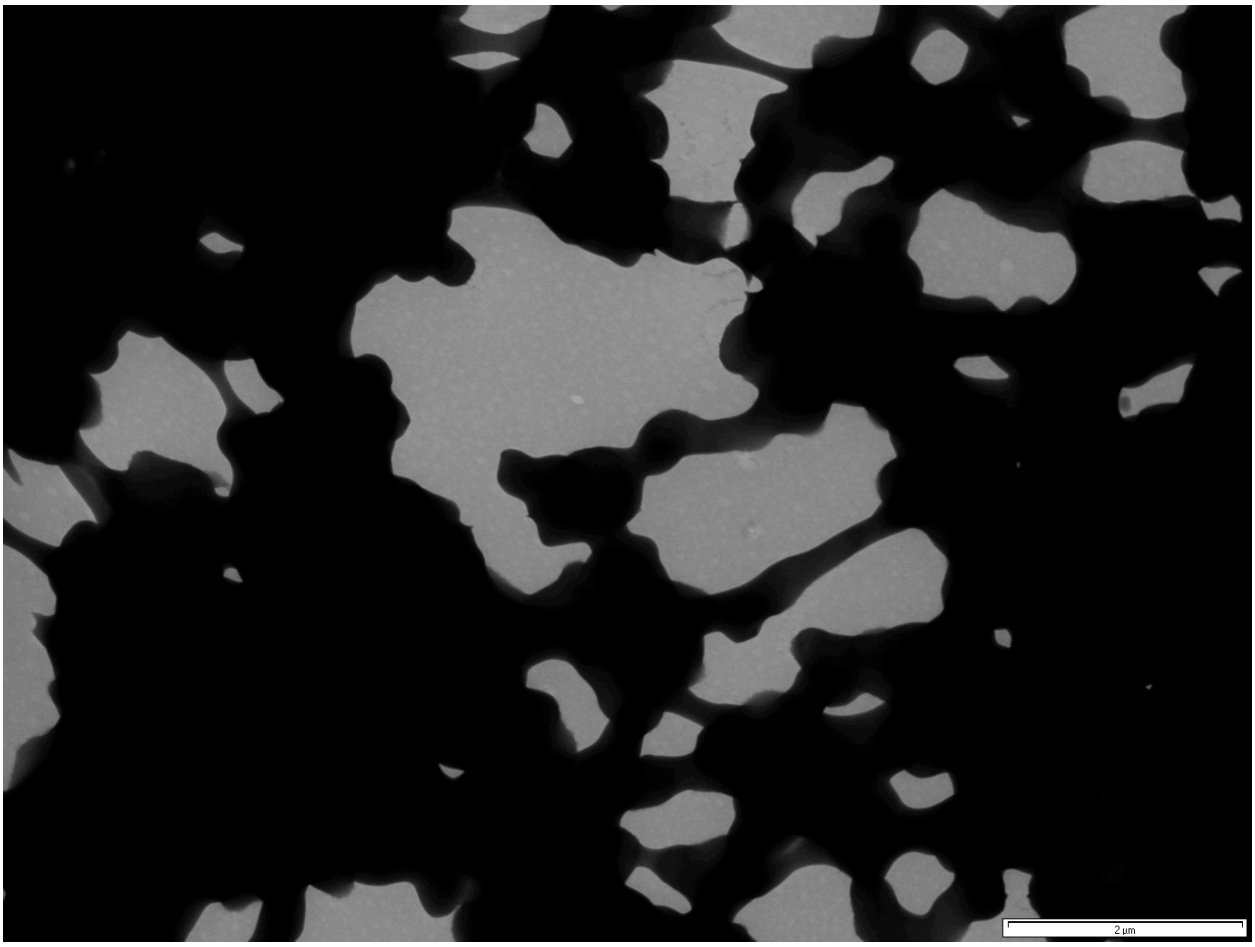

Figure 2.16. Transmission electron microscopy image of GAPDH incubated with $Cu([9]aneN_3)Cl_2$. Imaged is the beads-on-a-string morphology GAPDH adopts during incubation with **1**. The arrow is pointing to an example of the beads-on-a-string morphology.

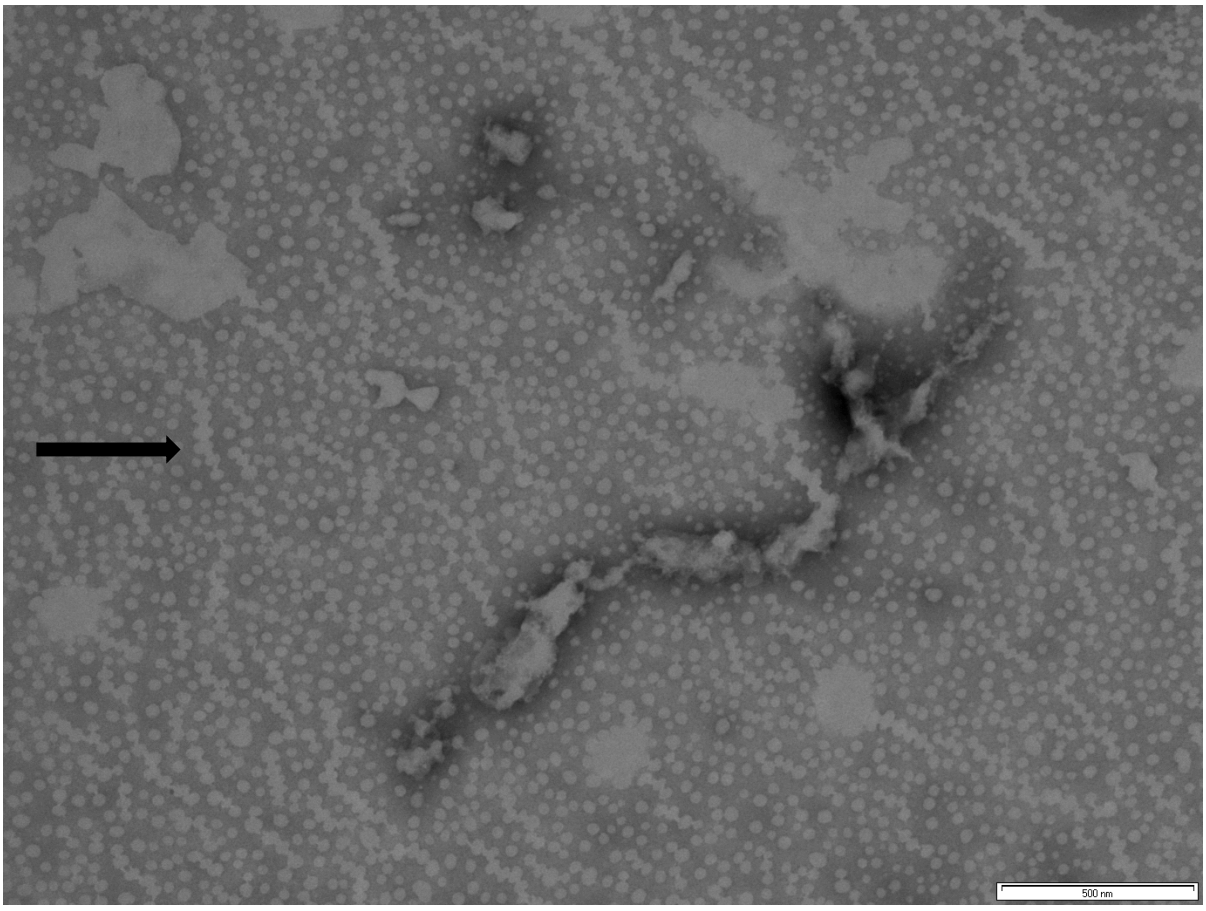

Figure 2.17. Congo Red electronic absorbance assay of BSA incubated with **1**. The solid trace (—) is the absorbance of the dye. The dotted trace (…) is the result of mixing the Congo Red dye with copper complex incubated BSA, a slight red shift to lower energy resulting upon mixing suggests the formation of possible fibrils.

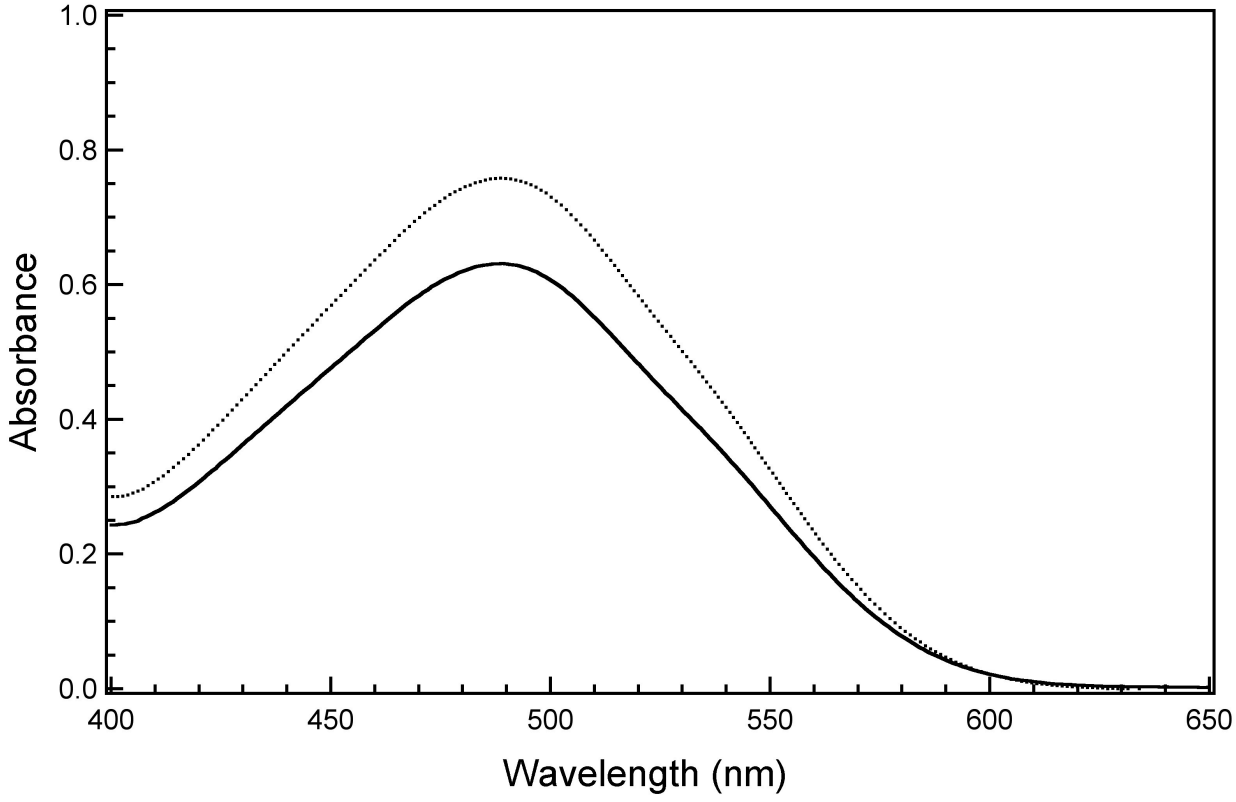

Figure 2.18. CD spectroscopy comparison of BSA in phosphate buffer to BSA incubated with Cu([9]aneN$_3$)Cl$_2$. The solid trace (—) is BSA in phosphate buffer. The dotted trace (…) is BSA after incubating with **1** for 48 hrs at 50 °C. Both BSA spectra display two virtually identical negative absorbance features at 208 and 222 nm indicating the α-helical structure of BSA is not altered during incubation with Cu([9]aneN3)Cl2.

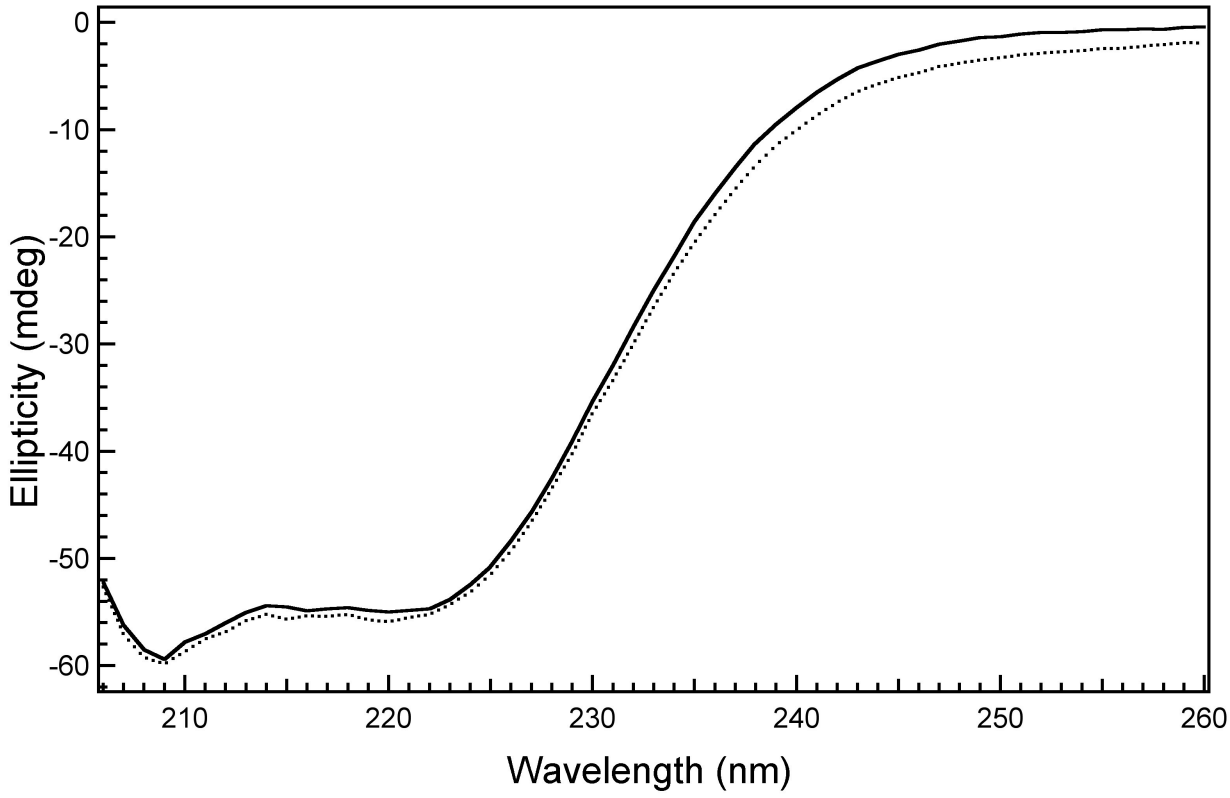

Figure 2.19. Transmission electron microscopy image of BSA incubated with Cu([9]aneN$_3$)Cl$_2$. Imaging of the incubated BSA sample reveals the protein has started to form snowflake-like aggregates.

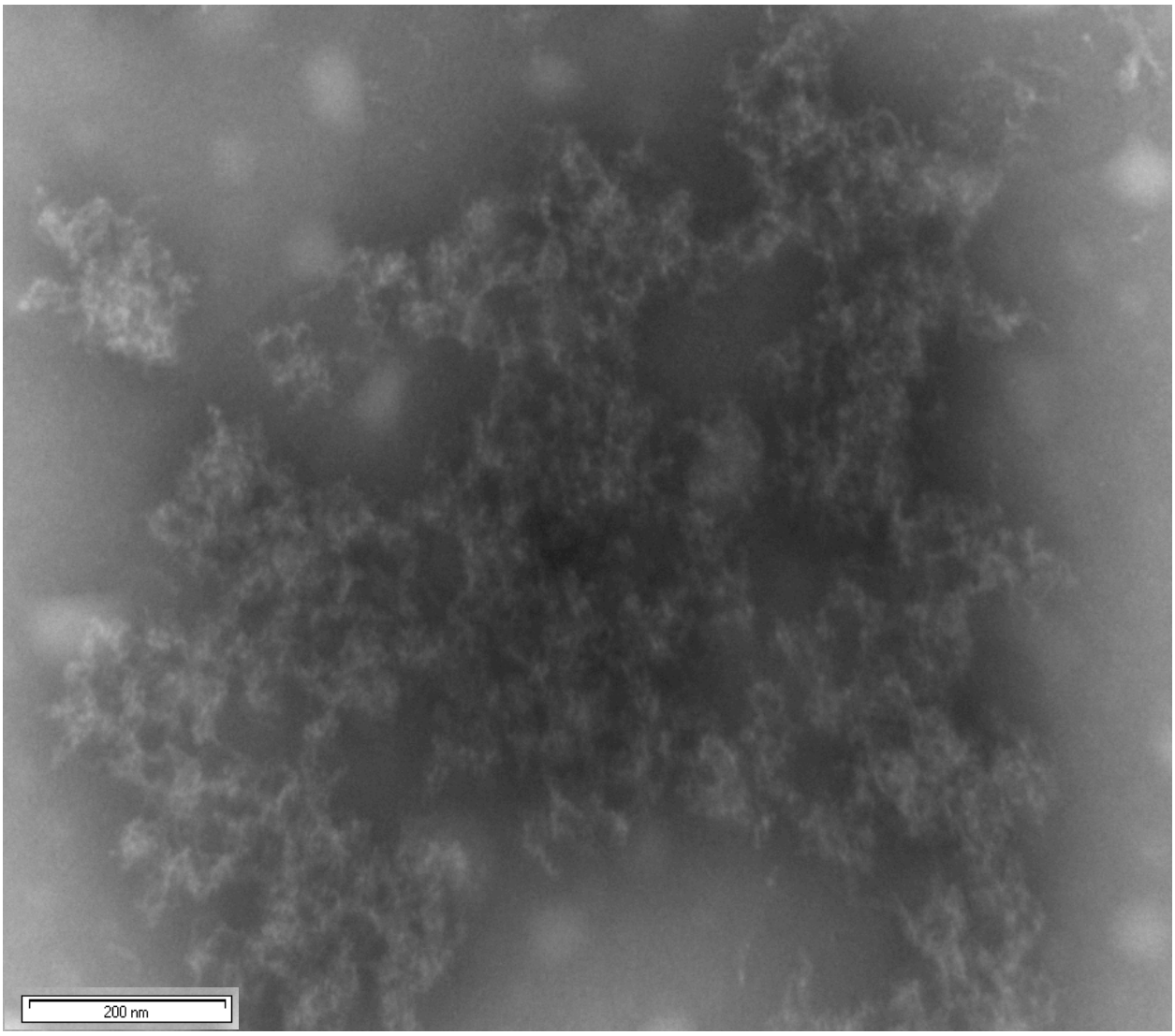

Figure 2.20. Example of the bifunctional small molecule cyclen-curcumin. The cyclen moiety chelates metals through the nitrogen atoms while the curcumin moiety is for targeting/interacting with Aβ.

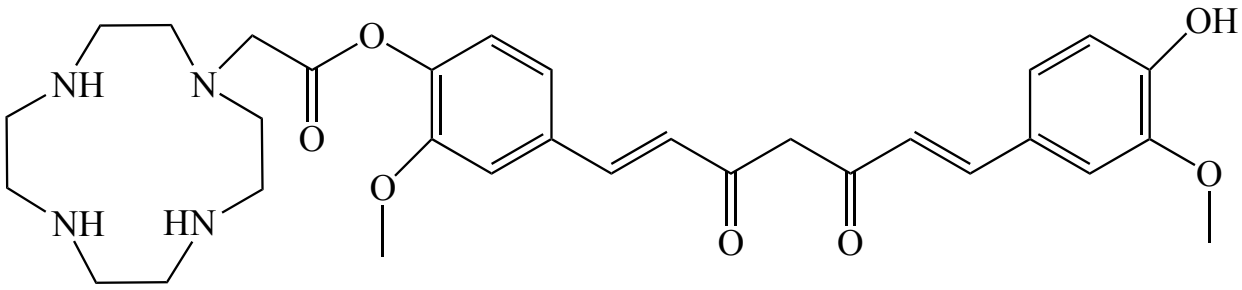

Cyclen Curcumin

Scheme 2.1. Possible mechanisms by which metal complexes promote the hydrolysis of amide bonds. Scheme taken from (*67*).

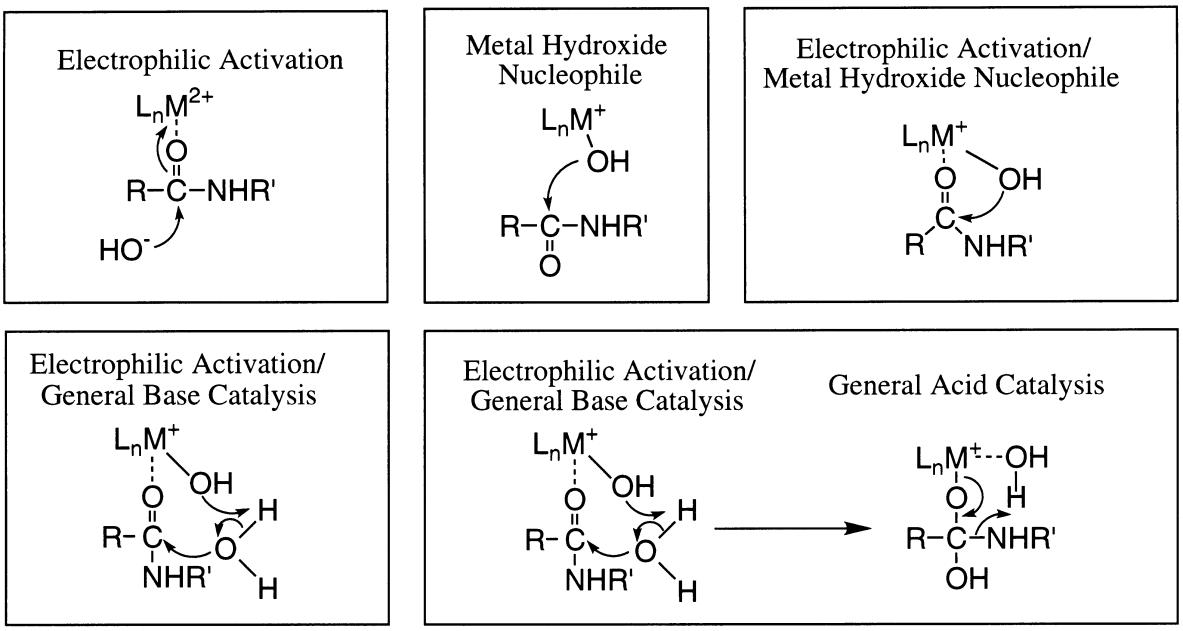

Scheme 2.2. Synthetic of $Cu([9]aneN_3)Cl_2$. Reaction of 2 mmol $CuCl_2 \cdot H_2O$ with 2 mmol TACN basified with NaOH results in the synthesis of $Cu([9]aneN_3)Cl_2$.

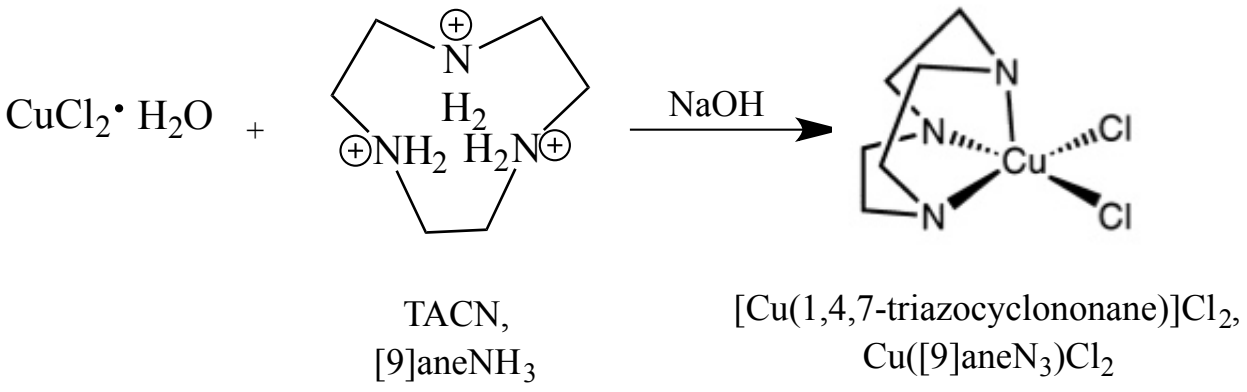

TACN,
$[9]aneNH_3$

[Cu(1,4,7-triazocyclononane)]Cl_2,
$Cu([9]aneN_3)Cl_2$

Chapter Three

Mass Spectral Characterization of *Rhodospirillum rubrum* Carbon Monoxide Oxidation Activator (CooA) Protein and *Drosophila melanogaster* Cystathionine β-Synthase (CBS)

Some data from this chapter were included in:

Su, Y.; Majtan, T.; Freeman, K. M.; Linck, R.; Ponter, S.; Kraus, J. P.; Burstyn, J. N. (2013) Comparative Study of Enzyme Activity and Heme Reactivity in *Drosophila melanogaster* and *Homo sapiens* Cystathionine β-Synthases, *Biochemistry*, *52*, 741-751.

The H/D exchange mass spectrometry experiments and data analysis were performed by Duc Tran and Jagat Adhikari in the laboratory of Professor Michael C. Fitzgerald at Duke University. The CBS expression and purification was performed by Dr. Tomas Majtan in the laboratory of Professor Jan P. Kraus at the University of Colorado. KMFP attempted in-house H/D exchange MS before expressing and purifying CooA for our collaborators at Duke University. The mass spectrometry analysis of hCBS and *Dm*CBS were performed by KMFP. This chapter was written by KMFP.

Introduction

The importance of protein allostery is reinforced by the observation that allostery is ubiquitous. Allosteric proteins possess a wide range of structures and functions all governed by a single principle: a binding event in one region of the protein is transmitted to another region, thereby modulating activity or function (*1-5*). Proteins are inherently dynamic, and this characteristic is essential for the allostery they exhibit. Allostery is more prevalent and diverse (*6*) than previously thought. In fact, many examples of allosteric regulation remain to be discovered. (*7, 8*). The new view of allosteric regulation incorporates thermodynamics and dynamics, replacing the static structure-based models (*5, 9-11*). The new view expands its definition to include: 1) proteins exist in ensembles rather than just two distinct conformational states, 2) it emphasizes allostery as a thermodynamic phenomenon, and 3) the existence of multiple conformational and dynamic states indicates multiple pathways through which energy is released from the allosteric site after a perturbation event.

One class of allosteric proteins is the heme-dependent gas sensors that respond to NO, O_2 and CO (*12-14*). An example is the heme protein carbon monoxide oxidation activator (CooA), a CO responsive transcription factor that induces the expression of a provisional CO-oxidation system found in the anaerobic CO-metabolizing bacterium *Rhodospirillum rubrum* (*15-17*). CooA is a 50 kDa homodimer with each monomer consisting of two domains: a helix-turn-helix DNA-binding domain, and a C-terminal effector-binding domain that contains a heme cofactor (Figure 3.1) (*18, 19*). Two long α-helices (termed the C-helices) form a leucine zipper/coiled-coil motif at the dimer interface of the protein. Each heme is bound by two protein-derived ligands, and changes in the identity of these ligands are associated with CO-dependent DNA-binding (Figure 3.2) (*16, 17*). In the Fe(III) state, the heme ligands are the N-

terminal proline (Pro^2), which comes from the opposite monomer of the homodimer, and a cysteine thiolate (Cys^{75}) (*20*). Upon reduction to the Fe(II) the heme undergoes a concomitant ligand switch where Cys^{75} is replaced by His^{77} and Pro^2 is retained (*21, 22*). In the Fe(II) state, the protein is poised for activation by CO, thus, CO replaces the less tightly bound Pro^2 ligand (*23-26*). CO binding concomitant with release of Pro^2 is the key event believed to be associated with the onset of DNA binding. Evidence to date suggests that the allosteric mechanism involves a structural change, including repositioning of the heme, the C-helices, and the DNA binding domain (see Figure 3.1) (*26, 27*).

Covalent-modification-coupled mass spectrometry is an excellent tool to gain knowledge about the structural and biophysical properties of proteins and protein-ligand complexes. Proteins fold into intricate three-dimensional structures in native solution conditions. However, it is important to recognize that solution-phase structures of proteins are not static. Proteins sample a gamut of conformational states in solution. An understanding of the structures, kinetics and thermodynamics involved in the conformational changes that proteins undergo in solution and during interactions with ligands is essential for gaining knowledge about the biological processes regulated by proteins. In the last decade, protein amide H/D exchange and oxidation reactions have been exploited in a number of different MS-based studies to characterize the conformational properties of proteins and protein-ligand complexes (*28-30*). Two such tools are stability of unpurified proteins from rates of H/D exchange (SUPREX) (*30-32*) and stability of proteins from rates of oxidation (SPROX) (*33, 34*). Those techniques provide a way to probe the mechanism of heme-dependent gas sensor allostery wherein binding of a small gas molecule to the heme cofactor initiates the allosteric mechanism. An advantage of the covalent-label-based mass spectrometry methods SUPREX or

SPROX is that they are sensitive to backbone amides or reactive side chains that undergo changes in solvent accessibility upon denaturation. In SUPREX, changes in H/D exchange as a function of denaturant concentration are used to extract unfolding free energies, ΔG. The SUPREX H/D exchange experiment is relatively insensitive to back exchange because the experiments are done under unfolding equilibrium conditions where dilution into a MALDI matrix or protease digestion buffer refolds the protein and protects the exchanged deuterons (Figure 3.3). Any back exchange that does occur decreases the overall change in mass, but the sensitivity of the method is such that only a few protected sites are required to obtain a SUPREX denaturation curve. Because the modified sites are protected upon refolding, SUPREX is compatible with digestion by most proteases (*32, 35*). Complementary unfolding free energies, ΔG, can be obtained using SPROX, in which limited oxidation by hydrogen peroxide is used to follow exposure of methionine residues as a function of denaturant concentration (*33, 34*). The SPROX method exploits the ease of methionine oxidization to a sulfoxide, by selectively oxidizing methionine residues that are exposed to solvent (Figure 3.4.). SPROX has several advantages: mass sensitivity, since each added oxygen atom contributes 16 mass units to the peptide in which it is located and irreversibility, since there is no potential for back exchange of the added oxygen. The hydrogen peroxide-mediated oxidation reaction is easily quenched by the addition of catalase, after which the modified protein may be digested with any desired protease. For ease of separation, immobilized catalase and proteases are employed (*30*). SUPREX and SPROX are complementary covalent-modification-coupled mass spectrometry tools being currently being used to correlate thermodynamic changes in the heme Fe(III) state with changes in protein structure and

dynamics. Ideally the SUPREX and SPROX methodologies will be expanded to include investigation of the Fe(II), Fe(II)-CO and Fe(II)-CO DNA-bound states of CooA.

Another allosterically regulated heme protein is cystathionine β-synthase (CBS). CBS is the only known enzyme to have both a pyridoxal-5'-phosphate (PLP) and a heme cofactor. The catalytic chemistry of CBS (Scheme 3.1) can be explained by a typical PLP-dependent mechanism (see Scheme 3.2) (*36*). The allosteric activator, *S*-adenosyl-L-methionine (AdoMet), increases CBS activity three-fold (*37*). The specific activity of human CBS (hCBS) for the condensation of homocysteine and serine in the canonical reaction (Scheme 3.1) is 109±4 units/mg protein compared to 424±27 units/mg protein when AdoMet is added to the reaction (*38*). It is of interest to know whether there is a connection between heme binding, enzyme activity and allosteric regulation by AdoMet. While the heme does not have a catalytic role, there is clear evidence that changes in the heme environment in hCBS affects enzymatic activity. For example, even though heme is not responsible for the catalytic chemistry, hCBS requires heme to achieve maximum activity (*39*). Furthermore, in all cases studied, disruption of the bond between the heme and its cysteine-thiolate ligand results in loss of enzyme activity (*40-45*). One plausible hypothesis is that heme and AdoMet regulation act in concert to regulate PLP affinity and enzyme activity. For example, yeast CBS (yCBS) does not bind heme and is not regulated by AdoMet (*46-48*), whereas hCBS has heme and responds to AdoMet stimulation with a 3-fold increase in activity. Yeast CBS has a significantly lower *in vitro* affinity for PLP than hCBS, and an hCBS variant with the heme binding N-terminal domain deleted exhibits a similarly low affinity for PLP (*39, 48*). Despite these correlations, the exact function of heme in CBS remains unknown.

To determine if there is a connection between heme binding, enzyme activity and

AdoMet regulation, response to AdoMet stimulation was probed in CBS of *Drosophila melanogaster* (*Dm*CBS). *Dm*CBS is similar to yet different from hCBS. Unlike hCBS, which is a tetramer, *Dm*CBS is a dimer as shown by X-ray crystallography (*49*) and native gel electrophoresis. The catalytic core region (residues 40–380) of *Dm*CBS exhibits high sequence similarity (85% homology, 62% sequence identity) to hCBS; the C-terminal domain (residues 381–522) of *Dm*CBS is almost the same size as that of hCBS but is less conserved (59% homology, 24% sequence identity); and the N-terminal domain (residues 1–39) of *Dm*CBS is significantly shorter, but does contain analogous residues to those that serve as heme ligands in hCBS (Figure 3.5). In the recently reported crystal structures of *Dm*CBS, heme indeed is coordinated to Cys^{22} and His^{34} (analogous to Cys^{52} and His^{65} in the human enzyme). Although the *Dm*CBS crystal structure does not contain AdoMet we analyzed the *Dm*CBS enzyme by mass spectrometry to determine whether or not the enzyme is purified with or binds to the allosteric regulator AdoMet.

Materials and Methods

Materials. Unless otherwise stated, all chemicals used were purchased from Sigma-Aldrich and were used as received.

Expression and Purification of CooA. Briefly, *E. coli* VJS6737 (*50*) bearing the pEXT20 expression vector containing the CooA gene (*51*) was cultivated in rich medium supplemented with 40 μM ferric citrate. Protein expression was induced by addition of isopropyl β-D-thiogalactopyranoside (IPTG) to 7 μM (final concentration), and cells were incubated for 18-20 h at 28°C. Cells were pelleted by centrifugation (10,000 x *g*, 10 min), resuspended in lysis buffer (50 mM MOPS, pH 7.5, 500 mM KCl and 0.5 mM DTT) and lysed by passage through a French press. A Ni-NTA column (Qiagen, 8 mL resin volume) was pre-equilibrated with 10 mM imidazole, 50 mM MOPS pH 7.5, 500 mM KCl. The cell supernatant (30 mL) was applied slowly, and the column was washed successively with 10 mM imidazole (2 column volumes) and 50 mM imidazole (1 column volume), in the same buffer. Finally, protein was eluted by addition of 220 mM imidazole. The protein was precipitated at 55%-saturated $(NH_4)_2SO_4$ (v/v) with incubation on ice for 30 minutes and brief centrifugation. The protein pellet was dissolved in 500 μL 25 mM MOPS, pH 7.4 and 500 mM KCl, applied to a buffer-equilibrated Sephadex G-25 column, and eluted in the same buffer. The desalted protein was stored at -80 °C. Protein concentrations were determined using the BCA method (Pierce, Rockford, IL); SDS-PAGE verified protein purity was >90%; heme content was determined using the pyridine hemochromogen assay (*52*).

The expression and purification of CooA for use in the H/D exchange unfolding experiments was the same as above except the protein pellet was solubilized and buffer-

equilibrated in 25 mM MES, pH 7.4, 100 mM NaCl. For the SPROX mass spectrometry experiments, the CooA protein was buffered exchanged using a Sephadex G-25 column into 30 mM phosphate buffer, pH 7.1 with 50 mM NaCl. Following determination of protein concentration by the BCA method (Pierce, Rockford, IL) and verification of protein purity with SDS-PAGE, protein samples were flash-frozen with liquid nitrogen. Frozen CooA protein samples were shipped on dry ice to Duke University for SUPREX and SPROX mass spectrometry analysis.

Mass Spectrometry of CooA. A pre-packed 10 mL Sephadex G-25 column (Pharmacia Biotech AB Uppsala, Sweden) was equilibrated with 10 mM ammonium acetate (NH_4Ac). As-isolated CooA (30 µL) was loaded on the column (13 µg/µL protein in 25 mM MOPS pH 7.4, 500 mM KCl). The sample was buffer exchanged using gravity and eluted in 10 mM NH_4Ac. The eluted sample was either stored on ice for immediate analysis or stored at – 80 °C until analyzed.

Mass spectrometry data were acquired using a 7T linear trap/FT-ICR (LTQ FT Ultra) hybrid mass spectrometer (Thermo Scientific Inc., Bremen, Germany) equipped with an automated chip-based nano-ESI source (Triversa NanoMate, Advion BioSciences, Ithaca, NY). The spray voltage was 1.3-1.7 kV relative to the inlet of the mass spectrometer. To aid ionization samples were mixed with acetonitrile (ACN) and acetic acid, 1% acetic acid in 60:40 HPLC-grade ACN to 10 mM NH_4Ac, prior to analysis.

SUPREX Mass Spectrometry Analysis of CooA. Denaturant stocks of 8 M and 0 M guanidine hydrochloride (GdnHCl) were prepared in 25 mM MES. The GdnHCl buffers were prepared using serial dilutions from the 0 M and 8 M GdnHCl stocks. Deuteration of the GdnHCl buffers

was achieved by dissolving 19 g guanidine hydrochloride in 25 mL D_2O. The final GdnHCl concentration was calculated using a refractometer for refractive index and Nozaki's equation (*53*). Samples were prepared by diluting 2 μL of 23 μM CooA protein into 16 μL SUPREX buffer with [GdnHCl] of 0, 1.27, 2.27, 3.24, 3.74, 4.27, 4.64, 5.27, 5.76, 6.25, 6.75 and 7.81 M. After 3 days of incubation in the SUPREX buffer 2 μL of sample was quenched with 6 μL 1M HCl. The sample was digested with 1.4 μg pepsin for 1 minute followed by the addition of 2,5-dihydrobenzoic acid matrix. MALDI mass spectra were collected on a Voyager DE Biospectrometry Workstation (Perspective Biosystems, Inc., Framingham, MA) in linear mode using a nitrogen laser (337 nm).

SPROX Mass Spectrometry Analysis of CooA. We modified the published SPROX protocol (*54*) to analyze Fe(III) CooA. The denaturing buffer was prepared with 30 mM phosphate buffer, pH 7.1, 50 mM NaCl containing an increasing gradient of denaturant ranging from 0 to 5.6 M GdnHCl. Specifically, 8 μL aliquots of denaturant buffers were prepared with GdnHCl concentrations: 0, 1.4, 2.0, 2.5, 2.9, 3.2, 3.6, 3.8, 4.3, 4.7, 5.2 and 5.6 M. To each aliquot of denaturant buffer 170 pmols of Fe(III) CooA was added and allowed to incubate at room temperature for 2.5 hours. The SPROX reaction was initiated by adding 1 μL of 9.8 M (30% wt/wt) H_2O_2. After 3 minutes the reaction was quenched by the addition of 200 μL of 300 mM L-methionine. An overnight tricholoracetic acid (TCA) precipitation was performed with 200 μL of 100% TCA solution. To pellet the protein the samples were centrifuged for 30 minutes. The supernatant was discarded and the pellet was washed twice with ethanol. Upon evaporation of ethanol, 10 μL of 0.1% RapiGest (Waters, Milford, MA) in 50 mM NH_4HCO_3, pH 8.0 was added. RapiGest is a surfactant that unfolds proteins so the sites of enzymatic cleavage are

freely accessible for digestion. Pellets were suspended with two rounds of vortexing and sonication for 10 minutes. Disulfide bonds in the samples were reduced with 10 mM DTT followed by alkylation with 20 mM iodoacetamide. Samples were digested overnight at 37 °C with 0.5 μg of trypsin. Following trypsinolysis, mass spectrometry data was acquired using a Q-TOF mass spectrometer (Agilent, Santa Clara, CA) equipped with a Chip Cube interface and an autosampler.

Cloning of DmCBS. The *Dm*CBS sequence was subcloned into a pGEX-6P1 vector following a similar strategy to that used for the human CBS expression construct (*55*). The resulting pGEX-6P1-DMCBS enabled us to express *Dm*CBS as a fusion protein with glutathione-S-transferase (GST), from which GST could be cleaved off with HRV 3C protease (AG Scientific) leaving a single extra residue (Gly) at the N-terminus of *Dm*CBS polypeptide. Briefly, the *Dm*CBS sequence was amplified by PCR from a first strand cDNA using a forward primer containing an ApaI site (5′- ctagGGGCCCcaaccgaagccatacgagagg) and a reverse primer containing a NotI site (5′-ctagGCGGCCGCgatcagaactggagaacgc). After cleavage with ApaI and NotI (NEB Biolabs), the *Dm*CBS fragment was purified and isolated by excision from a 1% agarose gel, and cleaned up using QIAquick gel extraction kit (Qiagen). Subsequently, *Dm*CBS was ligated into the ApaI-NotI linearized pGEX-6P1 vector, in which an internal ApaI site was abolished previously by site directed mutagenesis (*55*). The construct pGEX-6P1-DMCBS was transformed into *E. coli* XL1-Blue cells (Stratagene) and its authenticity was confirmed by DNA sequencing. Verified plasmid was transformed into *E. coli* Rosetta2 (DE3) expression host cells (Novagen).

Expression and Purification of CBS. Human CBS (hCBS) was expressed and purified as described previously (*56*). *Dm*CBS was purified in an otherwise identical fashion with the following specific modifications. After cleavage of the fusion protein with HRV 3C protease, GST was removed chromatographically on DEAE Sepharose Fast Flow (GE Healthcare). The column was equilibrated in 15 mM potassium phosphate pH 7.2, 1 mM EDTA, 1 mM DTT and 10% ethylene glycol. Under these conditions, both GST and *Dm*CBS proteins bind to the DEAE Sepharose resin. The separation of the GST from *Dm*CBS was achieved by elution with a linear gradient from 15 to 75 mM potassium phosphate pH 7.2, 1 mM EDTA, 1 mM DTT and 10% ethylene glycol. Unlike hCBS, *Dm*CBS elutes prior to the GST. Protein-containing fractions were analyzed by electrophoresis on 9% SDS–PAGE. The *Dm*CBS-rich fractions were pooled and subsequently concentrated on YM-30 membrane (Millipore). The buffer was exchanged by pressure dialysis to 20 mM HEPES pH 7.4, 1 mM TCEP and 0.01% Tween 20.

Mass Spectrometry of CBS. As-isolated and AdoMet-treated *Dm*CBS and hCBS were analyzed by mass spectrometry for the presence of AdoMet. Proteins were diluted directly into 0.1% acetic acid in 5:95 (v:v) methanol/water. AdoMet-treated *Dm*CBS and hCBS were diluted into and incubated with 0.36 mM AdoMet in 200 mM Tris (pH 8.6) buffer at 37°C for 20 min. All samples were then desalted at room temperature using two consecutive detergent removal spin columns (Pierce, Rockford, IL) according to manufacturer instructions. Columns were pre-equilibrated with 0.1% acetic acid in 5:95 methanol/water, and the CBS samples were eluted off the column into the same solvent. Prior to mass spectrometry analysis, the CBS samples were diluted with acetic acid and methanol to achieve 1% acetic acid in 50:50 (v:v) methanol/aqueous sample. Mass spectrometry data were acquired using a 7T linear trap/FT-

ICR (LTQ FT Ultra) hybrid mass spectrometer (Thermo Scientific Inc., Bremen, Germany) equipped with an automated chip-based nano-ESI source (Triversa NanoMate, Advion BioSciences, Ithaca, NY). The spray voltage was 1.3-1.5 kV relative to the inlet of the mass spectrometer.

Results

Mass Spectral Characterization of CooA To determine sample-handling conditions for CooA the as-isolated protein was analyzed by mass spectrometry. The sample requires a 60:40 ratio of acetonitrile to 10 mM NH_4Ac with 1% acetic acid to maintain a steady ionization current. The ion trap (IT) mass spectrum is shown in Figure 3.6A. Upon ionization the heme cofactor dissociates resulting in a mass peak at 616. The predominant mass peak from the IT spectrum, 980, was isolated for Fourier transform (FT) analysis. Figure 3.6B. displays the isotopic distribution of the 980 mass peak resulting from FT. The FT data reveals a mass of 25463 Da for a single 7-histidine-tagged CooA monomer (calculated mass 254478 Da). These data reveal the use of a Sephadex G-25 column as an efficient means to desalt the as-isolated protein without precipitation or loss of sample during mass spectrometry sample preparation.

SUPREX Mass Spectrometry Analysis of CooA To explore the thermodynamics of CooA's conformation stability the protein was analyzed by SUPREX. Establishing experimental conditions for the analysis of CooA was challenging. The high salt concentration in the standard CooA purification buffer (500 mM KCl, 25 mM MOPS, pH 7.4) interfered with MALDI detection of protein signal after H/D exchange. Therefore, CooA was purified in 100 mM NaCl, 25 mM MES, pH 7.4 to determine if decreasing the salt concentration yielded a better MALDI signal. When 2,5-dihydroxybenzoic acid was used as the matrix rather than sinapinic acid there was detectable protein signal. Because CooA is a multidomain protein the samples were digested with pepsin after the H/D exchange step to generate peptide fragments from the different domains. The purpose of the SUPREX experiment was to probe the thermodynamic properties of the global unfolding/refolding events. To probe an individual

protein domain unfolding/refolding event using SUPREX with protease digestion, the domain must undergo a large motion (i.e., exposure/burial of a substantial area of the protein). Peptides from regions of a protein's structure that undergo relatively small motion (i.e., only local unfolding) do not exhibit a denaturant dependent H/D exchange behavior in the SUPREX with protease digestion experiment. Figure 3.7 displays the SUPREX curves data from Fe(III) CooA after a 3-day H/D exchange. Two peptides from the DNA-binding domain were identified to undergo large changes in exposure/burial of surface area resulting in denaturant-dependent H/D exchange. From these curves the $C^{1/2}$ (the concentration of guanidine hydrochloride at the transition midpoint) values of 4.4 and 4.5 M GdnHCl were determined. The $C^{1/2}$ values were used to estimate a ΔG of 64 kJ/mol for the DNA-binding domain.

SPROX Mass Spectrometry Analysis of CooA Surveying the thermodynamics of Fe(III) CooA, the protein was analyzed by SPROX. While all methionine residues within a protein are susceptible to oxidation, SPROX probes the buried methionine residues. Just like the H/D exchange rates of globally protected amide protons in SUPREX, the oxidation rates of the globally protected methionine residues in SPROX are denaturant dependent. Analysis of the SPROX data revealed oxidation of Met^{124} from the helix rod connecting the DNA-binding and heme domains. The peptide was found to have a $C^{1/2}$ of 4.2 M, from which a ΔG of 28.65 kJ/mol may be estimated (Figure 3.8).

Mass Spectral Characterization of CBS To test whether *Dm*CBS binds to AdoMet, as-isolated and AdoMet-treated *Dm*CBS samples were analyzed by mass spectrometry. Ion trap mass spectra of *Dm*CBS, with and without preincubation with AdoMet, are shown in Figure 3.9. The

Fourier transform data (Figure 3.10) reveal a mass of 56870 Da for the *Dm*CBS protein; the calculated mass of the heme-free protein is 56882 Da. From these data, it is evident that heme dissociates upon ionization; furthermore, free heme may be seen in the mass spectrometry data and appears as a characteristic mass peak at 616 (FePPIX calculated mass 616.48). Control AdoMet solutions under similar experimental conditions exhibit a peak at m/z 399 (AdoMet calculated mass 398.14). Contrasting with the heme dissociation neither *Dm*CBS sample showed a mass peak at 399, demonstrating that *Dm*CBS does not bind to AdoMet and suggesting that *Dm*CBS is not natively isolated with the same allosteric effector as hCBS. Incubating *Dm*CBS with an excess of AdoMet did not result in binding, evidenced by lack of a mass peak at 399, the mass of AdoMet, indicating *Dm*CBS is not responsive to AdoMet stimulation. A similar mass spectrometric analysis was performed using hCBS as a control, since hCBS is known to bind AdoMet. The AdoMet mass peak was absent in the as-isolated hCBS spectrum, but present in the AdoMet-treated hCBS spectrum (data not shown). These results confirm that *Dm*CBS and hCBS are purified free of AdoMet; moreover, they demonstrate that upon incubation with AdoMet, hCBS was capable of binding AdoMet whereas *Dm*CBS was not, even under saturating conditions (i.e. [AdoMet] >> [*Dm*CBS]).

Discussion

Previous work has characterized CooA's three distinct conformations, Fe(III), Fe(II), and Fe(II)-CO, by measurement of their structural stabilities using guanidine hydrochloride (GdnHCl) denaturation (*57*). Using visible absorption, fluorescence and CD spectroscopies, Lee *et al.* (*57*) identified independent unfolding processes for each domain of CooA. All 3 CooA coordination states (Fe(III), Fe(II), and Fe(II)-CO) undergo unfolding of the DNA-binding domain between 2 and 3 M GdnHCl with a free energy of unfolding of ~17 kJ/mol. Unfolding of the heme domain is variable and dependent on the heme coordination state. Between 3 and 4 M GdnHCl, the heme domain unfolds and the protein reaches a second intermediate conformation. The free energy of heme domain unfolding is ~26 kJ/mol. Concentrations above 4 M GdnHCl, result in the final unfolding of the effector domain and dissociation of the monomers, with a free energy of ~54 kJ/mol. Our goal is to understand how CO binding to heme induces the change in protein conformation using mass spectrometry techniques to probe the dynamics of CooA.

CooA requires high salt concentration to stabilize the protein in solution therefore, the protein is purified in 500 mM KCl, 25 mM MOPS at pH 7.4. The high salt concentration presents a problem for mass spectrometry, since all the salt must be removed from the sample prior to analysis. Further, not only does CooA require high salt concentration, CooA also tends to stick to surfaces, a phenomenon compounded during the removal of salt from the protein. Use of a C4 column such as the commercially available Bruker-Michrom MicroTrap^{TM} column results in protein precipitation and loss of protein sample. The process of desalting the protein with the MicroTrap column appeared to increase the protein's affinity for the column in preference to any elution solution tested. A combination of methanol/water, acetonitrile/water

and gradients of ammonium acetate were tested as elution solutions. When using the Bruker-Michrom MicroTrap^{TM} C4 trap column, removal of CooA from the column requires column flushing with 70:30 formic acid to isopropyl alcohol; extremely harsh conditions that result in denaturation of the protein. To avoid loss and denaturation of CooA during sample preparation a Sephadex G-25 column was used for buffer exchange and desalting. Considering CooA's solubility in high salt conditions, ammonium acetate, a volatile salt at low pressure, is used for buffer exchange and desalting. Figure 3.6 provides evidence using a Sephadex G-25 column with ammonium acetate elution results in successful desalting of as-isolated CooA.

Successful sample preparation procedures were followed by initial attempts at using H/D exchange in collaboration with Michael C. Fitzgerald's research group at Duke University. The goal is to use H/D exchange and oxidation-based mass spectrometry measurement methods to probe the structure, dynamics and thermodynamics of Fe(III) CooA. The techniques SUPREX and SPROX allow the measurement and correlation among thermodynamic and structural changes associated with the relevant CooA states: Fe(III), Fe(II), Fe(II)-CO and Fe(II)-CO DNA-bound. Preliminary SUPREX data identify DNA-binding domain peptides with similar $C^{1/2}$ values of ~4.5 M GdnHCl that estimate a ΔG of 64 kJ/mol. The preliminary SPROX unfolding data reveal oxidation of Met^{124}, located in the helix rod connecting the DNA- and heme-binding domains, resulting in $C^{1/2}$ values of ~4.2 M GdnHCl, an estimated ΔG of 28.65 kJ/mol. The preliminary covalent-modification-based mass spectrometry results provide more evidence the DNA-binding and heme-binding domains of CooA are independently folded domains (*57*). It remains to be seen if changes in relative position and/or mobility of those domains regulate CooA activity. More work is required to understand the

thermodynamic and structural changes associated the states of CooA; our work with the Fitzgerald laboratory is ongoing.

*Dm*CBS contains heme but does not respond to AdoMet stimulation, suggesting that these two characteristics are not correlated with one another. *Dm*CBS is isolated as a heme-containing protein; the crystal structure reveals that His^{34} and Cys^{22} are ligands to the heme, with the guanidinium group of Arg^{235} and the amide backbone ofTrp^{24} within hydrogen bonding distance of the Cys^{22} thiolate moiety (*58*). This coordination sphere and associated hydrogen bonding network, as well as the spectral characteristics of Fe(III)*Dm*CBS reported by Su *et al* (*38*), are essentially identical to those of Fe(III)hCBS. *Dm*CBS is active in all three reactions (Scheme 3.1) tested, but the enzyme does not respond to AdoMet stimulation in catalyzing any of these reactions. In this regard, *Dm*CBS is more like yeast CBS, which also does not respond to AdoMet stimulation. The lack of response to AdoMet, combined with the fact that *Dm*CBS contains heme, suggests that heme and AdoMet are not functionally or evolutionarily connected.

The reported evidence herein reveal that *Dm*CBS does not bind AdoMet. There are multiple reasons why this CBS enzyme may appear unresponsive to AdoMet stimulation: 1) it may be unable to bind AdoMet; 2) it may be locked in a conformation that cannot be activated even though AdoMet binds, or 3) it may have a high affinity for AdoMet such that the molecule is always bound and it therefore does not respond to exogenous AdoMet but remains stimulated or hyperactive. For example, the C431S variant of hCBS is not activated by AdoMet because it does not bind AdoMet (*59*). However, the hCBS S466L variant binds AdoMet, but because this variant enzyme is constitutively activated, its activity does not increase in response to AdoMet binding (*60*). Yeast CBS is more similar to S466L hCBS, where constitutively high activity is

paired with high AdoMet binding affinity but no AdoMet-dependent activation (*61, 62*). There is no example yet known of a CBS protein where AdoMet is tightly bound at all times. No evidence of AdoMet was seen in the *Dm*CBS crystal structure (*58*); furthermore, when an AdoMet molecule was docked into the C-terminal domain of the protein, there was insufficient space to accommodate the AdoMet molecule (*58*). Thus, *Dm*CBS is not crystallized with a tightly bound AdoMet molecule and the crystallography implies that AdoMet may not bind at all. Our mass spectrometry experiments confirm *Dm*CBS is isolated free of any tightly-bound AdoMet molecule. In addition, we see no evidence of AdoMet-binding when *Dm*CBS is incubated with AdoMet. These results suggest that the high activity of *Dm*CBS is an intrinsic property of the enzyme and not a consequence of the enzyme being saturated by AdoMet when isolated. The mass spectroscopy results suggest that *Dm*CBS does not respond to AdoMet stimulation because the enzyme cannot bind AdoMet; however, we cannot rule out low affinity binding that does not survive the sample preparation procedures.

Future Directions

Carbon monoxide oxidation activator (CooA), is an allosterically regulated CO responsive transcription factor found in the anaerobic CO-metabolizing bacterium *Rhodospirillum rubrum*. Our goal is to elucidate the thermodynamics and dynamics of CooA. The application of mass spectrometry techniques to CooA has been challenging due to CooA's affinity for salt; the presence of salt interferes with ionization and data analysis. We utilize concentrated samples of CooA to ensure there is enough protein to generate a signal at the detector. Additional experiments are needed to determine if we are using enough guanidinium hydrochloride to unfold CooA. In conjunction with Fitzgerald group at Duke University, we have preliminary evidence that the DNA-binding and heme-binding domains of CooA are independently folded domains. Due to CooA's high affinity for salt, not surprising since CooA is a DNA binding protein, spectroscopic techniques, such as spin-labeling EPR, that permit the use of salt, may offer a more appropriate option for elucidating the thermodynamics and dynamics of CooA.

References

1. Monod, J., Changeux, J. P., and Jacob, F. (1963) Allosteric proteins and cellular control systems, *J. Mol. Biol. 6*, 306-329.
2. Swain, J. F., and Gierasch, L. M. (2006) The changing landscape of protein allostery, *Curr. Opin. Struct. Biol. 16*, 102-108.
3. Cui, Q., and Karplus, M. (2008) Allostery and cooperativity revisited, *Protein Sci. 17*, 1295-1307.
4. Goodey, N. M., and Benkovic, S. J. (2008) Allosteric regulation and catalysis emerge via a common route, *Nat. Chem. Biol. 4*, 474-482.
5. Tsai, C.-J., del Sol, A., and Nussinov, R. (2009) Protein allostery, signal transmission and dynamics: a classification scheme of allosteric mechanisms, *Molecular Biosystems 5*, 207-216.
6. Kuriyan, J., and Eisenberg, D. (2007) The origin of protein interactions and allostery in colocalization, *Nature 450*.
7. Lindsley, J. E., and Rutter, J. (2006) Whence cometh the allosterome?, *Proc. Natl. Acad. Sci. USA 103*, 10533-10535.
8. Gunasekaran, K., Ma, B., and Nussinov, R. (2004) Is allostery an intrinsic property of all dynamic proteins?, *Proteins: Struct., Funct., Bioinfo. 57*, 433-443.
9. Kern, D., and Zuiderweg, E. R. P. (2003) The role of dynamics in allosteric regulation, *Curr. Opin. Struct. Biol. 13*, 748-757.
10. Cooper, A., and Dryden, D. T. F. (1984) Allostery without conformational change. A plausible model, *Eur. Biophys. J. 11*, 103-109.

11. Tsai, C.-J., del Sol, A., and Nussinov, R. (2008) Allostery: Absence of a Change in Shape Does Not Imply that Allostery Is Not at Play, *J. Mol. Biol. 378*, 1-11.

12. Jain, R., and Chan, M. K. (2003) Mechanisms of ligand discrimination by heme proteins, *J. Biol. Inorg. Chem. 8*, 1-11.

13. Ascenzi, P., Bocedi, A., Leoni, L., Visca, P., Zennaro, E., Milani, M., and Bolognesi, M. (2004) CO sniffing through heme-based sensor proteins, *IUBMB Life 56*, 309-315.

14. Gilles-Gonzalez, M.-A., and Gonzalez, G. (2005) Heme-based sensors: defining characterstics, recent developments, and regulatory hypotheses., *J. Inorg. Biochem. 99*, 1-22.

15. Shelver, D., Kerby, R. L., He, Y., and Roberts, G. P. (1995) Carbon monoxide-induced activation of gene expression in Rhodospirillum rubrum requires the product of cooA, a member of the cyclic AMP receptor protein family of transcriptional regulators, *J. Bacteriol. 177*, 2157-2163.

16. Aono, S. (2003) Biochemical and Biophysical Properties of the CO-Sensing Transcriptional Activator CooA, *Acc. Chem. Res. 36*, 825-831.

17. Roberts, G. P., Kerby, R. L., Youn, H., and Conrad, M. (2005) CooA, a paradigm for gas sensing regulatory proteins, *J. Inorg. Biochem. 99*, 280-292.

18. Shelver, D., Kerby, R. L., He, Y., and Roberts, G. P. (1997) CooA, a CO-sensing transcription factor from *Rhodospirillum rubrum*, is a CO-binding heme protein, *Proc. Natl. Acad. Sci. USA 94*, 11216-11220.

19. Lanzilotta, W. N., Schuller, D. J., Thorsteinsson, M. V., Kerby, R. L., Roberts, G. P., and Poulos, T. L. (2000) Structure of the CO sensing transcription activator CooA, *Nature Struct. Biol. 7*, 876-880.

20. Reynolds, M. F., Shelver, D., Kerby, R. L., Parks, R. B., Roberts, G. P., and Burstyn, J. N. (1998) EPR and Electronic Absorption Spectroscopies of the CO-Sensing CooA Protein Reveal a Cysteine-Ligated Low-Spin Ferric Heme, *J. Am. Chem. Soc. 120*, 9080-9081.

21. Aono, S., Ohkubo, K., Matsuo, T., and Nakajima, H. (1998) Redox-controlled ligand exchange of the heme in the CO-sensing transcriptional activator CooA, *J. Biol. Chem. 273*, 25757-25764.

22. Shelver, D., Thorsteinsson, M. V., Kerby, R. L., Chung, S.-Y., Roberts, G. P., Reynolds, M. F., Parks, R. B., and Burstyn, J. N. (1999) Identification of Two Important Heme Site Residues (Cysteine 75 and Histidine 77) in CooA, the CO-Sensing Transcription Factor of Rhodospirillum rubrum, *Biochemistry 38*, 2669-2678.

23. Pinkert, J., Clark, R. W., and Burstyn, J. N. (2006) Modeling proline ligation in the heme-dependent CO sensor, CooA, using molecule analogs, *J. Biol. Inorg. Chem. 5*, 642-650.

24. Clark, R. W., Youn, H., PArks, R. B., Cherney, M. M., Roberts, G. P., and Burstyn, J. N. (2004) Investigation of the Role of the N-Terminal Proline, the Distal Heme Ligand in the CO Sensor CooA, *Biochemistry 43*, 14149-14160.

25. Youn, H., Kerby, R. L., and Roberts, G. P. (2004) Changing the Ligand Specificity of CooA, a Highly Specific Heme-based CO Sensor, *J. Biol. Chem. 279*, 45744-45752.

26. Coyle, C. M., Puranik, M., Youn, H., Nielsen, S. B., Williams, R. D., Kerby, R. L., Roberts, G. P., and Spiro, T. G. (2003) Activation Mechanism of the CO Sensor CooA: Mutational and Resonance Raman Spectroscopic Studies, *J. Biol. Chem. 278*, 35384-35393.

27. Kerby, R. L., Youn, H., Thorsteinsson, M. V., and Roberts, G. P. (2003) Repositioning about the Dimer Interface of the Transcription Regulator CooA: A Major Signal Transduction Pathway between the Effector and DNA binding Domains, *J. Mol. Biol. 325*, 809-823.

28. Yang, H., and Smith, D. L. (1997) Kinetics of Cytochrome c Folding Examined by Hydrogen Exchange and Mass Spectrometry, *Biochemistry 36*, 14992-14999.

29. Dai, S. Y., Gardner, M. W., and Fitzgerald, M. C. (2005) Protocol for the Thermodynamic Analysis of Some Proteins Using an H/D Exchange- and Mass Spectrometry-Based Technique, *Anal. Chem. 77*, 693-697.

30. Fitzgerald, M. C., and West, G. M. (2009) Painting proteins with covalent labels: what's in the picture?, *J. Am. Soc. Mass. Spectrom. 20*, 1193-1206.

31. Roulhac, P. L., Powell, K. D., Dhungana, S., Weaver, K. D., Mietzner, T. A., Crumbliss, A. L., and Fitzgerald, M. C. (2004) SUPREX (stability of unpurified proteins from rates of H/D exchange) analysis of the thermodynamics of synergistic anion binding by ferric-binding protein (FbpA), a bacterial transferrin, *Biochemistry 43*, 15767-15774.

32. Tang, L., Roulhac, P. L., and Fitzgerald, M. C. (2007) H/D exchange mass spectrometry-based method for biophysical analysis of multidomain proteins at the domain level, *Anal. Chem. 79*, 8728-8739.

33. West, G. M., Tang, L., and Fitzgerald, M. C. (2008) Thermodynamic analysis of protein stability and ligand binding using a chemical modification- and mass spectrometry-based strategy *Anal. Chem. 80*, 4175-4185.

34. West, G. M., Tucker, C. L., Xu, T., Park, S. K., Han, X., Yates III, J. R., and Fitzgerald, M. C. (2010) Quantitative proteomics approach for identifying protein-drug interactions in complex mixtures using protein stability measurements, *Proc. Natl. Acad. Sci. USA 107*, 9078-9082.

35. Hopper, E. D., Pittman, A. M. C., Tucker, C. L., Campa, M. J., Patz Jr., E. F., and Fitzgerald, M. C. (2009) Hydrogen/deuterium exchange- and protease digestion-based screening assay for protein-ligand binding detection, *Anal. Chem. 81*, 6860-6867.

36. Banerjee, R., Evande, R., Kabil, O., Ojha, S., and Taoka, S. (2003) Reaction mechanism and regulation of cystathionine b-synthase, *Biochim. Biophys. Acta 1647*, 30-35.

37. Finkelstein, J. D., Kyle, W. E., Martin, J. J., and Pick, A.-M. (1975) Activation of cystathionine synthase by adenosylmethionine and adenosylethionine, *Biochem. Biophys. Res. Commun. 66*, 81-87.

38. Su, Y., Majtan, T., Freeman, K. M., Linck, R. C., Ponter, S., Kraus, J. P., and Burstyn, J. N. (2013) Comparative study of enzyme activity and heme reactivity in Drosophila melanogaster and Homo sapiens cystathionine beta-synthases, *Biochemistry 52*, 741-751.

39. Oliveriusová, J., Kery, V., Maclean, K. N., and Kraus, J. P. (2002) Deletion Mutagenesis of Human Cystathionine beta -Synthase. Impact on Activity, Oligomeric Status, and S-Adenosylmethionine Regulation, *J. Biol. Chem. 277*, 48386-48394.

40. Smith, A. T., Majtan, T., Freeman, K. M., Su, Y., Kraus, J. P., and Burstyn, J. N. (2011) Cobalt Cystathionine ß-Synthase: A Cobalt-Substituted Heme Protein with a Unique Thiolate Ligation Motif, *Inorg. Chem. 50*, 4417-4427.

41. Cherney, M. M., Pazicni, S., Frank, N., Marvin, K. A., Kraus, J. P., and Burstyn, J. N. (2007) Ferrous Human Cystathionine β-Synthase Loses Activity during Enzyme Assay Due to a Ligand Switch Process, *Biochemistry 46*, 13199-13210.

42. Taoka, S., Green, E. L., Loehr, T. M., and Banerjee, R. (2001) Mercuric chloride-induced spin or ligation state changes in ferric or ferrous human cystathionine β-synthase inhibit enzyme activity, *J. Inorg. Biochem. 87*, 253-259.

43. Shintani, T., Iwabuchi, T., Soga, T., Kato, Y., Yamamoto, T., Takano, N., Hishiki, T., Ueno, Y., Ikeda, S., Sakuragawa, T., Ishikawa, K., Goda, N., Kitagawa, Y., Kajimura, M., Matsumoto, K., and Suematsu, M. (2009) Cystathionine β-synthase as a carbon monoxide-sensitive regulator of bile excretion, *Hepatology 49*, 141-150.

44. Taoka, S., Green, E. L., Loehr, T. M., and Banerjee, R. (2001) Mercuric chloride-induced spin or ligation state changes in ferric or ferrous human cystathionine β-synthase inhibit enzyme activity, *J. Inorg. Biochem. 87*, 253-259.

45. Celano, L., Gil, M., Carballal, S., Durán, R., Denicola, A., Banerjee, R., and Alvarez, B. (2009) Inactivation of cystathionine β-synthase with peroxynitrite, *Arch. Biochem. Biophys. 491*, 96-105.

46. Jhee, K.-H., McPhie, P., and Miles, E. W. (2000) Yeast Cystathionine β-Synthase Is a Pyridoxal Phosphate Enzyme but, Unlike the Human Enzyme, Is Not a Heme Protein, *J. Biol. Chem. 275*, 11541-11544.

47. Jhee, K.-H., McPhie, P., and Miles, E. W. (2000) Domain architecture of the heme-independent yeast cystathionine b-synthase provides insights into mechanisms of catalysis and regulation, *Biochemistry 39*, 10548-10556.

48. Maclean, K. N., Janosìk, M., Oliveriusov·, J., Kery, V., and Kraus, J. P. (2000) Transsulfuration in Saccharomyces cerevisiae is not dependent on heme: purification and characterization of recombinant yeast cystathionine β-synthase, *J. Inorg. Biochem. 81*, 161-171.

49. Koutmos, M., Kabil, O., Smith, J. L., and Banerjee, R. (2010) Structural basis for substrate activation and regulation by cystathionine beta-synthase (CBS) domains in cystathionine β-synthase, *Proc. Natl. Acad. Sci. USA*, 1-6

50. Stewart, V., Lu, Y., and Darwin, A. J. (2002) Periplasmic Nitrate Reductase (NapABC Enzyme) Supports Anaerobic Respiration by Escherichia coli K-12, *J. Bacteriol. 184*, 1314-1323.

51. Dykxhoorn, D. M., St. Pierre, R., and Linn, T. (1996) A set of compatible *tac* promoter expression vectors, *Gene 177*, 133-136.

52. Antonini, E., and Brunori, M. (1971) *Hemoglobin and myoglobin in their reactions with ligands*, North-Holland Publishing Company, Amsterdam.

53. Nozaki, Y. (1972) [3] The preparation of guanidine hydrochloride, In *Methods Enzymol.* (C. H. W. Hirs, S. N. T., Ed.), pp 43-50, Academic Press.

54. Strickland, E. C., Geer, M. A., Tran, D. T., Adhikari, J., West, G. M., DeArmond, P. D., Xu, Y., and Fitzgerald, M. C. (2013) Thermodynamic analysis of protein-ligand binding interactions in complex biological mixtures using the stability of proteins from rates of oxidation, *Nat. Protoc. 8*, 148-161.

55. Frank, N., Kent, J. O., Meier, M., and Kraus, J. P. (2008) Purification and characterization of the wild type and truncated human cystathionine β-synthase enzymes expressed in *E. coli*, *Arch. Biochem. Biophys. 470*, 64-72.

56. Majtan, T., Freeman, K. M., Smith, A. T., Burstyn, J. N., and Kraus, J. P. (2011) Purification and Characterization of Cystathionine Beta-Synthase Bearing a Cobalt Protoporphyrin, *Arch. Biochem. Biophys. 508*, 25-30.

57. Lee, A. J., Clark, R. W., Youn, H., Ponter, S., and Burstyn, J. N. (2009) Guanidine Hydrochloride-Induced Unfolding of the Three Heme Coordination States of the CO-Sensing Transcription Factor, CooA, *Biochemistry 48*, 6585-6597.

58. Koutmos, M., Kabil, O., Smith, J. L., and Banerjee, R. (2010) Structural basis for substrated activation and regulation by cystathionine beta-synthase (CBS) domains in cystathionine β-synthase, *Proc. Natl. Acad. Sci. 107*, 20958-20963.

59. Frank, N., Kery, V., Maclean, K. N., and Kraus, J. P. (2006) Solvent-Accessible Cysteines in Human Cystathionine β-Synthase: Crucial Role of Cysteine 431 in *S*-Adenosyl-L-methionine Binding, *Biochemistry 45*, 11021-11029.

60. Janosik, M., Kery, V., Gaustadnes, M., Maclean, K. N., and Kraus, J. P. (2001) Regulation of Human Cystathionine β-Synthase by *S*-Adenosyl-L-methionine: Evidence for Two Catalytically Active Conformations Involving an Autoinhibitory Domain in the C-Terminal Region, *Biochemistry 40*, 10625-10633.

61. Jhee, K.-H., McPhie, P., and Miles, E. W. (2000) Yeast cystathionine β-synthase is a pyridoxal phosphate enzyme but, unlike the human enzyme, is not a heme protein, *J. Biol. Chem. 275*, 11541-11544.

62. Maclean, K. N., Janosik, M., Oliveriusova, J., Kery, V., and Kraus, J. P. (2000) Transsulfuration in *Saccharomyces cerevisiae* is not dependent on heme: purification and characterization of recombinant yeast cystathionine β-synthase, *J. Inorg. Biochem. 81*, 161-171.

63. Lanzilotta, W. N., Schuller, D. J., Thorsteinsson, M. V., Kerby, R. L., Roberts, G. P., and Poulos, T. L. (2000) Structure of the CO-sensing transcription activator CooA, *Nat. Struct. Biol. 7*, 876-880.

64. Borjigin, M., Li, H., Lanz, N. D., Kerby, R. L., Roberts, G. P., and Poulos, T. L. (2007) Structure-based hypothesis on the activation of the CO-sensing transcription factor CooA, *Acta Crystallogr. Sect. D. Biol. Crystallogr. D63*, 282-287.

65. Weeks, C. L., Singh, S., Madzelan, P., Banerjee, R., and Spiro, T. G. (2009) Heme Regulation of Human Cystathionine β-Synthase Activity: Insights from Fluorescence and Raman Spectroscopy, *J. Am. Chem. Soc. 131*, 12809-12816.

Figure 3.1. Sequence map and structures of inactive, “off”-state Fe(II) *Rr* CooA (*63*) and active “on”-state Fe(II)-CO *Ch* LL-CooA (*64*). One monomer is shown as a ribbon, the other as a strand. The “on” structure is of a protein missing heme (red) in one monomer. The DNA-binding F-helices are colored blue, the 4/5 loop is green, and the hinge region is yellow. These regions change shapes or orientations between the “on” and “off” structures. The F-helices are in an orientation that prevents contacts with DNA in the “off” structure. An F-helix is exposed for DNA binding in the “on” structure.

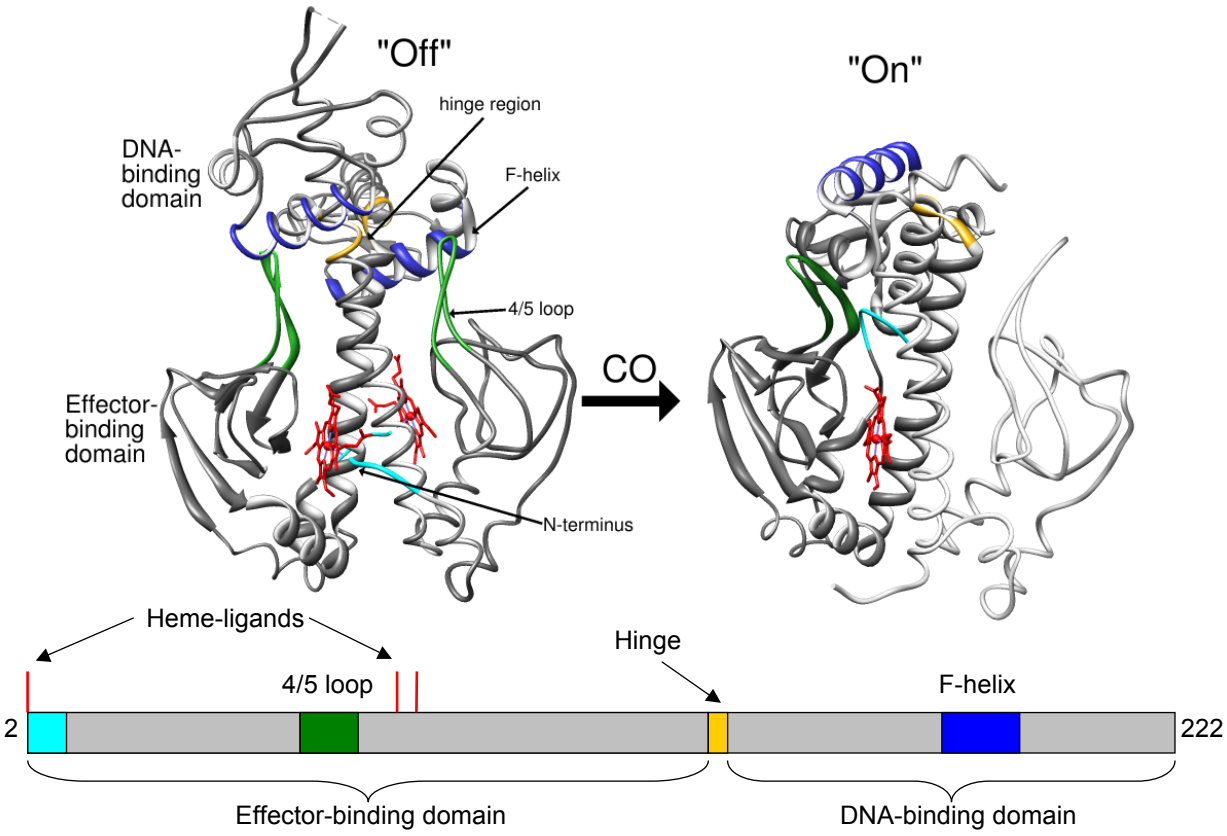

Figure 3.2. Coordination changes associated with CO sensing in CooA. Fe(III)CooA contains Cys^{75} as one ligand to the heme; Cys^{75} is replaced by His^{77} upon reduction to Fe(II)CooA. CO replaces Pro^2, and this change in heme coordination drives a global conformational change in the protein.

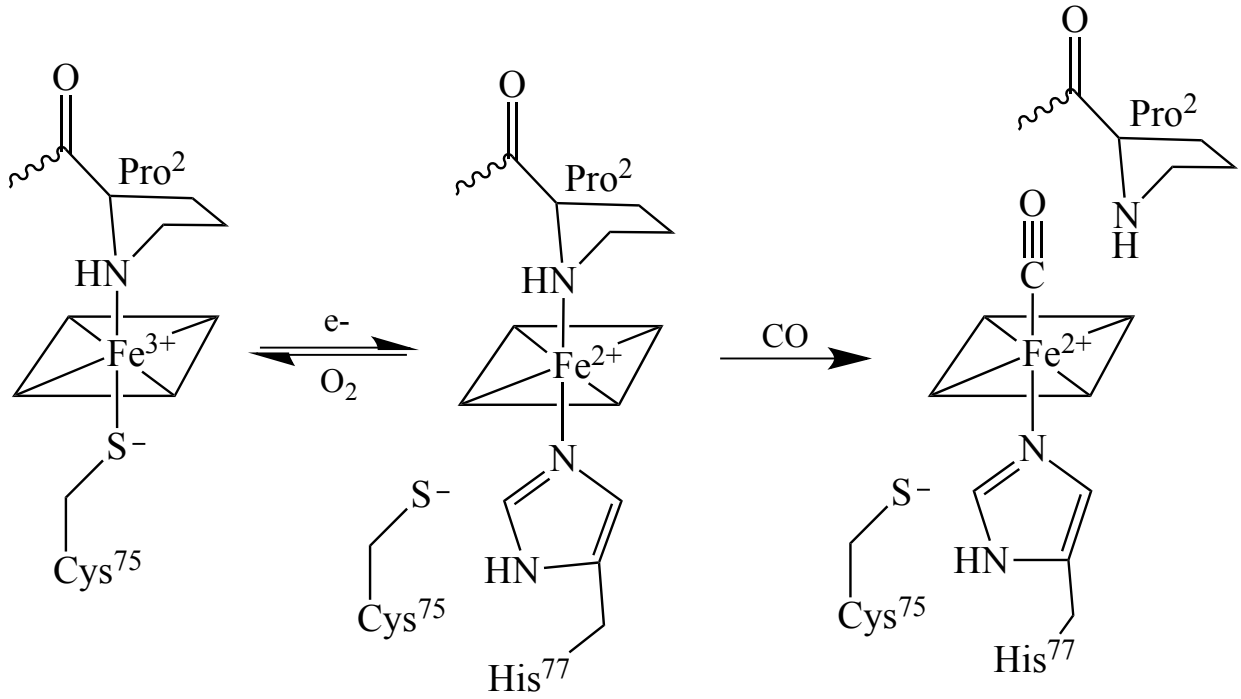

Figure 3.3. A schematic outline of the basic SUPREX (stability of unpurified proteins from rates of H/D exchange) method (*30*).

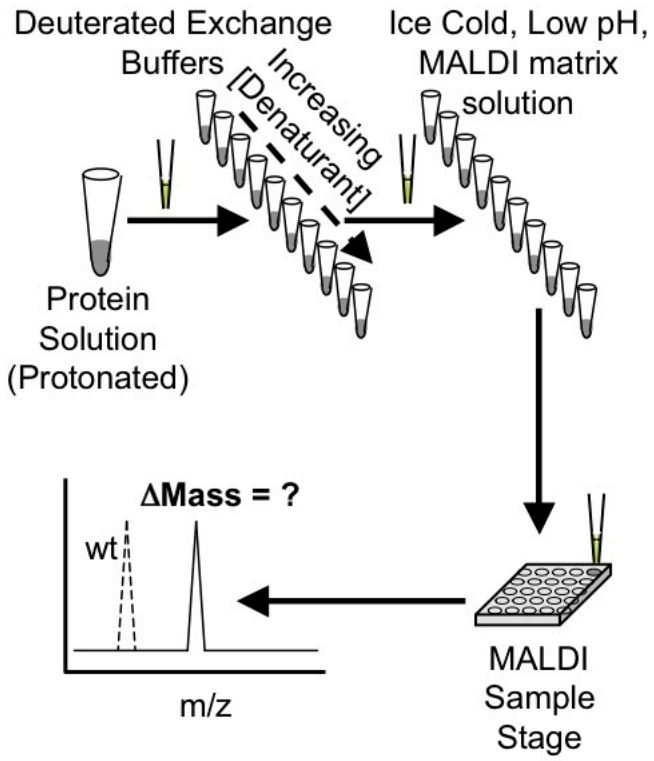

Figure 3.4. A) Schematic of the basic SPROX (stability of proteins from rates of oxidation) protocol (*33*). B) Locations of the five methionine residues on the structure of Fe(II) CooA.

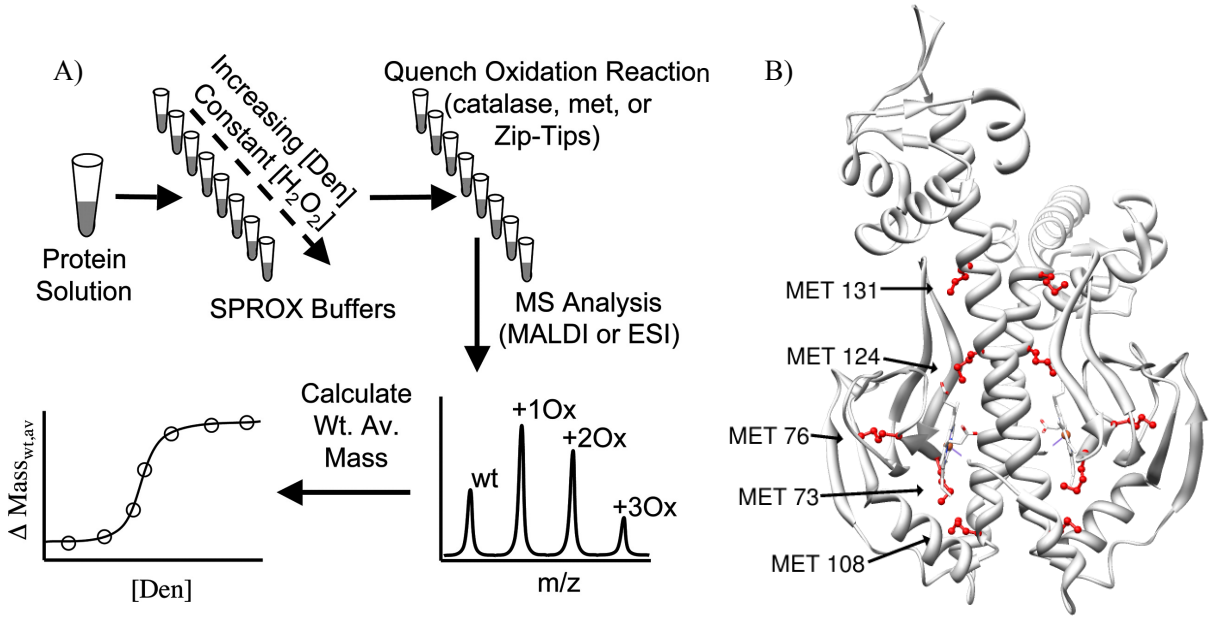

Figure 3.5 Sequence alignment of hCBS (UniProt ID P35520) and *Dm*CBS (UniProt ID Q9VRD9). The PLP and heme binding residues are marked with ▲. The residues hydrogen bonded to the PLP or heme in the crystal structures are marked with ●. The residues hydrogen bonded to the substrates/products in the crystal structures are marked with ○.

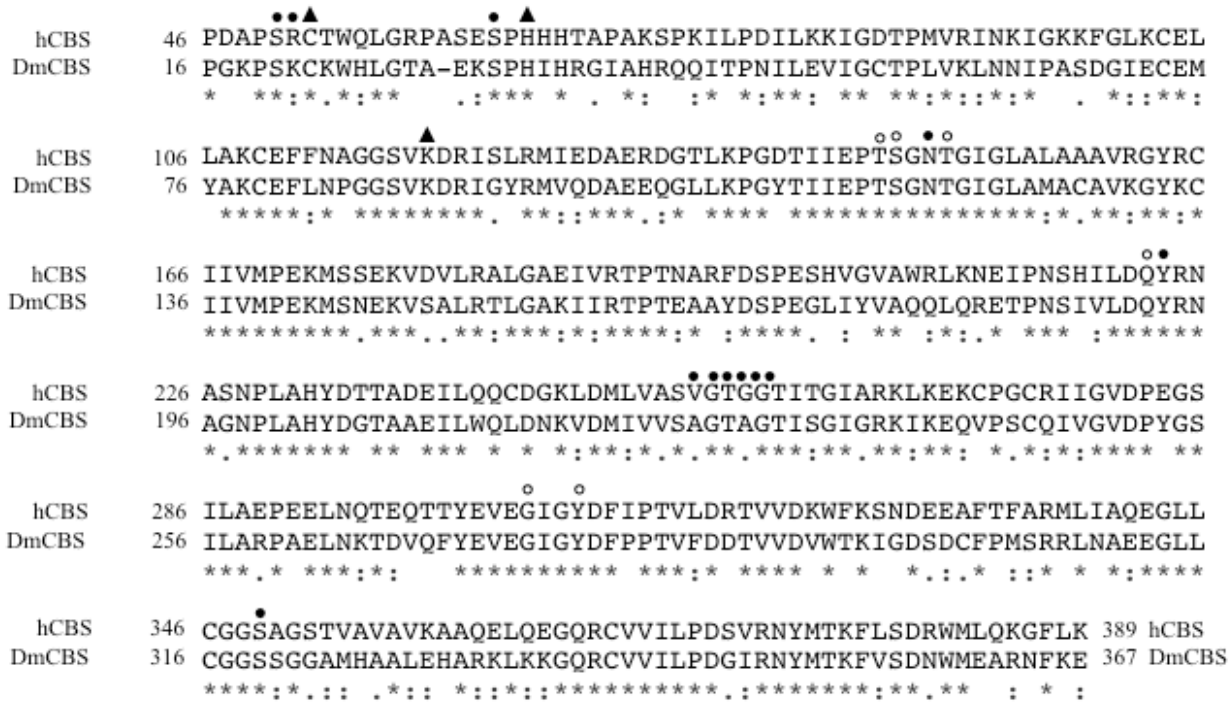

Figure 3.6. Ion trap mass spectrum of CooA (A) and Fourier transform mass spectrum of CooA (B). The mass peak at 616 is heme in the ion trap spectrum. The low mass peaks, at 436 and 527, were present in the respective background solvent samples. FT data acquired on predominant IT peak, 980, for 500 scans with resolution set to 400,000. FT spectrum displays the isotope distribution of CooA's 980 mass peak.

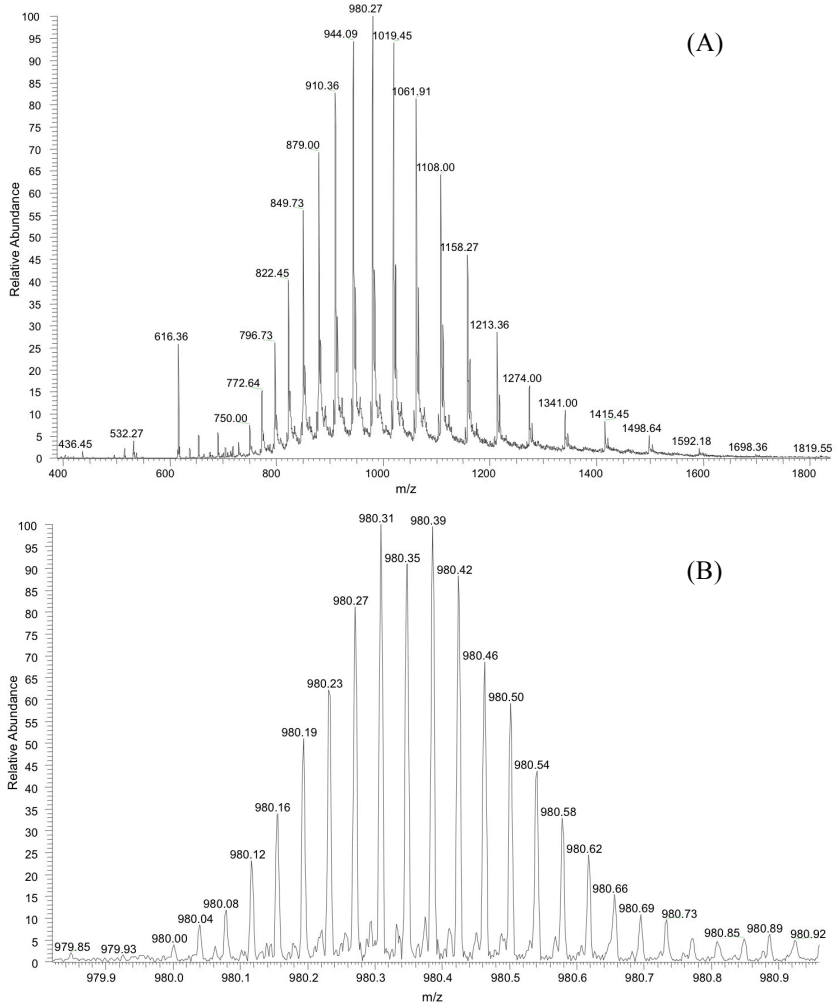

Figure 3.7. Mass spectrometry-based SUPREX assay of wild type Fe(III) *Rr*CooA. 23 μM *Rr*CooA protein H/D exchanged for 3 days with increasing guanidinium hydrochloride (GdnHCl) gradient (0-5 M). Pepsin digestion of the quenched SUPREX reaction followed by MALDI analysis resulted in identification of 2 DNA-binding domain peptides (depicted in gray).

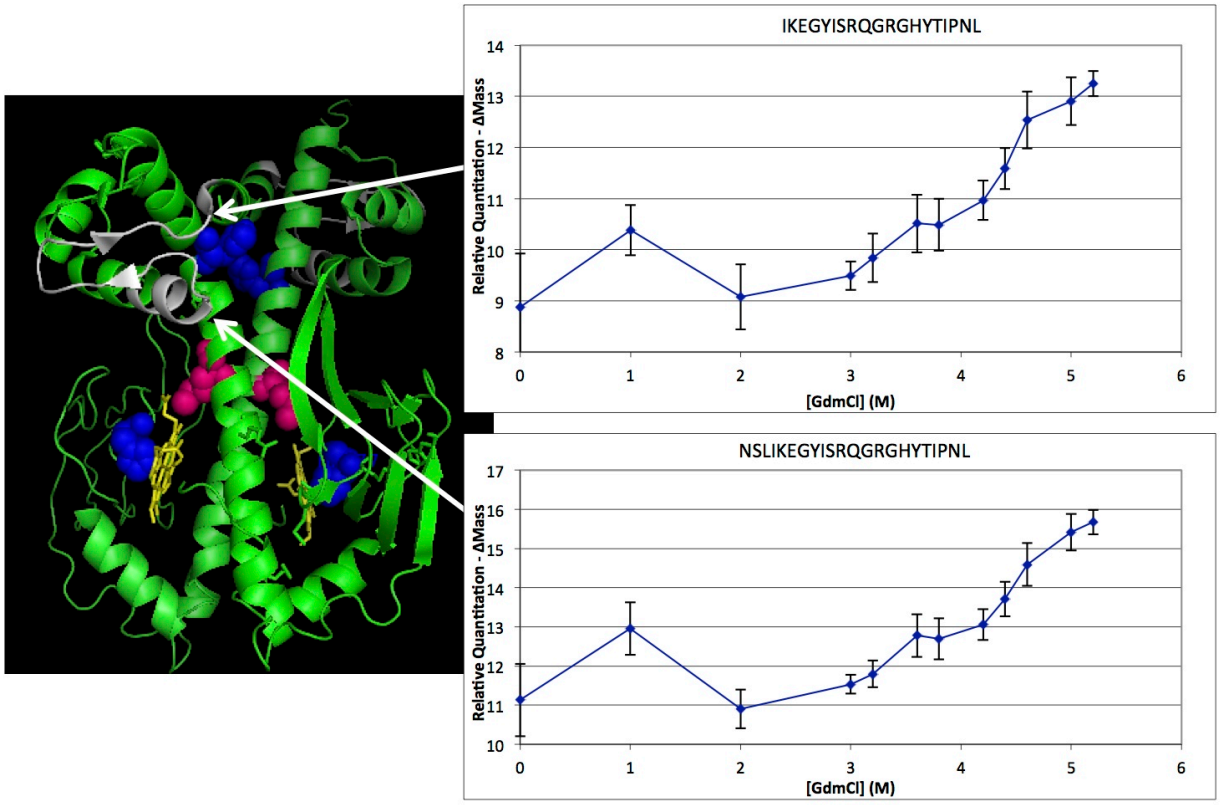

Figure 3.8. Mass spectrometry-based SPROX assay of wild type Fe(III) *Rr*CooA. 17 μM *Rr*CooA protein oxidized with 1 M H_2O_2 for 3 minutes with increasing gradient of GdnHCl. Trypsin digestion of the sample revealed Met^{124} (fushia residue) was oxidized.

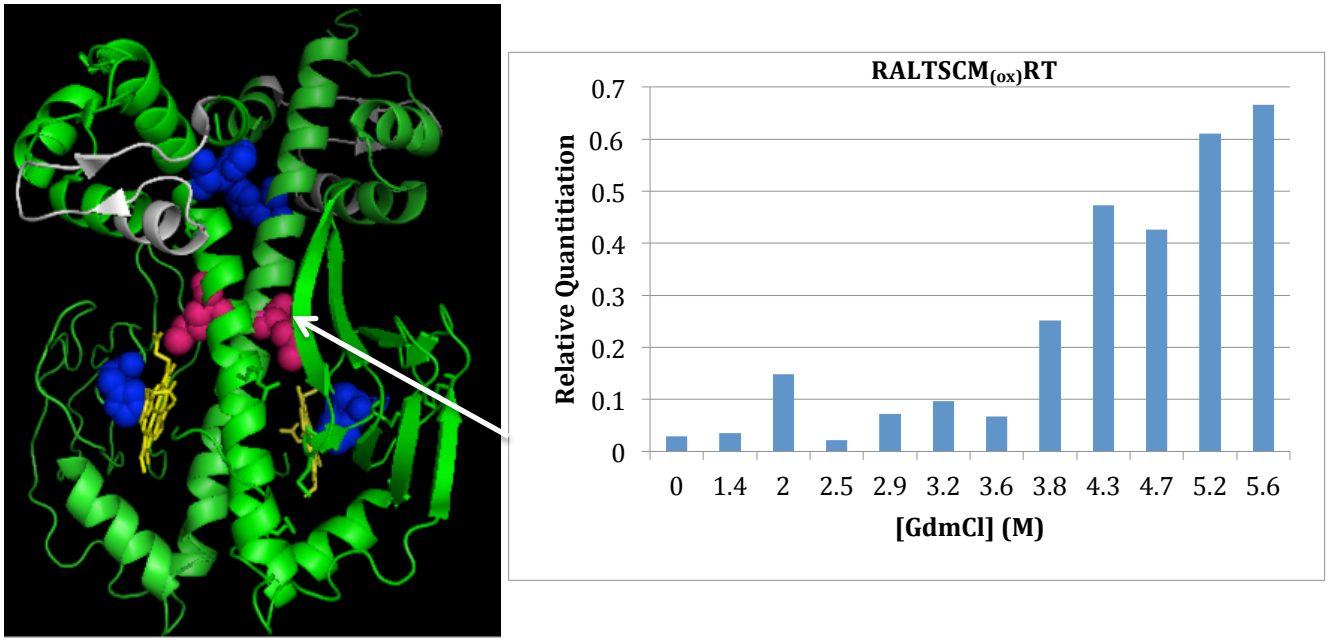

Figure 3.9. Ion trap mass spectra of as-isolated (A) and AdoMet-treated (B) *Dm*CBS. The mass peak at 616 is heme. Lack of a mass peak at 399 indicates the absence of AdoMet. The other low mass peaks, including those at 239 and 409, are common plasticizers that were present in the respective background solvent samples.

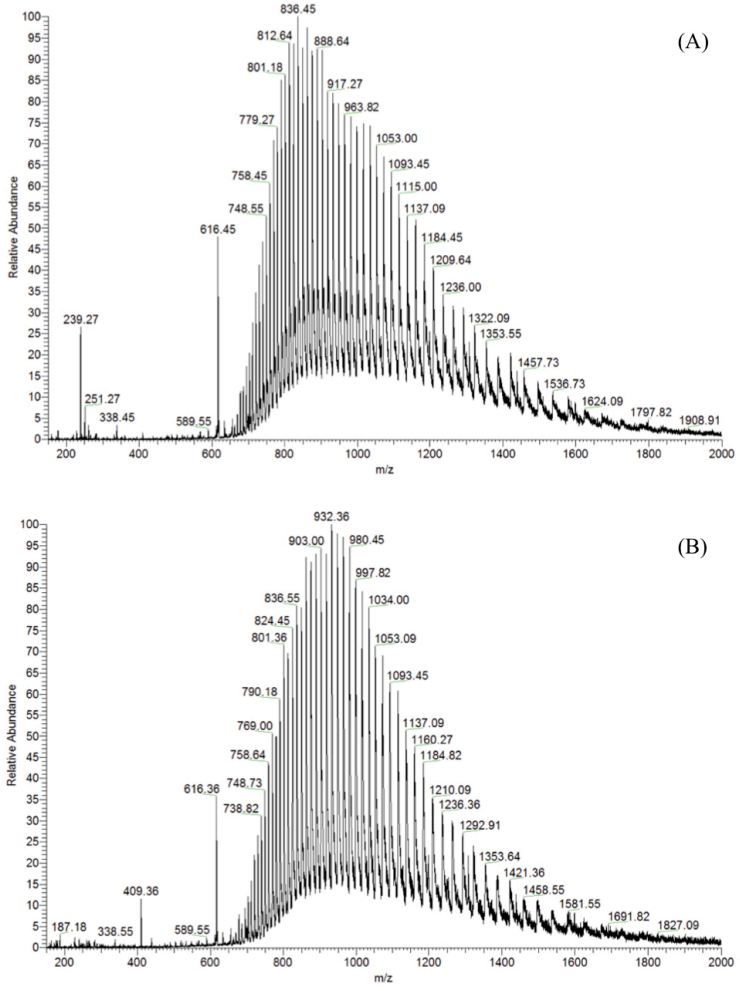

Figure 3.10. Fourier transform mass spectra of as-isolated (A) and AdoMet-treated (B) *Dm*CBS. The multiple charge states correspond to enzyme molecular weight of 56,870 Daltons for both as-isolated (A) and AdoMet-treated (B) *Dm*CBS.

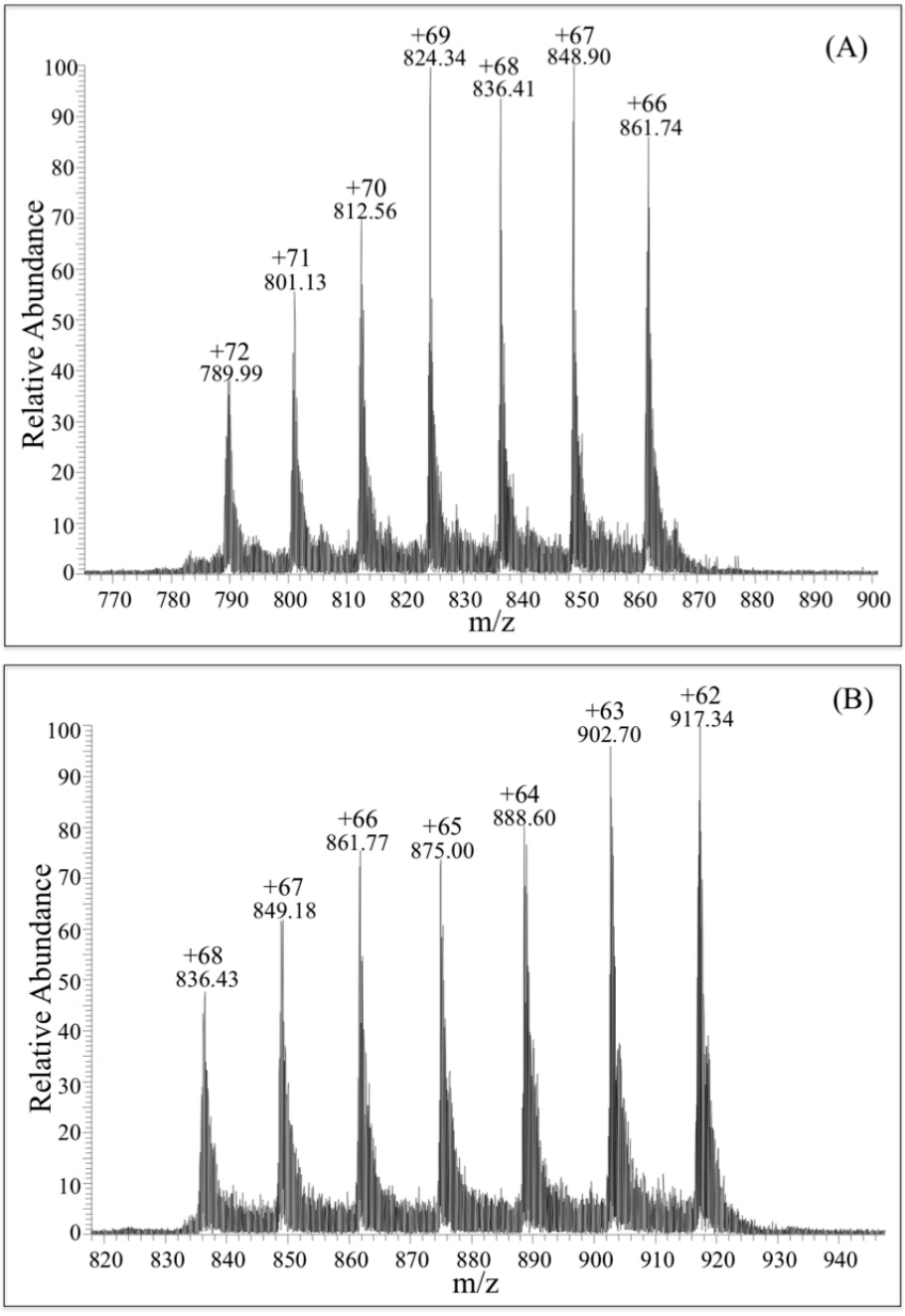

Scheme 3.1. CBS-catalyzed reactions. The canonical enzymatic reaction (top) condenses homocysteine and serine to form cystathionine. Alternative cysteine synthesis CBS-catalyzed reactions (bottom): the condensation of hydrogen sulfide with serine to form cysteine (Rxn 1) and the β–replacement reaction between hydrogen sulfide and *O*-acetylserine to form cysteine (Rxn 2).

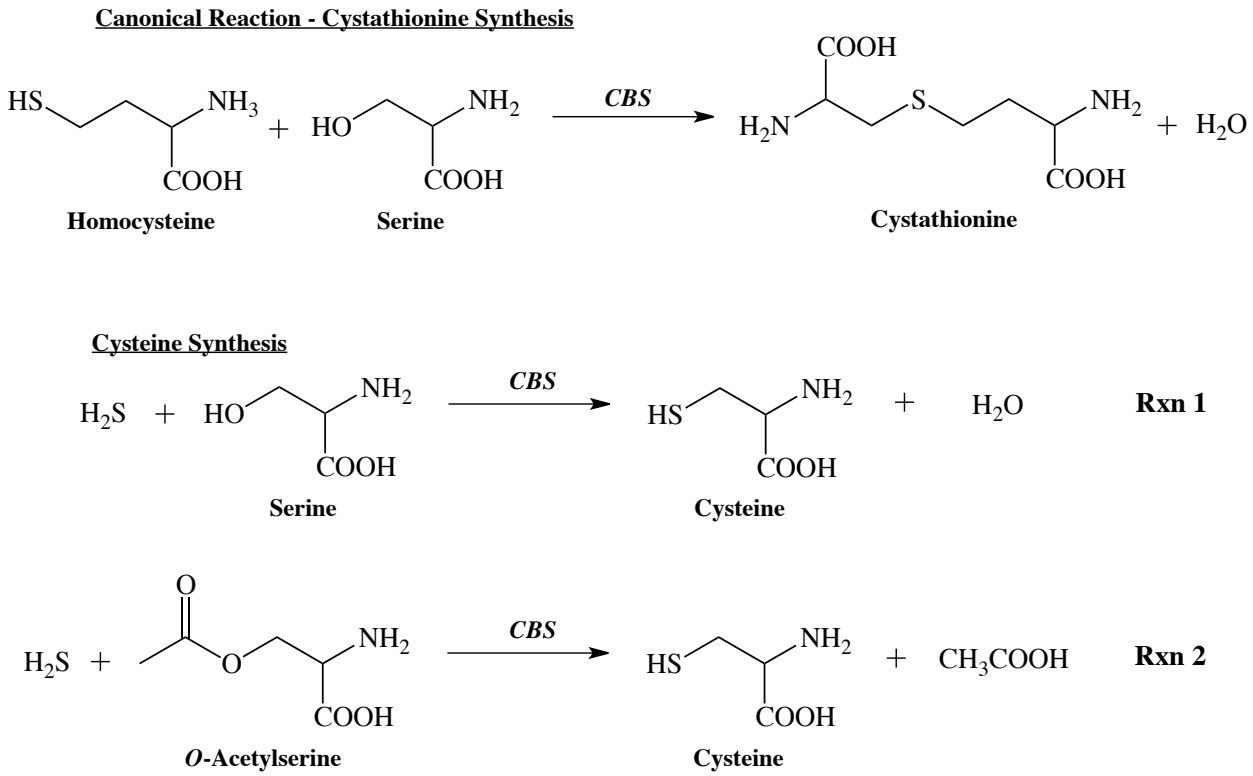

Scheme 3.2. Simplified PLP-dependent catalytic mechanism of cystathionine β–synthase (CBS) (*65*). In the canonical reaction (shown), CBS catalyzes the β–replacement reaction between homocysteine and serine to form cystathionine.

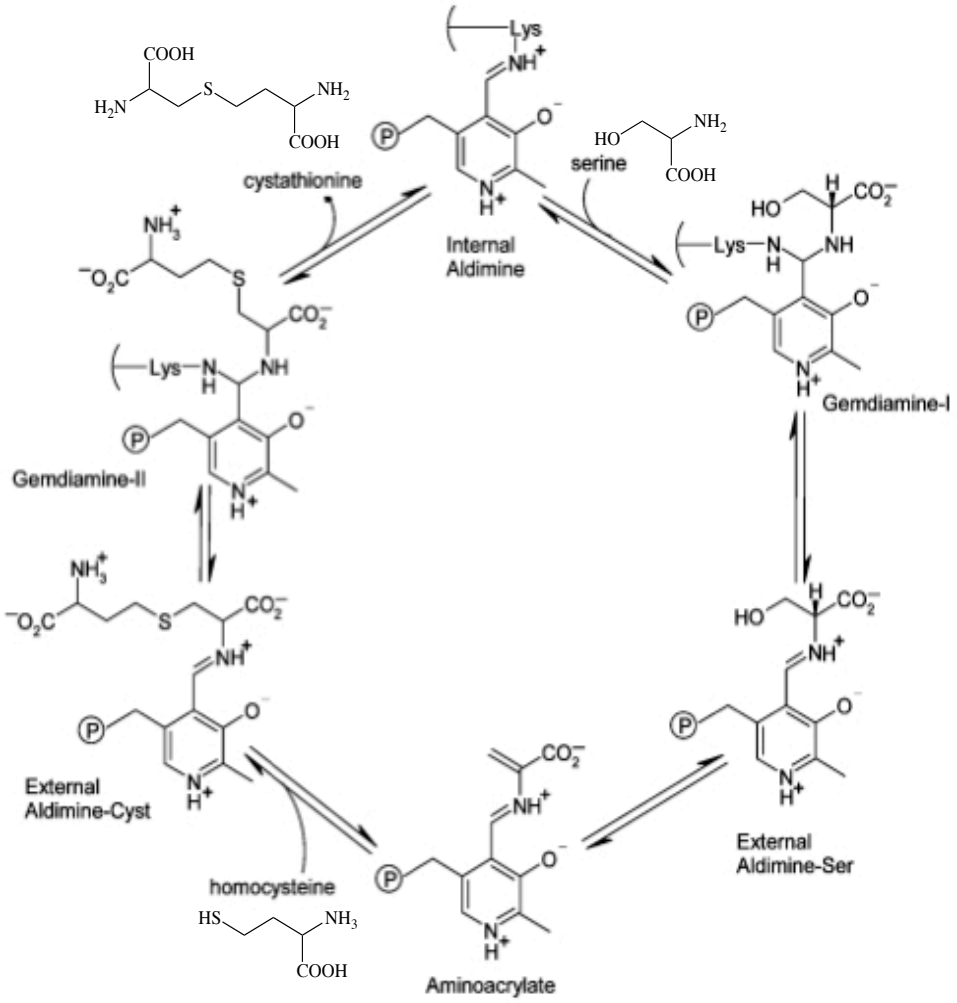

Chapter Four

Identification of Cys^{94} as the Distal Ligand to the Fe(III) Heme in the Transcriptional Regulator RcoM-2 from *Burkholderia xenovorans*

This chapter was published as:

Smith, A. T.; Marvin, K. A.; Freeman, K. M.; Kerby, R. L.; Roberts, G. P.; Burstyn, J. N. (2012) Identification of Cys^{94} as the distal ligand to the Fe(III) heme in the transcriptional regulator RcoM-2 from *Burkholderia xenovorans*, *J. Biol. Inorg. Chem*. *17*, 1071-1082.

All mutagenic work was performed by Dr. Robert L. Kerby in the laboratory of Professor Gary P. Roberts at the University of Wisconsin—Madison. Aaron T. Smith and Katherine M. Marvin performed the spectroscopic characterization of the RcoM-2 variant proteins. A prepublication version of this manuscript was included in Aaron T. Smith's dissertation. KMFP expressed and purified the RcoM-2 variants. KMFP prepared the final published manuscript.

Introduction

Small, gaseous diatomic molecules, such as O_2, NO and CO, are important signaling molecules in biological systems; one method nature employs to sense these gases is interaction of the diatomic molecule with a heme cofactor (*1-6*). Dioxygen binding to heme in Mb and Hb is a well-known paradigm. Examples of heme-based O_2 sensor proteins, in which the dioxygen-binding heme domain regulates function, include *Rhizobium meliloti* FixL (*7*), *Bacillus subtilis* HemAT (*8*) and *Escherichia coli* DOS (*9*). NO is produced endogenously by nitric oxide synthase; at physiological levels, NO plays a role in both neurotransmission as well as vascular regulation (*10*). Examples of heme-containing NO sensors include the bacterial H-NOX proteins (*11*), mammalian sGC (*12*), heme-regulated eIF2α kinase (*13*), and the putative NO-sensors *Drosophila melanogaster* DHR51 (*14*), *D. melanogaster* E75 (*15*), and *Pseudomonas aeruginosa* DNR (*16*). CO is also believed to function as a neurotransmitter in mammals, where it is endogenously produced by heme oxygenase (*17*). Examples of CO sensors include mammalian NPAS2 (*18*) and bacterial *Rhodospirillum rubrum* CooA (*19, 20*) as well as the putative CO sensors *D. melanogaster* E75 (*15*) and *D. melanogaster* DHR51 (*14*).

Recently, a new prokaryotic transcriptional regulator of CO metabolism (RcoM) was isolated from the aerobic, polychlorinated biphenyl (PCB)-degrading bacterium *Burkholderia xenovorans* (LB400) (*21, 22*). Two homologous proteins, *Bx*RcoM-1 and *Bx*RcoM-2, were identified in this bacterium and share 93% sequence similarity. These proteins contain a N-terminal PAS domain and a C-terminal LytTR domain. PAS domains frequently function as sensors of environmental signals through the binding of small molecules and may bind various cofactors (*23*). LytTR domains are DNA-binding domains that commonly function within transcriptional regulators and may be found in conjunction with PAS sensor domains (*24*). In

*Bx*RcoM-1 and *Bx*RcoM-2, the N-terminal PAS domain binds a *b*-type heme cofactor that controls CO-dependent DNA binding (*25*).

Studies of *Bx*RcoM-1 and *Bx*RcoM-2 revealed the ligation and oxidation state changes that occur at the RcoM heme. The *Bx*RcoM-1 and *Bx*RcoM-2 homologues were first isolated under aerobic conditions, yet they each contained a six-coordinate Fe(II)CO-bound heme (*21*). Aerobic photolysis of the Fe(II)CO species resulted in conversion to a six-coordinate, low-spin Fe(III) heme. Site-directed mutagenesis of *Bx*RcoM-1 identified His^{74} as the proximal ligand, and spectral characterization of Fe(III) *Bx*RcoM-2 definitively demonstrated that the protein bears a cysteine(thiolate) ligand *trans* to a neutral ligand, presumably the same His^{74}. *Bx*RcoM-2 was shown to undergo a redox-mediated ligand switch in which the cysteine(thiolate) ligand is lost upon heme reduction. The spectral signatures of Fe(II) *Bx*RcoM-2 were consistent with the presence of methionine *trans* to His^{74}; mutagenesis data suggested that the distal Fe(II) ligand for *Bx*RcoM-1, and by analogy *Bx*RcoM-2, is Met^{104} (*21, 26*). Methionine, a weaker ligand than histidine, may be more easily replaced by CO; consistent with this understanding, resonance Raman data of the heme-CO adduct in *Bx*RcoM-2 were indicative of CO binding *trans* to the proximal His^{74} (*26*). Thus, the proximal ligand His^{74} remains constant during redox- and CO-binding events while the distal ligand is exchanged in order to allosterically modulate *Bx*RcoM DNA-binding behavior to initiate transcription. Although the mutagenesis studies were on *Bx*RcoM-1 and the spectroscopic studies were on *Bx*RcoM-2, the presence of His^{74} and Met^{104} in the N-terminal PAS domains of both proteins implies that the same amino acids are the Fe(II) ligands in these two closely related homologues.

The identity of the cysteine ligand remained in question. Only three cysteine residues are found in the sequences of *Bx*RcoM-1 and *Bx*RcoM-2: Cys^{94}, Cys^{127} and Cys^{130}. All three

cysteine residues were considered as potential Fe(III) ligands, since they all occur within the heme-binding PAS domain. We examined sequences of 16 homologous RcoM proteins to determine the degree of conservation of these three cysteine residues (*21*). Cys^{94} and Cys^{127} are not well conserved. Cys^{94} appears in only three proteins, *Bx*RcoM-1, *Bx*RcoM-2, and the RcoM homologue of *Alkalilimnicola ehrlichei*. Cys^{127} appears only twice, in *Bx*RcoM-1, *Bx*RcoM-2. In contrast, Cys^{130} is moderately conserved, appearing in 8 of the 16 RcoM homologues. Thus, amino acid conservation suggests that Cys^{130} is the most likely candidate for the cysteine ligand. Examination of sequences of other *Burkholderia* species revealed evidence for two putative RcoM proteins in *Burkholderia cepacia*. Sequence alignments of *Bx*RcoM-1 and -2 with the postulated RcoM proteins from *B. cepacia* strains CH1-1 and BH160 show 88% and 85% amino acid identity, respectively (Figure 4.1). Two of the three cysteines are conserved among all four proteins: Cys^{94} and Cys^{130}. In place of Cys^{127} is Ser^{127} in the *B. cepacia* BH160 sequence, suggesting that Cys^{127} is least likely to be the heme ligand in the *Bx*RcoM proteins. Both Cys^{94} and Cys^{130} are conserved, and are therefore more likely candidates.

Herein, we present identification of Cys^{94} as the cysteine(thiolate) ligand to the Fe(III) heme in *Bx*RcoM-2. Because there were only three cysteines, we chose to isolate variants in which each of the three was altered; surprisingly, the evidence unequivocally identifies Cys^{94} as the thiolate ligand. Spectroscopic signatures of the three *Bx*RcoM-2 variants—C94S, C127S, and C130S—were studied using electronic absorption, resonance Raman (rR) and electron paramagnetic resonance (*27*) spectroscopies. The Fe(III) C94S variant exhibits differences in its spectroscopic features from those of WT Fe(III)*Bx*RcoM-2 and the other variants, and the spectral signatures of Fe(III) C94S are inconsistent with coordination of a cysteine(thiolate) ligand to the Fe(III) heme.

Materials and Methods

Materials. Glycerol (>99.5%) and all chemicals used in buffer preparation (≥99.5 %) were purchased from Sigma-Aldrich and used as received. Potassium ferricyanide ($K_3[Fe(CN)_6]$) (certified ACS grade) was purchased from Sigma-Aldrich and used as received. Sodium dithionite ($Na_2S_2O_4$, 85%) was purchased from Fluka and stored under $Ar_{(g)}$ at -20 °C until used. A CO gas (99.5%) cylinder was obtained from AGA.

Mutagenesis, Isolation, and Purification of Bx*RcoM-2 Variants*. Variant proteins were generated by mutagenesis of the cloned *Bx*RcoM-2 (*21*) according to the QuikChange protocol (Agilent Technologies [Stratagene], Santa Clara, CA). Sequences of all constructs were verified with BigDye v. 3.1 reaction chemistry (Life Technologies [Applied Biosystems], Carlsbad, CA) and subsequent analysis by the University of Wisconsin—Madison Biotechnology Center DNA sequencing facility.

Isolation and purification of the *Bx*RcoM-2 variants was similar to our previous reports (*21, 26*). Briefly, *E. coli* VJS6737 (*28*) bearing the pEXT20 expression vector (*29*) for the appropriate variant was cultivated in rich medium supplemented with ferric citrate. Isopropyl β-D-thiogalactopyranoside (IPTG) 7 μM was used to induce expression for 18-20 h at 28°C. Cells were pelleted by centrifugation (10,000 x *g*, 10 min), resuspended in lysis buffer (50 mM MOPS, pH 7.5, 500 mM KCl and 0.5 mM DTT) and lysed by passage through a French press. A Ni-NTA column (Qiagen, 8 mL resin volume) was pre-equilibrated with 10 mM imidazole, 50 mM MOPS pH 7.5, 500 mM KCl. The cell supernatant (25 mL) was applied slowly, and the column was washed successively with 10 mM imidazole (2 column volumes) and 50 mM imidazole (1 column volume), in the same buffer. Finally, protein was eluted with 220 mM

imidazole. The protein was precipitated at 55%-saturated $(NH_4)_2SO_4$ (v/v) with incubation on ice for 30 minutes and brief centrifugation. The protein pellet was dissolved in 500 μL 25 mM MOPS, pH 7.4 and 500 mM KCl, applied to a buffer-equilibrated Sephadex G-25 column, and eluted in the same buffer. The desalted protein was stored at -80 °C. Protein concentrations were determined using the BCA method (Pierce, Rockford, IL); SDS-PAGE verified protein purity was >90%; heme content was determined using the pyridine hemochromogen assay (*30*).

Electronic Absorption Spectroscopy. Electronic absorption (EA) spectra were recorded on a double-beam Varian Cary 4 Bio spectrophotometer set to a spectral bandwidth of 0.5 nm. Spectra were acquired at room temperature for samples of protein prepared, as indicated in the figure legends, in either 25 mM MOPS buffer, pH 7.4, or 25 mM EPPS buffer, pH 8.0, with 500 mM KCl. Oxygen was removed from anaerobic samples by flowing argon gas through the headspace of a septum-sealed cuvette for at least 10 minutes. Reduction of Fe(III) protein samples was accomplished either by adding an anaerobically prepared stock solution of sodium dithionite to achieve a final sample concentration of 1-5 mM or by adding a few solid crystals of sodium dithionite to the protein sample solution with argon gas flowing in the cuvette headspace. The Fe(II)CO adducts were prepared by the injection of CO via gas-tight syringe into the headspace of a septum-sealed cuvette containing the Fe(III) or as-isolated protein, followed by gentle agitation of the sample and addition of the dithionite reductant. Final protein and heme concentrations ranged from 7-10 μM, and 100-200 μL of CO gas was injected, as appropriate, to give complete conversion to the Fe(II)CO adduct.

Reoxidation of the Fe(II) Bx*RcoM-2 variants*. Protein that was present in the Fe(II) state to a significant extent after purification was reoxidized using potassium ferricyanide, $K_3[Fe(CN)_6]$. A stock solution of potassium ferricyanide (500 µL, 25 mM) was prepared by dissolving 4-5 mg of solid $K_3[Fe(CN)_6]$ in 500 µL of 25 mM MOPS pH 7.4 with 500 mM KCl. This stock solution was added to the protein sample to a final concentration of 1-2 mM. The mixture was allowed to react for 20-30 minutes. The protein solution was loaded onto a YM-30 Amicon Ultra spin concentrator (Millipore) and washed 4 times by concentration and dilution into fresh MOPS buffer (25 mM pH 7.4, 500 mM KCl) using a table-top centrifuge (RCF 15,000 x *g*) to remove excess $K_3[Fe(CN)_6]$. Final heme and protein concentrations were determined using the pyridine hemochromogen (*30*) and BCA assays (Pierce, Rockford, IL), respectively.

EPR Spectroscopy. X-band electron paramagnetic resonance (*27*) spectra were collected on a Bruker ELEXSYS E500 equipped with an Oxford ESR 900 continuous flow liquid helium cryostat and an Oxford ITC4 temperature controller maintained at 10 K. The microwave frequency was monitored using an EIP model 625A CW microwave frequency counter. Protein samples were prepared, as indicated in the figure legends, in either 50 mM borate, pH 8.0, or in 25 mM MOPS, pH 7.4, with 500 mM KCl. Samples were transferred to a quartz EPR tube via small-bore tubing (connected to a gas-tight syringe) and frozen in liquid nitrogen. Samples of approximately 150 µL had a final concentration range of 80-250 µM heme. For all samples, scans of 0 - 10,000 Gauss revealed no signals other than those reported.

Resonance Raman Spectroscopy. Resonance Raman (rR) spectra were obtained with an excitation wavelength of 413.1 nm from a Coherent I-302C Kr^+ laser. Low incident laser

powers of <20 mW were focused with a cylindrical lens onto the sample. The frozen protein samples, prepared as described for EPR (*vide supra*), were placed in a quartz dewar and maintained at 77 K in liquid nitrogen to reduce local heating. Light was scattered in an approximately 135° geometry (relative to the sample) and dispersed by an Acton Research triple monochromator with gratings of 2400 grooves/mm. Scattered light was detected using a liquid nitrogen-cooled CCD camera (Princeton instruments) under computer control using Spectrasense software. Peak positions were calibrated relative to the ice peak at 228 cm^{-1} or a Na_2SO_4 peak at 981 cm^{-1}. Windows centered at 650, 1250 and 1850 cm^{-1} were overlaid for a total frequency range of 150-2250 cm^{-1}. IGOR Pro software v. 6.0 (Wavemetrics, Inc.) was used to import and process all spectral data. Spectral deconvolutions were achieved using IGOR Pro software v. 6.0. Peaks were generated by direct combination of a series of Gaussian curves; the amplitudes and frequencies of the Gaussian curves were manually adjusted until the residuals between the native peak and the fitted peak were minimized. Major vibrational modes are assigned based on comparison with those of other heme proteins and the work of Kitagawa and Spiro (*31-35*).

Results

Characterization of C127S and C130S Bx*RcoM-2*. The electronic absorption spectra of purified C127S and C130S *Bx*RcoM-2 are most consistent with a low-spin, six-coordinate Fe(III) heme ligated by a cysteine(thiolate) and a neutral ligand, presumably His^{74} as in WT *Bx*RcoM. Thiolate-to-low spin Fe(III) charge transfer gives rise to an intense δ band and two low-energy ligand-to-metal charge transfer (LMCT) transitions, and these characteristic features are present in the electronic absorption spectra of C127S and C130S. The spectrum for C127S (Figure 4.2c) displays a well-resolved delta (δ) band at 354 nm; a sharp, intense Soret (γ) peak at 422 nm; a broad, asymmetric absorption envelope consisting of α and β bands at 562 and 537 nm, respectively; and a pair of weak LMCT transition bands at 648 and 728 nm. Peak positions for C130S are similar (Figure 4.2b). The electronic absorption spectra of these variants differ only marginally from those of WT, suggesting that the heme environments are similar (Figure 4.2, Table 4.1). Reduction (via addition of sodium dithionite) and CO binding to either C127S and C130S results in spectral changes nearly identical to those observed in WT *Bx*RcoM-2 (Table 4.1), suggesting that the reduction and CO binding behaviors of these variants are also similar to those of WT.

Comparison of the resonance Raman spectra of C127S and C130S to that of WT Fe(III)*Bx*RcoM-2 (Figure 4.3) support the presence of a low-spin, six-coordinate Fe(III) heme with a cysteine(thiolate) ligand in each variant. Porphyrin stretches in the mid-frequency region (1300-1700 cm^{-1}) are sensitive to the oxidation state of the heme iron (ν_4), its spin state and coordination number (ν_3, ν_2, ν_{10}) (*33, 34*). Assignments for these bands in WT Fe(III)*Bx*RcoM-2 were reported previously (*26*), and the high-frequency spectrum of C127S variant bears a striking resemblance to that of WT (Figures 4.3c and 4.3a, respectively). Similarly, the

spectrum of the as-isolated C130S protein overlaps closely with that of Fe(III) WT *Bx*RcoM-2 (Figures 4.4b and 4.4a, respectively); however, additional bands indicate there is a mixture of Fe(III) and Fe(II) in the as-isolated sample. The spectrum of C130S oxidized with potassium ferricyanide (Figure 4.3b) is almost identical to that of WT Fe(III)*Bx*RcoM-2, and is most consistent with a six-coordinate, low-spin Fe(III) heme; a shoulder persists in the oxidation-state marker band, ν_4, indicative of residual Fe(II) even after oxidation. Based on comparisons to rR spectra of other cysteine(thiolate)-ligated hemoproteins (*36-38*), an iron-sulfur stretching mode, $\nu_{Fe\text{-}S}$, was tentatively identified in the low-frequency region of the WT Fe(III)*Bx*RcoM-2 rR spectrum at 310 cm^{-1} (*26*). A similar, broad $\nu_{Fe\text{-}S}$ band is observed at 308 cm^{-1} for C127S (Figure 4.5c) and at 309 cm^{-1} for C130S (Figure 4.5b).

Electron paramagnetic resonance (*27*) spectroscopy is also indicative of a low-spin, six-coordinate Fe(III) ($S = ½$) heme with a cysteine(thiolate) *trans* to a second, neutral ligand in both C127S and C130S. The EPR spectrum of Fe(III) C127S (Figure 4.6c) displays a characteristic rhombic signal with *g* values of 1.91, 2.27, and 2.44 corresponding to g_x, g_y and g_z, respectively. Similarly, the rhombic EPR signal of Fe(III) C130S (Figure 4.6b) exhibits *g* values of 1.88, 2.27, and 2.50. For each variant, the *g* values are comparable to those obtained for WT Fe(III)*Bx*RcoM-2 (Figure 4.6a, Table 4.2). Slightly more basic pH and altered buffer conditions may account for differences in the observed *g* values among the variants and WT *Bx*RcoM-2. A second minor EPR signal with an axial *g* anisotropy ($g_\perp = 5.8$) is also observed for the variants C127S and C130S (both as-isolated and reoxidized). This signal is due to a small amount of high-spin Fe(III) heme present, consistent with rR spectra where a small five-coordinate high-spin band is observed at approximately 1490 cm^{-1} (ν_3) for both variants (Figure

4.3). Taken together, the electronic absorption, rR and EPR data for the Fe(III) C127S and Fe(III) C130S variants affirm the native His/Cys(thiolate) ligation motif is maintained.

Characterization of C94S Bx*RcoM-2*. Electronic absorption spectroscopy of purified C94S is strongly suggestive that Cys^{94} is the Fe(III) heme ligand in WT *Bx*RcoM-2. Unlike the C127S or C130S variants, electronic absorption spectra of C94S are most similar to those of Fe(III) hemes lacking a cysteine(thiolate) ligand (Figures 4.2d and 4.2e; Table 4.1). The as-isolated C94S Soret band at 418 nm is broader than that of WT *Bx*RcoM-2, and the α/β bands at 561 and 532 nm, respectively, are more well-defined than those expected for a six-coordinate, low-spin Fe(III) heme with Cys/His axial ligands. The pronounced, characteristic δ band of thiolate ligation is absent; in its place is a weak Soret shoulder near 360 nm. Only one LMCT band at 640 nm is observed, again suggesting that thiolate ligation is absent. Like the C130S variant, rR analyses initially indicated that C94S was purified as a mixture of the Fe(II) and Fe(III) oxidation states. In contrast to the C130S variant, however, only a weak EPR signal was initially detected (*vide infra*). Unlike the C130S variant, oxidation of the C94S variant by potassium ferricyanide resulted in a 3-nm blue-shift of the Soret band to 415 nm, a slight decrease in the intensity of the δ band shoulder, and slight shifts in the α/β band positions to 562 and 530 nm, respectively. Additionally, a band at 632 nm appeared suggesting that a high-spin Fe(III) heme was formed (*39*). The observed electronic absorption spectral features are most similar to proteins with a mixture of high- and low-spin Fe(III) hemes and without a cysteine(thiolate) ligand, such as metMb, *Ax*PDEA1H and *Mt*DosH (*39, 40*). Electronic absorption spectra of Fe(II) and Fe(II)CO C94S are virtually identical to those of WT *Bx*RcoM

(Table 3.1), suggesting that the reduction and CO binding behaviors of the C94S variant are unperturbed.

The rR spectrum for as-isolated C94S (Figure 3.4d) displays oxidation and spin-state marker bands consistent with a mixture of oxidation states, similar to those of the C130S variant. Addition of potassium ferricyanide to as-isolated C94S results in a sharpening of the oxidation state marker band with one major frequency exhibited at 1371 cm^{-1} (Figure 4.3d), indicative of Fe(III) as the majority heme iron oxidation state. A ν_3 shoulder, likely due to residual Fe(II), persisted in all of the studied samples. The high-frequency region that contains the spin and coordination-state marker bands (ν_3 and ν_2) displays broadened bands at 1493 and 1503 cm^{-1} (ν_3) and 1562 and 1577 cm^{-1} (ν_2). These band positions are indicative of a mixture of low-spin and high-spin Fe(III) hemes, which is most similar to what is observed in the met forms of Fe(III)*Ax*PDEA1H and Fe(III)*Mt*DosH (*40*). In addition, the spin-state marker band ν_{10} is not observed in the rR spectrum of C94S, unlike the ν_{10} band of the Fe(III) forms of WT, C130S and C127S *Bx*RcoM-2. Presumably, ν_{10} in C94S is shifted to lower energy and is hidden due to overlap with the strong, Gaussian-shaped $\nu_{c=c}$ band at 1622 cm^{-1}.

Distinct differences in the low frequency region of the resonance Raman spectrum of C94S support the conclusion that Cys^{94} is the native cysteine ligand. In the region where $\nu_{Fe\text{-}S}$ is typically seen, there is a band at 304 cm^{-1} that is sharpened and downshifted relative to the comparable band of WT *Bx*RcoM-2 (Figure 4.5). This 304 cm^{-1} mode might plausibly be attributed to a Fe-S(thioether) stretch, since Met^{104} is the distal Fe(II) ligand; however, we believe that this mode is actually a porphyrin vibration. Gaussian deconvolution of the broad $\nu_{Fe\text{-}S}$ bands of Fe(III) WT, C130S, and C127S *Bx*RcoM-2 (Figure 4.5) generated best fits with

three overlapping components. For the C94S spectrum a single Gaussian was sufficient to fit the sharp band at 304 cm^{-1}. Because the 304 cm^{-1} component peak is present in the low energy rR region of WT *Bx*RcoM-2 and all the variants, we assign this band to a porphyrin mode. We attribute the two higher-energy components (313 cm^{-1} and 321 cm^{-1}) of Fe(III) WT, C130S, and C127S *Bx*RcoM-2 to $\nu_{Fe\text{-}S}$. These $\nu_{Fe\text{-}S}$ bands overlap with the porphyrin mode centered at 304 cm^{-1}, like that of Cys-ligated NPAS2 (*41*). A new, intense band at 226 cm^{-1} is seen in the rR spectrum of C94S reacted with potassium ferricyanide, which we tentatively assign as the $\nu_{Fe\text{-}His}$ stretch of the proximal ligand His^{74}. The rationale for this assignment is the large resonance enhancement of the $\nu_{Fe\text{-}His}$ stretch, which typically appears in the 220-270 cm^{-1} region. This intense feature is typically observed in five- and six-coordinate ferrous hemoproteins with an axial His ligand, such as oxyMb, oxy and deoxyHb, microperoxidase, *Bj*FixLH, and *Mt*DosH (*40, 42-44*). A similarly intense Fe-His stretch is observed in five-coordinate ferric metMb (*45*).

EPR characterization of C94S provides confirmation that Cys^{94} is the sixth ligand to the Fe(III) heme in WT *Bx*RcoM-2. Data collected for the as-isolated C94S revealed no distinct set of rhombic signals between 2400 – 3800 G; however, a low intensity axial signal at $g_{\perp} = 5.8$ was observed, consistent with a high-spin Fe(III) heme. Addition of ferricyanide to the as-isolated form of C94S resulted in an increase in intensity (Figure 4.6d) of this high spin axial signal with $g_{\perp} = 5.82$ and $g_{||} = 2.00$. This axial spectrum is typical of high-spin hemoproteins such as aquo metMb and high-spin cytochrome *c* oxidase (*46, 47*). The EPR spectrum of the C94S protein (Figure 4.6d) also contains small rhombic signal that we attribute to the fraction of low-spin Fe(III). The g anisotropy of this low spin signal is comparable to those of WT *Bx*RcoM, C127S and C130S, suggesting that Cys^{127} or Cys^{130} may replace Cys^{94} in a fraction

of the C94S protein. The fact that the EPR spectrum of C94S exhibits predominantly high-spin Fe(III), and not low-spin Fe(III) like that of WT *Bx*RcoM-2, is clear evidence that the cysteine ligand has been lost in this variant. Taken all together, our spectral data implicate Cys^{94} as the distal Fe(III) heme ligand in *Bx*RcoM-2.

Discussion

Numerous heme proteins are implicated in sensing and transport of small molecules (*1, 4, 6*); discrimination among the gaseous signal transducers O_2, NO, and CO requires a recognition mechanism that is not based on charge, shape, or size because these gases cannot be readily differentiated by these methods. Instead, heme proteins must modify their affinity for small molecules by altering the iron redox potential, oxidation state, spin state, distal or proximal ligands, or interactions of the gas molecule with residues in the heme-binding pocket (*2*). Functional activity of gas-sensing heme proteins is frequently linked to the nature of the heme-binding environment. One element of control utilized to poise the heme for gas binding is a redox-mediated ligand switch; however, the discriminatory binding of gas molecules is modulated by a combination of factors that a redox-mediated ligand switch alone cannot confer. In many cases, a series of events occurs in which the heme iron atom changes oxidation and ligation states preceding gas binding; the final step of regulation is commonly achieved upon stabilization of the correct effector molecule in the heme-binding pocket.

In the O_2 sensor *Ec*DOS, binding of O_2 to heme regulates phosphodiesterase activity (*3, 48*). The *Ec*DOS Fe(III) heme, bound within a PAS domain, is coordinated by a histidine residue (His^{77}) and an exogenous water molecule (*49*). Reduction of the heme to Fe(II) results in replacement of the coordinated water by a methionine (Met^{95}) as the distal heme ligand (*50, 51*). O_2 binding to Fe(II)*Ec*DOS proceeds via replacement of the weakly-bound Met^{95} thioether group. Structural and spectroscopic studies have revealed that charge build-up on the coordinated O_2, which does not happen upon CO or NO binding, is neutralized via the guanidinium group of Arg^{97} (*49, 51, 52*). The environment of the heme-binding pocket in

*Ec*DOS enables the protein to enhance selectivity for O_2 over CO or NO and prevents autoxidation of the heme iron upon O_2 binding (*3, 52, 53*).

The heme-regulated eIF2α (HRI) kinase, which regulates globin synthesis in reticulocytes in response to available heme levels, is a multidomain heme protein with two distinct heme-binding sites, one of which is a low-spin, six-coordinate heme-thiolate center that functions as a NO sensor (*54, 55*). Cys^{409} of the kinase domain and a histidine (His^{119} or His^{120}) of the N-terminal domain serve as ligands to this NO-binding heme. Characteristics of cysteine(thiolate) coordination are lost following reduction, suggesting that either a ligand switch or protonation to a cysteine(thiol) occurs to stabilize the more electron-rich Fe(II) heme (*56, 57*). HRI kinase activity is specifically upregulated by formation of a five-coordinate NO adduct, which occurs due to the strong *trans* influence of NO and the weakly-coordinating nature of the His ligand. CO binding opposite the anchoring histidine, forming a six-coordinate species, suppresses activity in HRI, and reaction with O_2 results in autoxidation (*55*). It is postulated that NO binding releases inhibition by the HRI heme domain, while binding of other gas signaling molecules does not (*58*).

*Rr*CooA is the first-known and best-characterized CO gas sensor. This homodimeric protein binds a heme *b* cofactor within each monomer and utilizes heme-dependent control to regulate expression of genes encoding CO-metabolizing enzymes (*20, 59, 60*). The Fe(III) heme in *Rr*CooA is low-spin and six-coordinate; the axial ligands to the Fe(III) heme are a cysteine(thiolate) (Cys^{75}) and the N-terminal proline (Pro^{2}) from the other monomer of the dimer (*61-63*). Reduction of the heme iron results in replacement of the cysteine(thiolate) ligand (Cys^{75}) with histidine (His^{77}) (*63, 64*). *Rr*CooA is unusual in that the weakly coordinated N-terminal proline (Pro^{2}) is retained during the redox exchange and thereafter is replaced by

the exogenous CO molecule (*62, 65*). Binding of CO initiates conformational changes that are propagated along the dimer interface, ultimately resulting in DNA binding (*62, 65-68*). Addition of O_2 to Fe(II)*Rr*CooA results in autoxidation, which reverts the protein to the Cys-His axial coordination characteristic of the Fe(III) heme (*20*). NO reacts with either Fe(III) or Fe(II) *Rr*CooA to form a five-coordinate Fe(II)-NO heme, which is inactive toward DNA binding (*69*). Thus, *Rr*CooA is also able to discriminate between O_2, CO, and NO, and regulate the biological response of *R. rubrum* to its environment.

In a manner similar to *Rr*CooA, the isolated PAS-A domain of the mammalian CO sensor NPAS2 bears an Fe(III) heme that is low-spin and is ligated by a His/Cys(thiolate) motif. Upon reduction of the Fe(III) heme, the cysteine(thiolate) ligand (Cys^{170}) is replaced with a strong donor, postulated to be the deprotonated side chain of His^{171} (*41*). One of the histidines is then released to bind CO: whether this is His^{119} or His^{171} is not clear. CO-dependent signaling is transduced through the PAS-A domain via disruption of a hydrogen-bonding network, which ultimately causes dissociation of NPAS2 from its heterodimeric partner BMAL1. Dissociation of the DNA-binding NPAS2-BMAL1 complex prevents transcription of *per* and *cry* genes, both of which are involved in regulation of the circadian clock (*18, 41, 70*). NPAS2 is reported neither to bind O_2 reversibly nor to interact with NO (*18*). The structural basis for this discrimination is unknown, but it is hypothesized that secondary interactions in the heme-binding pocket contribute.

Recent spectroscopic studies and *in vivo* functional assays have linked the heme-containing *Bx*RcoM proteins to aerobic CO sensing (*21, 26*). Similar to other small-molecule sensor proteins that respond to O_2, CO, and NO binding, *Bx*RcoM function is modulated by the oxidation state of the heme iron and by the ligand environment of the heme cofactor. Our prior

studies demonstrated that *Bx*RcoM-2 is a cysteine-ligated heme protein that undergoes a redox-mediated ligand switch (*26*). In the Fe(III) state, the proximal ligand is inferred to be His^{74} based on sequence similarity to and site-directed mutagenesis studies of the homologous *Bx*RcoM-1 protein (*vide supra*) (*21*). The *Bx*RcoM-1 and -2 proteins contain three cysteine residues as the potential distal ligand to the Fe(III) heme: Cys^{94}, Cys^{127} and Cys^{130}. Given the involvement of cysteine(thiolate) residues in redox-mediated ligand switches, which appear to prime gas-regulated hemoproteins for effector-mediated response, we set out to identify the Fe(III) *Bx*RcoM cysteine(thiolate) ligand.

Herein, Cys^{94} was identified as the distal Fe(III) heme ligand in *Bx*RcoM-2. Sequence alignments of putative RcoM homologues suggested Cys^{130} was the more likely heme ligand candidate. Three cysteine-to-serine variants were generated, and unlike the other studied variants, spectral data strongly suggest that C94S does not possess the native low-spin Fe(III) heme with His/Cys(thiolate) coordination. The EPR spectrum of C94S was dominated by an axial signal characteristic of high-spin heme, providing the most compelling evidence that the strongly donating thiolate axial ligand was absent. A minor low-spin component was also observed, suggesting that a sixth ligand may bind in place of Cys^{94} in a small population of the Fe(III) C94S variant. Give the apparent g anisotropy of this weak low-spin signal, we speculate that Cys^{130}, the most conserved of the three cysteines, or possibly Cys^{127}, may replace the native Cys^{94}. The electronic absorption spectrum of C94S lacked the well-resolved δ band and the two weak LMCT bands in the visible region characteristic of a low-spin thiolate-ligated heme. Furthermore, rR data suggested that the Fe-S stretch was absent, and a new band at 226 cm^{-1} was tentatively assigned as a $\nu_{Fe\text{-}His}$ mode of a high-spin heme. Thus, all the spectral data point to Cys^{94} as the heme ligand in *Bx*RcoM-2 although this residue is not highly conserved

among RcoM proteins. It remains to be seen whether other RcoM proteins bear heme, whether they employ cysteine coordination, or whether Cys^{130} plays some other role in signal transduction in these proteins.

In combination with our past results on the *Bx*RcoM proteins, these data illustrate a mechanism by which the *Bx*RcoM proteins utilize changes in oxidation and ligation states at the heme cofactor to poise the protein to respond to CO (Scheme 4.1). *Bx*RcoM proteins are members of a family of cysteine(thiolate)-coordinated heme proteins that undergo redox-mediated ligand exchange and selective ligand replacement as components of the machinery to affect protein function. As shown in Scheme 1, reduction of the low-spin, six-coordinate Fe(III) heme center in *Bx*RcoM results in the loss of the cysteine(thiolate) distal ligand; this ligand is now known to be Cys^{94}. Loss of a cysteine(thiolate) ligand from a low-spin six-coordinate heme serves as a priming reaction that prepares *Bx*RcoM to respond to its effector molecule, similar to what is observed in *Rr*CooA and NPAS2. *Bx*RcoM Cys^{94} is replaced by a neutral, weakly-bound ligand, presumably Met^{104}; Met^{104} is then replaced by CO. Met^{104} serves an analogous function to Met^{95} in the heme-PAS O_2-sensor *Ec*DOS (*49, 71*), as the more weakly bound, more readily replaced ligand in a low-spin six-coordinate heme complex. Thus, the *Bx*RcoM proteins utilize a hybrid of the strategies seen in *Rr*CooA, NPAS2, and *Ec*DOS to ready themselves for gas-dependent transcriptional activation. Ultimately, the redox-mediated ligand switch from Cys^{94} [Fe(III)] to Met^{104} [Fe(II)] is crucial to maintaining the sensitivity of the *Bx*RcoM proteins to CO; however, the exact discriminatory nature of the RcoM proteins for CO over O_2 and NO, and the mode of propagation of this signal to the LytTR DNA-binding domain are still unknown.

Future Directions

Cys^{94} is the distal ligand to the Fe(III) heme in RcoM-2 and, by analogy, RcoM-1, the CO-responsive transcriptional regulators from *B. xenovorans*. In this study we altered all three cysteines, generating cysteine-to-serine variants (C94S, C127S and C130S). The electronic absorption, rR and EPR spectra of C127S and C130S variants are similar to those of WT *Bx*RcoM-2, consistent with retention of a Cys(thiolate) ligand to the Fe(III) heme. By contrast, the spectral features of the C94S variant spectral features are inconsistent with Cys(thiolate) ligation at the Fe(III) heme. In combination with our previous results, these data reveal a complete picture of the redox-mediated ligand switch that occurs at the heme cofactor in the RcoM proteins; however the mechanism by which CO binding is transmitted to the LytTR DNA-binding domain to regulate function is yet to be elucidated.

We believe one of the Fe(II) heme ligands of RcoM is methionine, with the other a neutral ligand (presumably histidine). To establish methionine as an Fe(II) ligand, I established a protocol for minimal media expression of selenomethionine-modified *Bx*RcoM-2. Incorporating selenomethionine into *Bx*RcoM-2 will enable spectroscopic characterization for the verification of methionine as one of the Fe(II) heme ligands. The *E. coli* VJS6737 (*28*) strain bearing the pEXT20 expression vector for *Bx*RcoM-2 requires a robust minimal medium; the key to cell growth is the presence of Kao and Michayluk vitamin solution (see Appendix for recipes).

References

1. Uchida, T., and Kitagawa, T. (2005) Mechanism for Transduction of the Ligand-Binding Signal in Heme-Based Gas Sensory Proteins Revealed by Resonance Raman Spectroscopy, *Acc. Chem. Res. 38*, 662-670.
2. Jain, R., and Chan, M. K. (2003) Mechanisms of ligand discrimination by heme proteins, *J. Biol. Inorg. Chem. 8*, 1-11.
3. Sasakura, Y., Suzuki-Yoshimura, T., Kurokawa, H., and Shimizu, T. (2006) Structure-Function Relationships of *Ec*DOS, a Heme-regulated Phosphodiesterase from *Escherichia coli*, *Acc. Chem. Res. 39*, 37-43.
4. Aono, S. (2008) Metal-containing sensor proteins sensing diatomic gas molecules, *Dalton Transactions 24*, 3137-3146.
5. Spiro, S. (2008) Metalloregulatory proteins and nitric oxide signalling in bacteria, *Biochem. Soc. Trans. 36*, 1160-1164.
6. Gilles-Gonzalez, M.-A., and Gonzalez, G. (2005) Heme-based sensors: defining characterstics, recent developments, and regulatory hypotheses., *J. Inorg. Biochem. 99*, 1-22.
7. Gilles-Gonzalez, M. A., Ditta, G. S., and Helinski, D. R. (1991) A haemoprotein with kinase activity encoded by the oxygen sensor of *Rhizobium meliloti*, *Nature 350*, 170–172.
8. Hou, S., Larsen, R. W., Boudko, D., Riley, C. W., Karatan, E., Zimmer, M., Ordal, G. W., and Alam, M. (2000) Myoglobin-like aerotaxis transducers in Archaea and Bacteria, *Nature 403*, 540-544.

9. Delgado-Nixon, V. M., Gonzalez, G., and Gilles-Gonzalez, M.-A. (2000) Dos, a Heme-Binding PAS Protein from *Escherichia coli*, Is a Direct Oxygen Sensor, *Biochemistry 39*, 2685-2691.

10. Ignarro, L. J. (1999) Nitric Oxide: A Unique Endogenous Signaling Molecule in Vascular Biology, *Angew. Chem. Int. Ed. 38*, 1882-1892.

11. Karow, D. S., Pan, D., Tran, R., Pellicena, P., Presley, A., Mathies, R. A., and Marletta, M. A. (2004) Spectroscopic characterization of the soluble guanylate cyclase-like heme domains from *Vibrio cholerae* and *Thermoanaerobacter tengcongensis*, *Biochemistry 43*, 10203-10211.

12. Ignarro, L. J., Degnan, J. N., Baricos, W. H., Kadowitz, P. J., and Wolin, M. S. (1982) Activation of purified guanylyl cyclase by NO requires heme, *Biochim. Biophys. Acta 718*, 49-59.

13. Igarashi, J., Sato, A., Kitagawa, T., Yoshimura, T., Yamauchi, S., Sagami, I., and Shimizu, T. (2004) Activation of Heme-regulation Eukaryotic Initiation Factor 2α Kinase by Nitric Oxide Is Induced by the Formation of a Five-coordinate NO-heme Complex. Optical Absorption, Electronic Spin Resonance, and Resonance Raman Spectral Studies, *J. Biol. Chem. 279*, 15752-15762.

14. de Rosny, E., de Groot, A., Jullian-Binard, C., Borel, F., Suarez, C., Le Pape, L., Fontecilla-Camps, J. C., and Jouve, H. M. (2008) DHR51, the Drosophila melanogaster Homologue of the Human Photoreceptor Cell-Specific Nuclear Receptor, Is a Thiolate Heme-Binding Protein, *Biochemistry 47*, 13252-13260.

15. Reinking, J., Lam, M. M. S., Pardee, K., Sampson, H. M., Liu, S., Yang, P., Williams, S., White, W., Lajoie, G., Edwards, A., and Krause, H. M. (2005) The Drosophila Nuclear Receptor E75 Contains Heme and Is Gas Responsive, *Cell 122*, 195-207.

16. Giardina, G., Rinaldo, S., Johnson, K. A., Di Matteo, A., Brunori, M., and Cutruzzolà, F. (2008) No sensing in *Pseudomonas aeruginosa*: Structure of the Transcriptional Regulator DNR, *J. Mol. Biol. 378*, 1002-1015.

17. Verma, A., Hirsch, D. J., Glatt, C. E., Ronnet, G. V., and Snyder, S. H. (1993) Carbon monoxide: a putative neural messenger, *Science 259*, 381-384.

18. Dioum, E. M., Rutter, J., Tuckerman, J. R., Gonzalez, G., Gilles-Gonzalex, M.-A., and Mcknight, S. L. (2002) NPAS2: A gas-responsive transcription factor, *Science 298*, 2385-2387.

19. Aono, S., Nakajima, H., Saito, K., and Okada, M. (1996) A novel heme protein that acts as a carbon monoxide-dependent transcriptional activator in Rhodospirillum rubrum, *Biochem. Biophys. Res. Commun. 228*, 752-756.

20. Shelver, D., Kerby, R. L., He, Y., and Roberts, G. P. (1997) CooA, a CO-sensing transcription factor from *Rhodospirillum rubrum*, is a CO-binding heme protein, *Proc. Natl. Acad. Sci. U.S.A. 94*, 11216-11220.

21. Kerby, R. L., Youn, H., and Roberts, G. P. (2008) RcoM: A New Single-Component Transcriptional Regulator of CO Metabolism in Bacteria, *J. Bacteriol. 190*, 3336-3343.

22. Chain, P. S. G., Denef, V. J., Konstantinidis, K. T., Vergez, L. M., Agulló, L., Reyes, V. L., Hauser, L., Córdova, M., Gómez, L., González, M., Land, M., Lao, V., Larimer, F., LiPuma, J. J., Mahenthiralingam, E., Malfatti, S. A., Marx, C. J., Parnell, J. J., Ramette, A., Richardson, P., Seeger, M., Smith, D., Spilker, T., Sul, W. J., Tsoi, T. V., Ulrich, L.

E., Zhulin, I. B., and Tiedje, J. M. (2006) *Burkholderia xenovorans* LB400 harbors a multi-replicon, 9.73-Mbp genome shaped for versatility, *Proc. Natl. Acad. Sci. USA 103*, 15280-15287.

23. Gu, Y.-Z., Hogenesch, J. B., and Bradfield, C. A. (2000) The PAS Superfamily: Sensors of Environmental and Developmental Signals, *Annu. Rev. Physiol. 40*, 519-561.

24. Nikolskaya, A. N., and Galperin, M. Y. (2002) A novel type of conserved DNA-binding domain in the transcriptional regulators of the AlgR/AgrA/LytR family, *Nucl. Acids Res. 30*, 2453-2459.

25. Kerby, R. L., and Roberts, G. P. (2012) Burkholderia xenovorans RcoMBx-1, a Transcriptional Regulator System for Sensing Low and Persistent Levels of Carbon Monoxide, *J. Bacteriol. 194*, 5803-5816.

26. Marvin, K. A., Kerby, R. L., Youn, H., Roberts, G. P., and Burstyn, J. N. (2008) The Transcription Regulator RcoM-2 from Burkholderia xenovorans Is a Cysteine-Ligated Hemoprotein That Undergoes a Redox-Mediated Ligand Switch, *Biochemistry 47*, 9016-9028.

27. Miskevich, F., Davis, A., Leeprapaiwong, P., Giganti, V., Kostić, N. M., and Angel, L. A. (2011) Metal complexes as artificial proteases in proteomics: A palladium(II) complex cleaves various proteins in solutions containing detergents, *J. Inorg. Biochem. 105*, 675-683.

28. Stewart, V., Lu, Y., and Darwin, A. J. (2002) Periplasmic Nitrate Reductase (NapABC Enzyme) Supports Anaerobic Respiration by Escherichia coli K-12, *J. Bacteriol. 184*, 1314-1323.

29. Dykxhoorn, D. M., St. Pierre, R., and Linn, T. (1996) A set of compatible *tac* promoter expression vectors, *Gene 177*, 133-136.

30. Antonini, E., and Brunori, M. (1971) *Hemoglobin and Myoglobin in Their Reactions with Ligands*, Vol. 21, North-Holland Publishing Co., Amsterdam.

31. Abe, M., Kitagawa, T., and Kyogoku, Y. (1978) Resonance Raman spectra of octaethylporphyinato-Ni(II) and *meso*-deuterated and 15N substituted derivatives. II. A normal coordinate analysis, *J. Chem. Phys. 69*, 4526-4532.

32. Woodruff, W. H., Adams, D. H., Spiro, T. G., and Yonetani, T. (1975) Resonance Raman spectra of cobalt myoglobins and cobalt porphyrins. Evaluation of protein effects on porphyrin structure., *J. Am. Chem. Soc. 97*, 1695-1698.

33. Spiro, T. G. (1975) Resonance Raman spectroscopic studies of heme proteins, *Biochim. Biophys. Acta 416*, 169-189.

34. Spiro, T. G., and Strekas, T. C. (1974) Resonance Raman spectra of heme proteins. Effects of oxidation and spin state., *J. Am. Chem. Soc. 96*, 338-345.

35. Kitagawa, T., Kyogoku, Y., Iizuka, T., Ikeda-Saito, M., and Yamanaka, T. (1975) Resonance Raman Scattering from Hemoproteins, *J. Biochem. 78*, 719-728.

36. Champion, P. M., Stallard, B. R., Wagner, G. C., and Gunsalus, I. C. (1982) Resonance Raman detection of an Fe-S bond in cytochrome P450CAM, *J. Am. Chem. Soc. 104*, 5469-5472.

37. Green, E. L., Taoka, S., Banerjee, R., and Loehr, T. M. (2000) Resonance Raman Characterization of the Heme Cofactor in Cystathionine β-Synthase. Identification of the Fe-S(Cys) Vibration in the Six-Coordinate Low-Spin Heme, *Biochemistry 40*, 459-463.

38. Liu, Y., Loccoz-Moënne, P., Hildebrand, D. P., Wilks, A., Loehr, T. M., Mauk, A. G., and de Montellano, P. R. O. (1999) Replacement of the Proximal Histidine Iron Ligand by a Cysteine or Tyrosine Converts Heme Oxygenase to an Oxidase, *Biochemistry 38*, 3733-3743.

39. Falk, J. E. (1964) *Porphyrins and Metalloporphyrins: Their General, Physical, and Coordination Chemistry, and Laboratory Methods*, Elsevier, Amsterdam.

40. Tomita, T., Gonzalez, G., Chang, A. L., Ikeda-Saito, M., and Gilles-Gonzalex, M.-A. (2002) A Comparative Resonance Raman Analysis of Heme-Binding PAS Domains: Heme Iron Coordination Structures of the *Bj*FixL, *Ax*PDEA1, *Ec*Dos, and *Mt*Dos Proteins, *Biochemistry 41*, 4819-4826.

41. Uchida, T., Sato, E., Sato, A., Sagami, I., Shimizu, T., and Kitagawa, T. (2005) CO-dependent Activity-controlling Mechanism of Heme-containing CO-sensor Protein, Neuronal PAS Domain Protein 2, *J. Biol. Chem. 280*, 21358-21368.

42. Kerr, E. A., Yu, N.-T., Gersonde, K., Parish, D. W., and Smith, K. M. (1985) Iron-Histidine Stretching Vibration in the Deoxy State of Insect Hemoglobins with Different O2 Affinities and Bohr Effects, *J. Biol. Chem. 260*, 12665-12669.

43. Walters, M. A., and Spiro, T. G. (1982) Resonance Raman Spectroscopic Studies of Axial Ligation in Oxyhemoglobin, Oxymyoglobin, and Nitrosylmyoglobin, *Biochemistry 21*, 6989-6995.

44. Othman, S., Lirzin, A. L., and Desbois, A. (1994) Resonance Raman Investigation of Imidazole and Imidazolate Complexes of Microperoxidase: Characterization of the Bis(histidine) Axial Ligation in *c*-Type Cytochromes, *Biochemistry 33*, 15437-15448.

45. Hirota, S., Mizoguchi, Y., Yamauchi, O., and Kitagawa, T. (2002) Observation of an isotope-sensitive low-frequency Raman band specific to metmyoglobin, *J. Biol. Inorg. Chem. 7*, 217-221.

46. Peisach, J., Blumberg, W. E., Ogawa, S., Rachmilewitz, E. A., and Oltzik, R. (1971) The Effects of Protein Conformation on the Heme Symmetry in High Spin Ferric Heme Proteins as Studied by Electron Paramagnetic Resonance, *J. Biol. Chem. 246*, 3342-3355.

47. Beinert, H., and Shaw, R. T. (1977) On the Identity of the High Spin Heme Components of Cytochrome *c* Oxidase, *Biochim. Biophys. Acta 462*, 121-130.

48. Tuckerman, J. R., Gonzalez, G., Sousa, E. H. S., Wan, X., Saito, J. A., Alam, M., and Gilles-Gonzalez, M.-A. (2009) An Oxygen-Sensing Digunalylate Cyclase and Phosphodiesterase Couple for c-di-GMP Control, *Biochemistry 48*, 9764-9774.

49. Kurokawa, H., Lee, D. S., Watanabe, M., Sagami, I., Mikami, B., Raman, C. S., and Shimizu, T. (2004) A redox-controlled molecular switch revealed by the crystal structure of a bacterial heme PAS sensor., *J. Biol. Chem. 279*, 20186-20193.

50. Hirata, S., Matsui, T., Sasakura, Y., Sugiyama, S., Yoshimura, T., Sagami, I., and Shimizu, T. (2003) Characterization of Met95 mutants of a heme-regulated phosphodiesterase from *Escherichia coli*. Optical absorption, magnetic circular dichroism, circular dichroism, and redox potentials, *Eur. J. Biochem. 270*, 4771-4779.

51. Park, H., Suquet, C., Satterlee, J. D., and Kang, C. (2004) Insights into Signal Transduction Involving PAS Domain Oxygen-Sensing Heme Proteins from the X-ray Crystal Structure of *Eschericihia coli* Dos Heme Domian (EcDosH), *Biochemistry 43*, 2738-2746.

52. Gonzalez, G., Dioum, E. M., Bertolucci, C. M., Tomita, T., Ikeda-Saito, M., Cheesman, M. R., Watmough, N. J., and Gillez-Gonzalez, M.-A. (2002) Nature of the displaceable heme-axial residue in the *Ec*Dos protein, a heme-based sensor from *Escherichia coli*, *Biochemistry 41*, 8414-8421.

53. Ishitsuka, Y., Araki, Y., Tanaka, A., Igarashi, J., Ito, O., and Shimizu, T. (2008) Arg97 at the Heme-Distal Side of the Isolated Heme-Bound PAS Domain of a Heme-Based Oxygen Sensor from Escherichia coli (Ec DOS) Plays Critical Roles in Autoxidation and Binding to Gases, Particularly O2, *Biochemistry 47*, 8874-8884.

54. Chen, J.-J., and London, I. M. (1995) Regulation of protein synthesis by heme-regulated eIF-2[alpha] kinase, *Trends Biochem. Sci 20*, 105-108.

55. Ishikawa, H., Yun, B.-G., Takahashi, S., Hori, H., Matts, R. L., Ishimori, K., and Morishima, I. (2002) NO-Induced Activation Mechanism of the Heme-Regulated eIF2Œ± Kinase, *J. Am. Chem. Soc. 124*, 13696-13697.

56. Igarashi, J., Murase, M., Iizuka, A., Pichierri, F., Martinkova, M., and Shimizu, T. (2008) Elucidation of the Heme Binding Site of Heme-regulated Eukaryotic Initiation Factor 2{alpha} Kinase and the Role of the Regulatory Motif in Heme Sensing by Spectroscopic and Catalytic Studies of Mutant Proteins, *J. Biol. Chem. 283*, 18782-18791.

57. Hirai, K., Martinkova, M., Igarashi, J., Saiful, I., Yamauchi, S., El-Mashtoly, S., Kitagawa, T., and Shimizu, T. (2007) Identification of Cys385 in the isolated kinase insertion domain of heme-regulated eIF2[alpha] kinase (HRI) as the heme axial ligand by site-directed mutagenesis and spectral characterization, *J. Inorg. Biochem. 101*, 1172-1179.

58. Uma, S., Yun, B.-G., and Matts, R. L. (2001) The Heme-regulated Eukaryotic Initiation Factor 2α Kinase: A Potential Regulatory Target For Control of Protein Synthesis by Diffusible Gases, *J. Biol. Chem. 276*, 14875-14883.

59. Roberts, G. P., Kerby, R. L., Youn, H., and Conrad, M. (2005) CooA, a paradigm for gas sensing regulatory proteins, *J. Inorg. Biochem. 99*, 280-292.

60. Kerby, R. L., Ludden, P. W., and Roberts, G. P. (1995) Carbon monoxide-dependent growth of *Rhodospirillum rubrum*, *J. Bacteriol. 177*, 2241-2244.

61. Reynolds, M. F., Shelver, D., Kerby, R. L., Parks, R. B., Roberts, G. P., and Burstyn, J. N. (1998) EPR and Electronic Absorption Spectroscopies of the CO-Sensing CooA Protein Reveal a Cysteine-Ligated Low-Spin Ferric Heme, *J. Am. Chem. Soc. 120*, 9080-9081.

62. Lanzilotta, W. N., Schuller, D. J., Thorsteinsson, M. V., Kerby, R. L., Roberts, G. P., and Poulos, T. L. (2000) Structure of the CO sensing transcription activator CooA, *Nature Struct. Biol. 7*, 876-880.

63. Shelver, D., Torsteinsson, M. V., Kerby, R. L., Chung, S.-Y., and Roberts, G. P. (1999) Identification of Two Important Heme Site Residues (Cysteine 75 and Histidine 77) in CooA, the CO-Sensing Transcription Factor of *Rhodospirillum rubrum*, *Biochemistry 38*, 2669-2678.

64. Aono, S., Ohkubo, K., Matsuo, T., and Nakajima, H. (1998) Redox-controlled ligand exchange of the heme in the CO-sensing transcriptional activator CooA, *J. Biol. Chem. 273*, 25757-25764.

65. Clark, R. W., Youn, H., PArks, R. B., Cherney, M. M., Roberts, G. P., and Burstyn, J. N. (2004) Investigation of the Role of the N-Terminal Proline, the Distal Heme Ligand in the CO Sensor CooA, *Biochemistry 43*, 14149-14160.

66. Kerby, R. L., Youn, H., Thorsteinsson, M. V., and Roberts, G. P. (2003) Repositioning about the Dimer Interface of the Transcription Regulator CooA: A Major Signal Transduction Pathway between the Effector and DNA binding Domains, *J. Mol. Biol. 325*, 809-823.

67. Youn, H., Kerby, R. L., and Roberts, G. P. (2003) The Role of the Hydrophobic Distal Heme Pocket of CooA in Ligand Sensing Response, *J. Biol. Chem. 278*, 2333-2340.

68. Yamamoto, K., Ishikawa, H., Takahashi, S., Ishimori, K., Morishima, I., Nakajima, H., and Aono, S. (2001) Binding of CO at the Pro2 side is crucial for the activation of CO-sensing transcriptional activator CooA. 1H NMR spectroscopic studies., *J. Biol. Chem. 276*, 11473-11476.

69. Reynolds, M. F., Parks, R. B., Burstyn, J. N., Shelver, D., Thorsteinsson, M. V., Kerby, R. L., Roberts, G. P., Vogel, K. M., and Spiro, T. G. (2000) Electronic absorption, EPR, and resonance Raman spectroscopy of CooA, a CO-sensing transcription activator from R. rubrum, reveals a five-coordinate NO-heme, *Biochemistry 39*, 388-396.

70. Kitanishi, K., Igarashi, J., Hayasaka, K., Hikage, N., Saiful, I., Yamauchi, S., Uchida, T., Ishimori, K., and Shimizu, T. (2008) Heme-Binding Characteristics of the Isolated PAS-A Domain of Mouse Per2, a Transcriptional Regulatory Factor Associated with Circadian Rhythms, *Biochemistry 47*, 6157-6168.

71. Tanaka, A., Takahashi, H., and Shimizu, T. (2007) Critical role of the heme axial ligand, Met95, in locking catalysis of the phosphodiesteraze from *Escherichia coli* (*Ec*DOS) toward cyclic diGMP, *J. Biol. Chem. 282*, 21301-21307.

Table 4.1. Comparison of electronic absorption peak positions (nm) for the CxxS *Bx*RcoM-2 variants with WT *Bx*RcoM-2 in the Fe(III), Fe(II) and Fe(II)CO states.

Electronic Absorption							
Fe(III)	**Ligands**	**δ**	**Soret**	**β**	**α**	**LMCT**	**Ref.**
WT *Bx*RcoM-2	Cys/His	354	423	541	565	640, 730	(*26*)
C130S[b]		356	422	539	561	640, 720	a
C127S[b]		354	422	537	562	648, 728	a
C94S[b]		sh[c]	418	532	561	640	a
C94S + ferricyanide		sh[c]	415	530	562	632	a
Fe(II)							
WT *Bx*RcoM-2	Met/His		425	532	562		(*26*)
C130S			425	532	562		a
C127S			424	532	562		a
C94S			425	532	562		a
C94S + ferricyanide			426	531	562		a
Fe(II)CO							
WT *Bx*RcoM-2	His/CO		423	540	570		(*26*)
C130S			423	540	569		a
C127S			423	539	568		a
C94S			423	540	570		a
C94S + ferricyanide			423	540	570		a

[a]This work. [b]This data is provided for the protein *as isolated*; the sample may contain a fraction of the Fe(II) form. [c]Shoulder.

Table 4.2. Comparison of EPR *g* values for the CxxS *Bx*RcoM-2 variants with WT *Bx*RcoM-2.

EPR						
Protein	Ligands	g_z	g_y	g_x		Ref.
WT *Bx*RcoM-2	His/Cys	2.52	2.28	1.88	pH 8.0	(*26*)
C130S[b] *Bx*RcoM-2		2.50	2.28	1.87	pH 7.4	a
C127S *Bx*RcoM-2		2.44	2.27	1.91	pH 7.4	a
		$g_\perp$		$g_\parallel$		
C94S[b] *Bx*RcoM-2		5.82		2.00	pH 7.4	a

[a]This work. [b]The spectrum was obtained after reaction of the as-isolated protein with ferricyanide.

Figure 4.1. Sequence alignments of *B. xenovorans* RcoM-1 (UniProt accession no. Q13YL3; NCBI gi:123168453) and -2 (UniProt accession no. Q13IY4; NCBI gi:122969446) with two putative RcoM proteins from *B. cepacia* H160 (UniProt accession no. B5WBI7) and *B. cepacia* CH1-1 (UniProt accession no. D5NG05). All Cys residues are boxed in black; the appropriate numbering is indicated above an inverted arrow (⮟). The alignments show high amino-acid conservation among all sequences, including complete conservation of Cys^{94} and Cys^{130}, but not Cys^{127}.

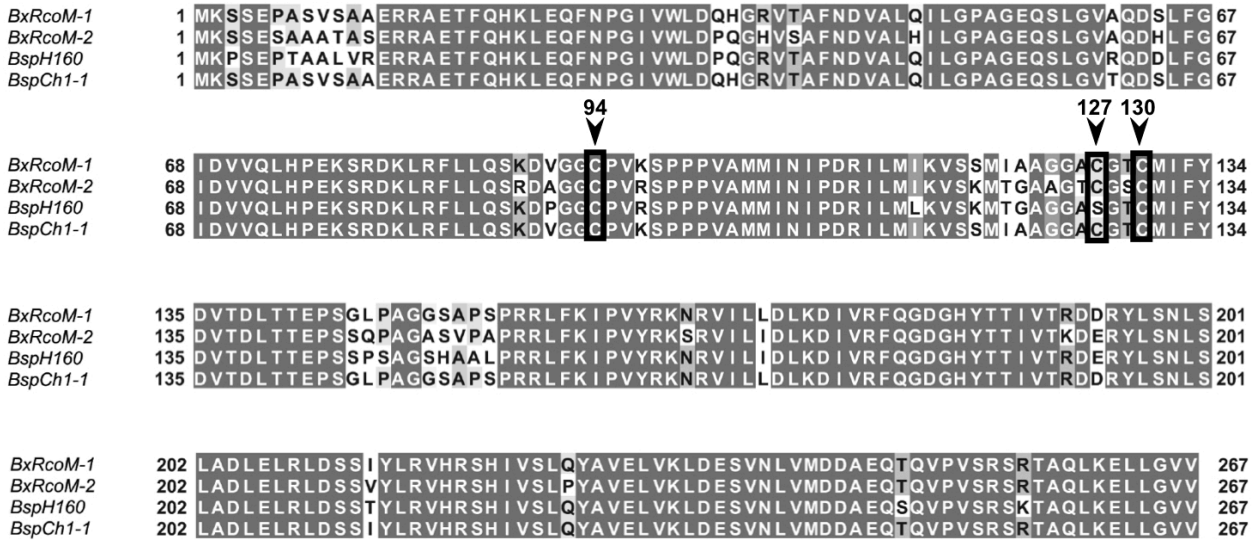

Figure 4.2. Electronic absorption spectra of purified a) WT *Bx*RcoM-2, b) C130S, c) C127S, d) C94S and e) C94S reacted with potassium ferricyanide. Spectra of samples a-d were taken of the protein as isolated; the spectrum of sample e was taken after oxidation of the protein with potassium ferricyanide and removal of excess oxidant via a spin concentrator. Sample a) contained 12 μM heme in 25 mM EPPS pH 8.0 with 500 mM KCl; samples b-e) contained 8-10 μM heme in 25 mM MOPS pH 7.4 with 500 mM KCl.

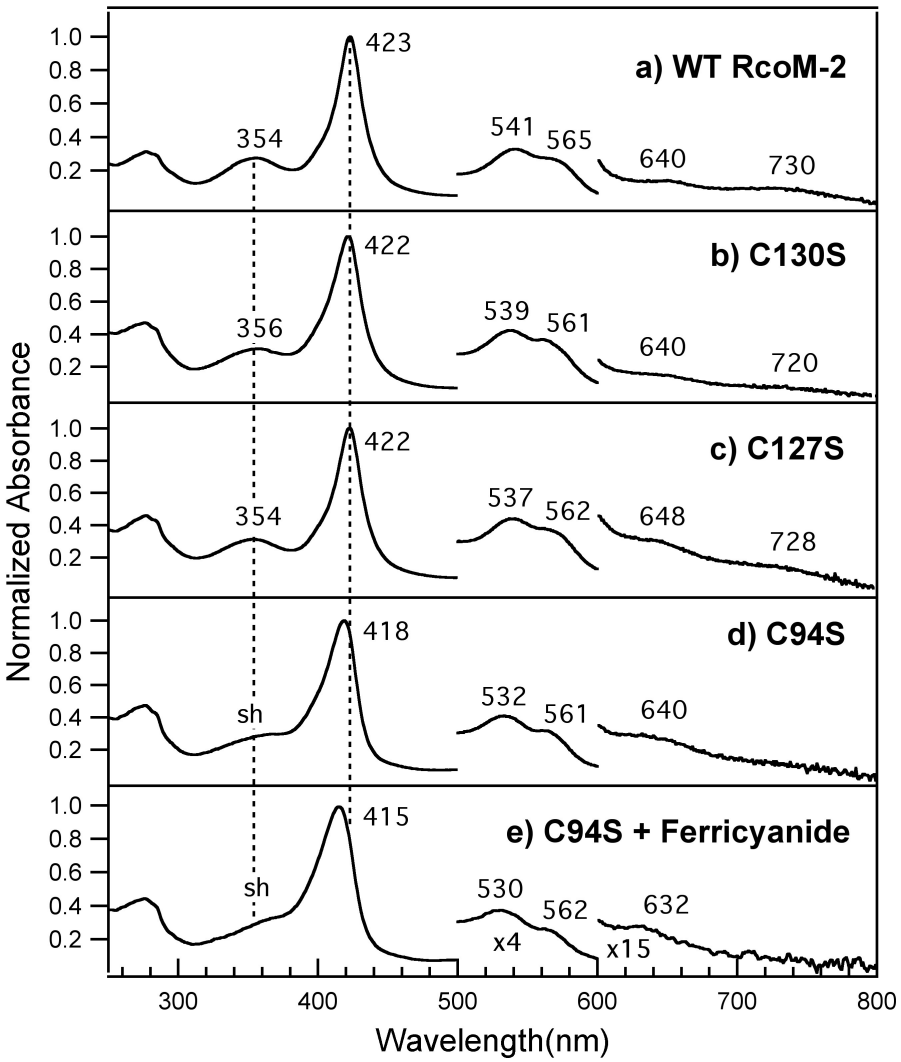

Figure 4.3. Resonance Raman spectra of a) WT Fe(III)*Bx*RcoM-2 compared to b) C130S reacted with potassium ferricyanide, c) C127S and d) C94S reacted with potassium ferricyanide. Sample a) contained 250 μM heme in 50 mM borate pH 8.0 with 500 mM KCl; samples b-d) contained 80-170 μM heme in 25 mM MOPS pH 7.4 with 500 mM KCl. Spectra were acquired with 8-15 mW of power at the frozen (77 K) sample using the 413.1 nm Kr^+ laser line. Key porphyrin stretching modes are noted, including major oxidation and spin state marker bands (ν_2, ν_3, ν_4 and ν_{10}) and the putative Fe-S stretch band ($\nu_{Fe\text{-}S}$).

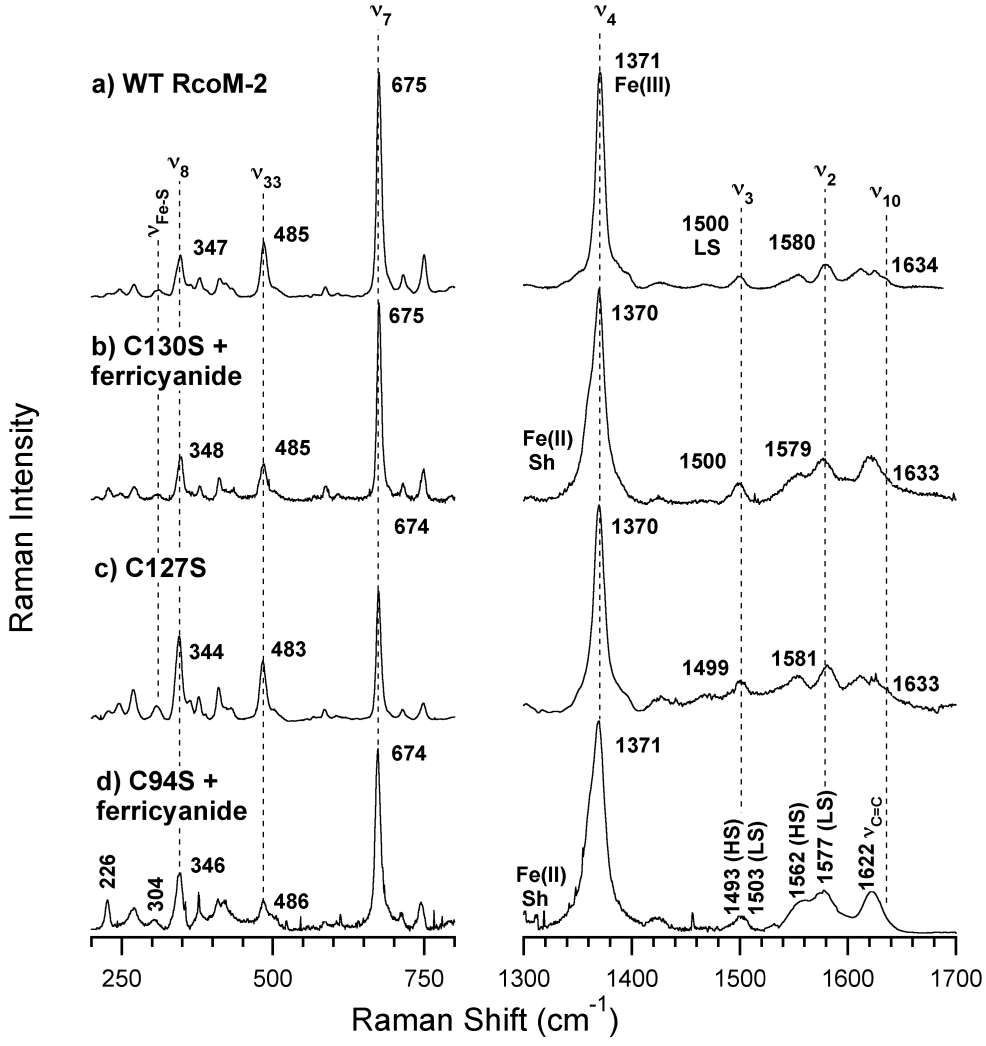

Figure 4.4. Resonance Raman spectra of a) WT Fe(III) *Bx*RcoM-2 compared to b) C130S *Bx*RcoM-2, c) C127S *Bx*RcoM-2 and d) C94S *Bx*RcoM-2 as isolated. Sample a) contained 250 μM heme in 50 mM borate pH 8.0 with 500 mM KCl; samples b-d) contained 80-170 μM heme in 25 mM MOPS pH 7.4 with 500 mM KCl. Spectra were acquired with 8-15 mW of power at the frozen (77 K) sample using the 413.1 nm Kr^+ laser line. Key porphyrin stretching modes are noted, including major oxidation and spin state marker bands (ν_2, ν_3, ν_4 and ν_{10}) and the putative Fe-S stretch band ($\nu_{Fe\text{-}S}$).

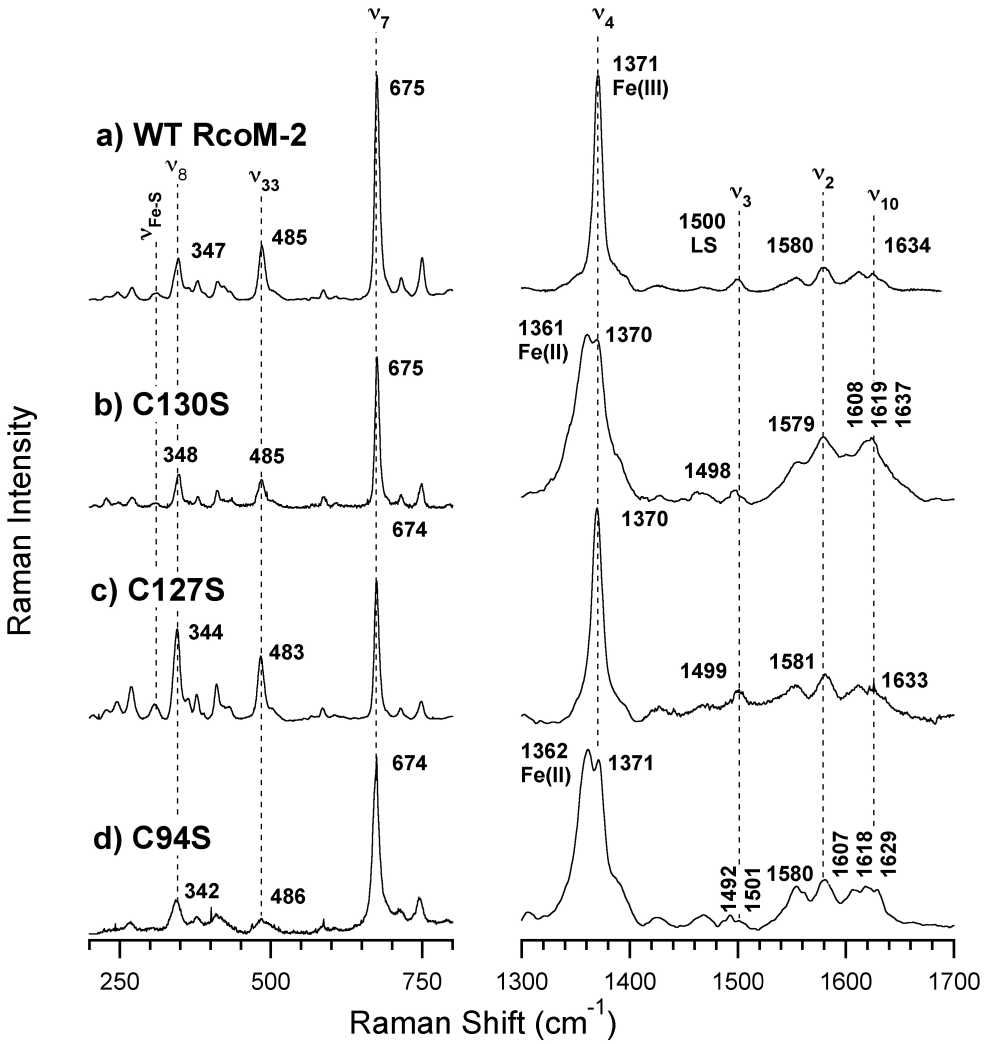

Figure 4.5. Low frequency resonance Raman spectra of a) WT Fe(III)*Bx*RcoM-2 compared to b) C130S reacted with potassium ferricyanide, c) C127S and d) C94S reacted with potassium ferricyanide. Sample a) contained 250 μM heme in 50 mM borate pH 8.0 with 500 mM KCl; samples b-d) contained 80-170 μM heme in 25 mM MOPS pH 7.4 with 500 mM KCl. Spectra were acquired with 8-15 mW of power at the frozen (77 K) sample using the 413.1 nm Kr^+ laser line. Key stretching modes are noted, including the Gaussian deconvolution of the putative Fe-S stretch band, $\nu_{Fe\text{-}S}$, the overlapping porphyrin mode, ν_{Por}, and the putative $\nu_{Fe\text{-}His}$ stretch. Peak positions are indicated for the putative porphyrin stretching mode ν_{Por} that overlaps with $\nu_{Fe\text{-}S}$.

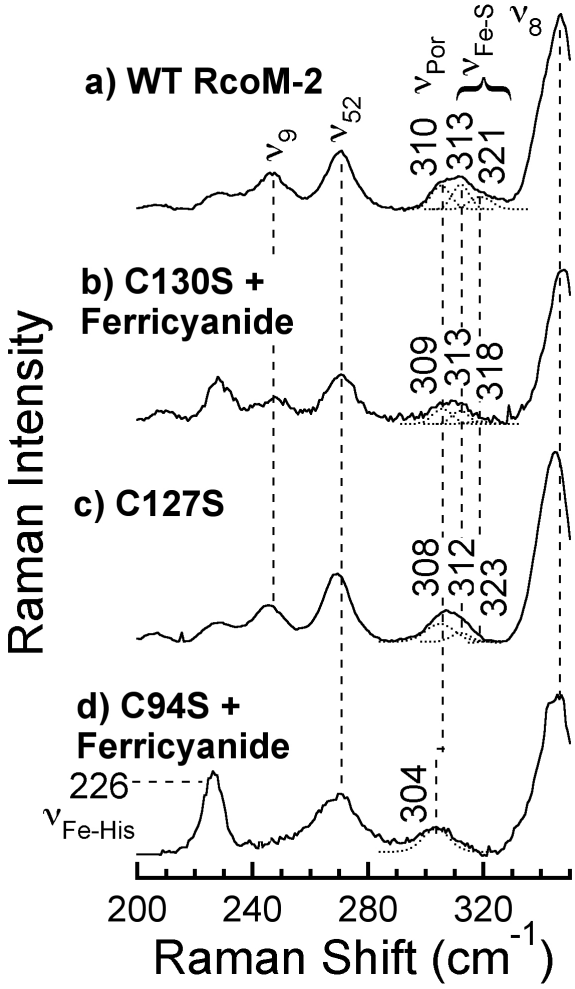

Figure 4.6. X-band EPR spectra of a) WT Fe(III)*Bx*RcoM-2 compared to b) C130S reacted with ferricyanide, c) C127S and d) C94S reacted with ferricyanide. Sample a) contained 250 μM heme in 50 mM borate pH 8.0 with 500 mM KCl; samples b-d) contained 80-170 μM heme in 25 mM MOPS pH 7.4 with 500 mM KCl. The spectra were recorded at 10 K, 9.38 GHz microwave frequency, < 5 mW microwave power, 65 dB receiver gain, 8.00 G modulation amplitude, 100 kHz modulation frequency, 81.92 ms time constant and used 20 added scans, each containing 2048 data points, except for: a) 9.36 GHz microwave frequency, 8.31 G modulation amplitude, 163.84 ms time constant; c) 9.36 GHz microwave frequency, 8.31 G modulation amplitude, 10 averaged scans; d) 10.02 mW microwave power.

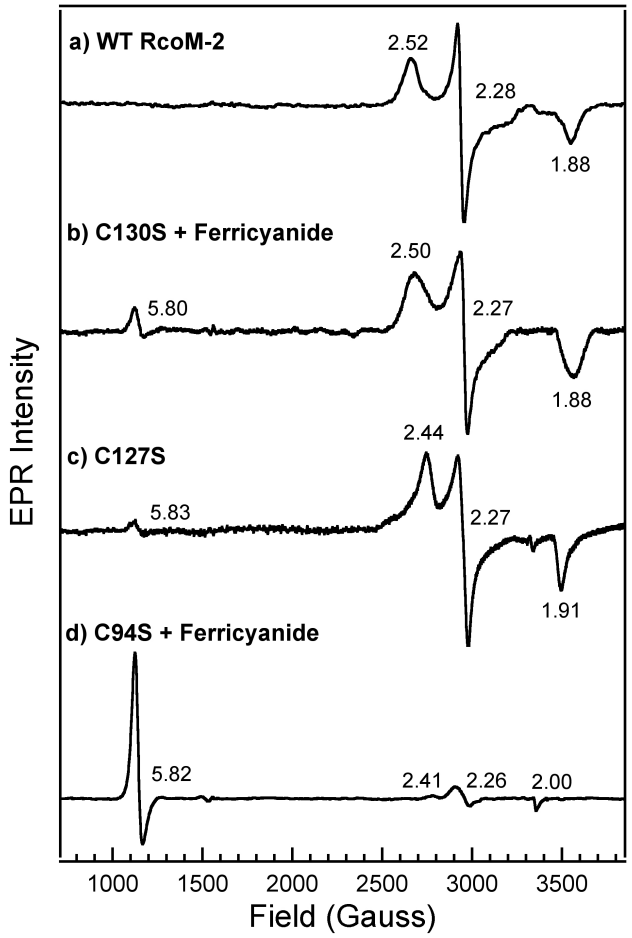

Scheme 4.1. Pictorial depiction of the varying heme coordination environments in *Bx*RcoM. Reduction of the Fe(III) heme to Fe(II) results in loss of the cysteine(thiolate) ligand (Cys^{94}) which is replaced by a nearby methionine (Met^{104}). Introduction of CO results in replacement of the weakly-bound Fe(II) distal Met^{104} ligand to form a carbon-monoxy adduct. In all states, the proximal ligand is a histidine (His^{74}) that is retained.

Burkholderia xenovorans RcoM

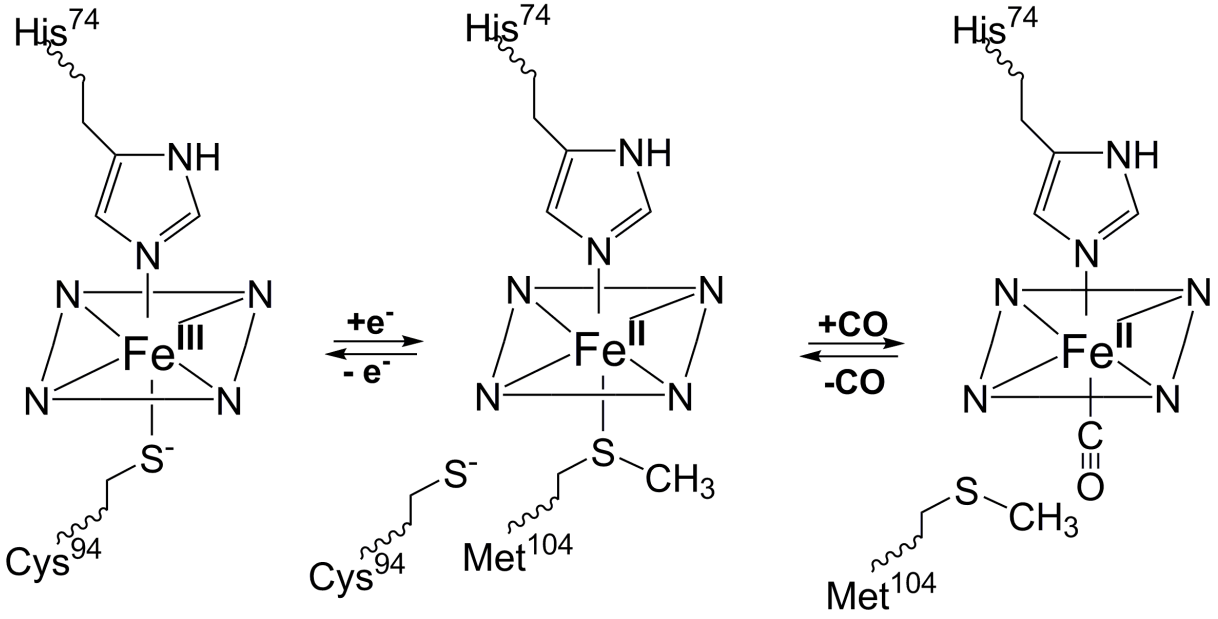

Chapter Five

Purification and Characterization of Cystathionine β-Synthase Bearing a Cobalt Protoporphyrin

A version of this chapter was published as:

Majtan, T.; Freeman, K. M.; Smith, A. T.; Burstyn, J. N.; Kraus, J. P. (2011) Purification and characterization of cystathionine β-synthase bearing a cobalt protoporphyrin, *Arch. Biochem. Biophys. 508*, 25-30.

All expression, purification, and activity assays of CoCBS were performed by Tomas Majtan in the laboratory of Professor Jan P. Kraus at the University of Colorado. Aaron Smith performed electronic absorption measurements. KMFP performed the metal analysis of CoCBS. This chapter was substantially edited and rewritten from the published manuscript by KMFP.

Introduction

Cystathionine β-synthase (CBS) is the first enzyme in the transsulfuration pathway in which the toxic intermediate homocysteine is converted to cysteine and ultimately to glutathione. A deficiency in CBS activity, primarily due to the presence of missense mutations, is the most common cause of homocystinuria, an inherited metabolic disease characterized by elevated plasma homocysteine and methionine levels and by symptoms such as dislocated optic lenses, vascular manifestations, skeletal deformities and mental retardation (*1*).

Human CBS is a homotetramer composed of 63 kDa subunits each with 551 amino acid residues. Each subunit has a modular structure consisting of three domains: an N-terminal heme binding domain, a highly conserved pyridoxal-5'-phosphate (PLP)-binding catalytic core, and a *S*-adenosyl-L-methionine (AdoMet)-binding C-terminal regulatory domain. PLP serves in the catalytic chemistry of CBS via a well-established mechanism (*2-4*). AdoMet allosterically activates the enzyme up to 8-fold. Removal of the C-terminal regulatory domain leads to a change in oligomeric status from tetramer to dimer and loss of response to AdoMet. Binding of AdoMet causes a conformational change with displacement of an autoinhibitory region from the catalytic site (*5, 6*). As a consequence, the 45 kDa C-terminal truncated enzyme has comparable activity to the AdoMet-stimulated full-length CBS.

The role of heme in CBS is not clear; however, our previous results demonstrate that heme does not function in redox sensing, ligand binding or the CBS catalytic step (*7-13*). The presence of heme in the CBS enzyme seems to be limited to higher eukaryotes. The crystal structure of the dimeric 45 kDa truncated human CBS shows that the heme cofactor is relatively surface-exposed and axially coordinated by Cys^{52} and His^{65}, both located on the loop within the N-terminus, in which the heme is nested (*8, 14*). The iron is 6-coordinate and low

spin in both reduced and oxidized states (*15*). In oxidized CBS, the Fe(III) heme does not bind exogenous ligands and appears to be a poor target for small molecule-mediated regulation. However, in reduced CBS, the Fe(II) heme binds CO, NO, CN^- and various isonitriles. Binding affects CBS activity and generally leads to inactivation by disruption of thiolate coordination (*13, 16, 17*). The redox properties of CBS heme and its effect on CBS activity suggested that the heme might function as a redox sensor (*14, 15, 18, 19*). However, this theory is undermined by the complex redox behavior of CBS, which exhibits pH and temperature dependence incompatible with simple redox regulation (*10-12*). Taken together, the complex behavior of the CBS heme iron suggests that allosteric regulation by small molecule ligand binding or changing heme redox state in CBS is unlikely.

A plausible alternative hypothesis is that heme plays a role in the structural stability of CBS. When expressed in a *S. cerevisiae* strain deficient in heme biosynthesis, the CBS enzyme does not accumulate in the absence of exogenous heme. Remarkably, heme may be replaced by the metal free protoporphyrin (PPIX) or with various alternate metalloporphyrins to yield accumulation of the CBS protein. The expression and activity of CBS are almost completely restored by inclusion of the chemical chaperone trimethylamine-N-oxide (TMAO) in the growth medium of the heme-requiring yeast cells, which implicates a folding defect in the absence of heme (*20*). When expressed in heme biosynthesis-deficient *E. coli* RP523 cells, CBS accumulation was similarly dependent on exogenous porphyrins and CBS protein containing MnPPIX and CoPPIX were isolated. These proteins were functional; however the yields and activity of CoCBS and MnCBS when anaerobically expressed in the presence of CoPPIX and MnPPIX, respectively, were lower than for FeCBS isolated from wild type *E. coli* cells in the presence of δ-aminolevulinic acid. While studying effects of cobalt on *E. coli*

metabolism, we have developed a new method for introduction of cobalt into PPIX, which can be conveniently utilized for preparation of CoPPIX substituted heme proteins (*21*). Herein we present the purification and characterization of cobalt-substituted human CBS (CoCBS) expressed in *E. coli*.

Materials and Methods

Materials. Unless stated otherwise, all chemicals were purchased from Sigma or Fisher Scientific. Protoporphyrins were purchased from Frontier Scientific. L-[^{14}C(U)]-serine was obtained from PerkinElmer Life Sciences.

Expression and purification of CoCBS. The construct pGEX-6P1-hCBS WT (*22*) was transformed into an improved bacterial host, *E. coli* Rosetta 2 (DE3) (Novagen), for expression. Cells were grown in M9 minimal medium. Media were always supplemented with 100 μg/ml ampicillin and 30 μg/ml chloramphenicol for selection of CBS expression plasmid and pRARE2 plasmid, respectively. After overnight cultivation, cells were inoculated into fresh M9 minimal medium supplemented with $CoCl_2$ at the final concentration of 150 μM and grown overnight. The cells were passaged seven times (7×) or twelve times (12×) in this medium, and the last culture served as an inoculum for the large-scale expression. The expression M9 minimal medium (pH 7.4) was supplemented with 0.5% glucose, 0.4% Casamino acids, 2 mM $MgSO_4$, 100 μM $CaCl_2$, 0.001% thiamine-HCl, 300 μM δ-aminolevulinic acid and 150 μM $CoCl_2$. Cells were grown at 30°C to an A_{600} ~ 1.0, then protein expression was induced with 500 μM IPTG and carried out overnight.

The CBS containing CoPPIX was purified as described previously for wild type FeCBS (*22*) with several modifications. Briefly, the cells were harvested in the stationary phase of growth for preparation of CBS. After cleavage of the fusion protein with PreScission protease, the GST tag was removed chromatographically on DEAE Sepharose Fast Flow (GE Healthcare). The column was equilibrated in 15 mM potassium phosphate pH 7.2, 1 mM EDTA, 1 mM DTT and 10% ethylene glycol. Under these conditions, both GST tag and hCBS

proteins bind to the DEAE Sepharose resin. The separation of the GST tag from CBS was achieved by elution with a linear gradient from 15 mM to 300 mM potassium phosphate pH 7.2, 1 mM EDTA, 1 mM DTT and 10% ethylene glycol. Protein-containing fractions were analyzed by electrophoresis on 9% SDS-PAGE. The CBS-rich fractions were pooled and subsequently concentrated on YM-100 membrane (Millipore). The buffer was changed by pressure dialysis for 20 mM HEPES pH 7.4, 1 mM TCEP and 0.01% Tween 20.

Pyridine hemochromogen assays. The pyridine hemochromogen assay was performed as described elsewhere (*20, 21*) using a HP diode array model 8453 spectrophotometer. For difference pyridine hemochromogen spectra of membrane-bound hemoproteins, the insoluble fractions of the cell lysates were washed twice with 120 volumes of Tris-saline buffer, pH 8.6. Difference spectra (i.e. reduced minus oxidized) were recorded from 650 to 380 nm with a Shimadzu 2401PC spectrophotometer.

Metal content determination. Metal content analysis was performed by inductively coupled plasma optical emission spectroscopy (ICP-OES) using a Perkin Elmer Optima 2000 DV in axial-view with an integrated AS-90 autosampler. The relevant measurement parameters were: plasma flow 15 L/min, auxiliary flow 0.2 L/min, nebulizer flow 0.6 L/min, power 1500 W, sample uptake 1 mL/min, single measurement mode with peak integration and high-resolution readout, background correction with manually selected 3-point interpolation, 10 s measurement time, 5 replicate measurements, 60 s wash between samples, 60 s read delay and 15 s flush time. Cobalt and iron were determined at commonly used analytical transitions of the atomic spectrum (228.616 nm for Co, 238.204 nm for Fe). Sample analysis was randomized to

eliminate systematic bias in the measurement. Each sample was analyzed 3 times allowing precise measurement with high signal to noise ratios. Data processing was performed automatically with the integrated instrument software.

Spectroscopic characterization. Electronic absorption spectra were measured on double-beam Varian Cary 4 Bio spectrophotometer set to a spectral bandwidth of 0.5 nm at 25°C. Solutions containing 10 μM of enzyme were in 500 mM CHES pH 9.0, 100 mM NaCl. CBS is isolated in the oxidized form i.e. with the metal ion in protoporphyrin cofactor oxidized (either Co(III)PPIX or Fe(III)PPIX). Samples were kept under argon atmosphere in septum-sealed cuvettes. Reduction of oxidized samples was carried out by adding an anaerobically prepared stock solution of sodium dithionite to a final concentration of 5 mM.

Activity assay. The CBS activity in the classical reaction was determined by a previously described radioisotope assay using [^{14}C] L-serine as the labeled substrate (*23*). CBS enzyme (420 ng) was assayed in a 100 μL reaction mixture for 30 min at 37°C. The reaction mixture contained 100 mM Tris-HCl pH 8.6, 10 mM L-serine, 0.3 μCi L-[^{14}C(U)]-serine and 0.5 mg/mL BSA. The extent of saturation of the enzyme with PLP was tested by running the activity assay in the presence or absence of 0.5 mM PLP. The reaction was performed in the presence or absence of CBS allosteric activator AdoMet in a final concentration of 0.3 mM. The reaction mixture with enzyme was incubated at 37°C for 5 min and the reaction was initiated by addition of L-homocysteine to final concentration of 10 mM. The colorimetric assay for the hydrogen sulfide-producing activity of CBS was essentially performed as described by Kayastha and Miles (*24*). CBS enzyme (5 μg) was assayed in a 200 μL volume

for 6 min at 37°C. The reaction mixture contained 50 mM Bicine pH 7.8, 40 mM L-cysteine, 50 mM β-mercaptoethanol and 0.5 mg/ml BSA. One unit of activity is defined as the amount of CBS that catalyzes the formation of 1 μmol of product in 1 h at 37°C under standard assay conditions.

Results

Purification of CoCBS. CoCBS was expressed as a GST fusion protein from a pGEX-6P1-hCBS WT construct transformed into the *E. coli* Rosetta 2 (DE3) expression stain. Expression of a GST-CBS fusion protein, where the fusion partner is specifically cleaved by PreScission protease leaving an extra glycine residue at the N-terminus, enabled us to rapidly isolate large amounts of highly purified CBS protein in a convenient two-step procedure. Unlike our previous procedure (*22*), we utilized a DEAE Sepharose column for the separation of the cleaved GST tag from CBS. After analysis of the fractions on 9% SDS-PAGE gels, the CBS-rich fractions were pooled and concentrated. To enhance solubility and prevent protein aggregation during concentration, we added a non-ionic detergent Tween 20 to a final concentration of 0.01%. We were typically able to recover 15 – 40 mg of highly purified CBS (> 97% pure according to inspection of the SDS-PAGE gel; Figure 5.1A) from 12 L of overnight culture with a 44% recovery from the crude extract (Table 5.1). CoCBS under native conditions migrated predominantly as a tetramer, as did wild type FeCBS, with some higher oligomeric forms detectable (Figure 5.1B).

Spectral properties of CoCBS. The visible spectrum of purified CoCBS was compared to the spectrum of wild type FeCBS. The A_{442}/A_{280} ratio is 0.93 suggesting purified CoCBS is fully saturated with CoPPIX. For comparison, the A_{429}/A_{280} ratio of wild type FeCBS is 0.94. The band shapes and positions of the peaks corresponding to the electronic absorption spectrum of CoCBS are distinct from those of wild type FeCBS and are indicative of a cobalt porphyrin in the +3 oxidation state (*25, 26*). The Soret peak of Co(III)CBS was red-shifted by 11 nm to 441 nm, relative to that of Fe(III)CBS. The well-resolved α/β-region revealed two discrete peaks at

587 nm and 553 nm, which are different from the broad absorption envelope of Fe(III)CBS (Figure 5.2A). The electronic absorption spectrum of Co(III)CBS also displays a distinct and well-resolved δ band at 367 nm. The combination of these spectral characteristics make Co(III)CBS unique among the family of cobalt-substituted heme proteins (*27-31*). The reduction of Co(III)CBS was much slower compared to that of wild type Fe(III)CBS. The Soret peak of Co(II)CBS was blue-shifted by 48 nm to 401 nm, relative to that of Fe(II)CBS. The broad adsorption envelope of Co(II)CBS around 554 nm with an ill-defined shoulder near 526 nm is different from the well-resolved α/β region of Fe(II)CBS revealing two discrete peaks at 573 nm and 540 nm (Figure 5.2B).

Metalloporphyrin analysis. To confirm the presence of CoPPIX in the isolated CBS enzyme, we characterized the *bis*-pyridine adducts of the metalloporphyrin contained within the protein. The spectra of pyridine hemochromogen adducts were recorded in the oxidized and reduced states and compared with appropriate standards, i.e. oxidized or reduced FePPIX and CoPPIX, respectively (Figure 5.3). The pyridine hemochromogen spectra of the protoporphyrins released from CoCBS closely resemble the spectra of the CoPPIX standard (Figure 5.3, Table 5.2). Similarly, the pyridine hemochromogen spectra of wild type FeCBS were almost identical with the spectra of the FePPIX standard (Figure 5.3, Table 5.2). The presence of iron and cobalt, respectively, in FeCBS and CoCBS is clearly visible from the positions of the Soret, α and β peaks of the oxidized (Figure 5.3A) and reduced (Figure 5.3B) pyridine hemochromogen spectra (Table 5.2).

Metal content analysis. Quantitative determination of iron and cobalt content in CoCBS was carried out using ICP-OES analysis (Table 5.3). CoCBS 7x protein was expressed in cells subjected to seven passages in cobalt-supplemented minimal medium prior to the induction of CBS expression. This enzyme was composed of 86.7% cobalt and 13.1% iron. The percentage of cobalt increased with five additional passages; the CoCBS 12x protein bore 92.4% cobalt and 7.6% iron. For comparison, wild type FeCBS expressed in cells similarly grown in the presence of 150 μM $FeCl_3$ contained only small amounts of cobalt. This minimal amount of cobalt may be attributed to cobalt in the growth medium; direct measurement of the minimal medium before supplementation with $FeCl_3$ by ICP-OES revealed 1.38 ppb Co and 2.15 ppb Fe.

The CoCBS activity measurements. Our previous results suggested that CoCBS prepared from cells grown under anaerobic conditions had 60% of the activity of FeCBS prepared from similarly cultivated cells. However, the activity of the wild type FeCBS isolated from anaerobically grown cells was substantially reduced compared to the wild type FeCBS isolated from aerobically grown cells (*20*). CoCBS, isolated after 12 passages of cells through $CoCl_2$-containing minimal medium, showed similar activity to wild type FeCBS in two different catalytic assays (Scheme 5.1): the classical condensation of L-serine and homocysteine to L-cystathionine, and an alternative condensation of L-cysteine and β-mercaptoethanol to yield *S*-hydroxyethyl-L-cysteine and hydrogen sulfide (Table 5.4). The CoCBS remains fully responsive to the allosteric activator *S*-adenosyl-L-methionine. Furthermore, we conclude that the presence of the different metalloporphyrin in CBS did not affect the saturation of the

enzyme with PLP, because similar increases in activity were observed for both CoCBS and wild type FeCBS when additional exogenous PLP was added.

Discussion

Mammalian cystathionine β-synthase (CBS) is the only known PLP-dependent enzyme to also contain heme (FePPIX); the role of heme remains unknown. CBS is principally responsible for the condensation of serine with homocysteine to form cystathionine. The catalysis of this reaction is attributed to the PLP cofactor via a classical β-replacement mechanism (*3, 7, 8, 32, 33*). Heme in CBS is not essential for the catalytic reaction, nor is heme involved in redox regulation or small molecule gas binding (*7-13*). A powerful approach to elucidate the role of heme in proteins is replacement of heme with a metalloporphyrin analogue or a porphyrin bearing different peripheral side chains. Typically, an effective method for preparing a hemoprotein with a substituted metalloporphyrin is reconstitution of the apoenzyme with heme analogues (reviewed in (*34*)); however, this approach relies on removal of the native heme using partially denaturing conditions and is therefore limited to proteins that can withstand the harsh replacement conditions. Thus, there is need for a different approach to replace or substitute heme in hemoproteins sensitive to partial denaturation and/or simultaneous removal of the heme moiety.

Our previous attempt at heme replacement in CBS employed *S. cerevisiae* and *E. coli* strains deficient in heme biosynthesis (*20*). The protein does not accumulate when expressing CBS in the heme biosynthetic-deficient yeast strain. However, addition of a chemical chaperone, or protoporphyrix IX and its metalloporphyrin analogues rescues CBS expression. Anaerobic expression of CBS in heme biosynthetic-deficient *E. coli* produced minimal yields of manganese-containing CBS and cobalt-containing CBS (*20*). Therefore, we developed a new method for aerobic expression of CoCBS dependent on iron-depleted cells in the presence of $CoCl_2$ that yields large quantities of high purity CoCBS sufficient for spectroscopic study.

We developed an alternative non-native metal insertion technique that uses the endogenous metal-insertion machinery of *E. coli* Rosetta2 cells to insert cobalt, in place of iron, into the PPIX macrocycle. Our strategy only works for cobalt. It fails at incorporating other divalent metal ions (e.g. Zn, Cu, Mn, Ni) that are not naturally inserted into porphyrin-derived macrocycles. We speculate that at high cobalt concentrations, cobalt is inserted into PPIX in place of iron by an endogenous chelatase. However, the nature of the adaptive response in *E. coli* Rosetta2 cells that permits cobalt insertion into CBS is not known.

A number of studies have explored the deleterious effects of cobalt on bacterial metabolism, revealing adaptive responses that occur in response to elevated cobalt concentration (*35, 36*). In particular, iron and cobalt compete with one another and elevated cobalt concentrations may disrupt iron-dependent metabolic processes (*37*). We observed that the cobalt-exposed *E. coli* Rosetta2 cells produce metabolites consistent with fermentative metabolism under aerobic growth suggesting suppression of iron-dependent pathways, since cobalt has been shown to inactivate aconitase and other key iron sulfur cluster enzymes in *E. coli* (*35*). The question still remains, how is cobalt inserted into PPIX, a porphyrin that does not usually contain cobalt? Studies in *Salmonella enterica* suggest that at elevated cobalt concentration, cobalt and iron compete for insertion into uroporphyrinogen III, a protoporphyrin IX precursor, via the CysG chelatase (*36*). In *E. coli*, an organism that does not synthesize cobalamin, CysG inserts iron in the pathway to siroheme, but this enzyme was also capable of inserting cobalt (*37, 38*). Human ferrochelatase will insert cobalt into PPIX; however, ferrochelatase from *Bacillus subtilis*, a cobalamin synthesizer, will not. The metal specificity of *E. coli* ferrochelatase (HemH) is not known (*39, 40*). There are two plausible hypotheses to explain cobalt insertion into CoPPIX in the *E. coli* Rosetta2 cells: 1) CysG

inserts cobalt into PPIX, as that cofactor builds up in the absence of iron; or 2) cobalt is inserted into PPIX by ferrochelatase. We do not have sufficient data to determine whether either mechanism is responsible for cobalt insertion into CoPPIX in *E. coli* Rosetta2 cells expressing CBS.

Our new method for expression of CoCBS yielded a protein virtually indistinguishable from wild type FeCBS with respect to its native conformation, enzyme activity and responsiveness to AdoMet. The enzymatic activity of CoCBS is practically identical to that of wild type FeCBS for the canonical and alternative substrate enzymatic reactions (see Scheme 5.1 and Table 5.4). The high activity of CoCBS is not due to FePPIX contamination, since loading of iron is only 7.6% with 92.4% incorporation of cobalt. Our results demonstrate not only is heme (FePPIX) not essential for the catalytic activity of CBS, but also that heme can be replaced by an alternative metalloporphyrin, particularly CoPPIX, without sacrificing enzymatic activity. Moreover, our data provides additional evidence the porphyrin moiety of CBS has a structural role (*12, 20*). The high yield of CoCBS allowed us to investigate the structural importance of heme in CBS by characterizing the coordination environment of CoPPIX in CoCBS with comparison to FePPIX in wild type FeCBS.

In a related spectroscopic study of CoCBS we found that cobalt is coordinated by Cys/neutral donor (presumably His) (*41*), the same coordination environment as iron in wild type FeCBS (Cys/His) (*42*). Structural similarities between CoCBS and wild type FeCBS emphasizes the structural significance of the metal-cysteine(thiolate) bond in the role of heme in CBS. Interestingly, thiolate coordination is not metal-dependent; the enzyme does not distinguish between cobalt and iron. In addition, substituting iron with cobalt does not perturb the secondary coordination sphere of the porphyrin in CBS (*41*). Maximal activity of wild type

FeCBS requires the electrostatic interaction of Arg^{266} with the axial ligand Cys^{52} (*43*). The fact that we observed indistinguishable activity between CoCBS and wild type FeCBS suggests the secondary coordination sphere is unperturbed. Our results suggest CBS does not discriminate between iron and cobalt, rather the metal center imparts a specific structure that supports enzymatic function, which is defined by the presence of a metalloporphyrin with a Cys/His ligation motif.

Future Directions

The ability to utilize *E. coli* for insertion of cobalt into PPIX rather than iron, yielding cobalt-substituted PPIX, is of interest to the Burstyn group to elucidate the role of heme in our heme-containing proteins. Using our *E. coli* VJS6737 strain (the strain bearing the pEXT20 expression vectors for CooA and RcoM) for expression of cobalt-substituted PPIX proteins will not yield protein. Cobalt is toxic to our *E. coli* VJS6737 strain; in addition, the strain requires a robust minimal media (see Appendix). To express in the presence of cobalt, we need to use *E. coli* Rosetta 2 (DE3) cells. Tomas Majtan forced a genetic mutation in the *E. coli* Rosetta 2 (DE3) cells during expression of CoCBS. We want to use *E. coli* Rosetta 2 (DE3) cells where we can induce the mutation(s) enabling incorporation of cobalt into PPIX rather than iron. It should also be noted that the presence of the CBS expression vector in *E. coli* Rosetta 2 (DE3) cells provides a protective benefit to cells growing in the presence of cobalt. If the *E. coli* Rosetta 2 (DE3) cells do not grow in the presence of cobalt, we should consider adding CBS to the expression vector to determine if we observe a protective benefit to our cells.

References

1. Mudd, S. H., Levy, H. L., and Kraus, J. P. (2001) Disorders of Transsulfuration, In *The Metabolic and Molecular Bases of Inherited Disease* (Scriver, C. R., Beaudet, A. L., Sly, W. S., Valle, D., Childs, B., Kinzler, K., and Vogelstein, B., Eds.), pp 2007-2056, McGraw Hill, New York.

2. Miles, E. W. (1986) *Vitamin B6. Pyridoxal phosphate. Chemical, Biochemical, and Medical Aspects. Part B*, John Wiley & Sons, New York.

3. Kery, V., Poneleit, L., Meyer, J. D., Manning, M. C., and Kraus, J. P. (1999) Binding of Pyridoxal 5'-Phosphate to the Heme Protein Human Cystathionine β-Synthase, *Biochemistry 38*, 2716-2724.

4. Banerjee, R., Evande, R., Kabil, O., Ojha, S., and Taoka, S. (2003) Reaction mechanism and regulation of cystathionine b-synthase, *Biochim. Biophys. Acta 1647*, 30-35.

5. Janosik, M., Kery, V., Gaustadnes, M., MacLean, K. N., and Kraus, J. P. (2001) Regulation of human cystathionine β-synthase by S-adenosyl-L-methionine: Evidence for two catalytically active conformations involving an autoinhibitory domain in the C-terminal region, *Biochemistry 40*, 10625-10633.

6. Shan, X., and Kruger, W. D. (1998) Correction of disease-causing CBS mutations in yeast, *Nat. Genet. 19*, 91-93.

7. Bruno, S., Schiaretti, F., Burkhard, P., Kraus, J. P., Janosik, M., and Mozzarelli, A. (2001) Functional Properties of the Active Core of Human Cystathionine β -Synthase Crystals, *J. Biol. Chem. 276*, 16-19.

8. Meier, M., Janosik, M., Kery, V., Kraus, J. P., and Burkhard, P. (2001) Structure of human cystathionine β-synthase: A unique pyridoxal 5'-phosphate dependent hemeprotein, *EMBO J. 20*, 3910-3916.

9. Oliveriusová, J., Kery, V., Maclean, K. N., and Kraus, J. P. (2002) Deletion Mutagenesis of Human Cystathionine beta -Synthase. Impact on Activity, Oligomeric Status, and S-Adenosylmethionine Regulation, *J. Biol. Chem. 277*, 48386-48394.

10. Pazicni, S., Lukat-Rodgers, G. S., Oliveriusová, J., Rees, K. A., Parks, R. B., Clark, R. W., Kraus, J. P., Rodgers, K. R., and Burstyn, J. N. (2004) The redox behavior of the heme in cystathionine β-synthase is sensitive to pH, *Biochemistry 43*, 14684-14695.

11. Pazicni, S., Cherney, M. M., Lukat-Rodgers, G. S., Oliveriusová, J., Rodgers, K. R., Kraus, J. P., and Burstyn, J. N. (2005) The Heme of Cystathionine β-synthase Likely Undergoes a Thermally Induced Redox-Mediated Ligand Switch, *Biochemistry 44*, 16785-16795.

12. Cherney, M. M., Pazicni, S., Frank, N., Marvin, K. A., Kraus, J. P., and Burstyn, J. N. (2007) Ferrous Human Cystathionine β-Synthase Loses Activity during Enzyme Assay Due to a Ligand Switch Process, *Biochemistry 46*, 13199-13210.

13. Vadon-Le Goff, S., Delaforge, M., Boucher, J.-L., Janosik, M., Kraus, J. P., and Mansuy, D. (2001) Coordination Chemistry of the Heme in Cystathionine β-Synthase: Formation of Iron(II)–Isonitrile Complexes, *Biochem. Biophys. Res. Commun. 283*, 487-492.

14. Taoka, S., Lepore, B. W., Kabil, O., Ojha, S., Ringe, D., and Banerjee, R. (2002) Human Cystathionine β-Synthase Is a Heme Sensor Protein. Evidence That the Redox

Sensor Is Heme and Not the Vicinal Cysteines in the CXXC Motif Seen in the Crystal Structure of the Truncated Enzyme, *Biochemistry 41*, 10454-10461.

15. Taoka, S., Ohja, S., Shan, X., Kruger, W. D., and Banerjee, R. (1998) Evidence for heme-mediated redox regulation of human cystathionine b-synthase activity, *J. Biol. Chem. 273*, 25179-25184.

16. Taoka, S., and Banerjee, R. (2001) Characterization of NO binding to human cystathionine β-synthase: Possible implications of the efects of CO and NO binding to the human enzyme, *J. Inorg. Biochem. 87*, 245-251.

17. Taoka, S., Green, E. L., Loehr, T. M., and Banerjee, R. (2001) Mercuric chloride-induced spin or ligation state changes in ferric or ferrous human cystathionine b-synthase inhibit enzyme activity, *J. Inorg. Biochem. 87*, 253-259.

18. Carballal, S., Madzelan, P., Zinola, C. F., Graña, M., Radi, R., Banerjee, R., and Alvarez, B. (2008) Dioxygen Reactivity and Heme Redox Potential of Truncated Human Cystathionine β-Synthase, *Biochemistry 47*, 3194-3201.

19. Singh, S., Madzelan, P., Stasser, J., Weeks, C. L., Becker, D., Spiro, T. G., Penner-Hahn, J., and Banerjee, R. (2009) Modulation of the heme electronic structure and cystathionine β-synthase activity by second coordination sphere ligands: The role of heme ligand switching in redox regulation, *J. Inorg. Biochem. 103*, 689-697.

20. Majtan, T., Singh, L. R., Wang, L., Kruger, W. D., and Kraus, J. P. (2008) Active Cystathionine β-Synthase Can Be Expressed in Heme-free Systems in the Presence of Metal-substituted Porphyrins or a Chemical Chaperone, *J. Biol. Chem. 283*, 34588-34595.

21. Majtan, T., Frerman, F., and Kraus, J. (2011) Effect of cobalt on *Escherichia coli* metabolism and metalloporphyrin formation, *BioMetals 24*, 335-347.

22. Frank, N., Kent, J. O., Meier, M., and Kraus, J. P. (2008) Purification and characterization of the wild type and truncated human cystathionine β-synthase enzymes expressed in *E. coli*, *Arch. Biochem. Biophys. 470*, 64-72.

23. Kraus, J. P. (1987) Cystathionine b-synthase (human), *Methods Enzymol. 143*, 388-395.

24. Kayastha, A. M., and Miles, E. W. (1991) A colorimetric assay for a pyridoxal phosphate-dependent b-replacement reaction with L-cysteine: Application to studies of wild-type and mutant tryptophan synthase a_2b_2 complexes, *Anal. Biochem. 193*, 200-203.

25. Falk, J. E. (1964) *Porphyrins and Metalloporphyrins: Their General, Physical, and Coordination Chemistry, and Laboratory Methods*, Elsevier, Amsterdam.

26. Dickinson, L. C., and Chien, J. C. W. (1975) Cobalt-Cytochrome C. I. Preparation, Properties, and Enzymic Activity, *Biochemistry 14*, 3526-3533.

27. Yonetani, T., Yamamoto, H., and Woodrow, G. V., III. (1974) Studies on Cobalt Myoglobins and Hemoglobins. I. Preparation and Optical Properties of Myoglobins and Hemoglobins Containing Cobalt Proto-, Meso-, and Deuteroporphyrins and Thermodynamic Characterization of their Reversible Oxygenation, *J. Biol. Chem. 249*, 682-690.

28. Yonetani, T., Yamamoto, H., and Iizuka, T. (1974) Sudies on Cobalt Myoglobins and Hemoglobins III. Electron Paramagnetic Resonance Studies on Reversible Oxygenation of Cobalt Myoglobins and Hemoglobins, *J. Biol. Chem. 249*, 2168-2174.

29. Wang, M. Y., Hoffman, B. M., and Hollenberg, P. F. (1977) Cobalt-substituted horseradish peroxidase, *J. Biol. Chem. 252*, 6268-6275.

30. Dickinson, L. C., and Chien, J. C. W. (1975) Cobalt-Cytochrome C. II. Magnetic Resonance Spectra and Conformational Transitions, *Biochemistry 14*, 3534-3542.

31. Wagner, G. C., Gunsalus, I. C., Wang, M. Y., and Hoffman, B. M. (1981) Cobalt-substituted cytochrome P-450cam, *J. Biol. Chem. 256*, 6266-6273.

32. Braunstein, A. E., and Goryachenkova, E. V. (1984) The β-Replacement-Specific Pyridoxal-p-Dependent Lyases, In *Adv. Enzymol. Relat. Areas Mol. Biol.*, pp 1-89, John Wiley & Sons, Inc.

33. Evande, R., Ojha, S., and Banerjee, R. (2004) Visualization of PLP-bound intermediates in hemeless variants of human cystathionine β-synthase: evidence that lysine 119 is a general base, *Arch. Biochem. Biophys. 427*, 188-196.

34. Fruk, L., Kuo, C.-H., Torres, E., and Niemeyer, C. M. (2009) Apoenzyme Reconstitution as a Chemical Tool for Structural Enzymology and Biotechnology, *Angew. Chem. Int. Ed. 48*, 1550-1574.

35. Ranquet, C., Ollagnier-de-Choudens, S., Loiseau, L., Barras, F., and Fontecave, M. (2007) Cobalt Stress in Escherichia coli the effect on iron-sulfur proteins, *J. Biol. Chem. 282*, 30442-30451.

36. Thorgersen, M. P., and Downs, D. M. (2007) Cobalt Targets Multiple Metabolic Processes in Salmonella enterica, *J. Bacteriol. 189*, 7774-7781.

37. Fazzio, T. G., and Roth, J. R. (1996) Evidence that the CysG protein catalyzes the first reaction specific to B12 synthesis in Salmonella typhimurium, insertion of cobalt, *J. Bacteriol. 178*, 6952-6959.

38. Spencer, J. B., Stolowich, N. J., Roessner, C. A., and Scott, A. I. (1993) The Escherichia coli cysG gene encodes the multifunctional protein, siroheme synthase, *FEBS Lett. 335*, 57-60.

39. Medlock, A. E., Carter, M., Dailey, T. A., Dailey, H. A., and Lanzilotta, W. N. (2009) Product Release Rather than Chelation Determines Metal Specificity for Ferrochelatase, *J. Mol. Biol. 393*, 308-319.

40. Frustaci, J. M., and O'Brian, M. R. (1993) The Escherichia coli visA gene encodes ferrochelatase, the final enzyme of the heme biosynthetic pathway, *J. Bacteriol. 175*, 2154-2156.

41. Smith, A. T., Majtan, T., Freeman, K. M., Su, Y., Kraus, J. P., and Burstyn, J. N. (2011) Cobalt Cystathionine ß-Synthase: A Cobalt-Substituted Heme Protein with a Unique Thiolate Ligation Motif, *Inorg. Chem. 50*, 4417-4427.

42. Meier, M., Janosik, M., Kery, V., Kraus, J. P., and Burkhard, P. (2001) Structure of human cystathionine β-synthase: A unique pyridoxal 5'-phosphate dependent heme protein, *EMBO J. 20*, 3910-3916.

43. Singh, S., Madzelan, P., Stasser, J., Weeks, C. L., Becker, D., Spiro, T. G., Penner-Hahn, J., and Banerjee, R. (2009) Modulation of the heme electronic structure and cystathionine β-synthase activity by second coordination sphere ligands: The role of heme ligand switching in redox regulation, *J. Inorg. Biochem. 103*, 689-697.

Table 5.1. CoCBS 12× purification table.

Fraction	Total activity (U)	Total Protein (mg)	Specific activity (U/mg of protein)	Recovery yield (%)
Crude extract	4520	6955	0.65	100
Glutathione Sepharose flow-through	1013	5279	0.19	22
Glutathione Sepharose wash	259	1140	0.23	6
GST-CBS fusion protein	2815	70	40.2	62
Cleaved fusion protein	3472	90	38.7	77
DEAE pool	1396	70	19.9	31
CoCBS 12×	2000	19	105.2	44

Table 5.2. Pyridine hemochromogen spectral peak positions.

Sample	Soret (nm)	α/β peaks (nm)
Fe(III)PPIX standard	396	ND*
Oxidized PPIX released from wild type FeCBS	399	ND*
Co(III)PPIX standard	423	534, 567
Oxidized PPIX released from CoCBS	429	542, 572
Fe(II)PPIX standard	416	522, 555
Reduced PPIX released from wild type FeCBS	419	524, 556
Co(II)PPIX standard	401	554
Reduced PPIX released from CoCBS	404	556

* ND: not detected; bands were broad and indistinct with a maximum beyond the spectral range recorded

Table 5.3. Metal content analysis of wild type FeCBS and CoCBS using ICP-OES. For the CoCBS samples, 7× and 12× denotes number of cell growth passages in minimal medium supplemented with 150 μM $CoCl_2$ prior induction of CBS expression. Metal content is reported as percentage of total metal content.

Sample	Iron content (μM)	Iron content (%)	Cobalt content (μM)	Cobalt content (%)
WT FeCBS	1.3 ± 0.1	97.1 ± 0.7	0.036 ± 0.006	2.9 ± 0.2
CoCBS 7×	0.061 ± 0.002	13.1 ± 0.1	0.39 ± 0.04	86.7 ± 0.3
CoCBS 12×	0.083 ± 0.003	7.6 ± 0.4	0.96 ± 0.06	92.4 ± 0.8

Table 5.4. Enzymatic activity of CoCBS and wild type FeCBS. The CBS activity was determined in two reactions. In the classical reaction, homocysteine and L-serine were used to generate cystathionine. In the alternative reaction, hydrogen sulfide was generated by condensing L-cysteine and β-mercaptoethanol. The extent of saturation of enzyme with the PLP was tested by running the activity assays in the presence or absence of 0.5 mM PLP. The reactions were performed in the presence or absence of CBS allosteric activator AdoMet in final concentration of 0.3 mM.

Activity assay	PLP	AdoMet	CoCBS	FeCBS
Classical L-cystathionine-generation (U/mg of protein)	–	–	75 ± 5	77 ± 9
	–	+	204 ± 13	217 ± 15
	+	–	95 ± 3	101 ± 4
	+	+	372 ± 19	404 ± 25
Alternative H_2S-generation (U/mg of protein)	–	–	91 ± 6	112 ± 10
	–	+	318 ± 21	329 ± 25
	+	–	124 ± 11	139 ± 6
	+	+	409 ± 24	341 ± 17

Figure 5.1. SDS-PAGE analysis of fractions from CoCBS purification (A) and native Western blot of purified CoCBS (B). (A) Each protein purification fraction was separated on a 9% SDS-PAGE gel and stained using Simply Blue Safe stain (Invitrogen). Lanes: M – Molecular weight marker (Biorad), 1 – crude extract (10 μg), 2 – Glutathione Sepharose flow-through (10 μg), 3 – Glutathione Sepharose wash (10 μg), 4 – GST-CBS fusion protein (10 μg), 5 – Fusion protein cleaved with PreScission protease (10 μg), 6 – DEAE Sepharose pool (2.5 μg), 7, 8, 9 – CoCBS (10 μg, 5 μg and 1 μg, respectively). (B) CoCBS and WT FeCBS were separated in 4-12% Tris-HCl native gel, transferred to PVDF membrane and probed with monoclonal anti-CBS antibody (Abnova).

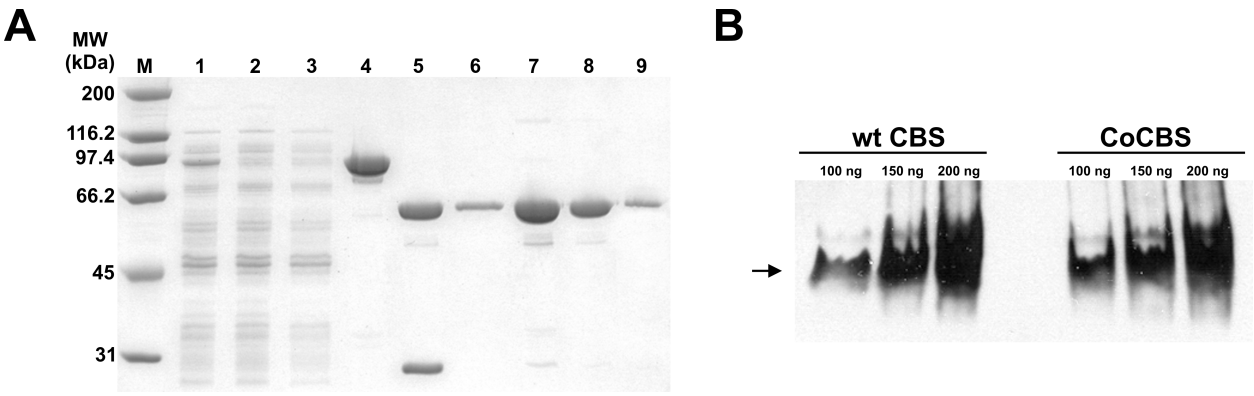

Figure 5.2. Electronic absorption spectrum of oxidized (A) and reduced (B) purified human CoCBS 12× (dashed) compared to that of wild type FeCBS (solid). Enzyme (10 μM) was in 500 mM CHES pH 9.0, 100 mM NaCl at room temperature. Reduction was performed under anaerobic conditions by using sodium dithionite as a reductant. Underlined values correspond to CoCBS.

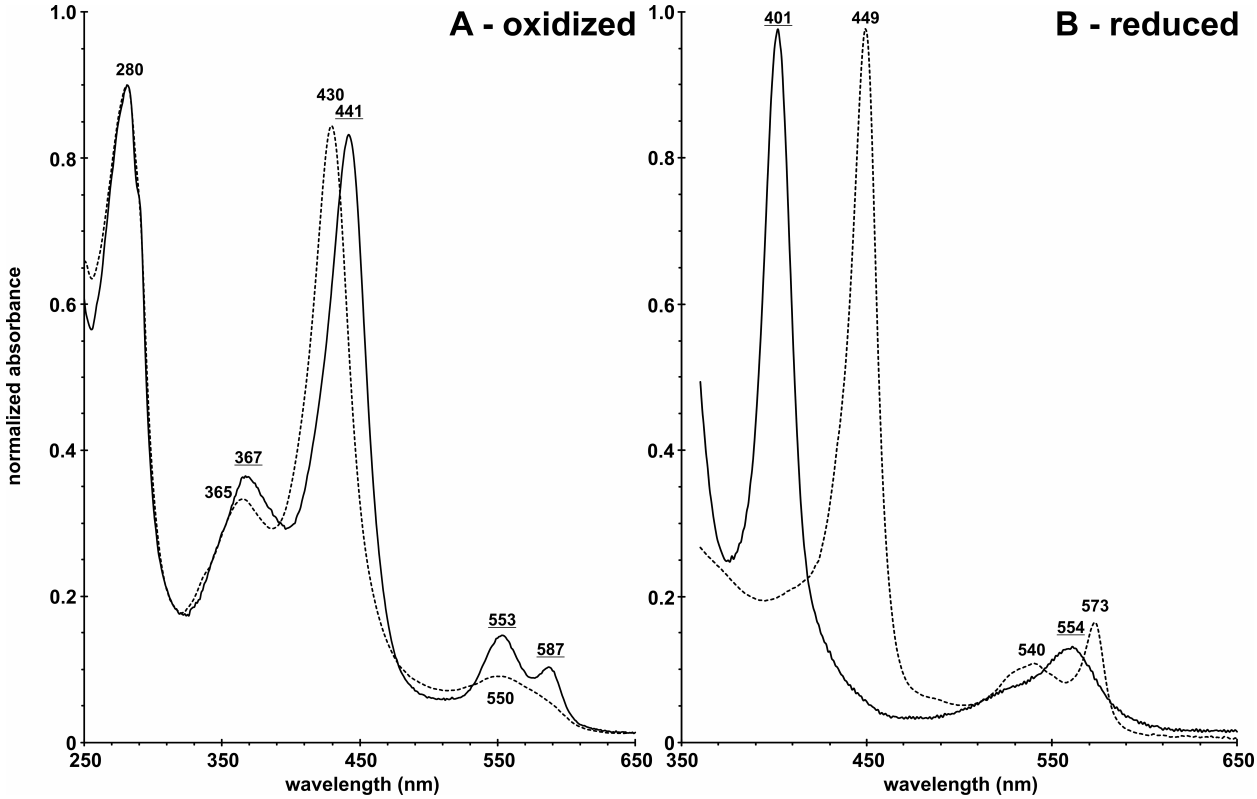

Figure 5.3. Pyridine hemochromogen spectra of oxidized (A) and reduced (B) protoporphyrins released from wild type FeCBS and CoCBS. Solid lines correspond to the spectra of metalloporphyrins released from the enzyme (black for wild-type FeCBS, red for CoCBS). Dashed lines represent the corresponding metalloporphyrin standard (black for FePPIX, red for CoPPIX).

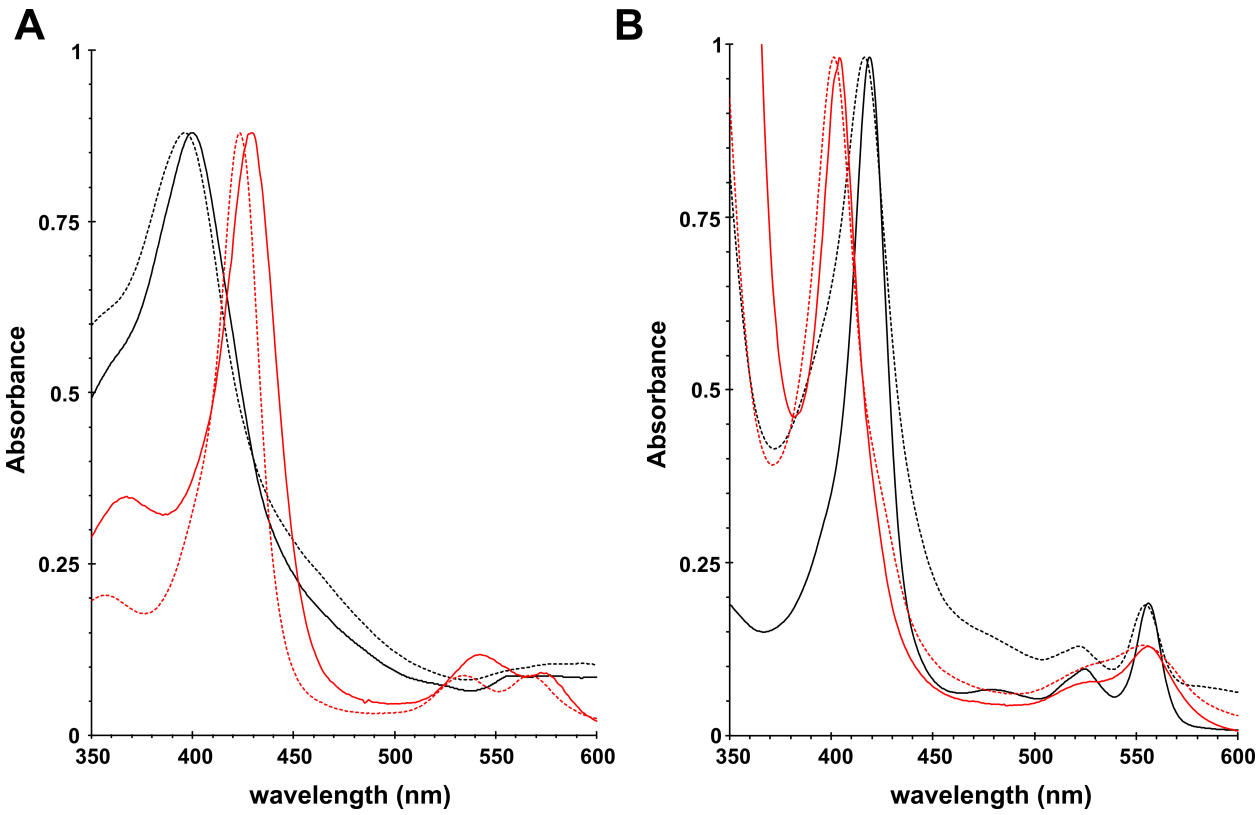

Scheme 5.1. The catalytic reactions of FeCBS and CoCBS. The classical reaction of CBS is the condensation of L-serine and homocysteine to form L-cystathionine. An alternative reaction is the condensation of L-cysteine and β-mercaptoethanol to yield *S*-hydroxyethyl-L-cysteine and hydrogen sulfide.

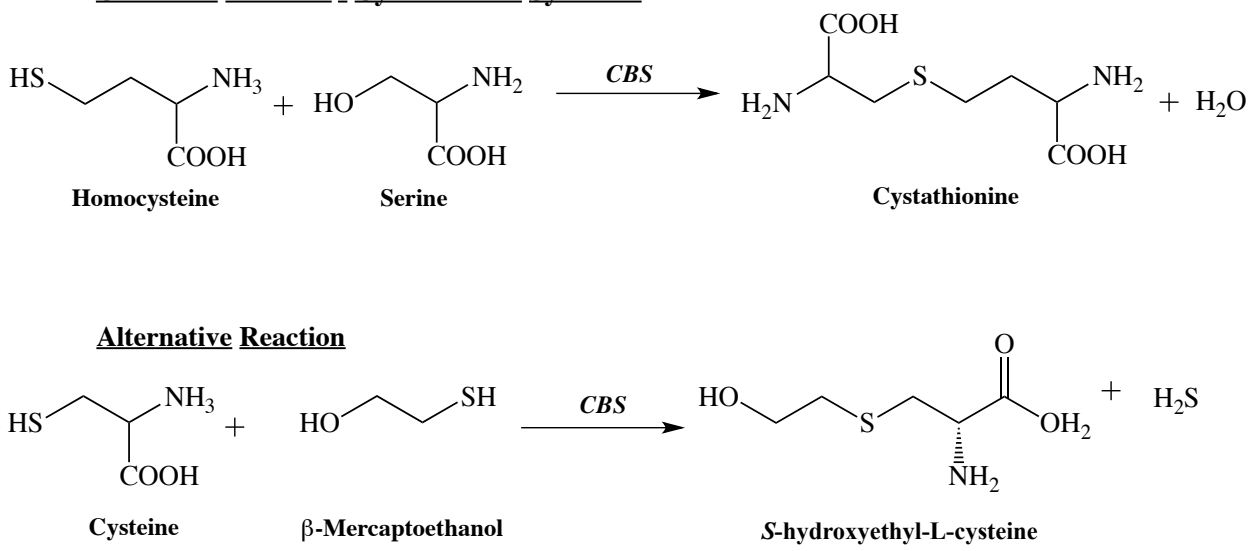

Appendix

Minimal Media Recipe for *E. coli* VJS6737 Strain

Stock/Buffer Component	Amount/L	Amount/500mL
2 M MOPS	75 mL	37.5 mL
0.5 M Tricine	8.0 mL	4.0 mL
0.1 M $FeSO_4 \cdot 7H_2O$	2.0 mL	1.0 mL
2 M NH_4Cl	15.0 mL	7.5 mL
1 M $MgSO_4$	5.5 mL	2.75 mL
1 M $CaCl_2$	2.0 µL	1.0 µL
5 M NaCl	10.0 mL	5.0 mL
0.88 M K_2HPO_4	2.0 mL	1.0 mL
40 % Glucose	18.0 mL	9.0 mL
2 mM Thiamine	10.0 mL	5.0 mL
10X Soluble Amino Acids	100 mL	50 mL
100X Insoluble Amino Acids	10.0 mL	5.0 mL
100X Mineral Solution	15.0 mL	7.5 mL
100X Kao Vitamins (Sigma)	10.0 mL	5.0 mL
Sterile DI H_2O	720 mL	350 mL

100X Kao Vitamins Mix Recipe

Component (mg/L)*	Kao and Michayluk Vitamin Solution
p-Aminobenzoic Acid	0.02
L-Ascorbic Acid	2.0
Biotin	0.01
D-Calcium Pantothenate	1.0
Choline Chloride	1.0
Folic Acid	0.4
myo-Inositol	100.0
Nicotinamide	1.0
Pyridoxine • HCl	1.0
Riboflavin	0.2
Thiamine • HCl	1.0
Vitamin A (Retinol)	0.01
Vitamin B_{12}	0.02
Vitamin D (Cholecalciferol)	0.01

*Concentrations listed are final concentrations when used at recommended dilution.